The relationship between the morphology and the rheology of mycelial fermentations.

Simon John Curtis WARREN.

PhD Biochemical Engineering.

University College London.

ProQuest Number: 10045770

All rights reserved

INFORMATION TO ALL USERS
The quality of this reproduction is dependent upon the quality of the copy submitted.

In the unlikely event that the author did not send a complete manuscript
and there are missing pages, these will be noted. Also, if material had to be removed,
a note will indicate the deletion.

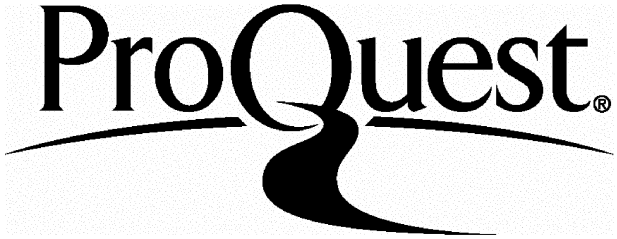

ProQuest 10045770

Published by ProQuest LLC(2016). Copyright of the Dissertation is held by the Author.

All rights reserved.
This work is protected against unauthorized copying under Title 17, United States Code.
Microform Edition © ProQuest LLC.

ProQuest LLC
789 East Eisenhower Parkway
P.O. Box 1346
Ann Arbor, MI 48106-1346

Abstract.

The rheology and morphology of culture broths are believed to influence the production of many secondary metabolites during fermentation. Consequently these topics have been the subject of intense research interest in the past and several researchers have postulated that morphology of filamentous microorganisms determines the rheology of the fermentation broth. However, no unequivocal evidence exists to support this hypothesis and the question of the factors that influence the rheology of the broth still remains open.

In this thesis an investigation was made to study the factors determining the rheology of three industrial strains of Actinomycete specifically *Streptomyces rimosus*, *Actinomadura roseorufa* and *Streptomyces erythraeus* (recently re-classified as *Saccharopolyspora erythraea*).

The rheological data were collected using two different viscometers; a Brookfield 2HAT DVII and a Contraves Rheomat 115. All rheological data collected with the Brookfield were in good agreement with the data from the Contraves and were analysed using Mitschka's technique[115]. These measurements revealed that all culture broths studied were highly viscous, pseudoplastic and could be characterised using a power law relationship. Both the flow behaviour index ($0.2 < n < 1$) and the consistency coefficient ($0.001 < K < 15$ Pa.s^n) were monitored and were found to vary throughout the course of the fermentation.

A sophisticated image analysis technique has recently been developed for morphological studies of filamentous microorganisms at the Department of Chemical and Biochemical Engineering at UCL (and the department of Chemical Engineering at Birmingham University). In this investigation a Magiscan image analyser was used for the rapid collection and accurate analysis of morphological parameters, namely total hyphal length, main hyphal length, branch length, number of tips and the length of the hyphal growth unit. These parameters were collected because they

have been shown to be reasonably sensitive to changes in the conditions of the culture.

The results of these measurements indicated that the morphology of the microorganisms changed during the whole of the fermentation period. However no observable correlation could be detected between these measurements and the rheology of the culture. The variation in the rheology of the culture broth was found to depend on the biomass concentration and on the pH of the culture. The culture rheology changed rapidly and dramatically from an initial Newtonian behaviour (n=1) to a highly pseudoplastic behaviour (n≈0.3) within forty hours of the fermentation inoculation, after which the flow behaviour index of the culture remained practically unchanged for the remainder of the fermentation. Additionally the consistency coefficient (K) was found to depend on biomass concentration during the initial growth phase for all three Actinomycete cultures. The data for *S. erythraeus* indicated that the consistency coefficient (K) increased with increasing biomass concentration and then dropped as biomass concentration decreased after the initial growth phase. These observations, however, could not be confirmed for *S. rimosus* and *A. roseorufa* beyond the initial growth phase because of experimental difficulties associated with measurements of biomass concentration during this phase.

Theories on suspension, flocculation and precipitation of particles (e.g protein particles) and limited measurements of zeta potential of microorganisms suggest that interparticle forces can under certain circumstances cause changes in the rheology of the mixture and pH is shown to influence these interaction forces. A limited number of experiments were conducted during which the pH of the culture was changed to establish whether this concept could be extended to fermentation broths. The results indicated that the rheology of the culture was strongly influenced by its pH indicating that charges around the microorganisms influence the rheology.

I dedicate this thesis to my family and friends, who have supported and encouraged me for the last four years.

"By perseverance the snail reached the ark."

I wish to thank Pfizer Limited, The Chemical and Biochemical Engineering Department at UCL and the SERC for their support and funding. In particular, I would like to thank Keith Dixon, Malcolm Lilly, Colin Thomas and Parvis Shamlou for their encouragement and patience.

Table of contents.

1 Introduction.

The basis of this thesis was an investigation into the relationship between the morphology of filamentous microorganisms, specifically Actinomycetes, and the rheology of the resulting fermentation broth. It has been postulated [1, 2 and 3] that the morphology of these microorganisms was one of the major determinants of the fermentation rheology and, therefore, the microorganism morphology had a significant effect on productivity since the rheology of the broth would have significant effects upon mixing and gas transfer in the fermenter.

Image analysis was recently developed to characterise the morphology of filamentous microorganisms. The technique was used in this work for the rapid and accurate collection of the morphology data.

The rheological data was collected using a Brookfield viscometer system. This viscometer was calibrated carefully against a Contraves system to ensure accuracy.

Pfizer UK, Sandwich, the collaborating industrial company in the project, has considerable expertise in all scales of Actinomycete fermentations. The company provided all the information, equipment and cultures necessary to perform and analyse fermentations from laboratory scale to production scale.

1.1 Actinomycetes.

1.1.1 General.

The three organisms studied in this project *Streptomyces rimosus, Streptomyces erythreus, and Actinomadura roseorufa* all belong to the taxonomical order known as the Actinomycetes. Actinomycetes constitute a unique group on the basis of nucleic acid sequencing, paring studies and a general ability to grow branched filaments, although some show many different morphological forms during their life cycle (pleomorphic).

Actinomycetes are a successful and widely distributed group of bacterium. They are found mainly in soil, compost, and water. They utilize dead organic matter with ease because of their filamentous nature and production of extracelluar enzymes; these properties favour them over other saprophytic microorganisms (microorganisms that feed on organic matter).

Actinomycetes have held a significant role in the pharmaceutical industry for many years because of their ability to produce antibiotics, vitamins and enzymes.

1.1.2 History.

Buchanan [4] conceived the order of Actinomycetes in 1917. The group was described, in general terms, as microorganisms with an ability to form branching hyphae at some stage of their development. But not until the 1950s did the determination of their fine structure and chemical composition indicate that Actinomycetes are Prokaryotes.

The study of actinomycetes began in the late 19th century by workers examining diseased material from humans, animals and plants. Actinomycetes have been shown to cause many human and animal infections; these include some widespread and well known diseases such as diphtheriae (*Corynebacterium diphtheriae*), tuberculosis (*Mycobacterium tuberculosis)* and leprosy (*Mycobacterium leprae*). In the early 20th century, Waksman [5] demonstrated the widespread occurrence of actinomycetes, particularly streptomycetes, in soil.

Actinomycin was the first purified antibiotic to be obtained from an actinomycete [6]. Once the potential medical and commercial value of this product (secondary metabolite) was realised, future research on actinomycetes was directed to similar compounds. The Actinomycin discovery was superseded by Streptomycin [7] which was used effectively to control tuberculosis. Many more antibiotics were soon revealed. Although most originated from streptomycetes, other genera such as actinoplanes,

actinomadura and micromonospora also produced useful antibiotics. In recent times the number of new antibiotics has diminished but other useful metabolites from actinomycetes are still being unearthed. For example, Clavulanic acid from *S. clavuligerus* [8] was found to inhibit β-lactamase and hence overcome bacterial resistance to existing β-lactam antibiotics. Research during 1940-70 has tended to concentrate on the detection and selection of potentially useful strains of streptomycetes and the optimization of their fermentations. In recent years, with the dwindling supply of metabolites from streptomycetes, the other saprophytic actinomycetes have regained favour.

1.1.3 Classification.

The actinomycetes have been traditionally considered to be prokaryotic bacteria with elongated cells or filaments that usually show some degree of branching. Despite the diverse morphology of these organisms, they may still be placed in either of the following groups: nocardioform or sporoactinomycetes [9].

The nocardioform bacteria form hyphae which eventually fragment into coccoid or rod-like elements that generate new mycelia [10].

The sporoactinomycetes encompass considerably greater extremes of morphology but all have the ability to form spores in or on defined parts of the mycelium [10]. The actinomycetes used during this project belong to this latter group.

1.1.3.1 Streptomycetes.

The streptomycete family are soil dwelling (terrigenous), Gram-positive sporoactinomycetes that are highly aerobic. The streptomycete family contains a number of gener including streptomycetes. *Streptomyces rimosus*, one of the organisms used in this project, belongs

to the streptomycete genus [11]. All members of the genus form an extensive branching substrate mycelium with an aerial mycelium which can bear chains of three or more spores; the substrate mycelium rarely fragments. Streptomycetes have a wall chemotype I.

1.1.3.2 Maduromycetes.

These are sporoactinomycetes with a wall chemotype III that contains the sugar madurose. This group may be artificial since a number of the gena present are poorly studied. One of these gena called actinomadura contains *Actinomadura roseorufa*, an organism used in this project. The genus is Gram-positive with a branching substrate mycelium that only rarely becomes fragmented.

1.1.3.3 Micropolyspora.

The genus saccharopolyspora [12] are aerobic, Gram-positive, sporoactinomycetes and form a substrate mycelium (0.4 - 0.6μm in diameter) that fragments into rod-shaped elements (1 x 0.5μm), though much less pronounced than in nocardioform actinomycetes [13]. They have a wall chemotype IV and have only been isolated from sugar cane plantations.

In 1987 Labeda [14] re-classified the organism *S. erythraeus* from the original family of streptomycetes into the family of micropolyspora. The organism was placed in the genus saccharopolyspora and renamed Saccharoployspora erythraea.

1.1.4 Growth and morphology.

Actinomycetes show a wide variety of morphologies, from simple rods and cocci to a highly complex mycelium. When an actinomycete propagule, such as a spore, is allowed to grow on a solid substrate, it usually gives rise to hyphae which branch at intervals and spread radially. The

growth is from the apex (apical) and then takes place by elongation from either end of the axis of the cell (polar elongation). The apical extension by hyphae of actinomycetes occurs at the tip, known as the extension zone. This phenomenon of preferential incorporation of new material at the apex is associated with a difference in structural strength in this region. Da Riva Ricci and Kendrick [15] suggest that there exists an apical 'unset' wall that is elastic and capable of yielding and stretching in response to pressure differentials, hence allowing growth. Conversely, an inelastic and non-deformable apical 'set' wall must exist as an anchor point at the other apex.

Branching is initiated by the resumption of plasticity in a previously hardened cell wall [16], often as a result of localized depletion in gaseous or other nutrients in the area around the branch point. The network produced offers the opportunity for the movement of nutrients from one position to another over a wide area.

The mycelium produced consists of hyphae that either grow across the surface or penetrate the substrate. This maybe described as primary or vegetative growth. This type of growth enables the actinomycetes to degrade insoluble organic material by the secretion of extracelluar enzymes [17].

In some microaerophilic forms of actinomycetes a different growth system occurs. The propagate generates extended filaments by synthesizing new wall material at both poles [18].

Nocardioform actinomycetes show a further complexity of growth; the mycelium produced in the early stages of growth subsequently becomes fragmented into rods or cocci [19]. The fragmentation results from the formation of a dividing partition (septation) and then breakage at these natural separation points of the hyphae (disarticulation), see figure 1. The fragmentation depends upon growth rates, which are influenced by many environmental factors [20]. The breakdown into numerous autonomous elements

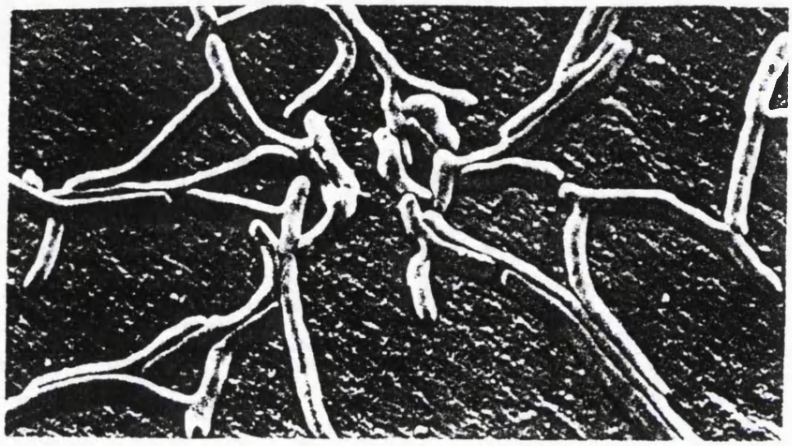

Figure 1: Fragmentation of *Nocardio asteroides* (4000x).

occurs at the end of the growth cycle, when nutrients are depleted, to ensure dispersion. The fragmentation of the mycelium achieves a similar effect to the production of spores in sporogenous actinomycetes. Thus it tends to occur in strains either devoid of spores or producing them in limited numbers only. The fragments often begin growth immediately contributing to further colony development. Thus the colony becomes polycentric.

However, the majority of actinomyctes are sporoactinomycetes (spore forming) and produce a non-fragmenting branched mycelium. The mycelium develops from the growth of a single propagule (monocentric).

Comparing figures 2 and 3 demonstrates the morphological differences between actinomycetes.

Although actinomycetes use surface growth in nature, submerged growth is the preferred method for industrial applications. In liquid culture the mode of growth can vary; pellets (up to 0.5mm in diameter), mycelial fragments (2-3μm in length), and well dispersed growth are all possible. The tendency to form fragments in liquid culture may be correlated to a reduction in ability to synthesise antibiotics. Similarly, Bushell [21] suggests that metabolites are inhibited by pellet formation in both fungal and actinomycete systems. Most pelleting strains will also produce filamentous culture depending on inoculum

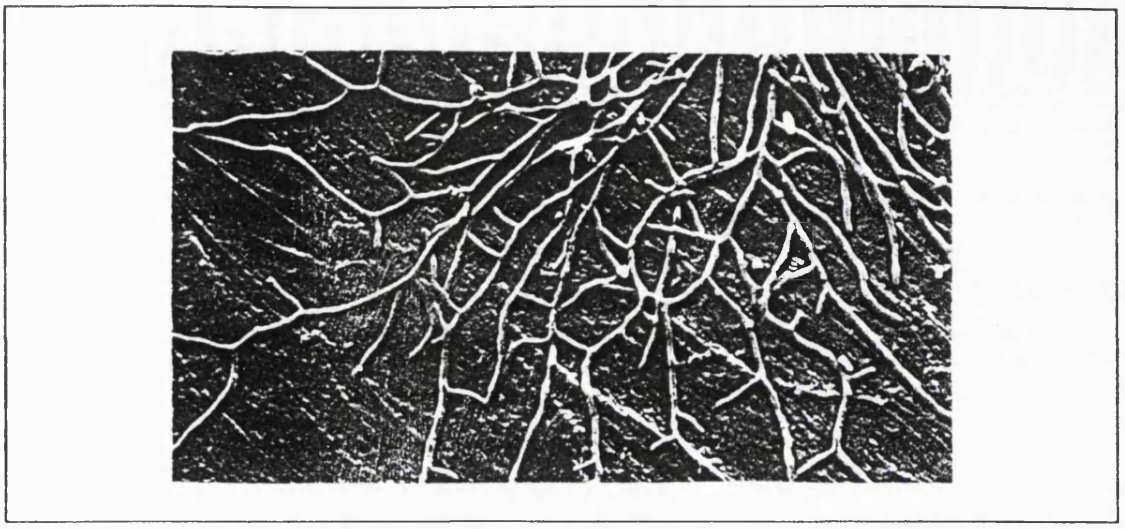

Figure 2: Branching hyphae of *Nocardia asteroides* (2000x).

concentration, dissolved oxygen tension, culture shear, and pH. König and Schügerl [22] grew *Penicillium chrysogenum* in a pellet form to reduce viscosity of the fermentation broth. In summary, a well dispersed mycelial growth gives optimal antibiotic production, both pelleting and fragmentation of the organisms should be avoided.

Kretschmer et al [23] formulated equations to describe filamentous mycelial growth in actinomycetes.

$$\frac{\partial L_h}{\partial t} = \alpha \cdot N_h \qquad (1)$$

and:

$$\frac{\partial N_h}{\partial t} = \beta \cdot L_h \qquad (2)$$

L_h - total length of hyphae per unit of culture volume.
N_h - number of hyphae tips per unit of culture volume.
α - mean apical growth rate.
β - the mean branching rate.
The ratio L_h/N_h is called the hyphal growth unit (HGU) which is used by mycologists to represent the fundamental unit of mycelial growth [24]. The image analysis section describes other equations to quantify the morphology of a filamentous microorganism.

1.1.5 Regulation of secondary metabolism.

The primary metabolism for all living organisms is essentially the same; an interconnected series of enzyme-mediated catabolic and anabolic pathways, providing biosynthetic intermediates and energy for the synthesis of essential macromolecules [25]. In contrast, secondary metabolism is not essential for growth although it probably plays a role in survival of the organism in nature.

Generally the course of events associated with secondary metabolite (idiolite) processes is a rapid growth

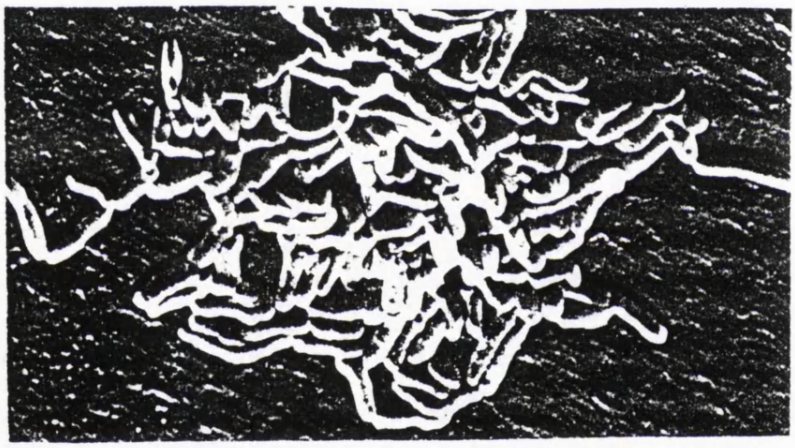

Figure 3: Rod-shaped cells of *Rhodococcus globerulus* (4000x).

phase (trophophase) followed by a phase of product synthesis (idiophase). Aharonowitz and Demain [26] have observed that these phases do not always occur at different times. This process timing is useful to the microorganism since species are often sensitive to antibiotics during the trophophase and only become resistant in the idiophase.

Observations suggest that the idiolite synthetase genes are generally expressed only at sub-maximum growth rates. Physiological control of antibiotic biosynthesis has been simplified into two mechanisms:

In the first model a co-repressor or inhibitor must be

depleted before antibiotic synthesis can occur. In the second, an inducer or activator must be synthesised prior to the initiation of biosynthesis.

The former model is consistent with observations on carbon regulation, nitrogen regulation and phosphate control. Glucose, due to a high specific utilization rate, interferes with the biosynthesis of many idiolites, hence other slow feed carbon sources such as polysaccharides, oligosaccharides and oils are often used in preference for production. Interfering carbon sources act by repressing synthesis and inhibiting activity of sythetases of secondary metabolism.

Repression and inhibition of idiolite biosynthesis by ammonium ion or certain amino acids are common. The use of soyabean meal in actinomycete fermentations results from its slow breakdown, thus avoiding large accumulations of repressive ammonium ions and amino acids.

Many idiolites are optimally produced when concentrations of phosphate are sub-maximal for growth. There are two mechanisms for the phosphate effect:

Phosphate represses and/or inhibits phosphatases involved in idiolite biosynthesis.

Or in the more general case, phosphate or some intracellular effector produced from extracelluar phosphate (such as ATP) represses or inhibits synthetases other than phosphatases.

Some secondary processes seem to be initiated by a low growth rate alone, whilst others need a specific type of nutrient deficiency to lower the growth rate and begin production of the idiolite. For the latter model induction is frequently involved in idiolite biosynthesis. The inducer is often an amino acid but it may be an unusual molecule such as A-factor required for the production of Streptomycin by *S. griseus* [26,27].

The termination of secondary metabolism is caused by either of the following: irreversible decay of one or more enzymes of the idiolite synthesizing pathway or the feed back effect of the accumulated product.

1.1.6 Oxygen requirements.

Oxygen requirements of actinomycetes vary; some are fermentative, growing under low concentrations of oxygen, whereas others are oxidative, requiring a high level of oxygen concentration. This second example includes the microorganisms used in this project. In most cases involving filamentous microorganisms broth viscosity increases as the fermentation progresses and thus can cause oxygen transfer problems. In these situations good mixing is vital for cell growth as it is controlled by both the rate of oxygen transfer from the gas to the broth and the uniform distribution of the dissolved oxygen throughout the vessel.

Viscosity influences most aspects of a biotechnological process. Thus, mixing, heating, mass transfer and aeration are affected by any factors that influence viscosity such as substrates and products. Bushell [21] states that the most significant factor on viscosity, in the case of actinomycetes, is morphology of the filamentous cells.

Banks [28] argued that mycelial suspensions and polymer solutions have similar rheological behaviour; polymer solutions are pseudoplastic. Banks stated that much of the published information on the rheology of mycelial suspensions was incomplete or contradictory. Metz et al [29] suggested this was due to the difficulties involved in obtaining reliable data on such heterogenous suspensions (see table from Atkinson and Mavitna [30]).

Deindorfer and West [31] stated that the rheogram obtained depends on the age of the mycelium; the study was on an *S. griseus* fermentation. Initially the culture broth showed Newtonian behaviour, then Bingham plastic behaviour as the lengthening hyphae aligned, and finally Newtonian rheology returned because of hyphal fragmentation and lysis. Charles observed a similar progression in a similar fermentation [2].

The oxygen solution rate OSR is determined as follows:

$$OSR = K_L a \ (C^* - C) \qquad (3)$$

$K_L a$ - the volumetric transfer coefficient (s^{-1}).

C^* - the concentration of dissolved oxygen in equilibrium with the partial pressure of oxygen in the gaseous phase ($mol.m^{-3}$).

C - the concentration of dissolved oxygen in the liquid ($mol.m^{-3}$).

In a Newtonian fluid of given viscosity the oxygen transfer coefficient, $K_L a$, depends on the degree of agitation. However, in a shear-thinning fermentation broth, agitation using a standard impeller is likely to cause formation of a cavity around the impeller [129]. It has been shown that once a cavity is established mixing outside the cavity is relatively poor resulting in inadequate rates of mass transfer, see figure (4).

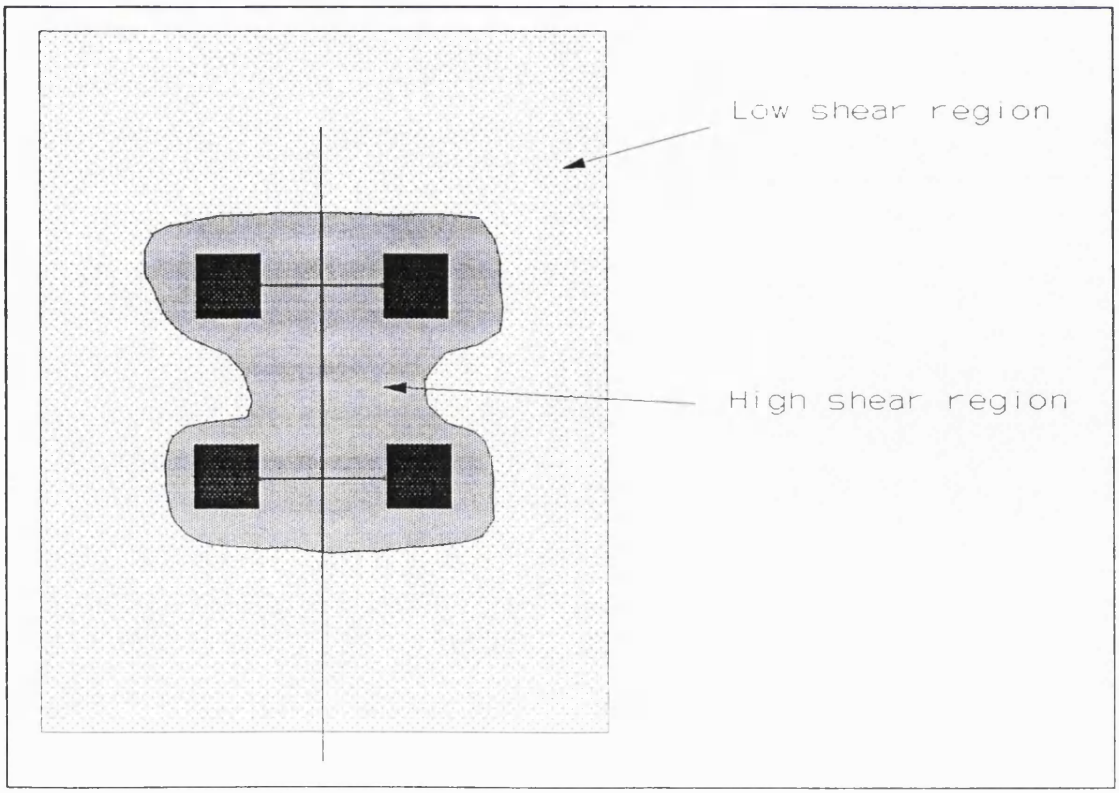

Figure 4: Variation of shear in a fermenter.

1.1.7 *S. erythraeus*.

The therapeutic importance of Erythromycin, a macrolide antibiotic, has stimulated a substantial amount of work on its production by *S.erythraeus*. The first erythromycin producing organism was isolated by Lilly Research Laboratories in 1950 [33 and 34] from a soil sample collected in the Philippine Islands. Most of the information on Erythromycin production, and hence the *S. erythraeus* fermentation, has not been published because of the commercial sensitivity of such work.

Generally, vegetative growth of *S. erythraeus* is not used to inoculate a fermentation medium until after 48-72hr on a shaker at 30-32°C.

The production of Erythromycin in a complex medium follows a fairly well defined course with respect to time. The amount of Erythromycin synthesized varies but biosynthesis has been correlated with such factors as period of growth, presence of carbohydrate and the absence

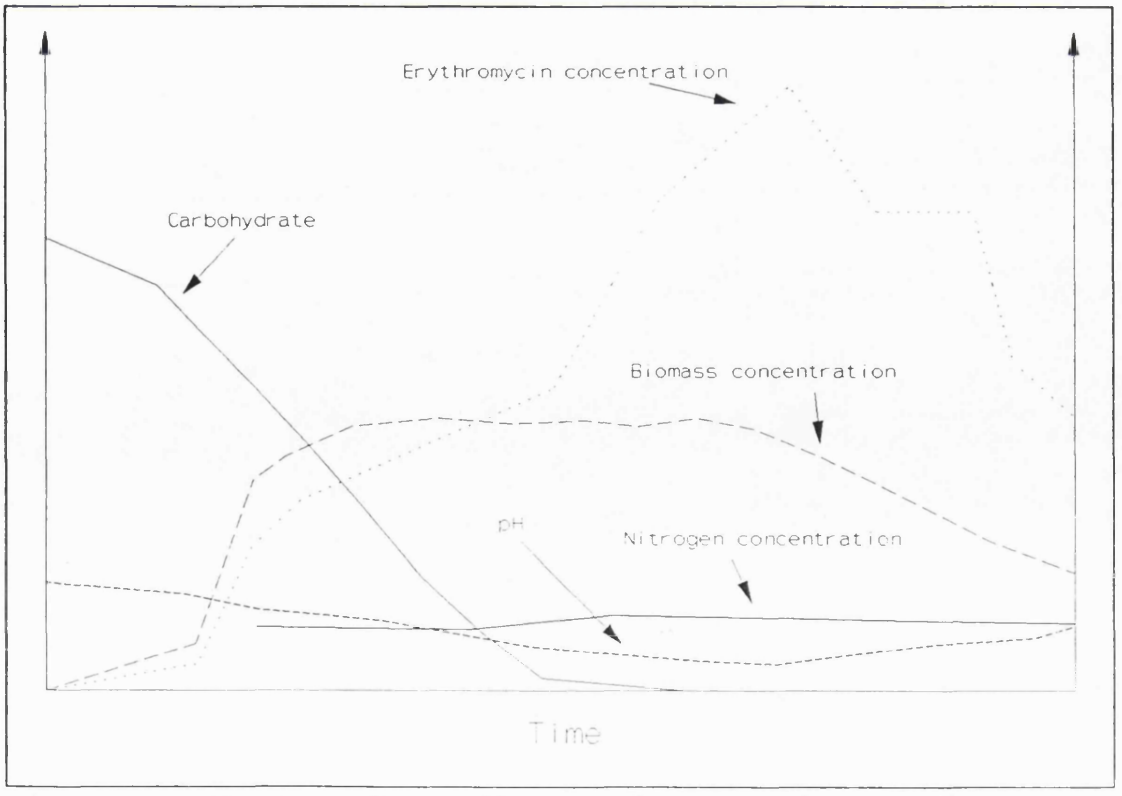

Figure 5: Typical *S. erythraeus* fermentation profile.

of nitrogen [35]. Figure 5 shows a typical *S. erythraeus* fermentation. It can be seen that the utilization of carbohydrate and nitrogen, as predicted by the growth curve, begins immediately. Only when nitrogen suitable for mycelial growth has been depleted does carbohydrate become available for Erythromycin synthesis. Antibiotic is not released into the medium until after the increase in the mycelium has halted. Smith et al [36] suggests this is because of growth consuming the intermediates, energy, or co-factors that would otherwise result in Erythromycin production. The biosynthesis of Erythromycin starts after approximately 24 hr and the antibiotic level increases at a linear rate until the carbohydrate is depleted.

Variation in pH of the medium during the fermentation appears to follow a typical pattern. The initial pH of slightly above neutrality drops rapidly to between 6 and 6.5 where it remains for 72-96 hr. A rise in pH follows and continues until near the end of the fermentation. The increase in pH is probably due to the disappearance of the carbohydrate and the subsequent utilization of the intermediate organic acids, as well as the appearance of nitrogenous compounds arising from lysis of the cells. Rapid synthesis of Erythromycin coincides with a rise in pH and continues until all available carbohydrate has been exhausted. Osman et al [37] suggests that biosynthesis of Erythromycin by *S. erythraeus* was most efficient at pH7.

The mineral requirements for the Erythromycin fermentation have been determined [35]. The requirements for magnesium and phosphate appear to be the most critical, followed by a need for iron, zinc, cobalt and calcium. When either the magnesium or the phosphate is excluded, both cell growth and the Erythromycin synthesis become diminished.

S. erythraeus has recently been taxonomically re-classified[14] to *Saccharopolyspora erythraea* in the family Micropolyspora. Since this re-classification was only discovered recently, the text for this project has been

completed using the name *S. erythraeus* rather than *S. erythraea*.

1.1.8 *A. roseorufa.*

This organism was isolated by Pfizer Limited, Sandwich. The commercial importance of *A. roseorufa* which produces a therapeutic agent and also the recent discovery of the process means that no literature has been published on the subject.

The European patent [38] describes a microbiological process for producing an acidic polycyclic ether anticoccidial antibiotic, previously only available by chemical means. The process involves the use of *A.roseorufa* to produce the compound using fermentative methods.

1.1.9 *S. rimosus.*

The actinomycete *Streptomyces rimosus* was isolated from a soil sample by Finby et al [39] for Pfizer and Company, New York. *S rimosus* produces an antibiotic called Terramycin (Oxytetracycline).

Doskoăl et al [40] have divided the growth and development of *S. rimosus* into distinct phases. The lag phase, a period lasting several hours, during which no detectable changes in the culture occur. The primary mycelium then starts to grow; the dry weight of the mycelium increases accompanied by a parallel increase in oxygen uptake. Morphologically the filaments are long, thick and Gram-positive. Next the primary mycelium fragment and the growth of the secondary mycelium begins. These filaments are long, thin and Gram-negative. They grow from the fragments of primary mycelium; some do not germinate and remain in the medium without change, thus a variety of morphologies is present in the culture. Once the nitrogen and carbohydrate sources are depleted a

stationary phase commences and the mycelium gradually fragments.

1.2 Morphological measurement.

The purpose of this work was to investigate the relationship between the morphology of filamentous microorganisms and the rheology of the resulting fermentation broth. Adams [41] and other authors [2,3] have postulated that hyphal entanglement of these filamentous microorganisms can result in suspensions being highly viscous and non-Newtonian; causing both mass and heat transfer problems in the fermentation. Hence, a quantitative measurement of morphology could be a major determinate of fermentation rheology and consequently help in the design and operation of filamentous microorganism fermentations. The result of such work should be improved productivity.

Roels et al [1] reported that the concept of 'morphological modelling' could have several interesting applications:

a) Monitoring the morphology of a strain in the course of fermentation; with the possibility of correlation between production and morphology changes.

b) Prediction of rheological behaviour of a broth in an early stage of the process design (this is important from an engineering point of view)

c) Selection of strains which, with regard to the physical processes in large scale fermenters, have superior morphological characteristics, i.e. strains with a low ratio of their length to their diameter are expected to give lower viscosities which may be advantageous.

Adams and Thomas [41] and Packer and Thomas [42] have recently developed image analysis as a novel and powerful tool for characterising the morphology of filamentous microorganisms.

1.2.1 History of morphological measurement.

Metz et al [43] suggests that although the morphology of filamentous microorganisms plays an important role in the fermentation process, in the literature on the subject only qualitative characterisations of morphology are used. Phrases such as `short fragmented mycelium' and `highly branched mycelium' are used in the published papers. Often only a spartan amount of quantitative information on hyphae length and diameter can be found and these data come from a relatively small sample of particles.

There are few papers on the subject of morphological characterisation of filamentous microorganisms. Roels et al presented a paper [1] on the rheology of Penicillin broths. They claimed that this study was not limited to determination of viscosity, but that the ultimate goal was to provide the possibility of prediction of viscosity, in terms of shear rate, solids content and broth morphology. Using the Casson equation [45] and a theory for the rheological description of polymer solutions (known as the `excluded volume concept') a morphological model was devised. This model contains a morphology factor which can be used to give a quantitative description of mycelial morphology. The morphology factor may be determined experimentally by a simple viscosity measurement in combination with a mycelial dry weight determination. The morphology constant is defined as:

$$\delta = \frac{\tau_0}{X^2} \qquad (4)$$

where;

X - the mycelial concentration (grammes per litre).

τ_0 -the yield stress (Pa).

Roels suggests that it is well established that the morphology of a mould, and other filamentous microorganisms, changes as the batch fermentation progresses. This change was reflected in a change in the

morphology factor. The factor was constant for a period up to 80 hours, after which it gradually decreases. This is consistent with the observation of fragmentation of the mycelium after 80 hours, which gives a lower morphology factor value. The morphology factor, as defined from theory, gave reasonably good agreement with the experimental data, however modifying the defining equation, on the basis of the experimental data, allowed a far superior correlation to be obtained. The author blamed this anomaly on the fact that the morphology factor is completely dependent on the ratio of length to diameter of the mycelial hyphae. In reality, other morphological characteristics should also be considered; such as branching, the formation of large agglomerates and the proportion of mycelium in pellet form. Roels states that there are strong indications that the model may be applicable to mycelial broths other than those of Penicillin. This has been partially confirmed by Fatile [3], who used Roel's theory to show a relationship between Power law constants and the microbial concentration and shape of the mycelial aggregates of an *Aspergillus niger* fermentation. However, the `aggregates' mentioned in the paper appear to be pellets, in which case the use of Roel's morphology factor seems to be of limited use. Fatile criticised Roel's paper for using the Casson model. He suggests that over the limited range of shear rates used (one and a half decades) almost any model could have been used. Roels did in fact try using both the Power law and the Bingham plastic law before discarding them and resorting to the Casson law.

Van Suijdam and Dusseljee [46] defined a morphological parameter using the viscosity of the fermentation broth, however the approach was only tested at low cell concentrations.

Another successful method, not as theoretically based as Roels, was also devised by van Suijdam and Metz [47] for defining the influence of process conditions on the morphology of microorganisms. The technique uses

photomicroscopy and an electronic digitizer. Trials on this system (using the digitizer) have been run by Adams [41], Metz et al [43] and Smith et al [48] using *Streptomyces clavuligerus*, *Penicillin chrysogenum* and *Penicillin chrysogenum*, respectively. Despite the different organisms, similar procedures were employed: a fermentation broth sample was withdrawn and suitably diluted. The dilution allows the disintegration of any aggregates, hence preventing the biased selection of non-aggregated and thus possibly shorter and more compact particles and also reduces the chances of overlapping organisms. Aliquots were transferred to microscope slides, air dried and stained to aid detection of the organisms. Using a microscope, photographs of individual microorganisms were taken. The selection process was essentially random; the microscope-table was moved step-wise and a photograph was taken of any visible object, unless it was unsuitable because of several objects overlapping. The photographs of mycelial objects taken through the microscope were projected, by means of an adapted microfilm reader, onto an electronic digitizing table. The digitizing table, a Hewlett-Packard 9874A digitizer, with the aid of a computer, was capable of determining the X and Y coordinates of any position on the table touched using a special pen. By touching several points along the length of the hypha, the length of the hypha could be calculated, see figure 6. It was also possible to measure the number and length of mycelium branches. To characterise the hyphal morphology a number of useful morphological indices were defined:

a) The length of the main hypha.
b) The total length of all hyphae of a particle.
c) The hyphal growth unit (the length of the hypha per growth tip).

The system was calibrated by means of a standard millimetre, photographed through the microscope, to enable the determination of absolute values of hyphal lengths rather than the number of pixels.

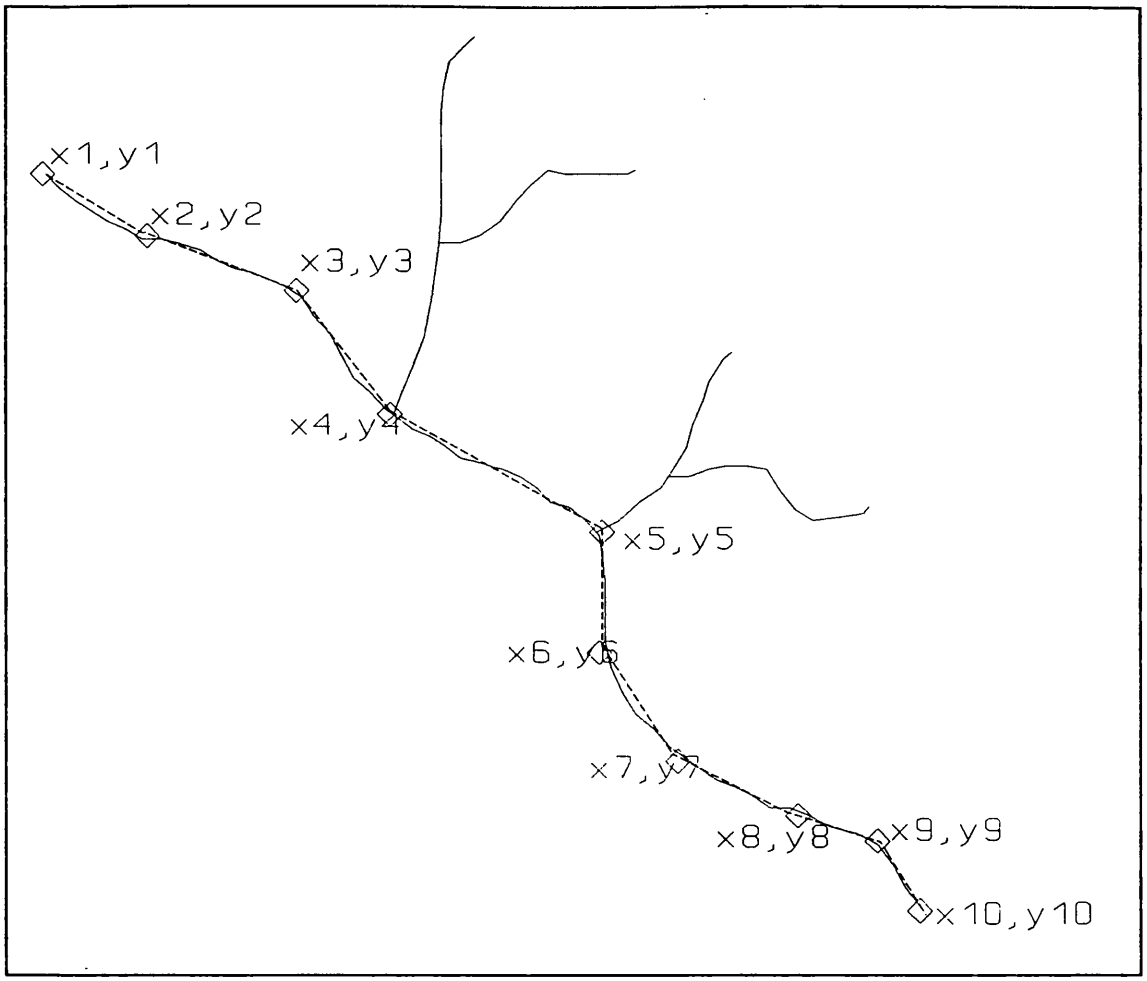

Figure 6: Digitising a filamentous microorganism.

Metz claimed that it was only necessary to analyze between 10 and 20 mycelial particles for every sample in order to determine the hyphal morphology properly.

Adams and Thomas [41] and Packer and Thomas [42] suggest the digitizing method has many disadvantages for its use as a tool for process control. The method is highly labour-intensive and time consuming. In order to analyze a reproducible sample of microorganisms (according to Adams and Thomas [41] over 1000 particles) the digitizing method would take approximately 83 hours, a considerable portion of which is due to the photography and film development required. The method is also highly dependent on the skill of the operator in using the digitizing pen, hence giving scope for operator variability and carelessness.

Because of these problems, the digitizing method would be impossible to use for morphological characterisations

that were either automatic or sufficiently rapid to allow the measurement of the large number of mycelia necessary if such characterisations were ever to be used routinely for process control of filamentous fermentations.

Adams demonstrated the use of image analysis to overcome the above problems in both semi-automated [41] and completely automated [42] forms.

1.2.2 Image analysis.

Image analysis involves the quantification and classification of objects of interest within images [49]. The human eye and brain, in combination, are constantly analysing images; viewing a scene and classifying its contents in a highly versatile manner. However, the `human' image analyzer finds exact quantification of what it sees difficult; hence the need for the digital image analyzer. Digital image analysis quantifies such parameters as size, number, shape, position, and object density of identifiable parts of an image, thus allowing the digital system to classify the scene.

The principle steps in image analysis, using the image analysis system at UCL as a typical example, are:

a) Image capture.
b) Segmentation.
c) Object detection.
d) Measurement.
e) Analysis.

Image capture is the conversion of an image into an electronic signal suitable for digital processing and storage. The system captures images using a television camera mounted on a microscope. The image from the camera is then converted into a grid of picture elements, or pixels, each of which is assigned a tonal intensity level representing the tone in the locality of the pixel in the original image.

Segmentation describes the act of separating the regions of interest within a captured image from the

background. The method most often used is called Thresholding. This allows selection of a tonal level; where upon all tones below the level are treated as black and all tones above as white. The system may then, for instance, treat black as of interest and white as background or the user may choose another convention. Modern systems, like the system at UCL, allow two thresholds to be set, allowing a slice of grey tone to be taken that is of interest while the darker and lighter tones which are below and above the slice are treated as background.

Thresholding works well in situations where illumination can be carefully controlled so as to have the same level across the entire scene, since the brightness of an object depends upon its illumination as well as its ability to reflect or transmit light. If illumination were a problem other techniques such as 'edge finding' and 'region growing' are available.

Object detection is a data-reduction step which produces a description of each object which is considerably more compact than a list of co-ordinates of every pixel it encompasses. These sets of descriptions, which fully characterise each object, are stored and used in subsequent measurement operations. The word `object' is defined in image analysis terms as the individual regions of interest within the whole scene.

Measurement is the gathering of quantitative data for the objects identified. Then the results from measuring are analysed to allow some sort of decision or classification to be made.

Mitev and Popova [50] used a simpler image analysis system for the morphological analysis of Baker's yeast.

1.2.2.1 A typical system.

The system discussed below is based around the image analysis system (Magiscan 2A, Joyce Loebl Ltd., Gateshead, England) used in the Biochemical Engineering Department at UCL, see figure 7.

Input device: this is a Nikon Optiplot microscope (Nikon U.K. Ltd., Telford, England) plus the necessary mechanical arrangements for mounting the camera, illuminating the image and carrying the microscope slide to ensure a clear, stable image is produced.

Lamp and lamp controller: in order to obtain consistent quantitative measurements, the system must have a non-fluctuating source of illumination. The system can be stabilised by controlling the voltage supplied to the lamp on the basis of the peak white level of the video signal.

Motorised stage, automatic focus actuator and controllers: these are used to speed up examination of the samples on the microscope slides. The automatic focus works by carrying out a preliminary focus check on the four corners of the specimen slide. The system measures the exact focus lengths at each of four positions and it can then interpolate the focus distances at intermediate points.

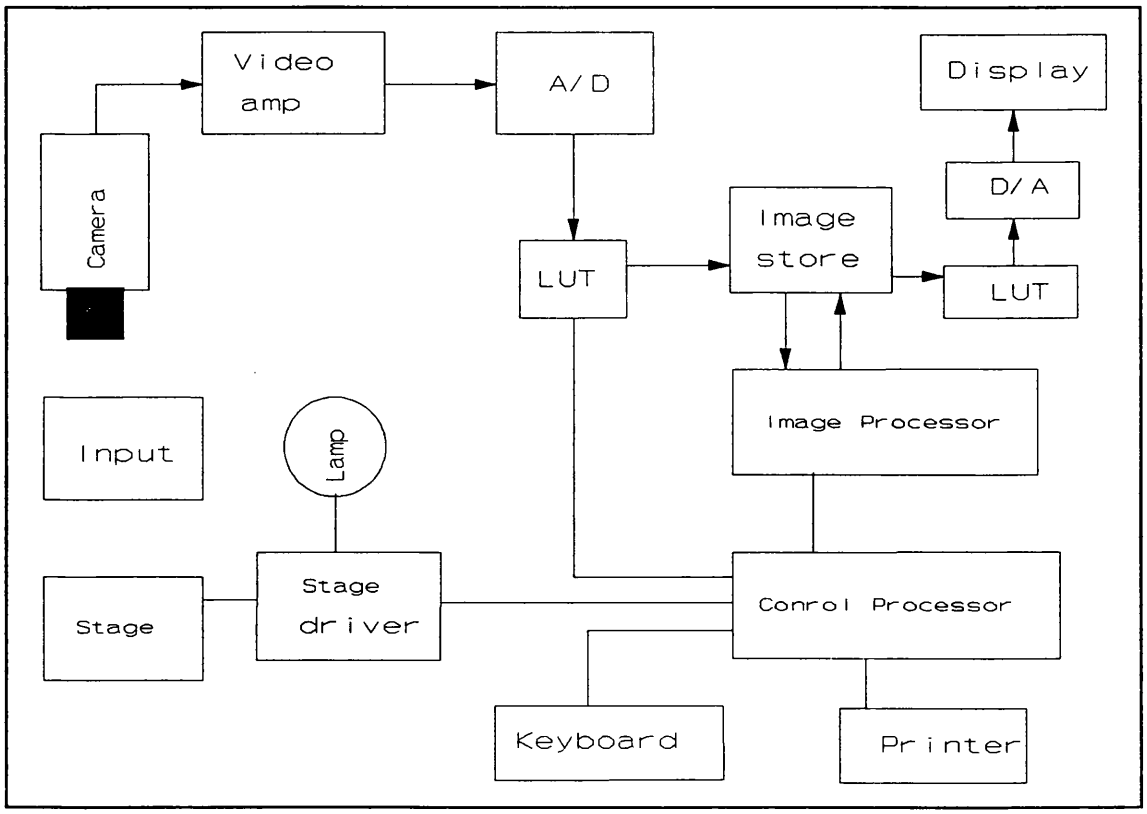

Figure 7: The UCL image analysis system.

Camera: this is a high quality commercial close-circuit television camera, with good geometry and high resolution desirable for a quantitative system. The system at UCL uses a charged-couple device (CCD).

Video amplifier: this consists of two parts, one located extremely close to the face of the tube, so that the amplified signal is resistant to the introduction of noise, and the second completes amplification and may be situated in the body of the camera or in the main body of the instrument.

Analogue to digital converter (A/D): this converts the cameras analogue video signal to a digital form. Once the signal is transformed, it is completely insensitive to noise or drift in amplification, within the design constraints of the digital processing system. Because the system is susceptible to stray electronic noise which may be induced in the video signal before conversion, the electronics are shielded in a conducting case.

Display: a television-type monitor is used to display an image of the sample, in full tonal range, with binary image overlay of what is being measured. Another display is also used to give a pseudo-colour display since the main monitor is monochrome.

Look-up table (LUT) converter: often the digitised video signal may require altering, either to produce a more readily interpreted display, or for purposes such as densitometry. The operation involves converting the grey level of a given pixel to another value by reference to a predetermined function. This function does not take into account the grey level at any other position. Since the number of possible values for inputs are limited (up to 256) it is quicker to precalculate a table of function results than to carry out the computation each time, hence the term LUT.

Control processor: sometimes contained in the instrument, but often an attached computer will exercise control on the image analysis system as well as performing data processing.

1.2.2.2 Measuring techniques.

The following is a description of the measurement software and options available on the UCL image analysis system; however all these techniques apply equally to other image analysis systems:

A sample of the filamentous microorganism is fixed to a microscope slide and dyed. The slide is placed under a microscope and, using a television camera mounted on the microscope, a video picture is passed to a computer capable of image processing and analysis.

Initial work on image analysis of filamentous microorganisms used supplied software and required considerable manual intervention. Although the method used by Adams and Thomas [41] has been shown to be more accurate and considerably quicker than the digitising method, it is clear that the image analysis system can only show its full potential by additional automation. This complete automation required development of application-specific software, such software has been written by Packer and Thomas [42]. This morphological characterisation program was designed to be highly flexible; running automatically but with manual options at various intervals throughout. The basic algorithm of the program is shown in figure 8; this shows the optional editors for manual intervention. The program has three main phases:

a) Setting-up.

b) Image processing.

c) Measurement.

The setting-up phase involves inputting parameters that are needed for each running of the program. As described previously, the sizing calibration is achieved using a graticule scale. Next, an active measuring frame must be established; this is a boundary which prevents objects, at the edge of the image, from being truncated and causing inaccurate results. The width of this boundary must be greater than the longest microorganism to be measured. The microorganisms that intersect the measuring

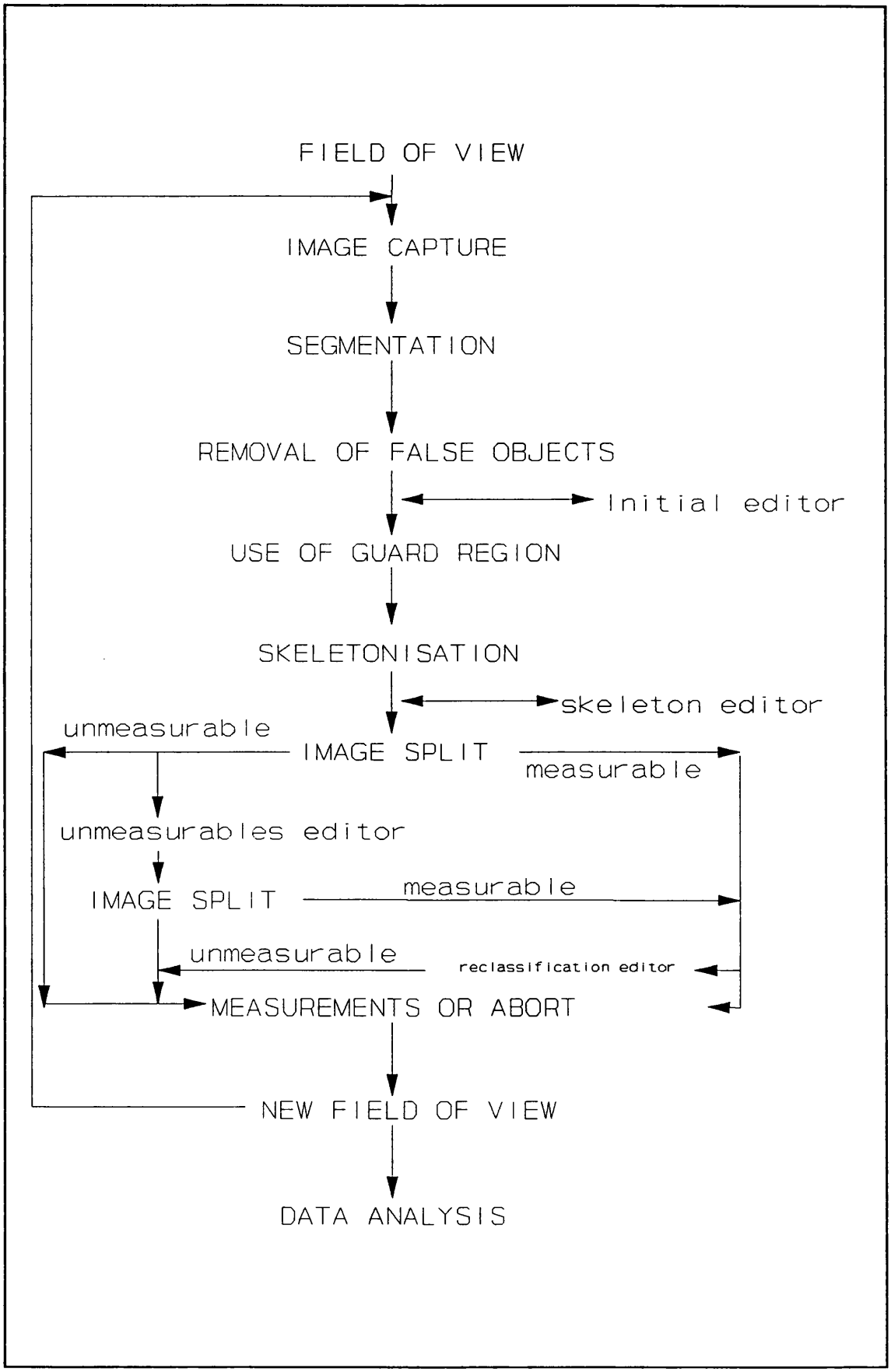

Figure 8: Image analyser program.

frame are only considered significant if their lowest hyphal tip is in the frame. The program drives an automatic microscope stage and the motion of this stage is set for abutting measuring frames in two directions, giving complete coverage of any region of interest. Finally, some parameters involved with image processing are set, and options for the level of manual editing are chosen.

Once the image has been captured, the image processing begins with segmentation. Then the binary image must be cleared of false objects, for example, media particles and dust. This is achieved by the use of a preset circularity parameter. This has a maximum value of unity for a perfect circle and decreases with increasing departure from circularity. Hence the long fibres of the filamentous microorganisms have a low value. Objects with a circularity value higher than the preset value (those objects which are too circular) are removed.

The objects remaining should all be microorganisms; these are skeletonised, that is, the pixels medial between the edges of the object are found, outlining skeletons for analysis. Noise spikes are often formed during this process, this may be due to media debris or an artefact of the skeletonisation process. Noise spikes of lengths less than a preset number of pixels are removed from the skeletons to prevent the software from treating them as branches.

The binary skeleton images are divided into two groups; measurable microorganisms and clumped (aggregated) material. Clumps are distinguished because they contain loops or holes, for the purpose of image analysis this means regions of background enclosed within the object. Objects in each of these two groups are analysed separately.

As mentioned above, the processing phase has a number of optional manual editors available. These can be selected during setting-up if appropriate. In some instances a fully automated system can mis-classify an object, editing allows any such error to be corrected, but

it significantly slows processing and makes the process much more labour intensive. Within the editing option the following procedures are available:

Accept - select objects of interest and reject the remainder.

Reject - reject uninteresting objects and the select remainder.

Fill - fill an object (with foreground colour) to prevent it being classified as a clump.

Draw - draw on additions to an object to give a more accurate representation.

Erase - as above, but removing a section of an object.

Kill - cancel all editing.

In the measurement phase both field and object measurements are taken:

Field measurements [49] are ones in which the contribution of each object is not individually known or recorded, but information recorded at pixel level is merely summed to provide a single measurement for the entire view. By taking a total pixel count of both images, the proportion of unmeasurable (clumped) and measurable material can be estimated.

Object measurements, as the name implies, are measurements on each individual object. The objects can then be classified by their individual measurements. For each measurable microorganism the longest connected path through the object is found. This is considered to be the main hypha and its length is estimated using the sum of the inter-pixel distances [41]. This hypha is then erased from the image, and the next longest connected path is found. By this recursive algorithm each branch and sub-branch of a microorganism is found and measured. Total hyphal length, number of tips and length of hyphal growth unit are calculated. The results are passed to a data file for subsequent statistical analysis using proprietary software.

As far as image analysis is concerned, clumping of the microorganisms can create measurement problems, but in this investigation this was not found to be a problem since

clumping did not occur with any of the microorganisms used in this work.

1.3 Rheology.

Rheology is defined as the study of the flow and deformation of matter. It is the science concerned with the mechanics of deforming bodies [51].

Rheologists apply methods for the measurement of rheological properties; these are methods for establishing the relationship between stress, strain and time for some test material.

1.3.1 Introduction to rheology.

Walters [52] distinguishes between the two objectives of rheological measurement:

a) To determine the behaviour of non-Newtonian liquids (fluids that do not follow Newton's law of viscosity) in a simple rheological flow situation, and hence establish a correlation between molecular structure and material behaviour.

b) More sophisticated and difficult is the prediction of behaviour in complex flow situations from the results of simple rheological experiment. Fortunately, many industrial processes involve relatively simple flow geometries so that the material functions determined in simple flow situations are adequate in many applications. Viscoelastic systems are the exceptions.

The deformation of a body maybe elastic, viscous or a combination of both. If the body is ideally elastic then the mechanical energy required to deform the body is recovered when the body spontaneously regains its original form. Whereas, for an ideal viscous body the mechanical energy used to deform the body is lost as heat as the body sustains flow.

Rheologists regard materials that obey Hooke's law of elasticity or Newton's law of viscosity as special; they

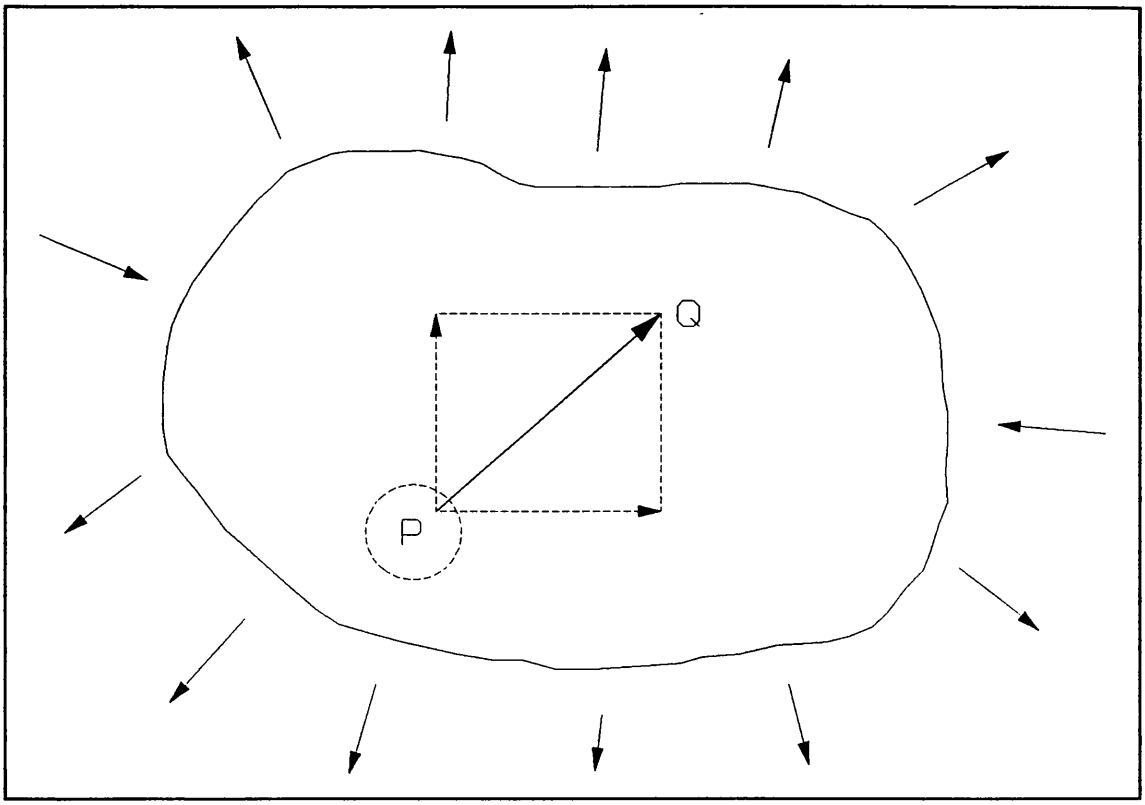

Figure 9: A body under stress.

are limiting cases of more general behaviour. Rheologists usually study materials that do not obey one of these laws either because of their nature or because they are subject to large deformations.

1.3.1.1 Shear stress.

The force per unit area acting on, or within, a body to cause a deformation is known as a stress. Stress magnitude is usually expressed in Pascals (Pa).

Whorlow [53] gives the following explanatory example, see figure 9. Suppose that external forces are acting on a continuous volume of solid or liquid. Now consider a plane area around a point, P, inside the material. In general, the material to one side of this plane, for example above, will exert a force, F, on the material on the other side. The material below the plane will exert an equal and opposite force on the material above the plane. Such internal forces are essential for the equilibrium of the parts of the body. If the area of this

plane is varied, then the force will vary. He assumed that as the area around P decreases, the ratio of F/A tends to a limit, known as the traction across the area at P. The traction is a vector quantity, represented by line PQ in the figure. Thus it must be specified as either a magnitude and direction or the magnitudes of its components along three appropriate coordinate axes. A body in which tractions are present is said to be under stress. The traction across a plane may be divided, as shown, into a component normal to the plane, known as the normal stress, and a component parallel to the plane, known as the shear stress.

This analysis of stress must be developed further to explain certain rheological concepts, see figure 10. Oxyz are a set of rectangular cartesian axes at a point O in a stressed body. Consider the stresses acting on the surfaces of a small rectangular block near O. The traction on face ABCD may be divided into stress components P_{xx}, P_{xy} and P_{xz} parallel respectively to Ox, Oy and Oz.

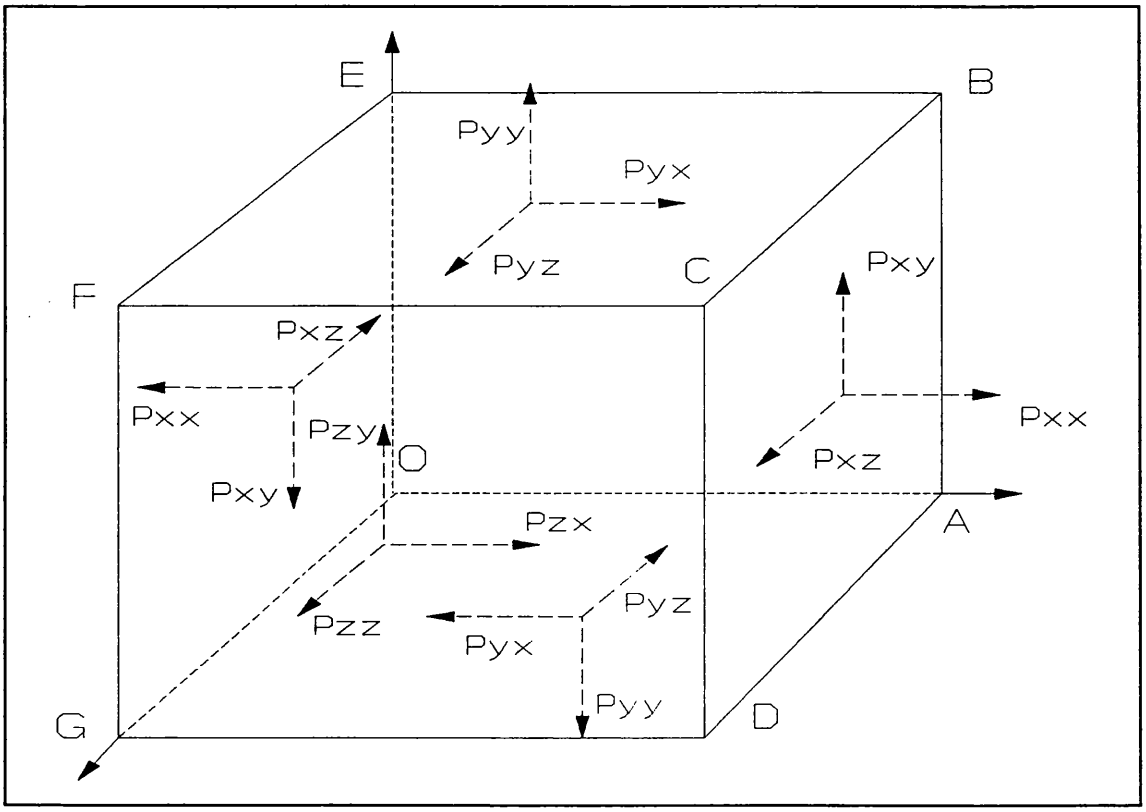

Figure 10: Stresses acting on a block.

The first subscript on the symbol for these components indicates the plane considered , in this case ABCD is normal to the x coordinate direction, and the second subscript denotes the direction in terms of cartesian axes. P_{xx} is taken to be positive when acting outwards from the surface of the element, that is, exerting a tension, not a pressure. Stress components on the other five faces of the block are denoted in an analogous fashion.

The stress components p_{xy} exert a couple on the element of magnitude, $p_{xy}.V$. V is the volume of the element. For stability:

$$p_{xy}.V = p_{yx}.V \tag{5}$$

so that;

$$p_{xy} = p_{yx} \tag{6}$$

Similarly;

$$p_{xz} = p_{zx} \quad also \quad p_{yz} = p_{zy} \tag{7}$$

There are thus only six independent components of stress relative to these axes. The traction across any plane area near O can also be expressed in terms of these six components.

Thus the stress acts in three directions on all six faces of the cube, so that there are altogether 18 components of stress. However, the stress components acting on the opposite faces of the cube are identical so that the state of stress is defined by nine components.

$$p_{ij} = \begin{matrix} p_{xx} & p_{xy} & p_{xz} \\ p_{yx} & p_{yy} & p_{yz} \\ p_{zx} & p_{zy} & p_{zz} \end{matrix} \tag{8}$$

p_{ij} is known as the stress tensor.

A particular rectangular coordinate system in common use in discussions of shear flow is shown in figure 11. The directions are distinguished by numbers rather than letters. The axis Ox_1 is chosen to be along the direction

of the streamlines, the axis Ox_3 to lie in a surface of constant velocity and the axis Ox_2 lies in the direction of maximum velocity gradient. The velocity components, relative to O, of a fluid particle are:

$$\dot{x}_1 = \dot{y}.x_2 \tag{9}$$

$$\dot{x}_2 = \dot{x}_3 = 0 \tag{10}$$

A symmetry argument shows that:

$$p_{23} = p_{31} = 0 \tag{11}$$

Using equation (7), the stress tensor reduces to:

$$\begin{matrix} p_{11} & p_{12} & 0 \\ p_{12} & p_{22} & 0 \\ 0 & 0 & p_{33} \end{matrix} \tag{12}$$

In many fluids only the shear stress, p_{12}, will be considered. However, for other fluids, particularly polymer solutions and melts, the normal stress differences

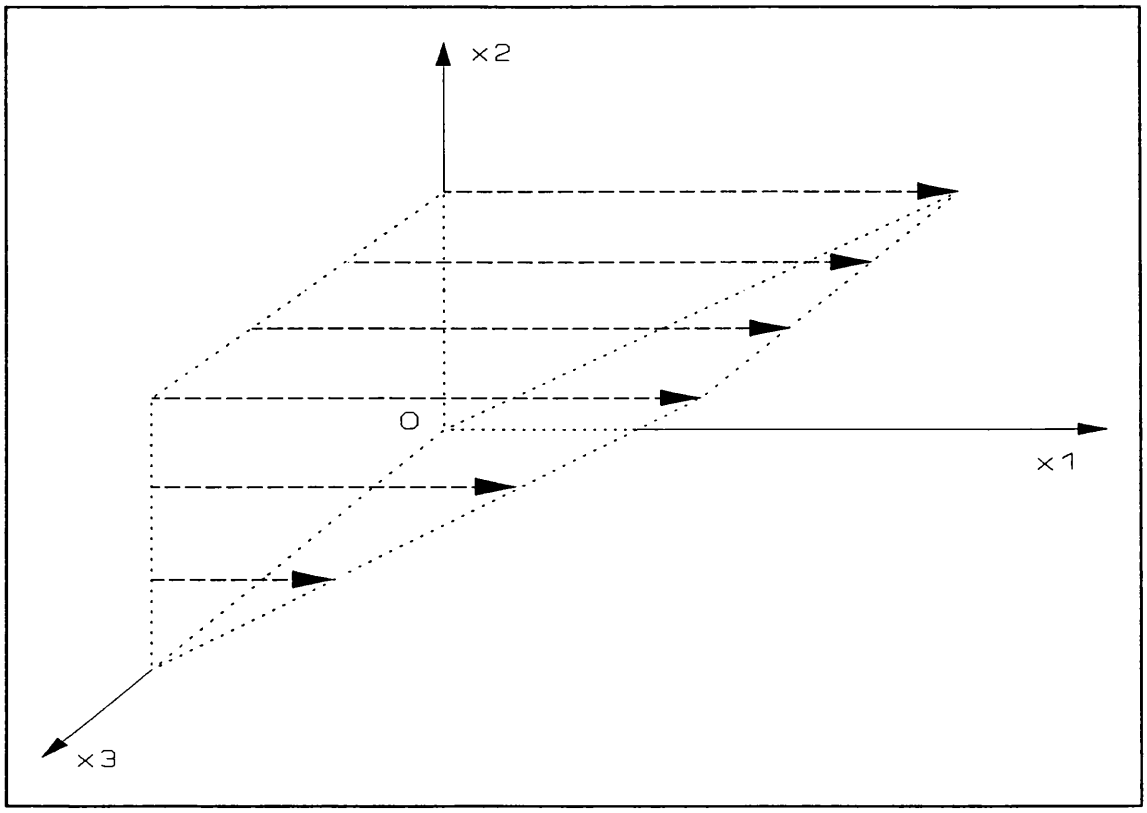

Figure 11: Shear flow.

may be important; for example phenomenon such as the Weissenberg effect are discussed later in this chapter.

The first normal stress difference is equal to

$$p_{11} - p_{22} = \nu_1 \qquad (13)$$

The second normal stress difference is equal to

$$p_{22} - p_{33} = \nu_2 \qquad (14)$$

1.3.1.2 Strain.

Applying a stress to a body causes deformation which is known as strain. The magnitude of the strain is derived from calculating the change in separation of any two points in the body or the change in angle between any two directions. A special case is that of steady simple shear strain, this provides a system under strain which can be studied easily. Such a flow can be generated in various viscometer geometries [54].

In steady simple shear strain successive layers of material move, in their own planes, relative to a reference layer in such a way that the displacement of a layer is proportional to its distance from the reference layer. The deformation is shown in figure 12. The relative displacement of two layers divided by their separation, $\partial l_i/l_i$, is called the simple shear strain. Lines originally perpendicular to the reference layer rotate through an angle Y, where;

$$\tan Y = \frac{\partial l_i}{l_i} \qquad (15)$$

If the deformation is sufficiently small, Y, the angle of shear, expressed in radians, equals the shear strain. There is no change in the dimension perpendicular to the plane of shear, lengths such as AB remain constant.

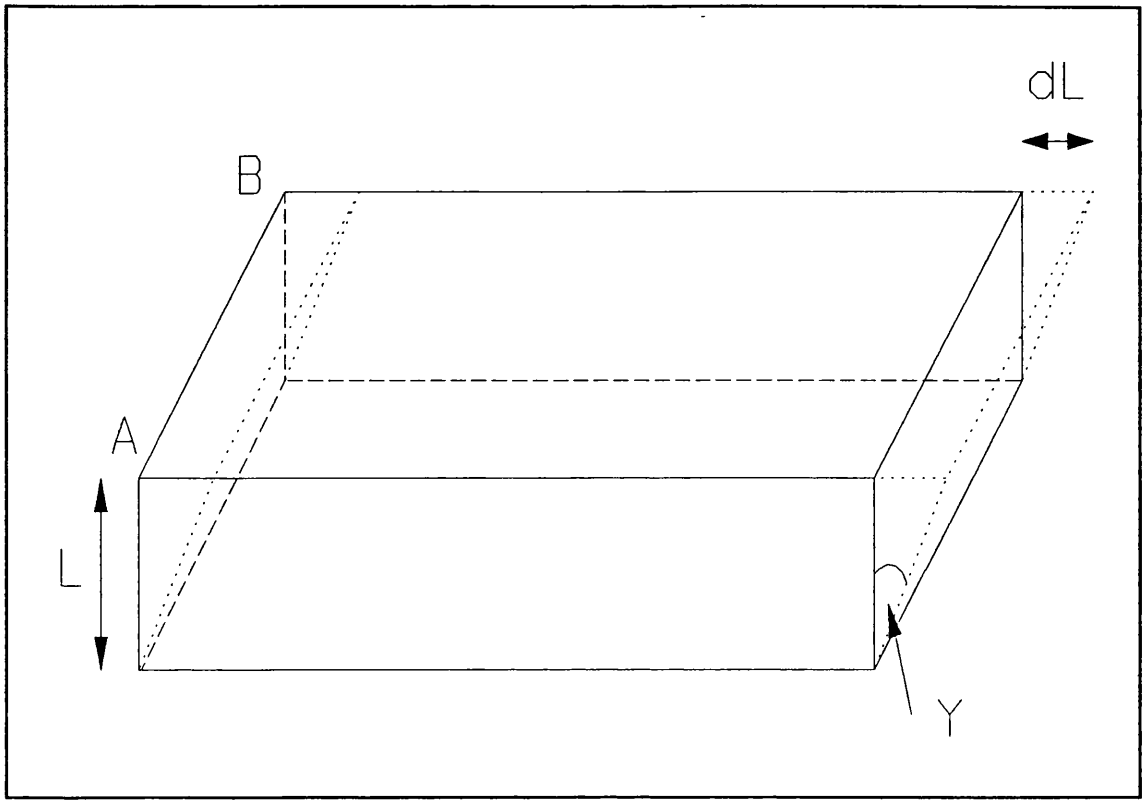

Figure 12: Steady simple shear strain.

The instantaneous rate of strain, or shear rate is;

$$\frac{\partial Y}{\partial t} = \dot{Y} \qquad (16)$$

When the flow is linear a layer at distance l from a reference layer and moving with velocity, v, will travel a distance $\partial l_i = v.\partial t$ in an infinitesimal time ∂t so that;

$$\dot{Y} = \frac{d}{dt}\left(\frac{\partial l_i}{l_i}\right) = \frac{v}{l_i} \qquad (17)$$

The type of flow shown in figure 12 is a particular example of streamline flow. The fluid particles which are successively at a particular point all follow the same path known as a stream line. This type of flow is known as laminar whereas all other forms of flow are turbulent. Normally, only the simple shear field produced by laminar flow provides useful rheological data.

Viscous deformation is the change in the velocity of

flow for a distanced measured at right angles to the direction of flow. Figure 13 shows three examples of deformation: (A) is used in Newton's definition of viscosity, (B) represents the flow pattern for a rotational viscometer and (C) represents the flow present in a capillary-tube viscometer. (A) and (B) are examples of simple shear strain.

1.3.2 Types of rheological behaviour.

In order to analyse the results obtained from viscometers assumptions are made about the general nature of the rheological properties of the material under test. In the following two sections, some of the most important forms of rheological behaviour will be described and some of the mathematical models to describe these types of behaviour will be discussed. These models are presented in a restricted form, as relationships between shear stress and shear rate. They provide a means to correlate the

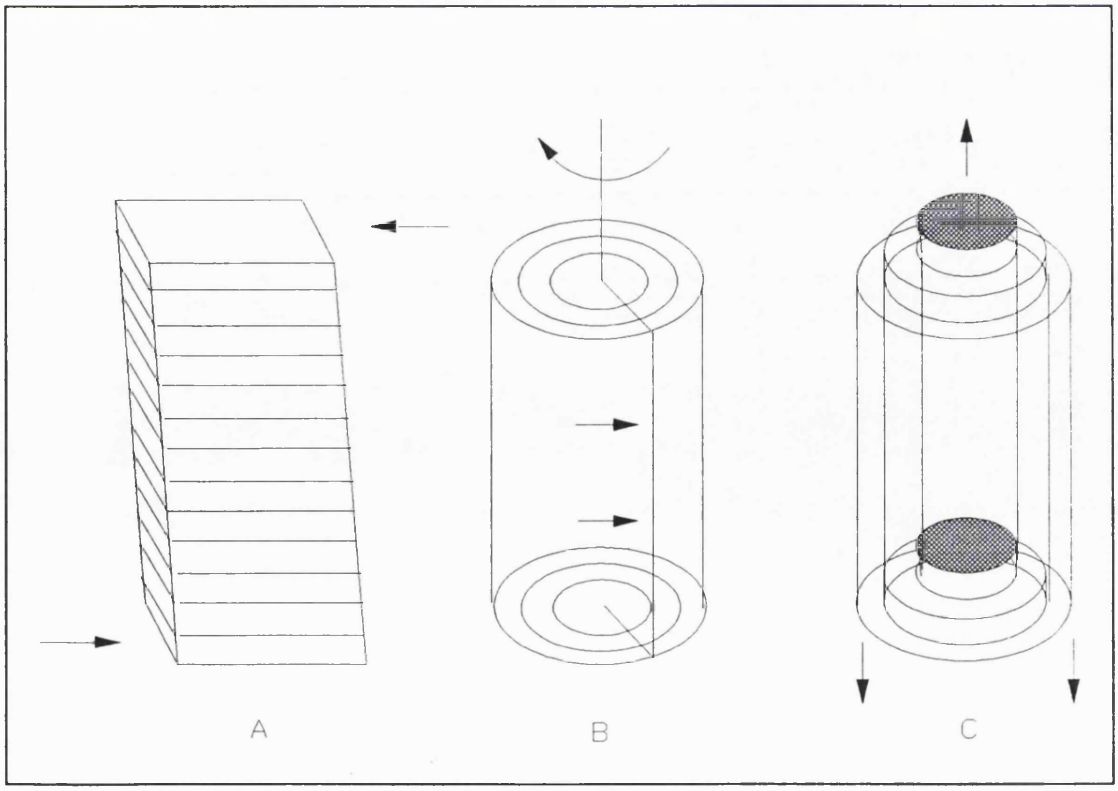

Figure 13: Examples of deformation.

data from one type of shear deformation to other types of flow, for example, elongational flow. In this project only simple shear systems will be used.

Suppose that a layer of material under consideration is subjected to a shear stress. If the stress is removed after deformation has occurred, the strain may, or may not, return to zero. If the strain does not eventually return to zero we say that flow has occurred. If flow occurs, even for a vanishingly small shear stress, the material is said to be liquid, otherwise it is a solid. A vanishingly small shear stress must be defined because many solids, for example clay, flow under the action of finite stress. If no recovery occurs then these materials are termed inelastic. Some liquids show a partial recovery, such materials are called elastic liquids.

The deformation and recovery of a solid may be almost instantaneous, these are said to be ideally elastic. If the response is not immediate, as with some polymers, the material is said to be viscoelastic. Often it is not possible to establish if a viscoelastic material is behaving as a solid or a liquid.

1.3.2.1 Elasticity.

An ideal elastic body is defined as a material that deforms reversibly and for which strain is proportional to the stress. Recovery to the original form occurs immediately the stress is removed. The ratio of stress to strain is known as the elastic modulus. A body may exhibit many elastic moduli, however, comparisons are generally made between the Shear modulus of a body, see equation 18, and the viscosity of a fluid, see equation 24.

$$Shear\ modulus,\ G' = \frac{Shear\ Stress}{Shear\ Strain} = \frac{(\partial F/A)}{(\partial L/L_0)} \qquad (18)$$

The Shear modulus of a body and the viscosity of a fluid are shown in figures 14 and 15, respectively. A plot of

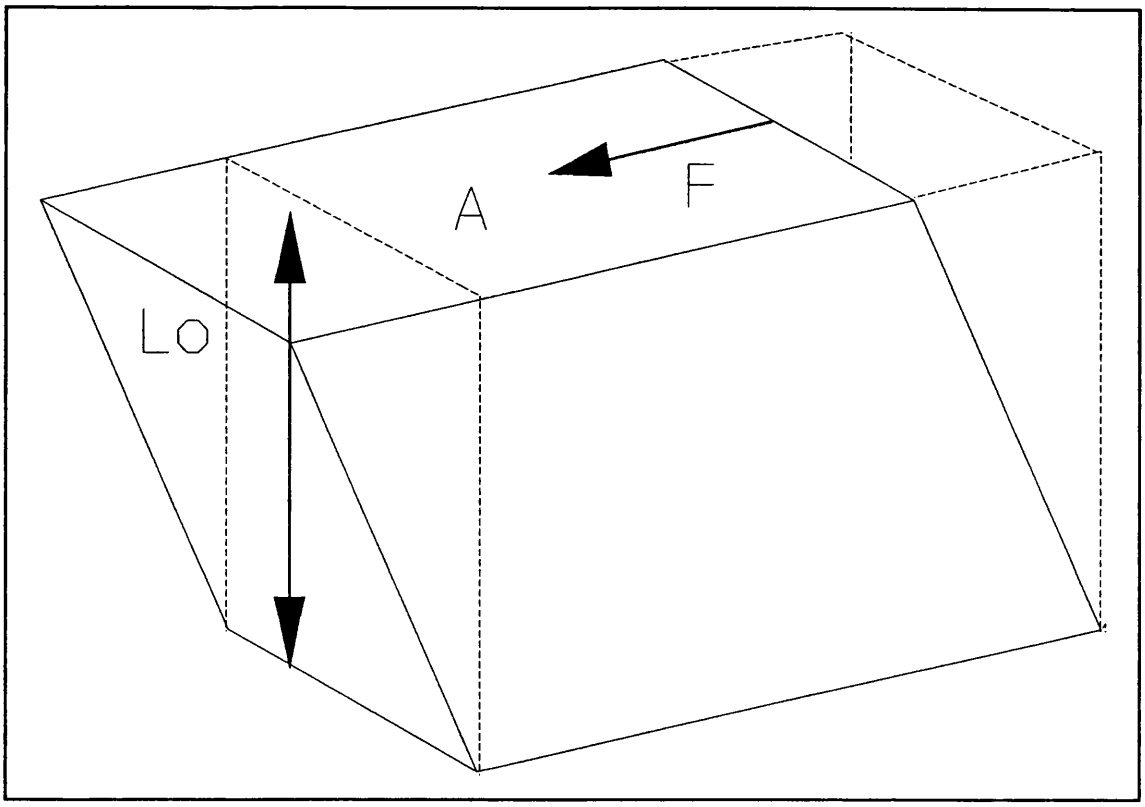

Figure 14: Shear modulus of a body.

stress against strain will produce a straight line through the origin. The strain must change instantaneously when the stress changes and remain constant until the stress again changes. A material represented by the model is therefore not viscoelastic, nor does flow occur. No solids were used in this project.

1.3.2.2 Viscosity.

This is the property of a fluid whereby it resists the relative motion of its parts - often known as internal friction.

The nature of this fluid friction was surmised by Newton. Figure 15 shows a viscous fluid undergoing laminar flow and, in particular, two parallel layers of area, A, separated by a small distance, ∂x, and whose velocities are v and $v+\partial v$. The upper layer of area, A, will exert an accelerating force, F, on the lower layer and the lower layer will exert a retarding force, F, on the upper layer. As a result of these viscous forces the relative motion of the layers will dissipate unless there

is some external force acting on the liquid to maintain the relative motion. Newton suggested that the frictional force between the layers is proportional to the area, A, and the velocity gradient, $\partial v/\partial x$, thus:

$$F \propto A \cdot \frac{\partial v}{\partial x} \tag{19}$$

This equation (19) can be re-written using further definitions. The fluid velocity gradient is known as the shear rate of the fluid.

$$\dot{\gamma} = \frac{\partial v}{\partial x} \tag{20}$$

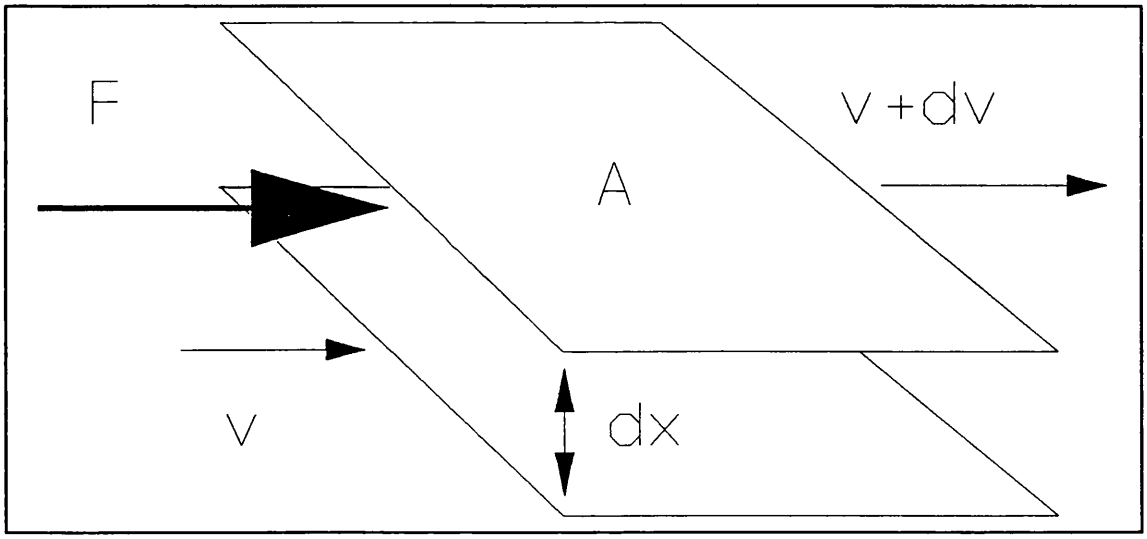

Figure 15: Viscous fluid in laminar flow.

And the force per unit area, causing the fluid to flow, is known as the shear stress.

$$\tau = \frac{F}{A} \tag{21}$$

Putting equations (20) and (21) into (19) gives:

$$\tau \propto \dot{\gamma} \tag{22}$$

Therefore:

$$\tau = \mu \cdot \dot{\gamma} \tag{23}$$

Hence:

$$\mu = \frac{\tau}{\dot{\gamma}} \qquad (24)$$

Equation 24 defines Newton's law of viscosity. The ratio of the applied shear stress to the shear rate is known as the coefficient of viscosity. The magnitude of the coefficient is measured in Pascal-seconds (Pa.s). Fluids following the law are called Newtonian; they have a constant viscosity regardless of shear rate. Newton's law applies to all gases and many liquids, particularly low molecular weight liquids. The Newtonian relationship often holds over a wide range of shear rates and these fluids show no elastic properties. Figure 16 (line A) shows a plot of shear stress against shear rate for a Newtonian fluid.

A wide range of industrially important fluids, such as solutions of polymers, colloids, suspensions and emulsions exhibit more complex behaviour; this is termed non-Newtonian behaviour. In such fluids, the viscosity is a function of shear rate. As the ratio of shear stress to shear rate is not a constant, the viscosity of a non-Newtonian fluid is labelled as an apparent viscosity and must be quoted with an associated shear rate. Figure 16(b-f) shows typical rheograms for several types of non-Newtonian behaviour.

Pseudoplastic fluids (or shear thinning) show a decrease in apparent viscosity with increasing shear rate under steady shear flow, see figure 16b. Tuffile and Pinho demonstrated that the fermentation broths of two Streptomyces cultures displayed pseudoplastic behaviour [55]. Also, Taguchi et al [56] showed pseudoplastic properties in an Endomyces culture broth.

Dilatant fluids (or shear thickening) show an increase in apparent viscosity with increasing shear rate, under steady flow conditions, (see figure 16c). No dilatant fermentation systems have been reported in the literature.

Bingham plastic fluids cannot flow until a limiting shear stress, termed the yield stress or yield value, is

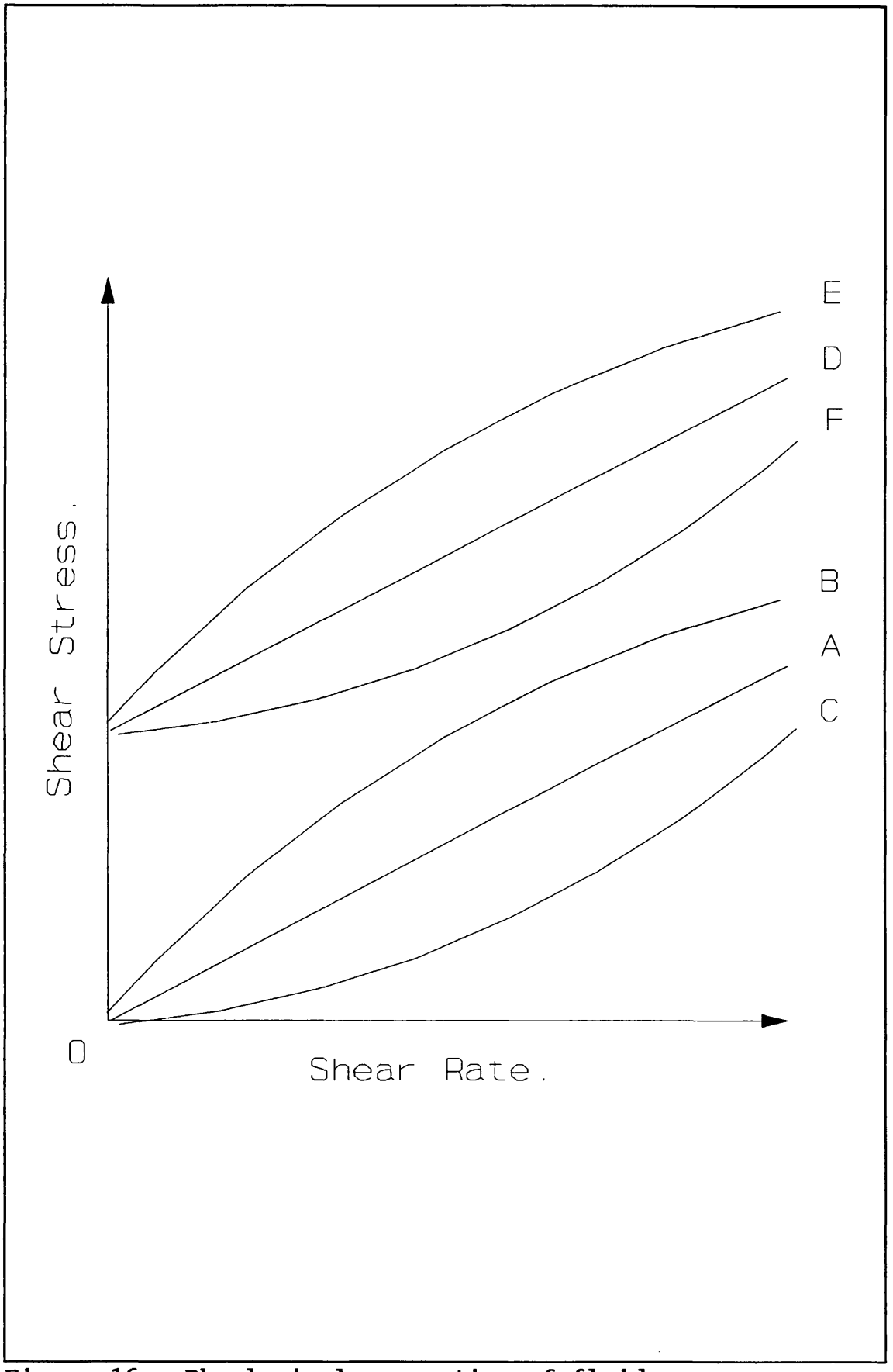

Figure 16: Rheological properties of fluids.

overcome. All plastic substances exhibit the properties of solids at stresses below the yield value and the properties of a liquid at higher stresses. The Bingham model represents a solid but is only applied when flow occurs. According to Whorlow [53], the elastic deformation before flow begins is almost invariably ignored because the corresponding strain is small compared with the strain due to flow, see figure 16d. Sato [57] related the rheological properties of a Kanamycin broth to the Bingham plastic behaviour.

The fluids displayed in figures 16e and 16f also exhibit a yield stress, but once the limiting shear stress has been exceeded a pseudoplastic or dilatant behaviour follows, respectively.

Many fluids exhibit time related flow or sample history effects; these effects may, or may not, be reversible. A thixotropic substance becomes more fluid with increasing time of flow under steady state conditions. The opposite effect, when a material becomes more resistant to flow with increasing time of flow under steady state conditions is termed rheopexy. Figure 17 shows the variation with the shear rate of the apparent viscosities corresponding to zero time and infinite time of shearing for a thixotropic material. Van Wazer et al [58] suggest that the thixotropic fluid falls from an initial value of μ_0 (a) to a final value of μ_∞ (b) over a given period of time.

Many examples of thixotropy represent a very fast change in shearing. This emphasizes the fact that the time constants of the thixotropic and rheopectic effects may vary considerably and that it is virtually impossible to determine time-dependent changes which occur in extremely short times during flow of a material. Van Wazer states that it can be argued that pseudoplastic flow (no yield value) results from immediately concluded thixotropic behaviour, exhibiting an infinitely short time to go from $\mu_{\theta=0}$ to $\mu_{\theta=\infty}$. Similarly, dilatant flow results from immediately concluded rheopectic behaviour.

When a shear stress is applied suddenly to a fluid the

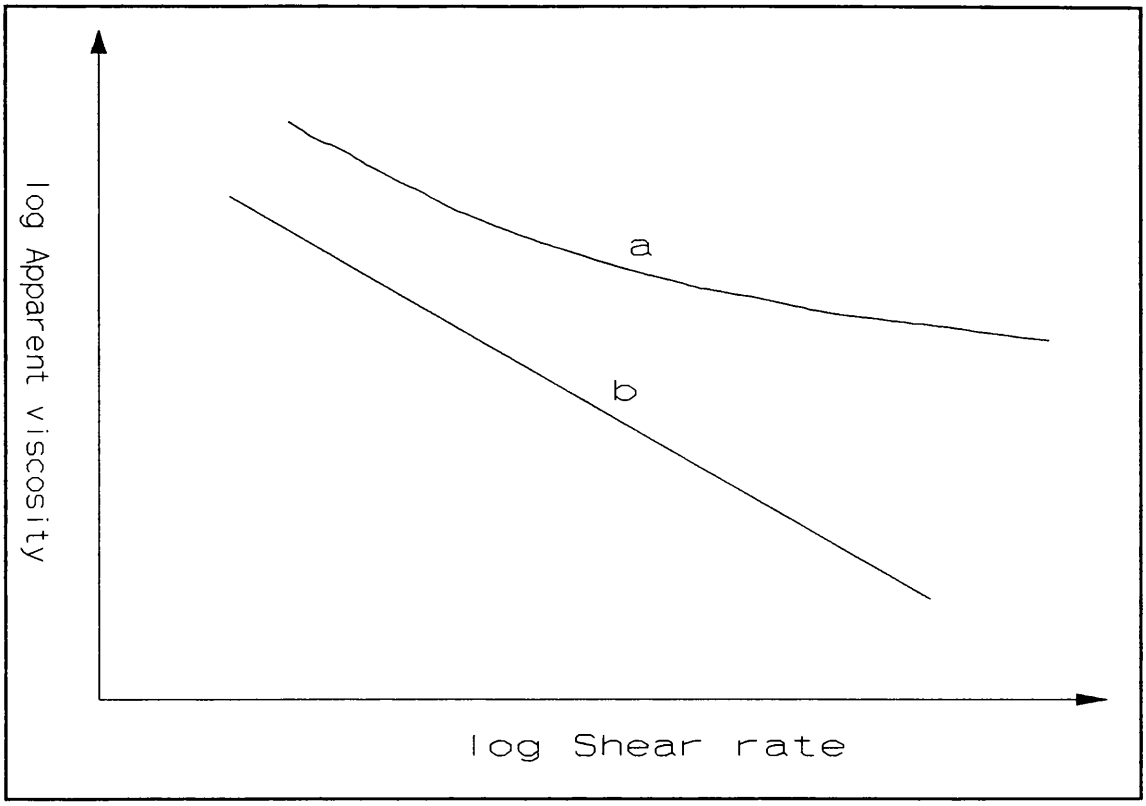

Figure 17: Properties of thixotropic materials.

initial shear rate may not be maintained for two distinct reasons, apart from inertial effects.

a) Part of the mechanical energy supplied to the material may be stored as elastic energy. As the maximum stored energy for a particular stress is reached, the rate of supply of energy falls to that necessary to maintain flow, so that the shear rate falls.

b) The second reason for a change of shear rate is that the structure of the material changes in some way. Sometimes a limiting value of shear is reached, but often the change continues for the duration of the experiment.

According to Van Wazer et al [58] non-Newtonian flow observed in suspensions and other dispersed systems can be explained by interaction between particles, interaction with the continuous phase and particle deformation, see figure 18. The fluids shown are composed of the following:

a) Asymmetric particles in solution.

b) Polymer solutions with long entangled and looping molecular chains.

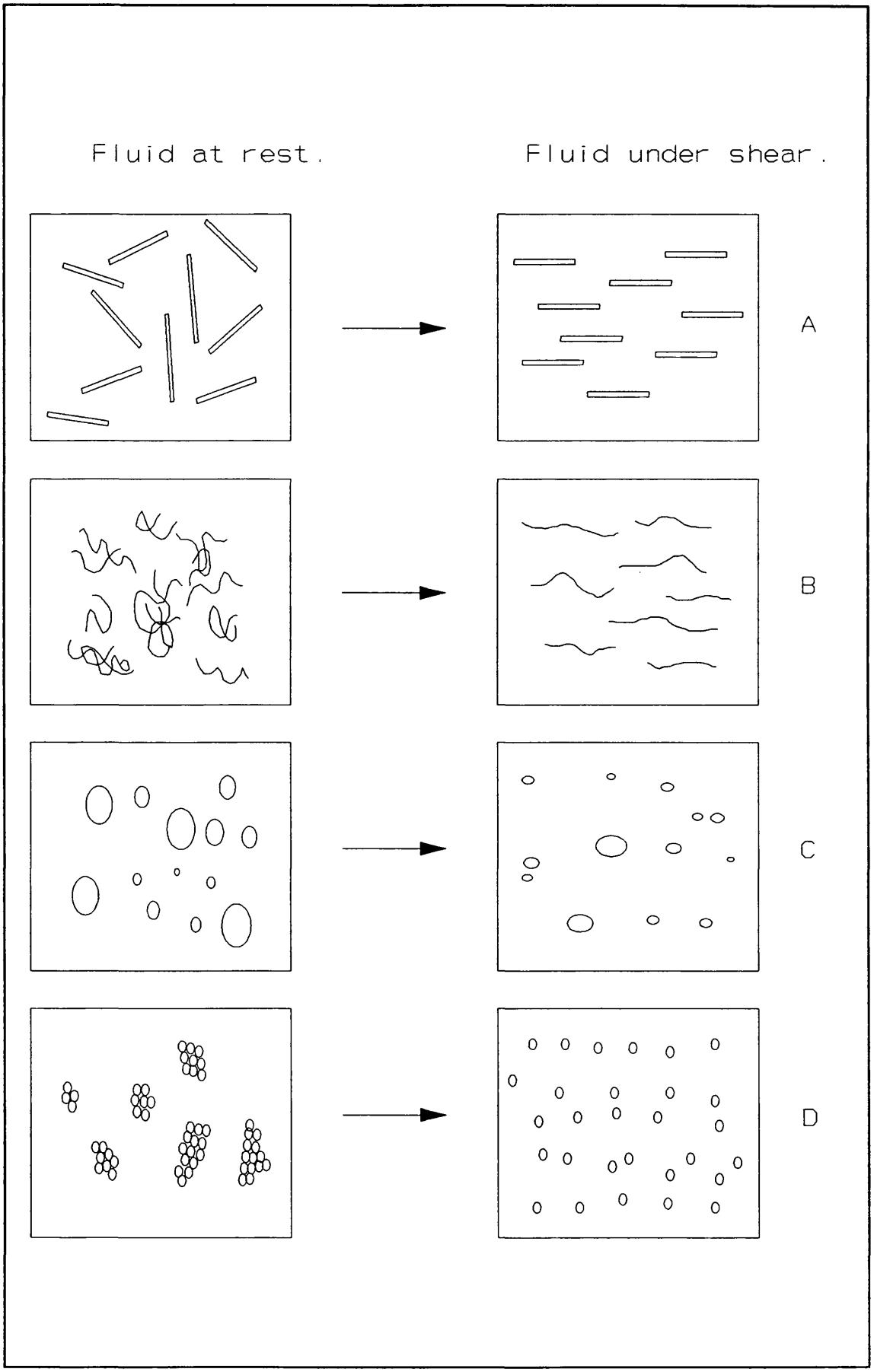

Figure 18: Structural changes in thixotropic materials.

c) Droplets of one liquid dispersed in another liquid.

d) Agglomerates of particles in solution.

At rest all of these systems will display random motion (Brownian movement) creating an irregular internal order and correspondingly a high resistance to flow. Hence these systems will be highly viscous. However, under the influence of a given shear rate the internal order of these systems becomes more organised. The asymmetric particles become orientated to achieve least flow resistance. The long chain molecules of the polymer solution become disentangled, stretched and orientated parallel to the direction of flow. In addition, the stretching of the molecules causes liquid previously bound to the molecules to be released; this causes a dilution of the molecules present. The liquid droplets become deformed. These alignments, dilutions, and deformations of the particles enables them to flow past each other more readily, which manifests itself as a reduction in viscosity. As the shear rate increases so does the extent of the dilution, alignment and deformation of the particles and therefore the reduction in viscosity also increases. Also different interparticular attractions may account for some pseudoplastic properties. Van der Waal's forces, electrostatic charges and hydrogen bonding cause aggregation and entanglement of particles. The shear field could break these bonds and allow for increased alignment and thus lower viscosities.

For most fluids the shear thinning effects are reversible once the shear field has been removed. However, sometimes the decrease in the fluid's viscosity is irreversible caused by damage to the particles, the fluid is then said to have suffered shearbreakdown or rheodestruction.

The shear thinning properties of pseudoplastic fluids are not uniform over extremes of the shear rate range, see figure 19. At low shear rates the Brownian movement of molecules ensures all particles remain in a random state

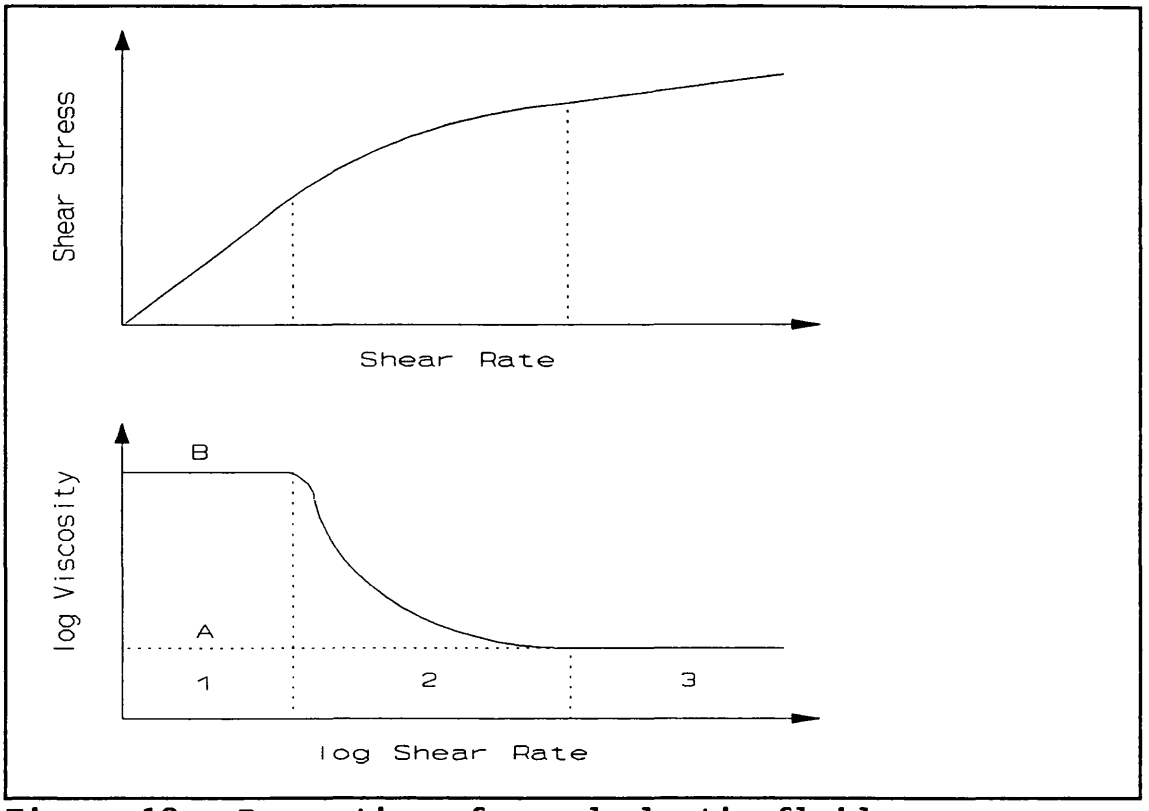

Figure 19: Properties of pseudoplastic fluids.

despite the initial effects of the shear. Hence, at low shear rates (region one) pseudoplastic fluids show the flow behaviour of a Newtonian fluid with viscosity, $\mu_{0\ (A)}$, independent of the shear rate. Then follows a period (region two) when the shear rate induced particle orientation or deformation exceeds the randomising effect of Brownian movement and pseudoplastic flow properties are observed. Finally the viscosity approaches a finite level (region three), $\mu_{\infty\ (B)}$. Higher shear rates cause no further shear thinning as the optimum orientation and deformation has been reached. Once again, the flow properties become Newtonian. These two periods of Newtonian behaviour are known as the first and second Newtonian ranges. These ranges which show different flow properties mean that equations to model a particular flow behaviour are only valid over a certain range.

In general, dilatant flow behaviour is found in highly concentrated suspensions. The particles are densely packed and the quantity of continuous phase is just sufficient to fill the voids between particles. At rest

or at low shear rates the continuous phase fully lubricates the particle surfaces and hence allows smooth positional changes of the particles. At higher shear rates the particles will wedge against others causing a general volume increase. The continuous phase is no longer sufficient to fill the voids and keep the particle surfaces lubricated hence the system becomes more viscous. Dilatancy in fluids is rare, examples include slurries in water and wet sand on a beach.

Plastic systems are classified as both solids and liquids. The fluids are dispersions which at rest can build up an intermolecular/interparticular network of forces. The types of forces may be Van der Waal's, hydrogen bonding, electrostatic bonding or polar attractions. These forces prevent the movement of the volume elements within the substance and thus give the system the character of a solid. At low shear stresses the forces hold the network together and the solid can only deform elastically. When the shear stress overcomes the network forces, the volume elements can change positions and the system behaves like a fluid. The threshold shear stress that causes the network to collapse is known as the yield stress.

Many dispersions show the potential in their particles or molecules for orientation or interaction. These

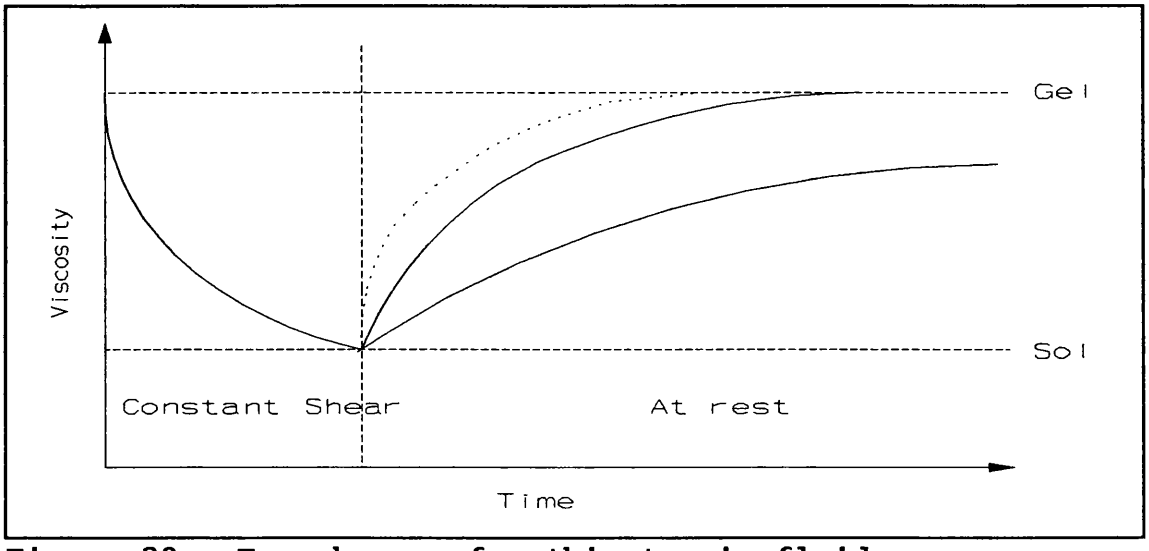

Figure 20: Two phases of a thixotropic fluid.

interactions create three dimensional network structures which are known as gels (the solid form of a substance that can be a solid or a liquid). The interactions are composed of weak hydrogen or ionic bonds which rupture easily when the dispersion is subjected to shear over an extended period of time. As the network breaks down the viscosity reduces until eventually it reaches a minimum for a given shear rate. This minimum viscosity describes a status known as sol (liquid form of a substance that can be a solid or liquid) for the dispersion.

A thixotropic fluid has the potential to reform structure when the substance is allowed to rest for an extended period of time. Figure 20 shows a graph of viscosity against time for the two phases of a thixotropic fluid: the gel form changes rapidly to a sol form when subjected to a given shear rate, then, once the shear field has been removed, the sol form transforms back to a gel form. It may take seconds or minutes to break down a thixotropic fluid but often requires minutes, hours or longer to fully recover. When a low shear rate is applied to a concentrated dispersed system it is often found that a steady value of shear stress is not recorded immediately. Instead, the latter decreases over a period of time due to structure breakdown until it eventually reaches a steady value, where an equilibrium is established between the rate of breakdown and the rate of structure redevelopment. The

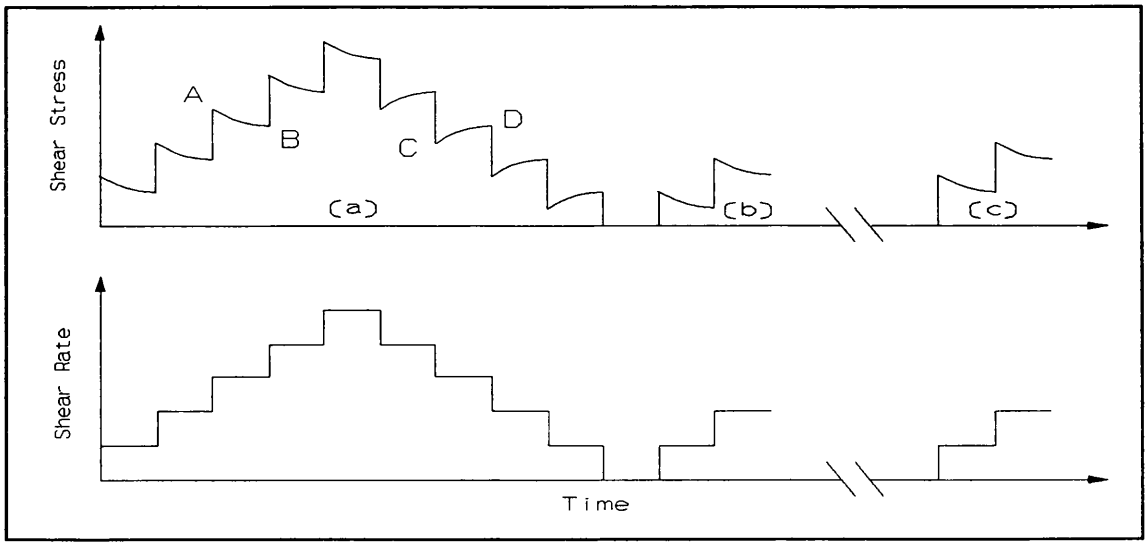

Figure 22: Further properties of thixotropic fluids.

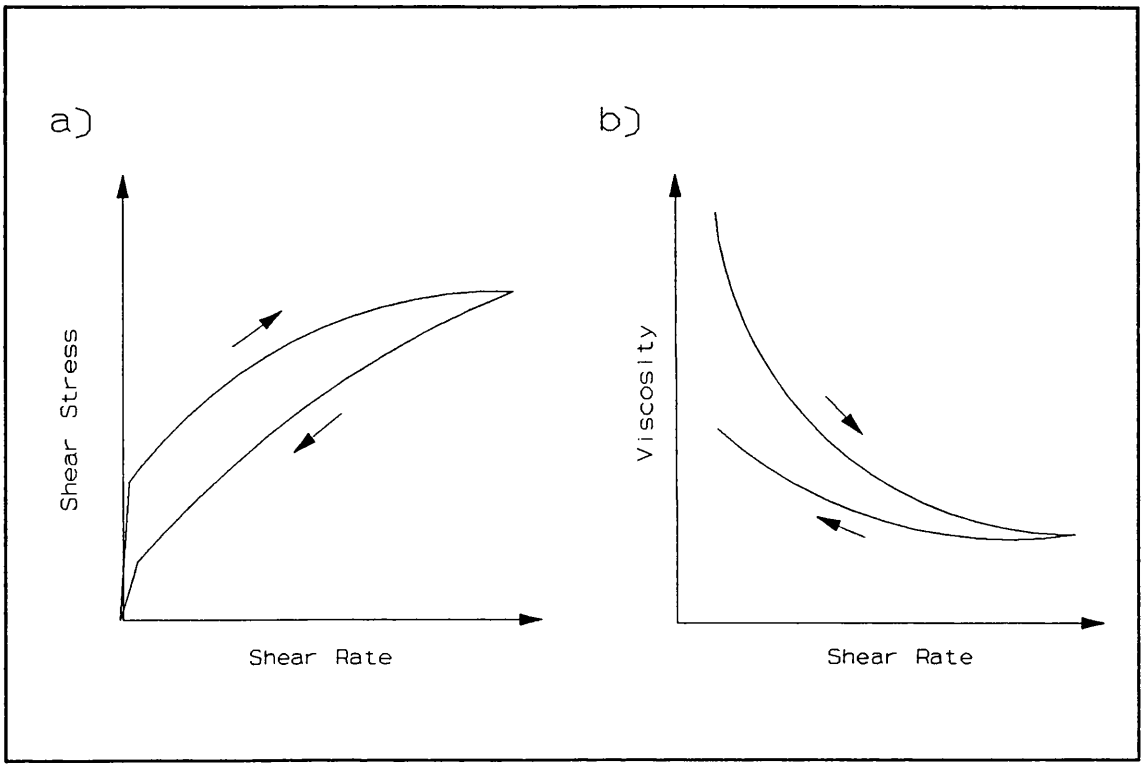

Figure 21: Rheograms of thixotropic fluid.

time interval required for equilibrium to be established decreases as the shear rate increases. This phenomenon is often referred to by Freundlich [59] as the equilibrium between gel and sol states.

Figure 21a shows the flow curve for a thixotropic system on a graph of shear stress against shear rate; the up-curve and down-curve do not superimpose causing a hysteresis effect. Figure 21b shows the corresponding viscosity against shear rate graph: with increasing shear rate the viscosity decreases because of a breakdown in the fluid structure and alignment of molecules or particles. When the shear rate is decreased, after the shear rate increases, the viscosity increases but does not have sufficient time to recover to the up-curve values. Although the orientation component of the total viscosity can be lost as quickly as it was established, the interactions or bonds component cannot be re-established as rapidly.

Figure 22 shows the variation of stress with the time for a thixotropic fluid during a stepped sequence of shear

rate changes.

a) The unsheared material.

b) After a short rest period.

c) After prolonged resting.

After a short rest, the initial peaks of each speed may not be as high as the original tests (b), but if the observed changes are entirely due to thixotropy, the original values of peak stress will be achieved after a long rest (c).

As the shear rates increase, the shear stress values can be observed immediately peaking and then reducing with time (line AB in the figure). This is typical thixotropic behaviour, however, similar rheograms can be produced by certain viscometers. The momentum of the viscometer's motor can cause a speed overshoot, which although it is rapidly corrected, can have a significant effect on the rheogram.

Immediately after each abrupt fall in shear rate (associated with a reduction in speed) a small increase in stress is shown (see line CD in the figure). Such an increase is not always observed, either because the material tested does not show recovery of viscosity while being sheared, or because of limitations in the rate at which the instruments can respond.

Observations from figure 23 suggests that if readings were taken 5s after each change of speed (not 15s), then the thixotropic loop would have been of the form shown by line ABC rather than line DEF. Whorlow [52] states that the area of the loop is not a satisfactory measure of the degree of thixotropy shown by the material. He suggests another approach to quantify thixotropic behaviour, from figure 22, if the curve AB were continued it might approach, asymptotically, a limiting stress. Similarly, if the curve CD approaches the same limit from below, an equilibrium stress may be determined for this strain rate. Plotting such equilibrium values would give the line EG in figure 23. The material may then be categorised by :

a) The equilibrium flow curve.

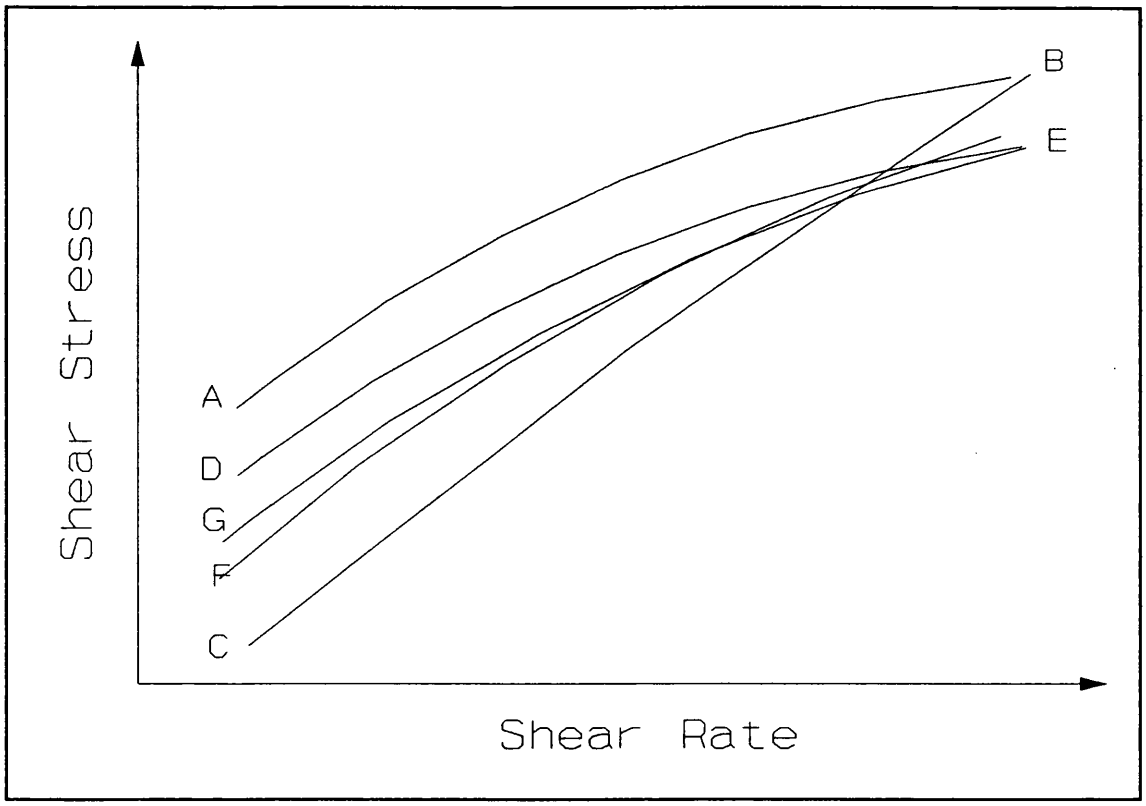

Figure 23: A rheogram showing the thixotropic loop.

b) Some measure of the rate of approach to equilibrium after a change in strain rate.

The theories of Moore [60], Chang [61] and Evans [62] are based on this concept.

From a practical point of view, thixotropic materials are seldom stable enough for an equilibrium flow curve to be determined. During the necessary long periods of shearing irreversible changes occur. Many materials show some rheodestruction as well as thixotropy.

Many rheologists, according to Whorlow [53], have published reports purporting to show thixotropic behaviour under conditions in which temperature changes were probably responsible.

Normally an increase in orientation within a system results in a reduction in viscosity since the particles are able to flow past each other more easily. However for Rheopectic systems the development of an ordered structure results in an increase in viscosity. Thus at high shear rates, when there is a good orientation of particles, the viscosity is higher than at low shear rates.

Coulson and Richardson [63] note that shear is not the only cause of time dependence on fluids. Many systems are prone to hydrolysis or bacterial action; such chemical changes produce effects similar to thixotropy or rheopexy and are irreversible.

Many fluids, particularly solutions of polymers such as microbial polysaccharides, exhibit an elastic response that is superimposed on a characteristic viscous behaviour; these fluids are known as viscoelastic. The complex stresses developed in viscoelastic fluids are responsible for a variety of phenomenon. Figure 24 shows two illustrations; part (a) shows a bob rotating in a purely viscous fluid, whilst part (b) shows the same bob rotating in a viscoelastic fluid. The fluid appears to climb the bob in part (b); this is known as the Weissenberg effect. Frederickson [64] provides a comprehensive review of viscoelastic behaviour.

Metzner and Reed [65] state that classification of fluids into general rheological categories constitutes a gross oversimplification of the actual situation. They suggests that it has been repeatedly shown that the classification of a particular fluid often alters depending upon the shear rate range used.

Charles [2] and Metzner say that fluids exhibit different rheological characteristics depending upon the

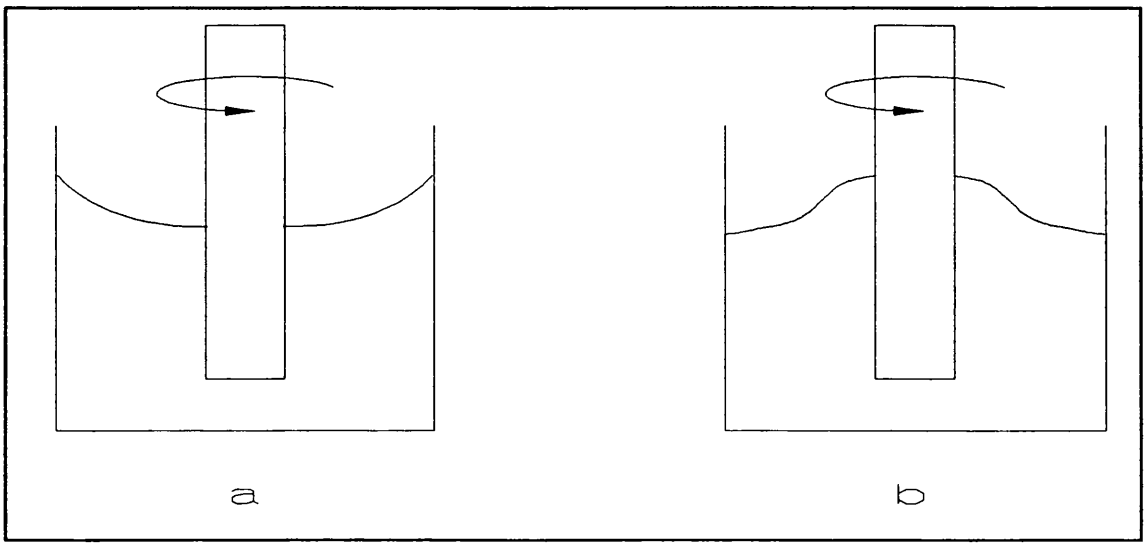

Figure 24: The Weissenburg effect.

shear rate range applied. However, Metzer adds that this phenomenon is frequently irrelevant since for most engineering problems the model only needs to portray the rheological properties over a known, limited range of shear rates.

1.3.3 Rheological models.

Mathematical models of rheological behaviour represent idealisation of actual material behaviour. Sometimes the idealisation is extremely accurate over a range of shear rates; at other times the idealisation is a crude approximation of the real behaviour but nevertheless useful in providing predictions on the effect of shear on a material.

The use of rheological models allows the behaviour of fluids to be described in quantitative terms, thus ensuring any changes in rheological characteristics are obvious. A variety of mathematical expressions has been developed to correlate viscosity data for fluids with various rheological properties. However, none of these expressions gives a completely satisfactory description encompassing all fluids or the entire shear rate range for a given fluid.

The Power law model, attributed to Ostwald [66], presumes the absence of a yield stress and can be used for both Newtonian and non-Newtonian fluids.

$$\tau = K \cdot (\dot{\gamma})^n \qquad (25)$$

τ - shear stress (Pa).
$\dot{\gamma}$ - shear rate (1/s).
K - consistency coefficient ($Pa.s^n$).
n - Power Law Index or Flow Behaviour Index (no units).

The consistency coefficient describes the apparent viscosity of the fluid when the shear rate is at unity. A quantitative rheological characterisation of the fluid is supplied by the Power Law Index. For pseudoplastic fluids

the dimensionless constant n is less than one, whereas for dilatant fluids it has a value greater than one. Newtonian fluids have an n value of one. The Power Law is often used in a logarithmic form:

$$\log \tau = \log K + n \,.\, \log \dot{\gamma} \qquad (26)$$

Thus for a time independent fluid ,a plot of log shear stress against log shear rate will produce a straight line. The slope of the line will equal the flow behaviour index and the intercept on the log shear stress axis will be equal to the logarithm of the consistency coefficient.

The Bingham plastic model postulates that the material behaves as an elastic solid for stresses less than the yield stress [67], the model describes Newtonian behaviour once flow has occurred.

$$\tau = \tau_0 + \mu_a \,.\, \dot{\gamma} \qquad (27)$$

τ - shear stress (Pa).
τ_0- yield stress (Pa).
μ_a - plastic viscosity (Pa.s).
$\dot{\gamma}$ - shear rate (1/s).

The Bingham model is one of a group of models for plastic materials; a number of fluids also demonstrate a yield stress but do not all behave as Bingham plastics (they do not exhibit Newtonian behaviour after the yield stress has been overcome). Metzner and Otto [68] state that many fluids, described in the literature as Bingham plastic, are in fact pseudoplastic with a yield stress. Most of these reported cases [69] involve fungal and mycelial cultures in which yield stresses are associated with the structure imposed by the mycelial mat and the subsequent break down of this structure on application of stresses exceeding the yield stress. Herschel and Bulkley developed a converted form of the Power law which is often applied to such fluids [70]:

$$\tau = \tau_0 + K \,.\, \dot{\gamma}^n \qquad (28)$$

or,

$$\tau - \tau_0 = K \cdot \dot{\gamma}^n \qquad (29)$$

Casson [45] described a type of non-Newtonian fluid, termed a Casson body, which behaves like a pseudoplastic fluid with a yield stress. His model for a Casson body is:

$$\sqrt{\tau} = \sqrt{\tau_0} + K_c \cdot \sqrt{\dot{\gamma}} \qquad (30)$$

K_c- Casson viscosity ($Pa^{\frac{1}{2}}.s^{\frac{1}{2}}$).
A plot of $\sqrt{\tau}$ against $\sqrt{\dot{\gamma}}$ will produce a straightline. The slope of this line will equal the Casson viscosity and the intercept of the y-axis will equal $\sqrt{\tau}_0$. Roels et al [1] have developed this rheological model for use with mycelial cultures. They found the Casson model superior to the Power law or the Bingham plastic model for correlating the rheological data from two different strains of *P. chrysogenum*. The behaviour of actual materials is often as represented in figure 25. As the applied stress increases from zero, no flow occurs until a stress X (at point A) is reached. Flow then begins abruptly at a rate that depends not only on the material properties but also on the characteristics of the measuring instrument. For most instruments the sudden strain at A results in a fall in the stress to a value represented by a point such as B. As the stress is again increased, the line BCD is followed. On decreasing the stress steadily, a line such as DEF is followed. It might be expected that a stress Y (at point F) could be sustained indefinitely by the material, the strain remaining constant. In practice, very slow flow occurs, and the stress that ultimately can be maintained without flow is often much less than Y.

The upper yield stress, X is important in many practical situations, for example when calculating the pressure needed to start a flow in a pipeline. The lower yield stress, Y, is required when the equation for the

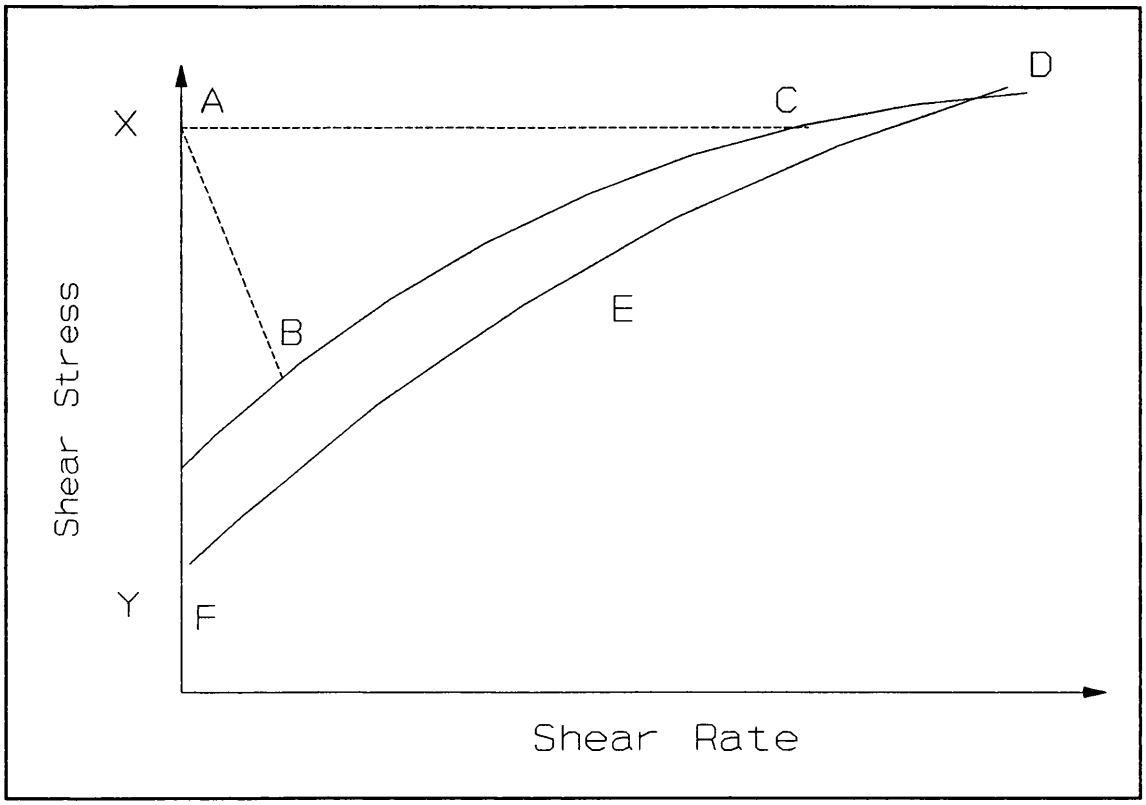

Figure 25: Bingham plastic fluid.

plastic material is to be used to represent the flow behaviour.

By using a new generation of constant stress rheometers, Barnes and Walters [71] demonstrate that yield stresses do not exist.

Sutterby [72] provides other mathematical models for describing rheological behaviour. As before, each model contains parameters which have their value determined by fitting the model to the viscosity data. These parameters can be used to characterise the flow behaviour of a particular fluid. Compared with the models previously outlined, the models used by Sutterby are complex and difficult to apply. None of these models have been used in the rheological literature covering filamentous microorganisms and so they will not be used in this project.

1.3.4 Rheology of fermentation broths.

In a fermentation broth, the presence of solid

particles and excreted microbial products may alter the rheological properties of the base fluid, water, producing a liquid with a more complex rheological behaviour [73].

Microorganisms, in submerged culture fermentations, are supplied with the nutrients they require for biochemical activity from their liquid environment. This liquid not only serves as a reservoir for the collection of metabolic end-products but also absorbs the heat liberated by the cells. The rate of transfer of heat and materials to and from the cells depends largely on the properties and motion of the fluid system in which the transport is carried out [74]. The more highly viscous and non-Newtonian the culture broth, the more acute the problems of mass and heat transfer in the fermenter. Hence characterisation of the fermentation broth rheology has an immense bearing on the design and operation of the fermentation, see figure 26.

A feature of batch fermentation is the variation of rheological properties with time. This may be due to

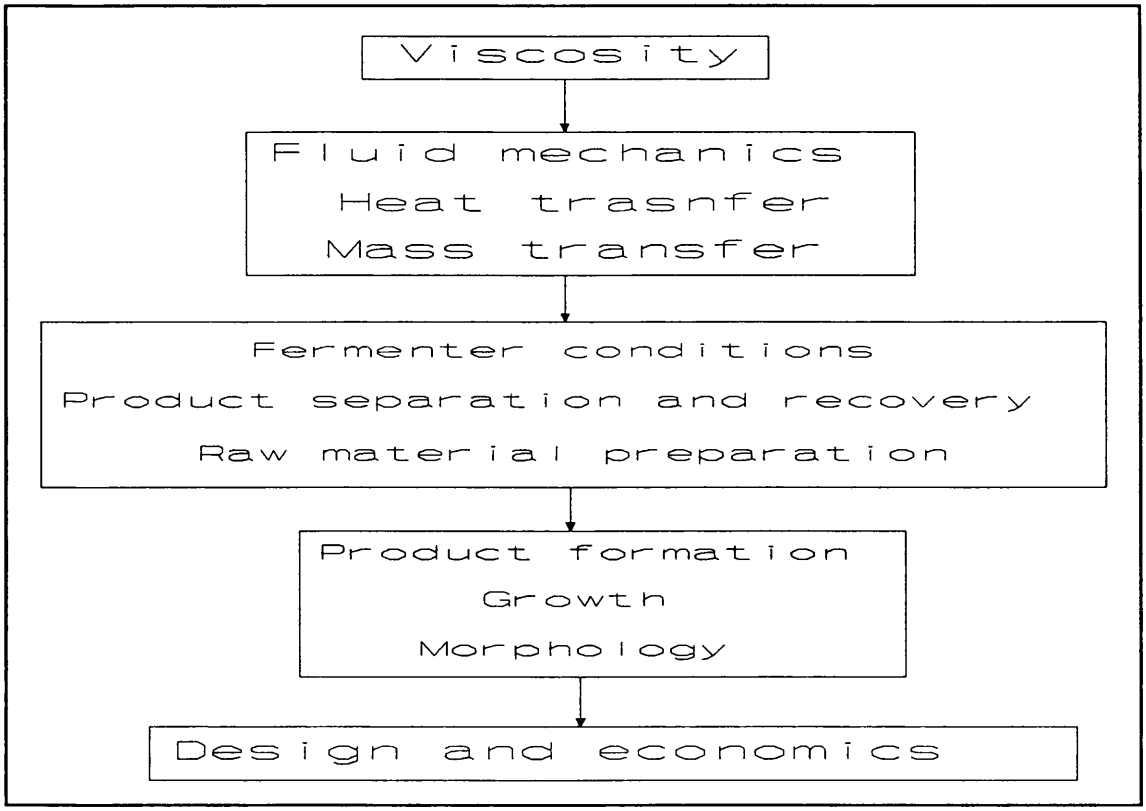

Figure 26: The influences of viscosity.

changes in biomass concentration, morphology of the microorganisms and, in some cases, to an increasing concentration of extracelluar products. According to Kemblowski and Kristiansen [73], at the cell concentrations normally encountered in bioreactors, single-cell organisms have little effect on the flow properties of the bioreactor broth. However, filamentous microorganisms can produce highly viscous, non-Newtonian suspensions even at relatively low biomass concentrations. The high viscosity is due to the structural rigidity of three-dimensional mycelial networks and the hyphae becoming highly entangled. An example is provided by Blanch and Bhavaraja [75] using *Penicillium chrysogenum*.

Certain microbial products, in particular exopolysaccharides, can also be major determinants of the rheological behaviour. Pace and Righelato [76] state that polysaccharide cultures are typified by highly viscous, non-Newtonian broths. The viscous nature of the medium is due to the presence of the high molecular weight linear polymers, the degree of flexibility in the long unidimensional particles causing non-Newtonian behaviour. These fluids are distinct from fungal and streptomycetes culture medium in which the mycelium causes the broth to be highly viscous and is discontinuous with the water phase. Thus, although mycelial and polysaccharide media may show equal viscometric behaviour, the heat and mass transfer characteristics of the broth may differ markedly. For example, Blakebrough et al [77] found that even though heat transfer coefficients of Xanthan broths measured in the laminar regime were in good agreement with a theoretical prediction accounting for fluid rheology, the heat transfer coefficients for *Aspergillus niger* broths were up to four times the predicted values. Both types of broths showed similar pseudoplastic behaviour over the shear rate ranges measured.

1.3.5 Measurement of rheological properties.

The study of rheology is important to many sciences and technologies. The data are particularly useful to the food processing, chemical and plastics industries, where many of the products and intermediates have a rheology which lies between the ideal extremes of Hookean solids and Newtonian liquids. Many instruments have been constructed to make manual, semi-auto, and automatic measurement of rheological properties. However, not all of the popular instruments measure viscosity as defined in section (1.3.4.2), some instruments only provide a relative viscosity value. The flow behaviour information can be of significant value as long as the instrument conditions remain consistent. In general the complex flow patterns produced in such instruments make them unsuitable for definitive measurement of viscosity. Walters [52] states that such an analysis would require complex mathematics. It should be noted that even when using instruments specifically designed to measure absolute viscosity considerable care must be exercised in analysing data for non-Newtonian fluids. Also, in most cases the empirical constants in any viscosity model are valid only over a limited range of shear rate and extrapolation beyond the range for which the constants were determined can produce serious errors. For example, the consistency coefficient, K, of the power law model is obtained by extrapolation to $1s^{-1}$; therefore it is quite possible that K will have no real physical significance at this shear rate. Also, the value of K and the flow index, n, generally vary with the range of shear rates considered. Hence, viscosities should be determined over the range of shear rates that will be encountered in the process of interest. This shear range will be a significant determinant on the choice of viscometer.

The following sections provide detailed information on the various types of viscometer presently available with special regard to the measurement of the rheological

properties of fermentation broths. The positive and negative aspects of each instrument will be outlined with respect to the analysis of these fluids which are typically dispersed particulate suspensions.

1.3.6 Capillary viscometers.

The capillary viscometer consists of a true-bore capillary (of accurately known diameter and length) attached to a pressurized reservoir containing the fluid under test. The whole system must be kept at a constant temperature. By measuring the volumetric flow rates for various pressure differences, the viscosity of the fluid may be measured. Corrections can be made for heat effects, viscoelasticity and other effects.

According to Charles et al [2], it is generally difficult to use a capillary viscometer to measure the viscosities of fluids containing suspended particles. Among the problems most frequently encountered are settling of particles and plugging of the fine capillary bores, particularly by filamentous organisms. Even in the absence of these problems, complications can be introduced by the 'tube-pinch' effect which is the migration of small particles away from the wall to the centre of the capillary, as described by Cohen and Metzner [78]. As a result of these difficulties capillary viscometers have not been used widely to study rheological properties of culture broths. However, the use of the larger tube viscometers has overcome many of the troubles mentioned above. The tube, or pipeline, viscometer is an extremely simple and commonly used rheological instrument. As with the capillary system, the Rabinowitsch-Mooney equation yields values of shear stress and shear rate.

Whorlow [53] states that when a tube rheometer is suitable for a particular fluid they are generally simpler, cheaper, more easily thermostatted over a wide temperature range, and of higher precision than the equilavent rotational viscometer. For extremely viscous materials

they may be more suitable at high shear rates because heat generation in the material will be reduced. Additionally, for friable fluids (substances that are easily broken up) or those that tend to slip over smooth metal the existence of a hydrostatic pressure along the tube may be advantageous.

Rheological measurements are determined from measurements of pressure drop and liquid flow rate, for a fluid moving through a pipe in fully developed laminar flow. It has been noted by Allen and Robinson [79], that for certain suspensions the measured shear stress at a given shear rate tends to decline with a decrease in pipe diameter. Allen suggests this peculiar behaviour can be attributed to the 'tube-pinch' effect. The fundamental nature of this phenomenon is not completely understood, however modifications to the Rabinowitsch-Mooney equation maybe made to alleviate such problems.

The problems encountered in such an instrument can be conveniently divided into two groups according to Whorlow [53]. The first group, which can in principle be allowed for by suitable experimental techniques includes end effects. The second group includes turbulence and other flow disturbances, viscosity changes due to variations in temperature or pressure during flow, particle migration and most wall effects. He states that it is important to recognise the presence of non-ideal conditions so that false conditions are not drawn.

Björkman [44 and 80] used an on-line system in a batch fermentation. Such a system was chosen to avoid the destruction of the broth sample that often occurs, according to the author, on removing it from the fermenter. The fermentation was the Penicillin V process, which uses a *Penicillium chrysogenum* strain. Blakebrough et al [77] measured the rheological properties of an air-lift fermentation of *Aspergillus niger*, using the downcomer as a the pipe viscometer.

Perley et al [81] used a tube viscometer to obtain a correlation between cell concentration and broth viscosity

for a fermentation of *Hansenula polymorpha*. The viscometer was chosen because it was inexpensive, easy to operate and could provide a continuous measurement.

An important disadvantage of pipe viscometers, especially in a research system, is that yield stresses cannot be determined.

1.3.7 Rotational viscometers.

According to Whorlow [52], instruments in which the test fluid is sheared between rotating cylinders or cones and plates have two fundamental advantages over tube viscometers:

a) A particular sample can be sheared for as long as desired so that changes in behaviour with time, either temporary or permanent, can be followed.

b) Using appropriate design, an approximately uniform shear rate can exist throughout the sample in contrast to the variation of the shear rate in a tube.

The major limitation of such systems is that the high shear rates cannot be achieved in even moderately viscous materials without a considerable temperature rise.

The basis of rotational viscometry can be explained as follows: the movement of a solid surface in contact with a fluid causes the fluid to move in a characteristic pattern which causes the development of forces against the solid surface. These forces must be continuously counter balanced (i.e. by a drive motor) in order to sustain the fluid motion. The nature of the flow pattern and the magnitude of the internal stresses and applied forces depend primarily on the geometry of the system, the rate of fluid motion, and the intrinsic rheological properties of the fluid.

There are many different types of rotational viscometers in use, the following sections describe the more common varieties.

1.3.7.1 The concentric cylinder viscometer.

Concentric cylinder or cup and bob viscometers are in widespread use. Figure 27 shows a simplified view of a concentric cylinder viscometer. The fluid to be analysed is contained between the inner and outer cylinders. The inner cylinder is then rotated, usually by a drive motor, and exerts a tangential force on the fluid in contact. This force is transmitted through the fluid to the outer cylinder. By measuring the torque required to maintain a particular rotational speed of the inner cylinder, values for shear stress and shear rate maybe determined.

Equations (31) and (32) allow shear stress and shear rate to be calculated for concentric cylinder viscometers.

$$\tau = \frac{M}{2.\pi.R^2.L} \qquad (31)$$

$$\gamma = \frac{2.\Omega}{[1-(\frac{r_i}{r_o})]^2} \qquad (32)$$

Many researchers [82, 83 and 84], in particular Yang and Krieger [86], have derived formulae to enable the determination of shear stress and shear rate data for a wide variety of fluids using concentric cylinder systems. The use of a system with a small annular gap allows these complex formulae to be simplified considerably. Viscometers have been constructed with very narrow annuli but this causes practical difficulties since the annular gap needs to be large compared with the dimensions of the suspended particles for accurate measurements to be obtained. According to van Wazer et al [58], most viscometers compromise with an annular gap of around 10% of the cylinder radius.

The major problems encountered when using a concentric cylinder system, or any system using a smooth rotating bob

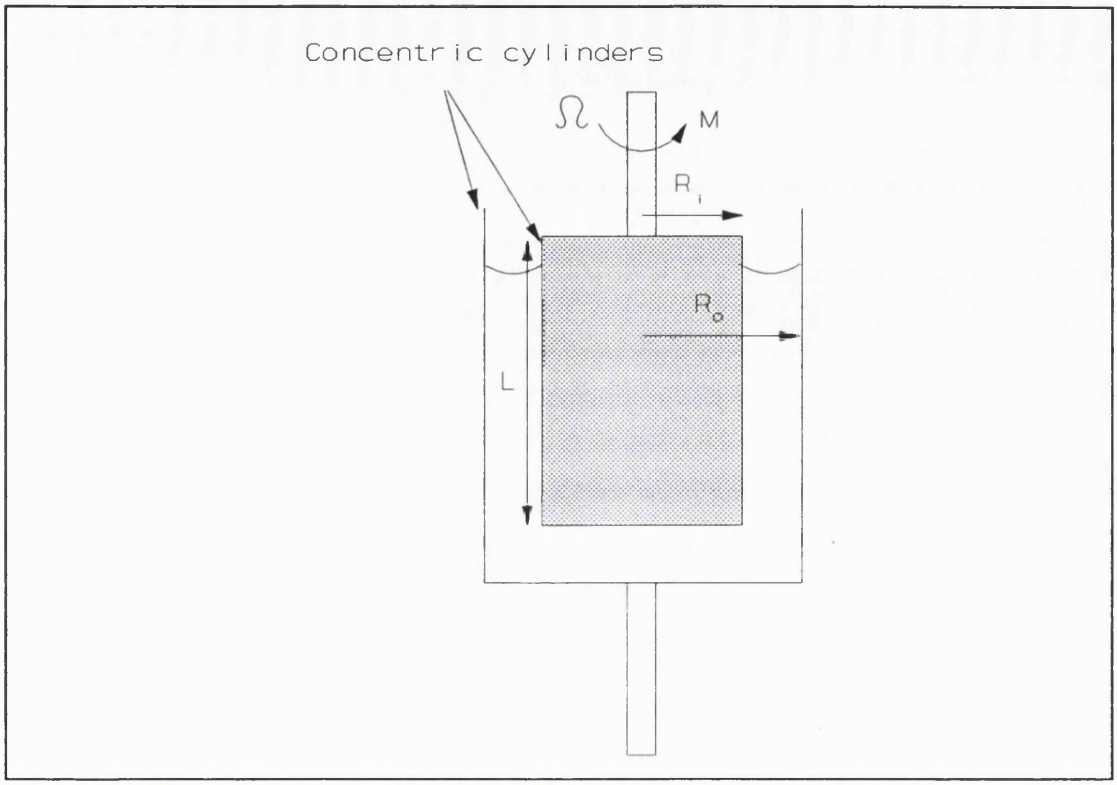

Figure 27: Concentric cylinder viscometer.

for measuring rheological properties of suspensions, are the tendencies for phase separation and gravity settling. The former manifests itself as a readiness for the particles in the suspension to move away from the immediate vicinity of the bob, creating a clear, less dense region next to the surface of the cylinder. The later, as the name suggests, is the settling-out of the particles, making the suspension heterogenous. Despite these problems many authors have used concentric cylinder viscometers: Barker and Worgan [87] used a Brookfield LV Synchro-lectric viscometer fitted with a U.L. spindle, to measure the rheological properties of a *Aspergillus oryzae* fermentation; whilst, Leduy et al [88],used a Brookfield LVT Synchro-lectric viscometer equipped with spindles 1, 2 and the U.L. adapter to study a *Aureobasidium pullulans* fermentation. Allen and Robinson [79] used a Haake Buchler model RV12 and a M150 measuring head on an *Aspergillus niger* fermentation. Ghildyal et al [89] used a Rheotest 2 with the S1 measuring head, for his rheological studies on *Streptomyces fradiae*. Wittler et al [90] used a Contraves Rheomat 115 with a

modified co-axial cylinders for studying *Penicillium chrysogenum*.

The equations used to calculate rheological data from concentric cylinder viscometers must account for various sources of error:

Since concentric cylinder viscometers are not infinite in length the torque per unit length readings must allow for end effects. The fluid below the cylinder exerts a torque which must be taken into account. Wilkinson [85] discusses end effects and other possible types of error.

In the theory of such systems, it is assumed that particles of fluid move in concentric circles about the axis of rotation of the instrument, except possibly in the edge zones. Any departures from this are caused by inertia. Inertial effects occur even with Newtonian fluids, but the type of flow disturbance depends on the geometry of the system. In concentric cylinder instruments, when the inner cylinder rotates, the fast-moving fluid near the inner cylinder tries to move

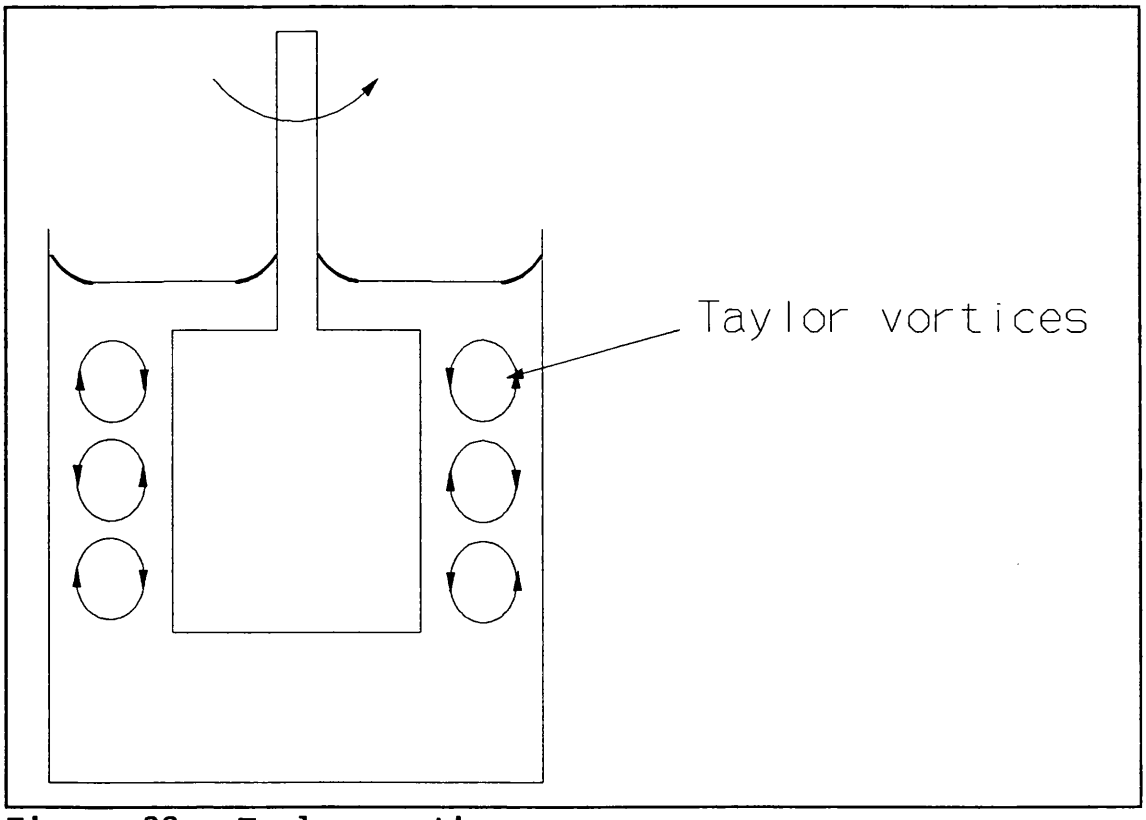

Figure 28: Taylor vortices.

outwards. Since it cannot do this en masse it circulates outwards locally forming Taylor vortices [91]. According to Schlichting [92], these vortices cause an increase in applied torque at a given rate of rotation, see figure 28.

If the outer cylinder rotates instead of the inner one, centrifugal action stabilises flow, and the maximum speed of rotation attainable without turbulence, for a given fluid, is considerably higher. Unfortunately, the cooling system on this particular geometry of concentric cylinder viscometer is highly complex.

As a sample of fluid can be sheared indefinitely in rotational viscometers temperatures often rise because of shear heating. Temperature changes can have significant effects on the rheological properties of the fluid. For Newtonian fluids corrections can be made to allow for such heating, however, Weltmann and Kuhns [93] state that for non-Newtonian systems accurate corrections are difficult. Therefore, the method of cooling in the viscometer must prevent any increase in temperature in the test fluid. The simplest method for accurately controlling the temperature of the sample in a concentric cylinder viscometer is to immerse the outer cylinder in a water bath (a liquid thermostat). This is considerably easier when the outer cylinder does not rotate.

In the theory it is assumed that the fluid adjacent to a metal surface moves with the velocity of that surface. A velocity difference can occur through slippage [94, 95 and 96]. Slippage takes place for several reasons: an oil film forms at the fluid-metal interface; the bonding surface alters the properties of the fluid under test, either, by causing alignment of polymer molecules, or, by a local reduction of concentration of suspended particles.

Often workers have used grooved or cross-hatched metal surfaces if slip was anticipated to prevent its occurrence. Wittler et al [90] used a Contraves Rheomat 115 with a modified co-axial cylinders for studying *Penicillium chrysogenum*. The inner surface of the outer cylinder and the outer surface of the inner cylinder were

ribbed with equidistant vertical grooves. A similar technique was also used by Tangsathitkulchai and Austin [97] for observing the rheological properties of concentrated particle slurries.

Vocadlo and Charles [98] stated that the yield stresses quoted in many papers are unsatisfactory because of slippage, to overcome this problem he describes a complex rheological apparatus.

Calibration of all rotational systems can be achieved by replacing the viscometer rotor with a drum, round which is wound a thread which passes over a pulley and supports a known load. A symmetrical system with two loads prevents undesirable side thrusts on the instrument bearings. In many cases Newtonian fluids of known viscosity are used to provide a calibration of the viscometer.

Most viscometers use a rather weak restoring spring so that large, easily measured, angular deflections occur; this is known as the soft torque system. In consequence they may give misleading results if readings are attempted after only short periods of rotation. After a small amount of shearing there is little deflection. Only after a longer period does the spring reach the equilibrium position when the shear rate is proportional to the angular velocity of the instrument. The alternative form of measuring system is known as the stiff torque system. Just such a system is described by Higma [99], this consists of a torque-sensitive crystal transducer and a torsion bar. Because of the small movements incumbent with such a system, the mechanism must be extremely accurate and will need regular calibration.

1.3.7.2 Cone and plate viscometer.

This type of rotational instrument is widely used because of ease of use. The reason for its popularity relies on the fact that the shear rate through out the fluid under test is approximately constant, as long as the cone angle is small (less than 3 degrees). Thus, shear

stress and shear rate values can be easily calculated using equations (33) and (34).

$$\tau = \frac{3.M}{2.R^3} \qquad (33)$$

$$\gamma = \frac{\Omega}{\theta} \qquad (34)$$

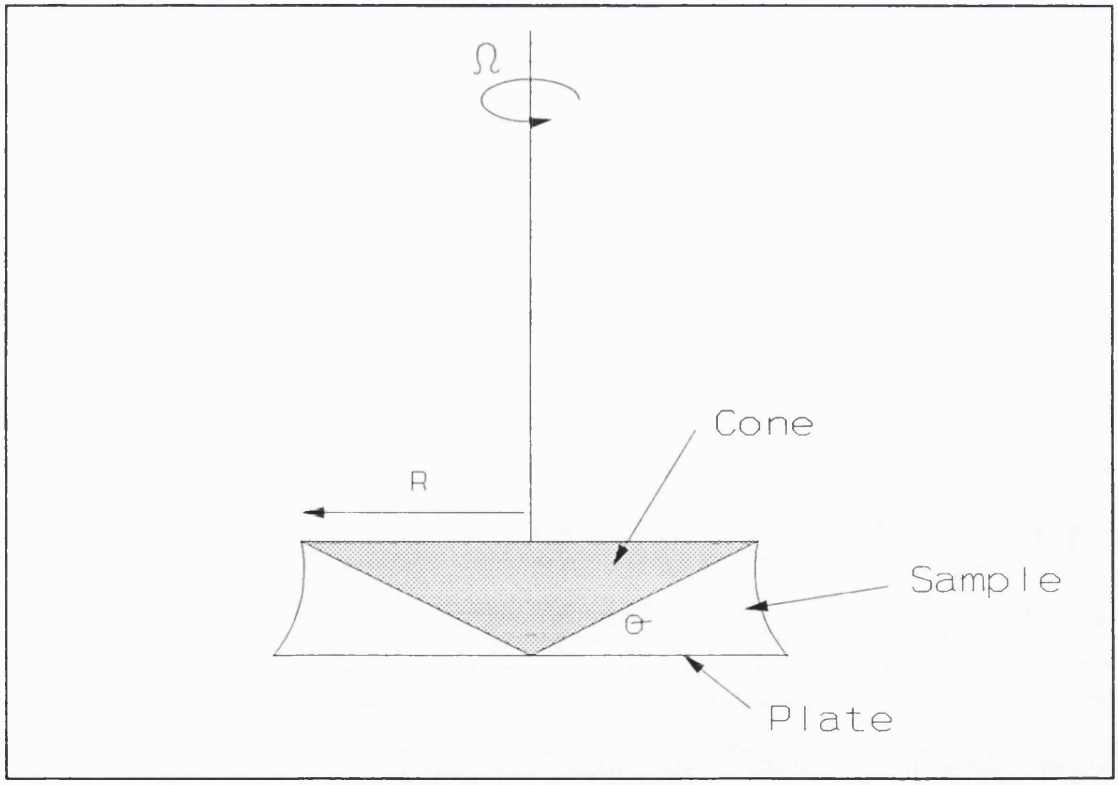

Figure 29: Cone and plate viscometer.

A Cone and Plate viscometer shears a fluid sample in the small angle between a flat surface and a rotating cone whose apex just touches the surface, see figure 29.

While cone and plate systems have been used extensively to study non-Newtonian fluids, their use in the study of rheological properties of suspensions and culture broths has been minimal. The reasons for their limited use are many. Charles [2] believed he observed phase separation near the rotating cone when suspensions were

under test, although not as pronounced as in the case of Couette viscometers. Another widely reported problem [100] is the tendency for particles, in the suspension, to be of the same order of magnitude as the gap, resulting in the destruction of the particles during measurement or the impairing of accurate readings.

1.3.7.3 Impeller viscometer.

While standard rotational viscometers are versatile, reliable and widely used, they are said to encounter many problems when used to study fermentation broths, particularly mycelial broths. These difficulties, according to Kemblowski and Kristiansen [73], result from the fact that broth is not a homogenous liquid, tending to be coarsely dispersed and unstable. The results obtained using the viscometers outlined so far on such fermentation may be of limited value because of one, or several, of the following:

a) Gravity settling of the suspended particles.
b) Other forms of phase separation, especially the formation of less dense layers next to the rotating surface.
c) Large particles, in the suspension, of the same order as the measuring gap of the instrument. This causes destruction of the particles in the shear field and impairment of accurate measurements.

Tube viscometers require large diameter pipes in order to cope with 3, and 1 and 2 may still be significant, according to Roels et al [1] and Bongenaar et al [100].

Charles [2] illustrates the problems encountered. Figure 30 shows a graph plotting Brookfield viscometer scale readings (proportional to viscosity) as a function of time at a speed of 30rpm, for a 1% (w/v) *Aspergillus niger* culture broth. From the graph it can be seen that the readings tend to decrease with time, appearing to indicate thixotropic behaviour. However, careful observation of

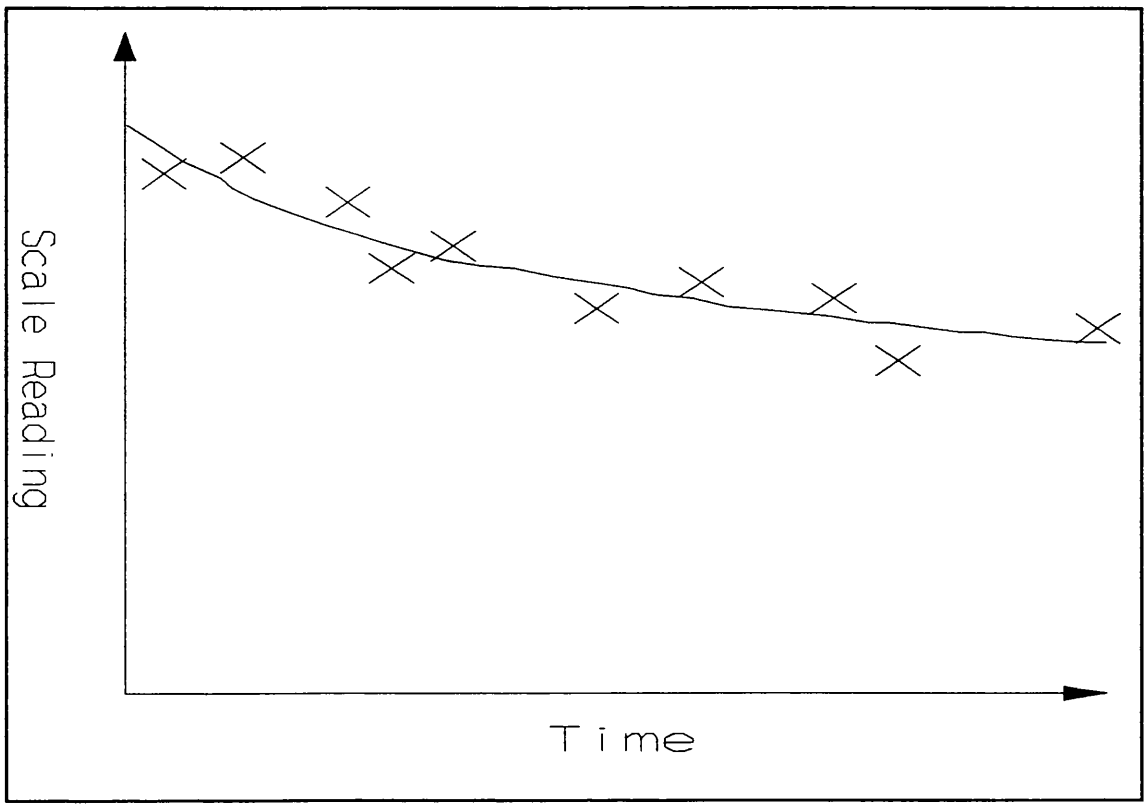

Figure 30: The effect of settling.

the sample reveals partial settling and also phase separation near the rotating spindle are responsible.

To prevent gravity settling whilst using a rotational viscometer system, Tangsathitkulchai and Austin [97] used organic liquids of similar densities to the solids present in the test fluid to prevent gravity settling. Whilst organic fluids may have no effect on the coal and quartz used in this work, they certainly will have an considerable effect on the cells of the microorganisms, hence such a technique cannot be used.

A more practical way of circumventing the experimental difficulties has been suggested by Roels et al [1] and Bongenaar et al [100]. They used an impeller viscometer which was shaped like a small Rushton turbine. This type of instrument avoids particle trapping and sedimentation problems. The flow field, at least qualitatively, is reminiscent of the flow field inside a standard fermenter and therefore should produce data of more relevance than the other viscometer systems previously described. Such a system was successfully used by Cooke et al [101] to show

similarities between the rheological characteristics of a paper fibre suspension and a filamentous fermentation.

Additionally, Kemblowski and Kristiansen [73] have developed an impeller measuring system to their own design and a procedure for calibrating the system. The theory has been formulated from the earlier work of Bongenaar et al [100] and Roels et al [1]. The authors claim that their approach allows for a more precise presentation of the theory and eliminates 'obvious' errors in the other impeller systems.

However, Björkman [80] states that impeller systems do have their drawbacks. The main obstacle is the constraint of a narrow shear range due to the requirement that the analysis must be completed under laminar flow conditions. Also, the turbine impeller establishes a relatively complex flow pattern which does not allow straightforward calculation of shear rate. Hence, there is doubt over the significance of the calculated viscosities. Charles [2] suggests that the instrument does not satisfy the requirements for measuring viscosity as defined formally and hence it is not clear whether any calculated quantity is an intrinsic property of the fluid. He states that the instrument maybe regarded as a 'practical' viscometer providing data that does not necessarily correlate simply or directly with viscosity.

Also, because of the complex flow field established during measurement, a number of different phenomena will occur simultaneously. Deformation-rate-dependant rheological phenomena will be either blurred or sometimes evened out.

Björkman [80] pointed out that the impeller rheometer is better suited for standardized routine measurements than conventional rheometers because of reduced operating problems and the internally consistent data produced.

Roels et al [1] provides the principle behind the measurement of viscosity using an impeller system. For a Newtonian fluid in a baffled mechanically agitated vessel the power consumption is normally expressed as:

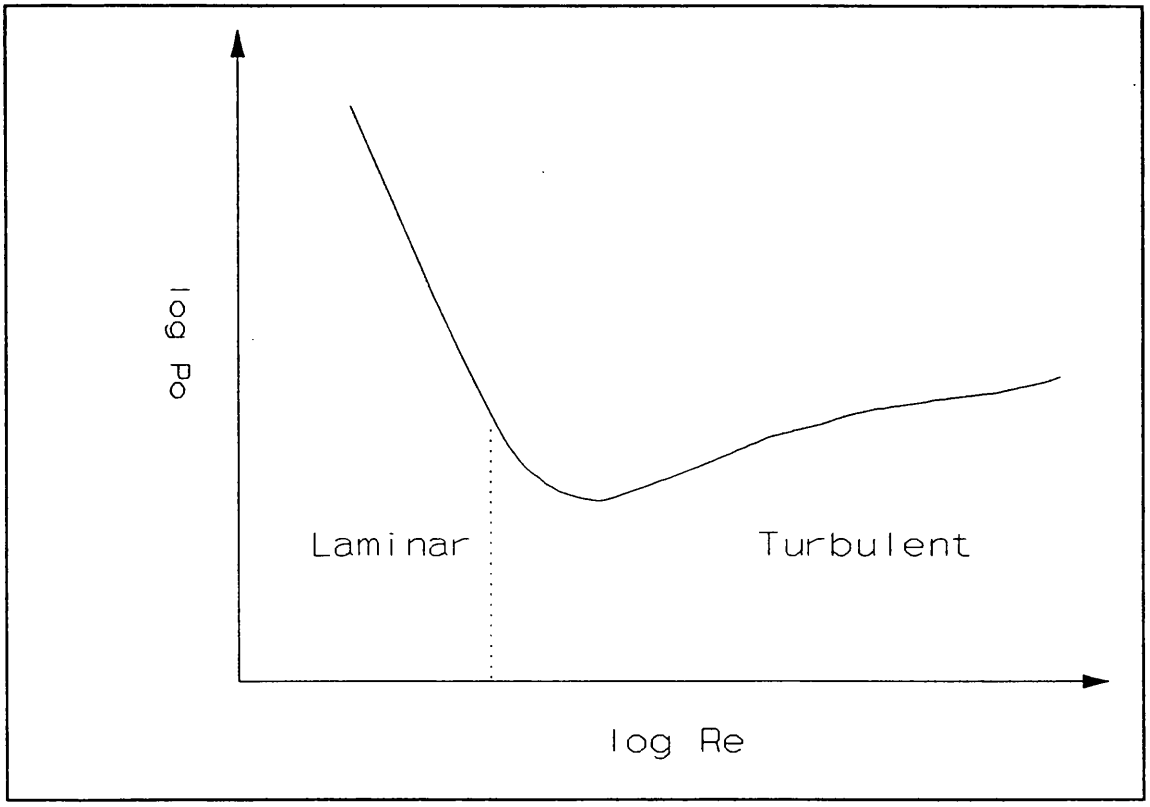

Figure 31: The laminar flow region.

$$P_o = fn\ (Re) \tag{35}$$

where;

$$P_o = \frac{P}{\rho . N^3 . d^5} \tag{36}$$

$$Re = \frac{\rho . N . d^2}{\mu_a} \tag{37}$$

P - power consumption (N.m/s).
P_0 - power number (-).
ρ - density of liquid (Kg/m^3).
N - impeller speed (1/s).
d - impeller diameter (m).
μ_a - apparent viscosity (Pa.s).

In the laminar region, see figure 31, the functional

relationship in equation (35) becomes:

$$P_o = \frac{K_p}{Re^{\beta}} \qquad (38)$$

Most investigators have provided a value of β equal to -1 in the laminar flow region.

For a non-Newtonian liquid with a shear dependent viscosity the Reynolds number is defined in terms of the apparent viscosity, μ_a, at a particular shear rate. Equation (38) can now be written as:

$$P = K_p . \mu_a . N^2 . d^3 \qquad (39)$$

The relationship between the power consumption and torque, M, on the stirrer is given by:

$$P = 2 \cdot \pi \cdot N \cdot M \qquad (40)$$

M - the torque (N.m).
from (38) and (39):

$$M = \frac{K_p \cdot \mu_a \cdot N \cdot d^3}{2 \cdot \pi} \qquad (41)$$

Assuming, the shear rate constant, k_s, is independent of the rheological characteristics of the liquid [2 and 65]. A comprehensive definition of k_s is provided overleaf.

Equation (41) suggests that for a given impeller speed, N, a measurement of torque, M, can give a value of apparent viscosity, μ_a, provided the magnitude of the impeller constant K_p is known. The impeller constant ,K_p, is a function of the impeller and vessel geometry and may be obtained experimentally. In the experimental work conducted in this thesis five different impellers were used; two, four, six and eight bladed vane impellers and a helical ribbon impeller (HRI). The K_p values for all these impellers were obtained experimentally and are given

in chapter eight.

In order to obtain a flow curve for a non-Newtonian fluid using an impeller viscometer it is necessary to obtain a relationship between the shear rate occurring in the vessel and the rotational speed of the impeller. Metzner and Otto defined an average shear rate, γ_{av}, in the vessel based on the following relationship:

$$\dot{\gamma}_{av} = k_s.N \qquad (42)$$

where the shear rate constant, k_s, is a function of impeller type and has a value of 10-15 for standard impellers such as turbines and propellers.[68] For any value of N the average shear rate can be calculated using equation (42).
Combining equation (42) with the viscosity definition equation i.e.

$$\tau = \mu_a \cdot \dot{\gamma}_{av} \qquad (43)$$

Gives:

$$\tau = \mu_a \cdot (k_s \cdot N) \qquad (44)$$

Using equation (40) to replace μ_a in equation (37) and re-arranging the resulting expression gives;

$$\tau = \left[\frac{2 \cdot \pi \cdot k_s}{K_p \cdot d^3}\right] .M \qquad (45)$$

In equation (45) the term in the bracket is a system constant, C, thus:

$$\tau = C \cdot M \qquad (46)$$

For any value torque the shear stress, τ, can be calculated using equation (46) and knowing the value of the shear rate

constant k_s and the impeller constant, K_p. Thus the flow curve (a plot of shear stress against shear rate) may be obtained from a series of measurements of rotational speeds and corresponding torques, given that laminar flow conditions exist in the vessel.

Roels et al(1), Bongenaar et al [100] and Reuss et al [102] used turbine systems for the viscosity measurement of *Penicillium chrysogenum* broths. Allen and Robinson [79 and 103] used similar systems for *Aspergillus niger* fermentation broths.

Charles [2] cites an on-line turbine impeller system. This was achieved by reducing the agitator speed in the fermenter to ensure laminar flow and then measuring power input as a function of agitator speed. They claim the *S. niveus* fermentation broth exhibited shear thinning behaviour characterised by a Power law relationship. However as the fermenter only allowed shear rates over a third of a decade the correlation is by no means incontrovertible.

For low viscosity fluids a modified impeller viscometer is recommended; the torsion wire viscometer, see figure 32. The value of torque is determined from the angle of rotation of the floating assembly, the torsion wire constant and geometry, and the stirrer speed.

Rapp and Wagner [104] used an anchor impeller to measure the degradation of cellulose in cultures of *Cellulomonas uda* grown on printed newspaper. This type of impeller was chosen because of its wider range of shear rates compared with the turbine impeller. Unfortunately, the system used proved to be insensitive to changes in torque, presumably because of the torque sensor used.

The use of equations (42) and (45) to obtain the flow curve for a non-Newtonian fluid does not require any assumption about the rheological nature of the fluid. Most fermentation broths appear to be shear thinning in their flow behaviour and over a limited range of shear rate their rheological characteristics can be described by a

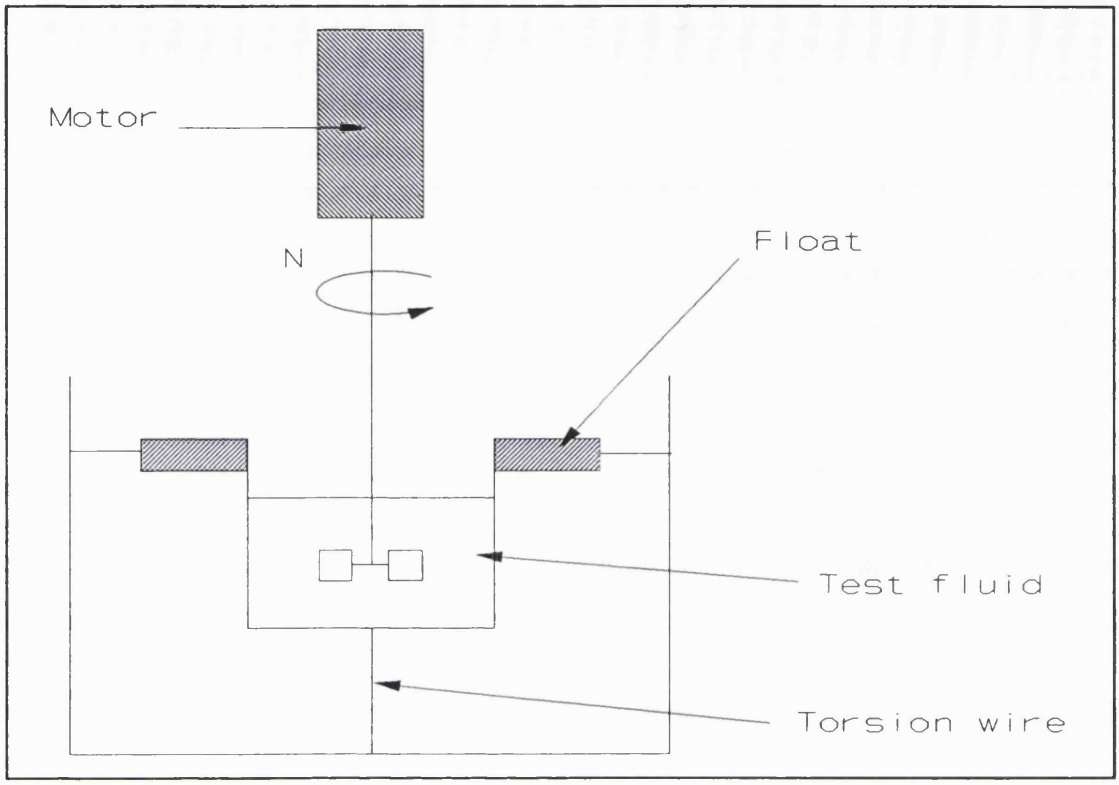

Figure 32: Torsion wire viscometer.

Power law relationship thus;

$$\tau = K \cdot \dot{\gamma}^{n} \qquad (47)$$

For any impeller viscometer the shear rate, γ, in equation (47) is replaced by the average shear rate, γ_{av}, and hence the shear dependent viscosity can be expressed as;

$$\mu_a = \frac{\tau}{\dot{\gamma}_{av}} = K\,(\dot{\gamma}_{av})^{n-1} \qquad (48)$$

In the laminar flow regime an alternative expression for the apparent viscosity, μ_a, can be obtained form equation (39). Making this expression equal to equation (48) gives;

$$\frac{P}{K_p . N^2 . d^3} = K(\dot{\gamma}_{av})^{n-1} \qquad (49)$$

substituting for P in equation (49), using equation (40)

results in;

$$\frac{2.\pi.M}{K_p.N.d^3} = K(k_s.N)^{n-1} \qquad (50)$$

from which the expression for torque, M, can be written as;

$$M = A.N^n \qquad (51)$$

and hence;

$$A = [\frac{K_p.K.d^3.k_s^{n-1}}{2.\pi}] \qquad (52)$$

By presenting the experimental data in the form of torque, M, as a function of rotational speed, N, it should be possible to evaluate the shear rate constant k_s provided the impeller constant K_p is known.

Kemblowski and Kristiansen [73] used their impeller viscometer (6 vane turbine) to analyse samples from a *Aureobasidium pullulans* fermentation broth and confirmed the applicability of this procedure.

In order to follow more closely the changing rheological properties of a broth during the course of the fermentation, Kemblowski and Kristiansen modified their original design to run on-line giving continuous rheological measurements [105 and 106].

Kemblowski and Kristiansen's basic design has been used by other researchers [69] to measure the rheology of concentrated suspensions.

1.3.7.4 Helical ribbon impeller viscometer.

Since any type of impeller gives a system specific result, the question arises whether a turbine or vane impeller is the most suitable agitator for the task. Metz et al [107] suggested that such turbine impeller systems may not completely prevent the gravity settling of the mycelium during measurement. Additionally, the use of a vane or turbine impeller means the range of shear rates involved are quite narrow since laminar conditions must be maintained. The viscosity model obtained may not be relevant under actual fermentation conditions because it is only valid over a limited range of shear rates and extrapolation is always hazardous. Hence, it appears that an impeller with superior mixing capability in the laminar flow region would be preferable. Furthermore, measurements over a wider range of shear rates should be possible. Kim et al [108] suggested that the range of Reynolds number attainable for the laminar flow region is about ten times greater with helical ribbon impeller compared with the turbine impeller used by Metz et al [107]. Thus, Reuss et al [102] chose helical ribbon impellers. Since mixing time with such impellers is known to be constant over a wide range of viscosities they should provide a more homogenous suspension as well as more uniform shearing conditions. In their papers Reuss, and also Allen and Robinson [79] measured the rheological properties of both *Penicillium chrysogenum* and *Aspergillus niger* with turbine and helical ribbon impellers. Both stated that the shear measurements from the turbine viscometer were significantly higher than those from other viscometers studied. Allen suggested that this effect resulted from a failure in the assumption that the average shear rate in this type of viscometer is proportional to the impeller speed and independent of the fluids rheological properties.

1.3.8 Other viscometers.

The following systems are considered viable methods for the determination of viscosity in filamentous fermentation broths, however, very little information exists on their use in this or a similar capacity.

1.3.8.1 The Convimeter.

The measuring principle of this system is as follows: a drive motor imparts a circular movement on the sensing device in the fluid being monitored. Due to a bend in the lower part of the drive shaft, the sensing device holds an inclined position and hence follows a gyratory path. The torque transmitted by the shaft is proportional to the viscosity of the fluid and detected by a metering spring. Rapp et al [104] used the device to continuously measure the cellulose degradation of a culture of *cellulomonas uda* grown on printed newspaper. The system is completely sterilizable.

1.3.8.2 Vibrating rod viscometer.

Picque and Corrieu [109] have attempted to resolve the difficult problems of on-line viscosity determination by the use of a vibrating rod sensor mounted in a bioreactor. The system works by the excitation of the rod under constant conditions with an electromagnet. The damping of rod vibrations by the viscosity of the liquid medium in which it vibrates is measured, vibration amplitude decreases as the viscosity of the medium increases. Electronic processing of the damped vibration phenomenon enables it to be translated in to a normalized voltage and related to viscosity. Electronic filtering of the signal damps the interfering effects of aeration and mechanical agitation.

The authors point out that the advantages of such a system are on-line capability, easy installation (fits most

fermenter fittings), thus overcoming the need for the external circulation loops as used by many authors, completely sterilizable within the fermenter due to its stainless steel construction and it will reliably maintain the asepsis of the bioreactor.

Unfortunately, the instrument is completely empirical; relative viscosity values only being obtained by reference to a calibration curve. The authors supplied no theoretical basis to their viscometer.

The calibration curve demonstrates the non-linear decrease in sensor signal with increased apparent viscosity. Hence, the sensitivity of the measurement depends considerably on the broth viscosity. The geometry of the instrument and its excitation frequency are at an optimum over a narrow viscosity range. Thus the geometry and dimensions should be designed on the basis of a specific fermentation.

Although this system has not been evaluated on a filamentous fermentation broth; it appeared to correlate well with a concentric cylinder system (Contraves Rheomat 30) when used to measure viscosity in a Xanthan fermentation.

1.3.8.3 Falling ball viscometer.

One method that may be used for rheological characterisation which is particularly useful at lower rates of shear, is the falling ball viscometer. The terminal velocity of a spherical particle is determined and the effective viscosity of the fluid is calculated by using Stoke's law.

2 Materials and methods.

2.1 Rheology.

Although a Brookfield viscometer was predominately used for this project, initially a Contraves system was used in parallel to validate the data produced by the Brookfield.

2.1.1 The Contraves Rheomat 115.

The Contraves has been used for many years as a research viscometer [73] because of an extensive shear rate range, high accuracy and the application of standard-geometry measuring heads. The Contraves is a rotational viscometer capable of utilising cup and bob, cone and plate and concentric cylinder systems. Both the cup and bob and the cone and plate systems have a range of dimensionally similar, incrementally sized geometries to allow measurements on fluids of widely differing viscosities. Whilst the concentric cylinder system is used only for ultra-low shear rate measurements, the other systems are used for general applications and are essentially interchangeable. The broths investigated in this work, typical of most industrial broths, were based around complex-media recipes. The particle sizes in complex-media can vary considerably, but the broths investigated in this work contained fragments up to 2mm in diameter. The Cone and Plate apparatus should only be used on broths containing particles smaller then its annular gap [52]. If the annulus was of a similar magnitude to either the media particles or the aggregated organisms then these bodies may become trapped or destroyed, so producing erroneous data. Because of the size of the media particles in the investigated fermentation broths, the use of a Cone and Plate system was deemed inadvisable. Since extremely low shear rates were not of particular interest there were no benefits in using the coaxial cylinder system. Hence, the

bob and cup apparatus was chosen for use in this work.

The Contraves uses the Searle principle of operation [110] for coaxial measuring systems. Hence, the inner cylinder or bob rotates at a defined speed. The outer cylinder or cup is held at rest. The rotating inner cylinder forces the liquid in the annular gap to flow. The resistance of the liquid to being sheared between the stationary and rotating sections results in a viscosity related braking torque. This torque works on the inner cylinder and counteracts the torque provided by the drive motor. A torque sensing element, in the Contraves a deflecting torsion bar, is situated between the drive motor and the shaft of the inner cylinder. The deflection in the torsion bar is related to the viscosity of the fluid sample. The torsion bar in the Contraves is considered a stiff torque measuring system. The use of the Searle rather than Couette system [110] allows for the provision of temperature control through a heating/cooling jacket around the outer cylinder. Good temperature control is required for any viscosity measurement because temperature is a strong function of viscosity.

Contraves supply four sizes of bob and cup measuring systems. These are coded 108, 114, 125 and 145. These configurations are dimensionally similar and conform to the D.I.N. 53019 specification. By providing a range of measurement head sizes the Contraves can be used to measure the rheological characteristics of fluids with a considerable variation in viscosity. The 145 system, the largest of the four, produces the highest torque reading for a given apparent viscosity, whilst the 108 system, the smallest, can be used to measure extremely viscous fluids, at which the larger sizes would produce off scale readings. The choice of measuring head was determined during the control experiments, see chapter three.

2.1.1.1 Preparation.

Figure 1 shows an exploded view of the sample holder

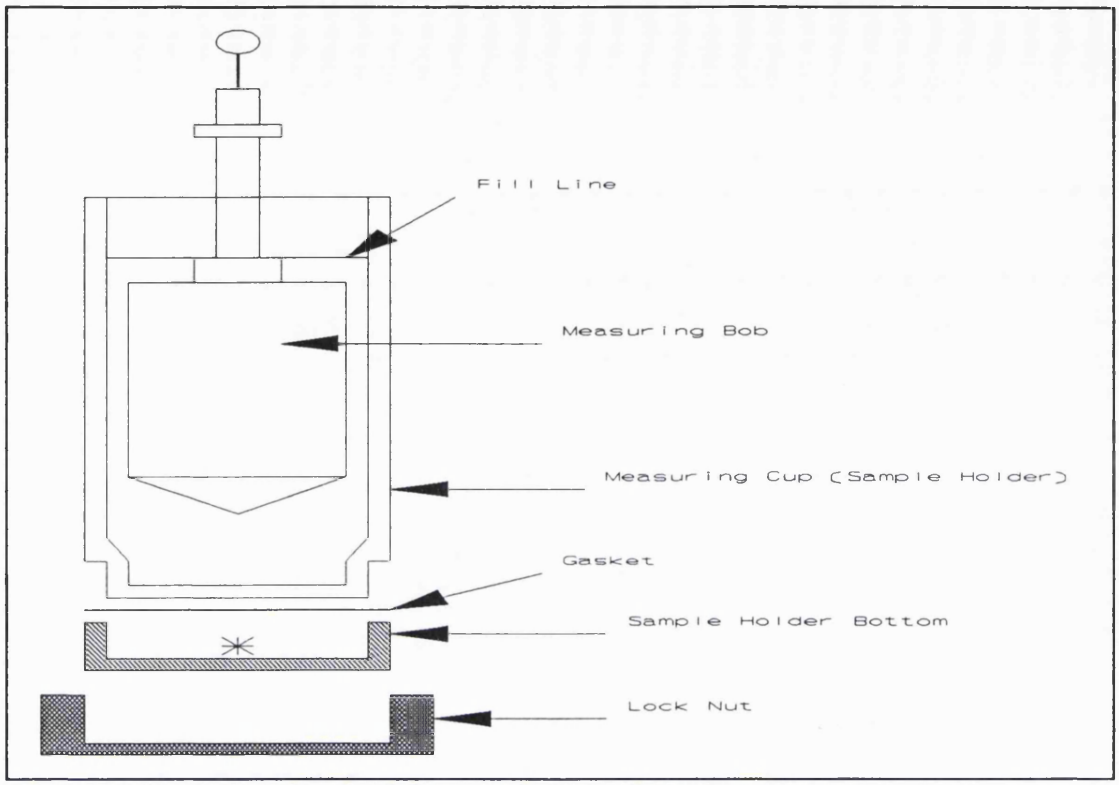

Figure 1: Sample holder and bob for Contraves.

from the Contraves viscometer. The sample holder bottom had to be screwed onto the measuring cup ensuring that a P.T.F.E. gasket was positioned correctly and undamaged. The use of a lubricant, such as high vacuum grease, on the screw threads ensured smooth and leak-free couplings. The measuring bob, or any desired rotor, could then be placed into the measuring cup. The fluid under examination was then poured carefully, to minimise air-entrainment, into the cup until the fill line level was reached.

Figure 2 shows the configuration of the Contraves system. The sample holder was slid into the stand from below and held in place by the lock nut. Only a quarter-turn was required to fasten the lock nut and secure the sample holder.

Before analysis could continue a series of checks had to be performed. Figure 3 shows detail of the Contraves stand and associated equipment. The stand was connected through a pump to a water bath. The water bath was of the thermostatically-controlled type; whilst a heater and thermocouple ensured the water was kept at a constant

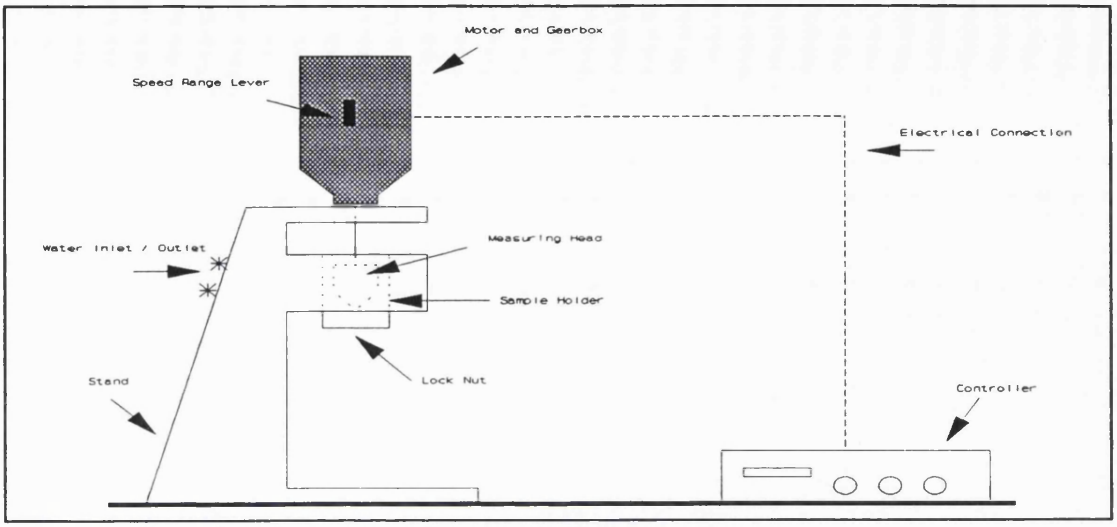

Figure 2: Contraves viscometer system.

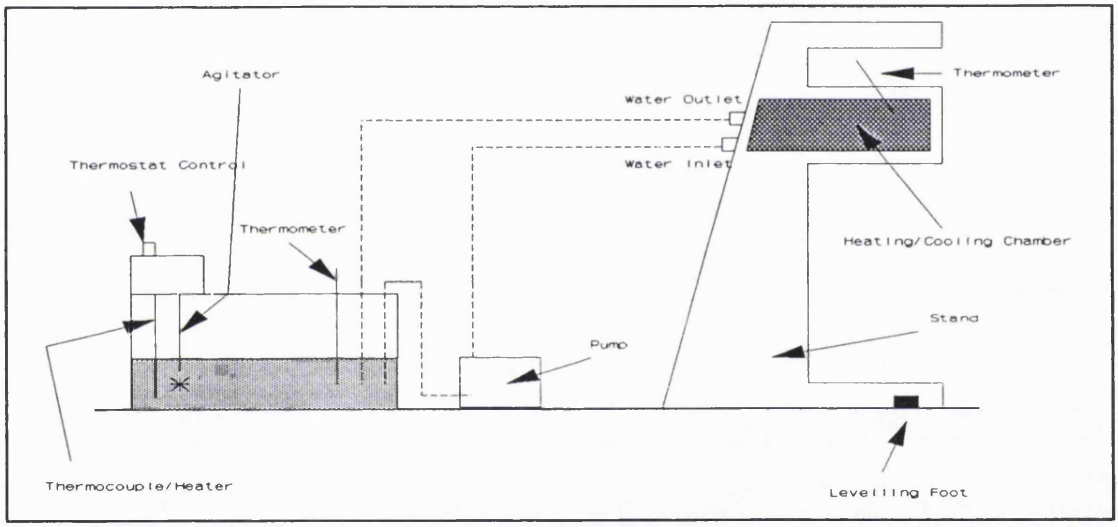

Figure 3: Cooling system for Contraves

temperature, an agitator ensured the temperature was uniform throughout the bath. A thermometer was used to confirm the set temperature was maintained to ±0.5°C. The water from the bath was circulated through the heating/cooling chamber in the stand using a centrifugal pump and silicon tubing. The pump speed was fast enough to limit cooling of the water as it passed from the bath to the stand to an acceptable level. A period of at least 30 minutes was always allowed for the heating/cooling system to reach equilibrium; at which point the thermometer in the stand gave a stable reading of 20°C +/- 0.5°C. Once equilibrium was reached the rheological measurements began.

The water bath was used for storage of the samples and the viscometer rotor prior to measurement. This ensured that all the elements required for a viscosity reading were at exactly the same temperature. The rotor was thoroughly dried before any measurements were taken.

Also shown in figure 3 is the levelling foot on the Contraves stand. This foot was screwed upwards or downwards until the stand acquired a horizontal position; this required the use of a spirit-level.

The motor/gearbox unit was placed onto the stand; the unit fitted securely into a countersunk hole in the top of the stand. The rotational position of the unit had no influence on the readings obtained, but the orientation shown in figure 2 was found to be satisfactory.

The viscometer was now ready to be zeroed. After actuating the mains switch on the control panel and setting the low pass filter to number three, the display panel produced an arbitrary reading. By turning the knob, positioned directly to the right of the display panel, the display was manipulated until a reading of +/- 0.00 was obtained. The motor was activated by pressing the motor switch. Pressure was applied to the universal coupling to obtain a torque reading; the use of the thumb and forefinger prevents de-centralisation of the driveshaft. Once the pressure was released the torque reading should drop back to zero, if not, the zeroing process was repeated.

The measuring bob could now be connected to the motor/gearbox unit. Figure 4 shows detail of the universal coupling. The sleeve was carefully pulled upwards thereby allowing the male section of the coupling, on the bob, to be inserted into the female universal coupling. See figure 4b. When the sleeve was then restored to its lower position the bob was locked in place. Particular care was taken to ensure that the bob was centralised correctly otherwise erroneous torque data could result.

The measuring bob and the universal coupling had to be

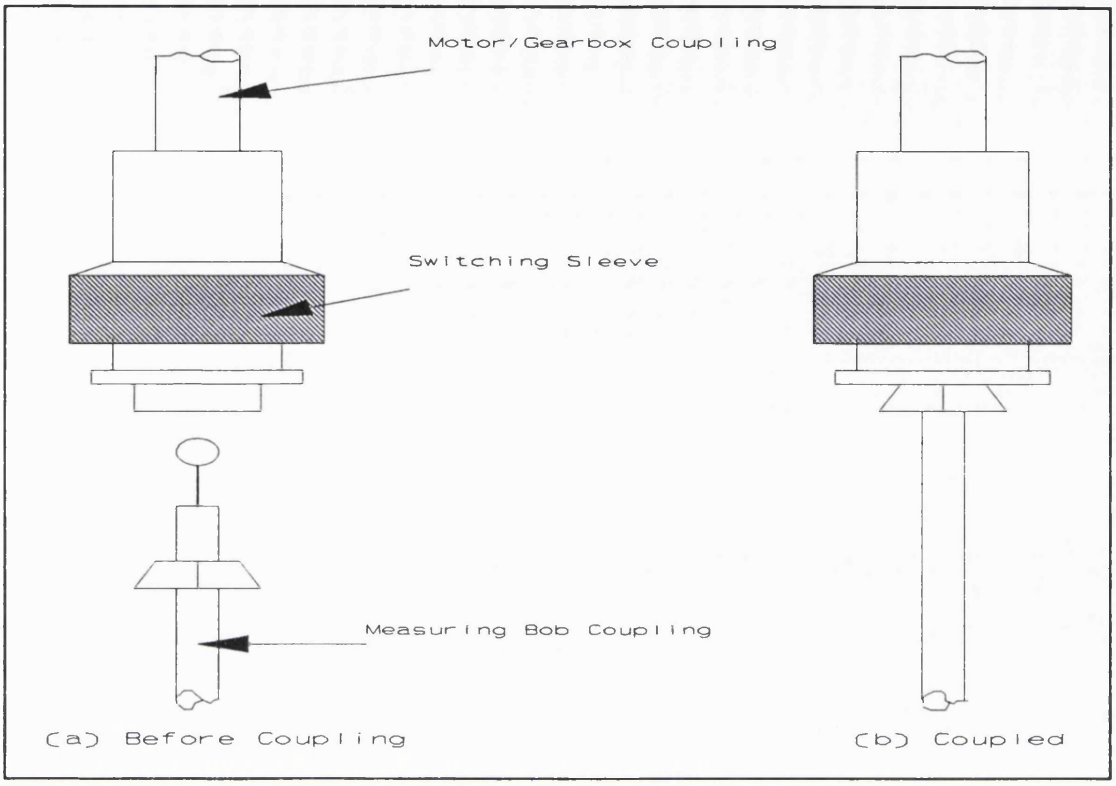

Figure 4: Bob coupling mechanism for Contraves.

correctly aligned before proper location could occur. By turning the bob slowly whilst offering it up to the universal coupling this particular arrangement could be found. This process had to be undertaken as gently as possible since any hefty movements might have ruined the zeroing. Once coupled there was no method for re-zeroing. If, for any reason, excessive force was used during coupling it would be wise to start the zeroing process again.

2.1.1.2 Analysis.

A rheological characterisation using the Contraves took about thirty minutes. The speed range lever on the motor/gearbox unit was set to the '100' position. Using the speed setting buttons, see figure 5, the speed step was set to one. Simultaneously, the motor button and a stop clock were activated. The readings were taken at a set time interval to allow the torque reading to reach a point of equilibrium; this period was called the 'equilibration

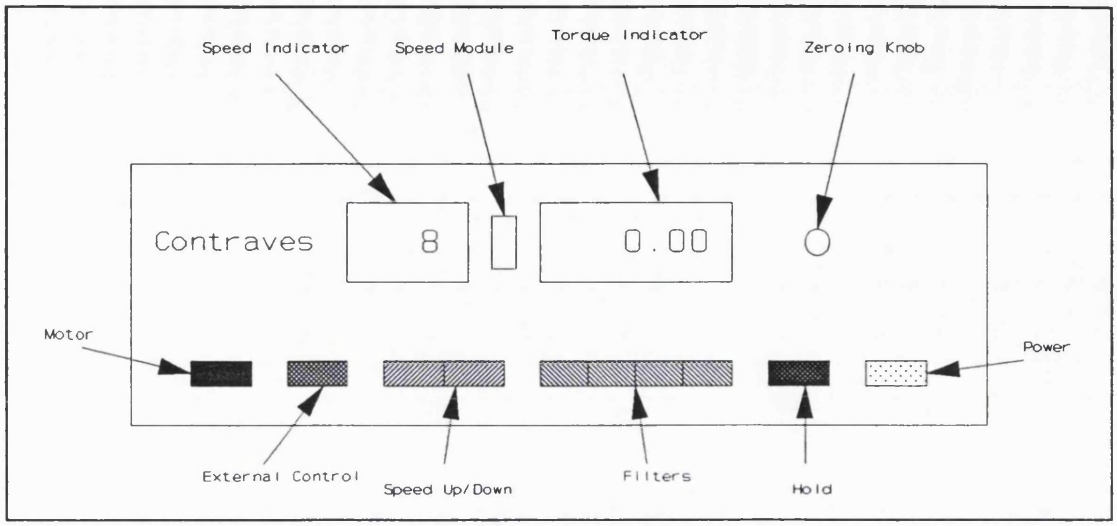

Figure 5: Control panel for Contraves.

time' (ET). After the desired ET the torque reading on the display indicator was recorded and the speed increased by one step to position two. This process was repeated until the final speed step, number thirteen, was reached; at this stage in the analysis the speed range lever had to be flipped to obtain a further set of higher rotation speeds. Once the torque reading at position thirteen had been recorded the following procedure was employed:

a) the motor was stopped.
b) the speed step was set to one.
c) the lever was turned to the 'N' position.
d) the motor was started 15s after initiation of (a).

After (c) the universal coupling was swivelled slightly to ensure the cogs in the gearbox meshed correctly.

The process continued as before. When the maximum rotational speed, position fifteen, was reached and the torque had been recorded, the subsequent torque readings were noted as the speeds were lowered one step at a time; moving down through the N range and then the 100 range. To switch back from the N range to the 100 range was the reverse of the procedure outlined above. This procedure was derived during the Control experiments, see chapter three.

The data collected during the analysis procedure were

placed on a spreadsheet for conversion from torque readings (N.m) and rotational speeds (RPM) to the more useful rheological units of shear rates (1/s) and shear stresses (Pa).

The spreadsheet used was Lotus Corporation's Lotus 123. Details for the conversion of Contraves parameters to characteristic rheological parameters are supplied in the Contraves Rheomat 115 operating instructions [112].

2.1.2 Brookfield 2HAT DV II.

A second type of viscometer was used during this work. The Brookfield Synchro-Lectric viscometer has a reputation for flexibility, durability, ease of use and value for money; for these reasons it has seen considerable industrial use [111]. Pfizer Limited use a Brookfield viscometer as a worldwide standard. A second viscometer was required because of a considerable demand for time on the Contraves. Therefore work at the Pfizer site was undertaken using one of the modern Brookfield viscometers. These contemporary machines have the same durable design as the original Brookfields; but the addition of electronic torque sensing has allowed a digital display, autozeroing and an RS232C port for data logging and chart recording. By correlating the Brookfield and the Contraves rheometers together, the Brookfield data were verified against a machine of excellent repute and high accuracy.

The Brookfield viscometer is of the rotational type. The instrument is powered by a synchronous induction type motor that ensures speed of rotation will be constant. Power is transmitted through a gear train with either four or, as in this case, eight speeds depending on the model. A calibrated spring is attached between the gear train and the pivot shaft. The pivot shaft is driven by the transmission but the power is first transferred through the calibrated spring. The relative angle of the pivot shaft to the gear train is detected by a rotary variable displacement transducer and is shown as a percentage of

maximum torque on a digital display. The spring in the Brookfield is considered a soft torque measuring system.

The Brookfield viscometer was supplied with a set of five RV spindles. The spindles each had the same design of stem but differed in the size or shape of disc attached to the stem. These disc spindles were numbered one to five in order of decreasing disc size. The spindles were attached through an external coupling to the pivot mechanism. When the spindle was immersed in the sample fluid, a viscous drag opposed the forces of the motor. This drag was detected as a strain on the spring which registers on the digital read out. The spring is made of beryllium copper and pre-calibrated at the factory; this particular model, the Brookfield 2HAT DVII, had a spring with a full scale deflection of 287.5×10^{-5} N.m (28,748 dyne.cm) of torque. The choice of spindle was made during the control experiments, see chapter three.

2.1.2.1 Preparation.

Figure 6 shows the Brookfield system without a chart recorder.

An analysis using the Brookfield took about ten minutes to complete. The viscometer body housed a spirit-level; by adjusting the three screw feet on the bottom of

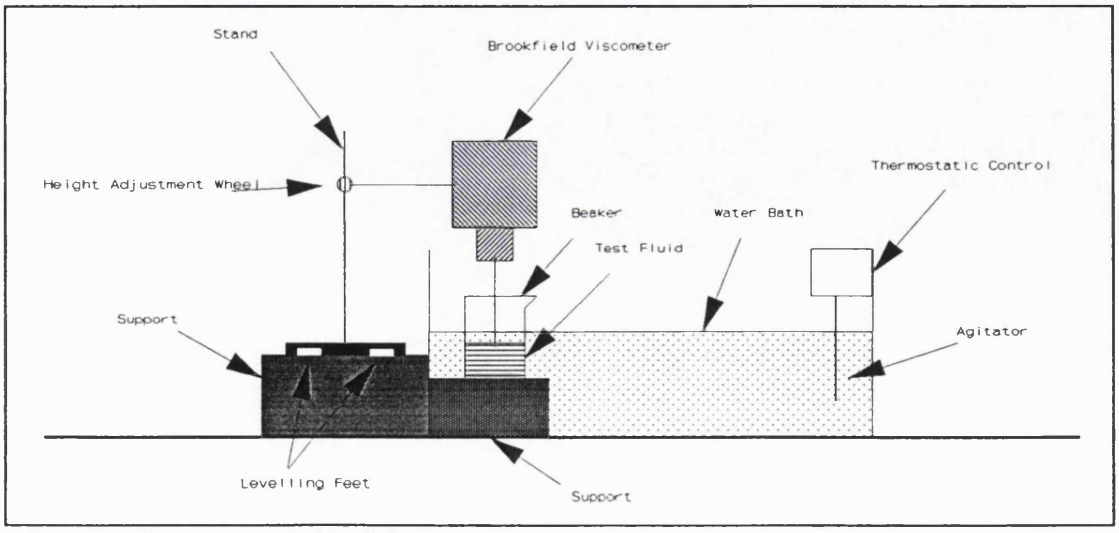

Figure 6: Brookfield viscometer system.

the Brookfield stand the viscometer could be levelled. An option available on the instrument was the attachment of a chart recorder allowing rates of changes in torque readings to be monitored continuously. Brookfield supply a recorder connection lead; the DIN plug end attaches to the viscometer, whilst the black and red wires at the other end connect to the 10mv positive and negative terminals respectively.

Figure 7 shows the control panel of the Brookfield viscometer. The 'power on' switch was flicked; the main

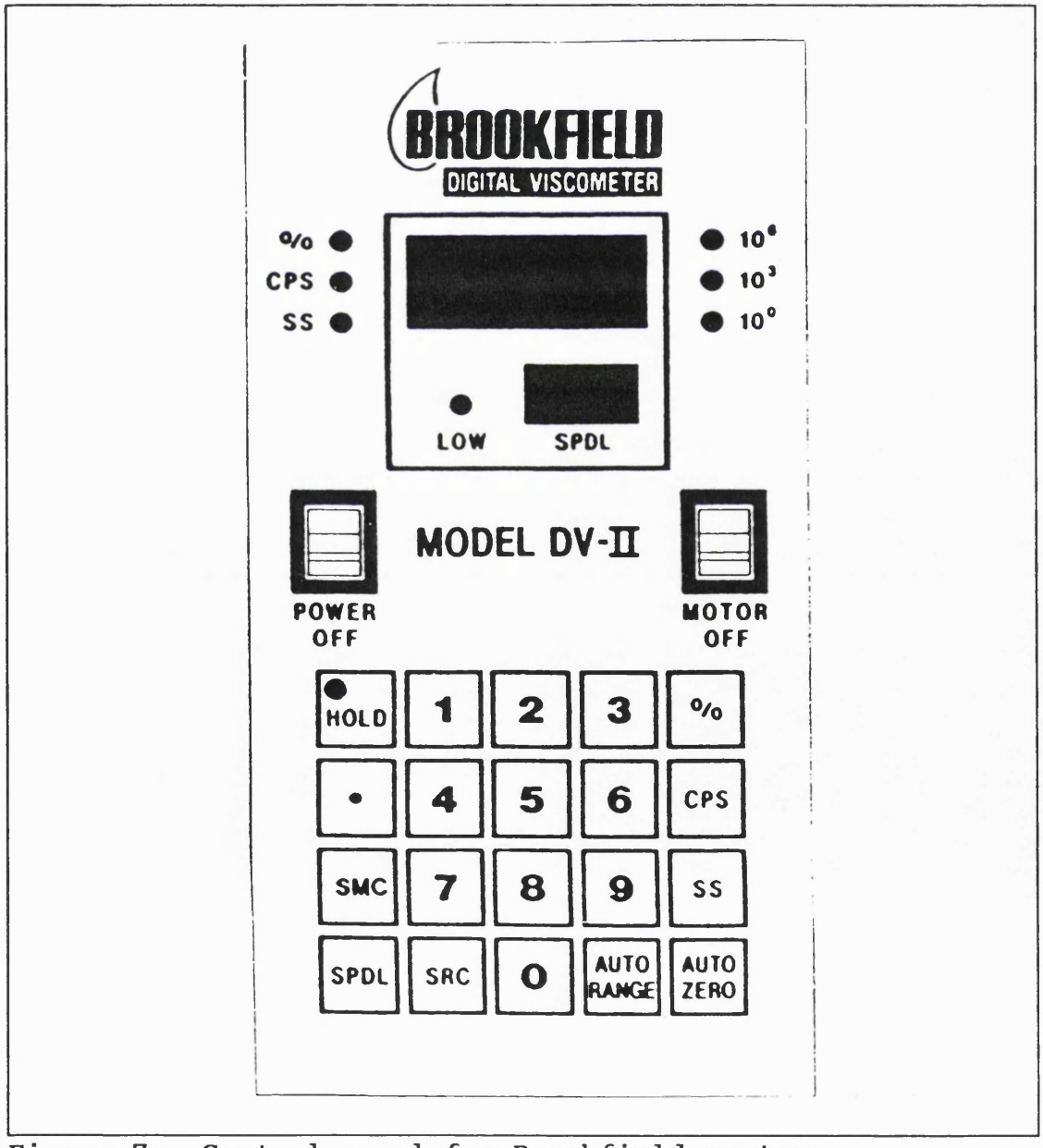

Figure 7: Control panel for Brookfield system.

display now read '___', whilst the spindle display showed 'EE'. The viscometer had to be zeroed. The motor switch was flicked on and the speed selector knob turned to indicate 10 RPM. The 'auto zero' switch was pressed thereby, zeroing the electronics and the shaft displacement pointer. The chart recorder, if required, was then zeroed. Note, the display now read '0.00' and the motor was off.

The sample fluid was poured carefully into a 500ml beaker to the level of the 400ml indication line. Care was taken to ensure no air-entrainment occurred. The beaker was placed on a support in the water bath, see figure 6. The water bath was maintained at a constant temperature to ±0.5°C. Since the sample storage flasks and the 500ml sample beaker were held in the water bath, prior to measurement no period of equilibration was required.

The Brookfield RV type 2 spindle was immersed at an angle into the sample fluid; by introducing the spindle to the fluid at an angle no air-bubble could become trapped beneath the spindle surface to cause erroneous data. The spindle was then attached to the driveshaft of the viscometer; a left-handed thread is used. The driveshaft had to be properly supported during this process by holding the shaft firmly with the thumb and forefinger; lateral forces on the shaft could result in premature deterioration of the bearings. The spindle was then raised or lowered, using the height adjustment wheel on the stand, so that the immersion groove on the spindle shaft coincided with the fluid's surface.

Before torque values could be measured the code for the particular spindle in use had to be entered; this allowed the internal microprocessor to calculate and display the particular rheological parameter selected by the operator. After pressing the spindle key, marked spdl, a universal code of double zero was entered. For the purposes of this work a reading of percentage of

maximum torque was wanted so the percentage key (the key marked '%') was then pressed.

2.1.2.2 Analysis.

The speed selector switch was set to 0.5 rpm. The stop clock and the motor were started simultaneously. Before the torque speed reading could be noted a period of equilibration took place. This equilibration time allowed the torque reading to stabilise. The length of the ET was determined during the Control experiments, see chapter three. After the torque reading had been noted the motor speed was increased. This process was repeated, up through the speed range to 100rpm and back down to 0.5rpm.

When the Brookfield viscometer was initially used in this project a 500ml beaker was used as suggested by the instruction manual [111]. However, subsequent experimentation revealed that 200ml of fluid in a 250ml beaker produced identical results. Since the broth supply was limited the smaller sample holder was used.

The recorded data were then transferred to a spreadsheet for conversion to more general rheological parameters. The calculations performed followed the work by P. Mitschka[113]. The work of Mitschka was verified and advanced by Williams [114].

2.1.3 Single point viscosity measurement.

Pfizer have a standardised procedure for the measurement of viscosity which is used in their production sites throughout the world. This method was used frequently in this project as a quantitative label to indicate a rheological difference between fermentation broths.

2.1.3.1 Preparation.

The viscometer used was the Brookfield LVF; this dial

reading model had eight speeds from 0.3 to 60 rpm, a specific set of spindles for the model and a torque spring with a maximum load of 6.74×10^{-5} N.m. Before analysis the viscometer was levelled using the spirit-level built into the casing.

The fermentation broth sample was poured into a 10 ml glass universal, care was taken to avoid air entrainment. The number three spindle was immersed at an angle into the broth, this action prevented an air bubble forming under the spindle. The spindle was then screwed to the viscometer's coupling, ensuring that the disc remains below the surface of the fluid. The spindle was centred in the glass universal to ensure that the sides of the disc do not touch the sample holder. The viscometer was switched to 60 rpm.

2.1.3.2 Analysis.

The viscometer motor was turned on and the spindle was allowed to rotate for ten revolutions. Then the pointer was clamped and the viscometer's motor turned off to enable the pointer reading to be taken. The Brookfield indication (in a range between 0 and 100) was multiplied by a factor of twenty to convert the reading to a value in centipoise; this factor was determined from Brookfield literature supplied with the viscometer.

2.2 Image analysis.

The image analysis system used was the Joyce Loebl Magiscan 2A. Although the system has been available for many years the fundamental theories on morphological analysis of filamentous microorganisms have remained almost unchanged. Hence, the modern generation of image analyzer tends to use the same procedures for measurement but at much faster processing speeds especially since the advent of parallel processing.

2.2.1 Sample preparation.

A flask of fermentation broth was again removed from storage after being used for a rheological analysis. One gram of the remaining broth was weighed onto a weigh boat. This broth was then washed carefully into a volumetric flask using de-ionised water from a wash bottle. The flask size was dependent on the dilution required. A small plastic funnel was used to ensure none of the sample was lost. Care was taken to wash all remnants of the broth from the weigh boat and the funnel. The volumetric flask was then filled to the meniscus mark using de-ionised water. To ensure uniform mixing, the stoppered flask was inverted several times.

The ideal dilution of the broth sample was assured by previously examining a range of dilutions during the control experiments, see chapter three. For the purposes of this section of work, the fermentation broth samples were assumed to have the same density as de-ionised water. Therefore, to make a one in fifty (1:50) dilution the one gram of broth would be aliquoted into a 50 millilitre volumetric flask. By examining the microscope slides prepared at various dilutions, a qualitative assessment was made on the following grounds:

1) The concentration of microorganisms present.
2) The amount of hyphal overlap between organisms.
3) The amount of debris present.

The slides needed a high concentration of microorganisms, at least five per field, to ensure a reasonable number of measured objects per field. If the concentration was too low the amount of time spent image analyzing became excessive. If the concentration was too high then the excessive hyphal overlap meant that either these objects were rejected due to clumping, or worse, the analyses will assume the objects to be a single entity and produced erroneous data. The debris present including ghost organisms (cell walls without any contents), dust, and dye particulates varied from sample to sample. These foreign

particles could have a significant effect on the analyses making object selection and measurement more difficult. Thus, a dilution was selected to allow for all these conditions. The natural variability of organism distribution across the slide ensured that a suitable section of slide could be found. Since each analysis scanned only a small portion of the slide many quite different measurement regions were available.

The contents of the volumetric flask were poured into a test-tube; at this stage any further dilutions could be completed although normally this was not necessary. Using a P100 Gilson automatic pipette, 50 µl of diluted sample were removed from the test-tube and spread over the surface of a labelled microscope slide. The slide was then allowed to air-dry on a level surface. Afterwards, the slides were dyed with a methylene blue solution. Enough dye was poured onto the slide to completely cover the surface. After a thirty second contact time, the dye was washed off using de-ionised water from a wash bottle. The slides were dried using blotting paper and stored in custom built containers.

All apparatus used was cleaned and dried. Pencil was used for slide labelling on the frosted portion of the slide.

2.2.1.1 Preparation of methylene blue solution.

The formulation of methylene blue dye solution used on image analysis slides was:

1) 0.3g methylene blue crystals (Loeffler's).
2) 30ml 95% (wt./wt.) solution of ethanol.
3) 100ml de-ionised water.

The methylene blue crystals were dissolved into the ethanol solution. Care was taken to ensure all residues of the crystals were dissolved. The de-ionised water was then added and the solution thoroughly mixed. The solution was then aliquotted into 250 ml screw capped bottles, labelled and stored for periods of up to one month.

2.2.2 Sample measurement.

The procedures described in sections 2.2.2.1 and 2.2.2.2 were followed for the operation of the image analyser and the microscope.

2.2.2.1 Magiscan operation.

Before the Magiscan 2A could be used for automatic

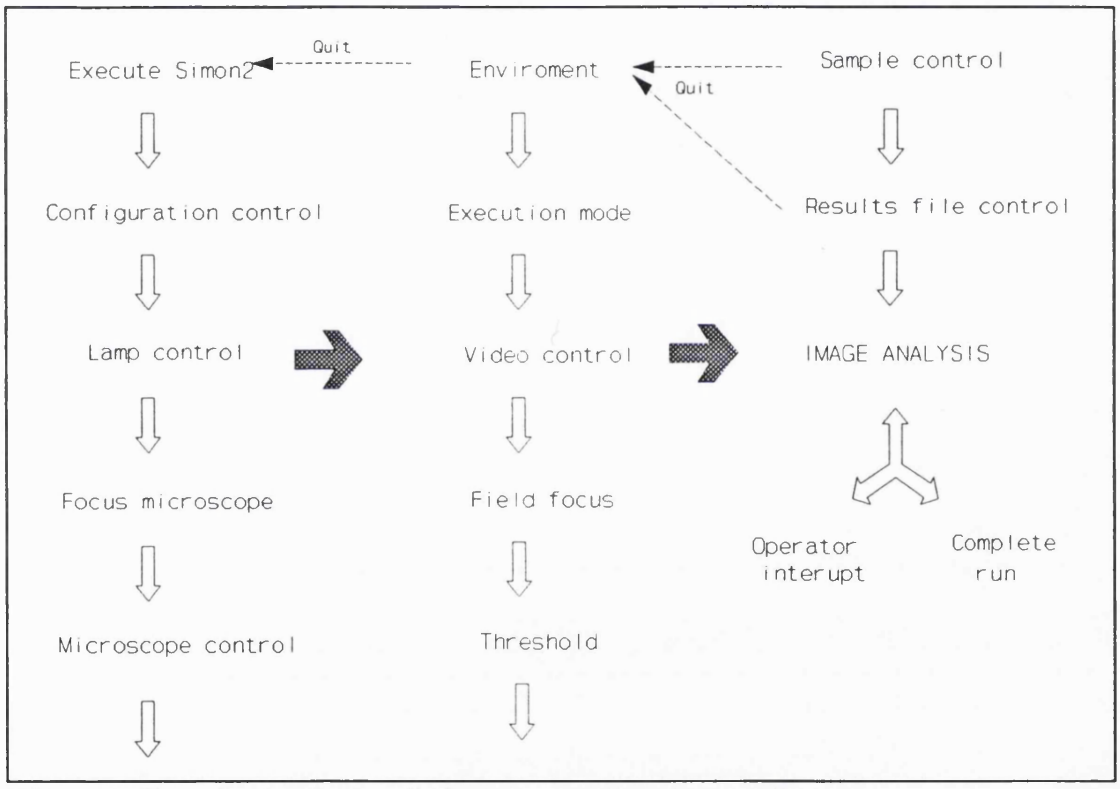

Figure 8: Overview of image analysis software.

image analysis, the software required some specific rules and information for operation, in particular, the calibration of pixels per micrometre for the chosen optical system and instructions for the movement of the microscope stage during analysis.

The calibration was performed in the environment section of the Magiscan software, see figure 8. A slide graduated in tenths of micrometres was placed on the microscope stage. The optical system to be used during

analysis was then selected; 40X objective and zoom lens set at 1.5X. The image analyser showed the microscope's view of the slide on a monitor. The light pen was used to point at any two markings on the graduated slide's image, then by entering the distance between the marks the analyser was able to calculate the calibration coefficient. This value was stored in the operator's environment file which had to be selected before each morphological analysis.

The instructions for movement of the microscope stage were also kept in the operator's environment file. In the environment section of the programme the operator selected the number of fields to analyse, the pattern of movement for the stage, and the inter-field distance.

The Magiscan 2A image analyser was switched on and booted, see figure 9. The operator was prompted to load the operating system. At the operating system main menu the option to execute a programme was selected. The original Joyce Loebl morphological analysis program was

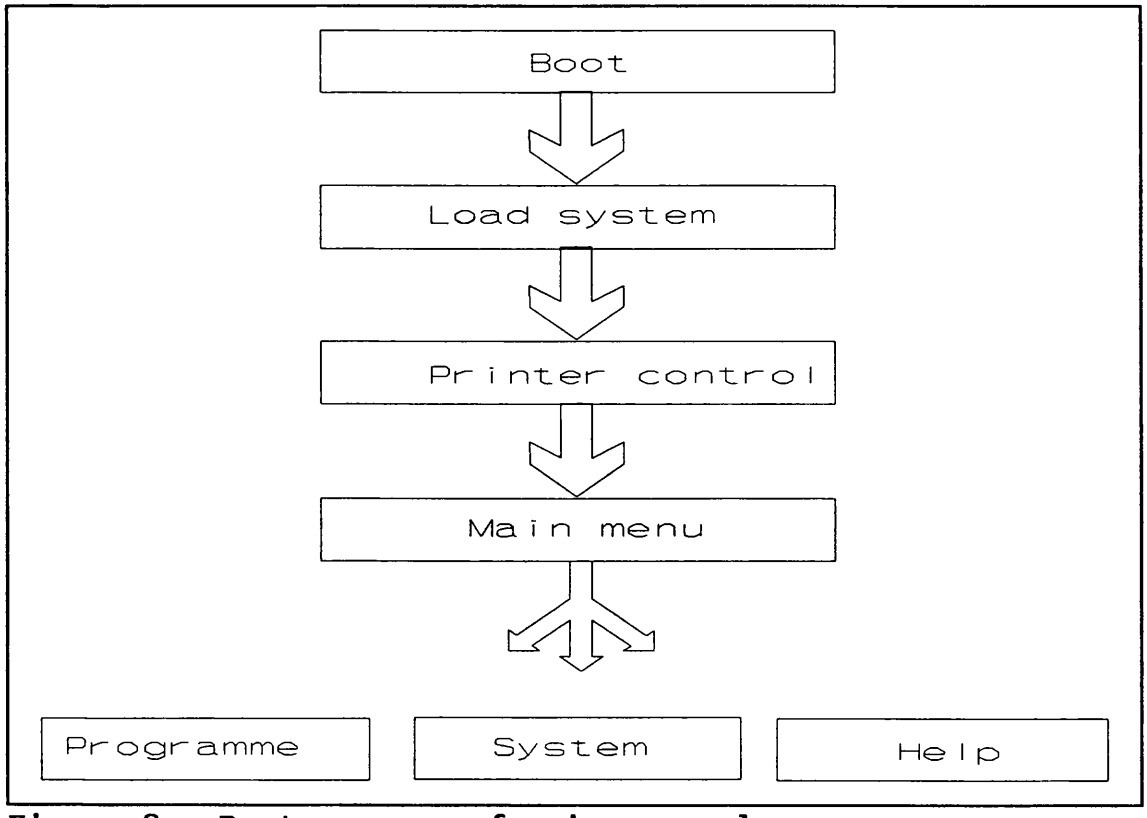

Figure 9: Boot sequence for image analyser.

known as Hyphal.code, however a modified form of this program was used called Morph.code.

Initially menus for configuration and lamp control were displayed, these require no modification since the default values were acceptable, see figure 8.

Then the microscope had to be focused. By using the microscope's focus control knob and the video monitor display the correct focus for the camera's image could be obtained. At this point the area of the sample slide for analysis was chosen. Different sections of the same microscope slide showed differences in the amount of cell overlap, cell concentration, and the presence of debris. A decision was made by scanning the slide until a suitable area was found. The contrast in regions of a slide were considerable, as the photographs in figure 10 indicate.

Figure 10 shows three different regions of the same image analysis slide. Figure 10a shows the ideal situation for image analysis with the microorganisms evenly distributed across the slide. Figure 10b shows the effect of several microorganisms grouping together, the image analyser will ignore these clusters. Figure 10c displays the effect of debris on the slide. The debris can confuse the image analyser and result in erroneous data.

The next menu for microscope control was not altered. At the environment menu the operator had to specify the previously designed environment file stored on the hard disk.

The execution mode menu allowed the operator to decide how much to participate during the analysis operation. If the image analysis editors were turned off for automatic operation then the operator took no part in the morphological analysis. This menu also allowed the analysis procedure to run faster. By default the machine would highlight the video image with colour any objects it had selected. This allowed the operator to gauge whether the software was selecting and rejecting objects as desired, but once satisfied, the option was abandoned as analysis was otherwise slowed considerably.

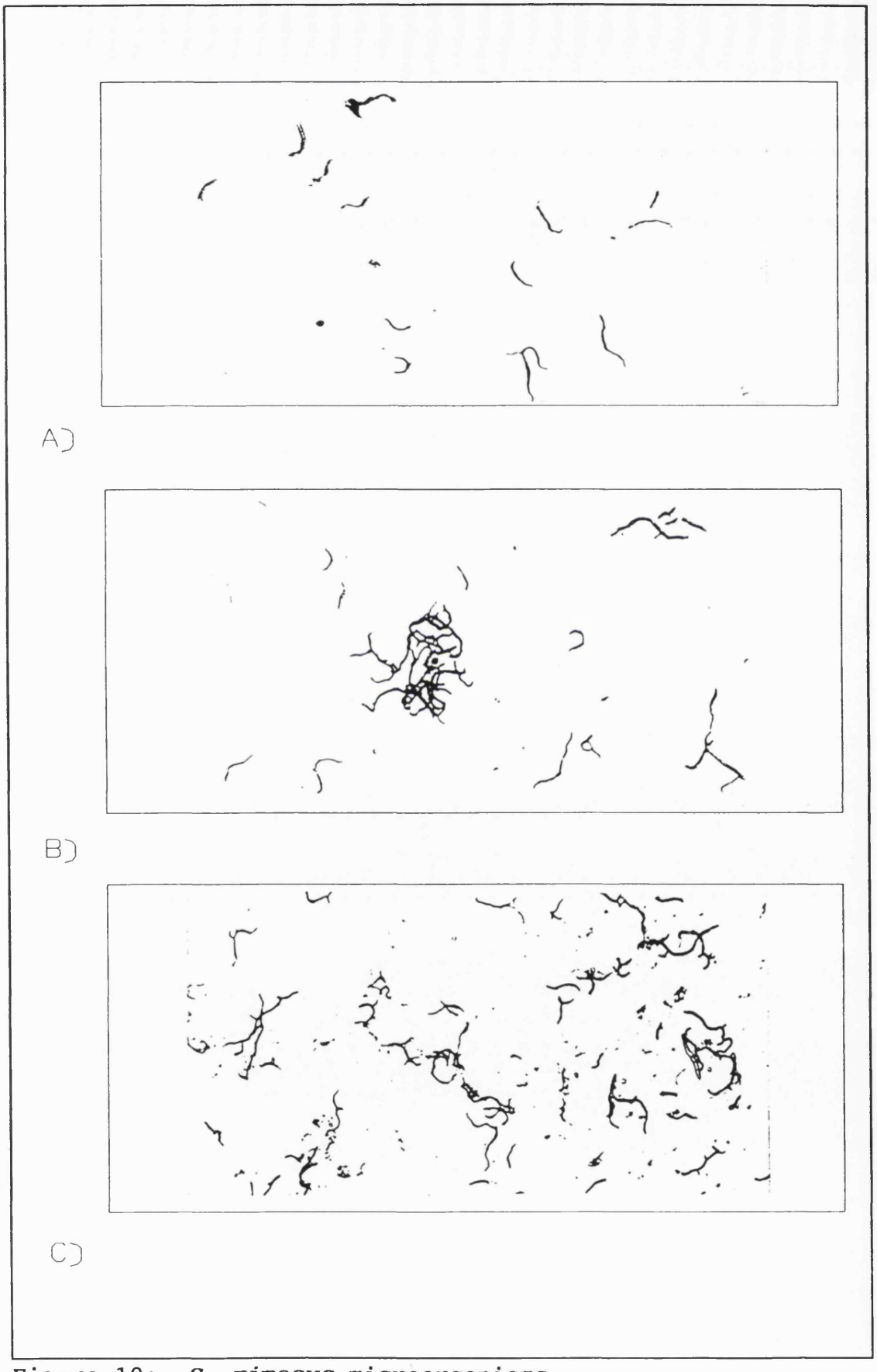

Figure 10: *S. rimosus* microorganisms.

At the video control menu the brightness of the microscope lamp was adjusted to an optimum level for image analysis. Selecting the brightness option caused the video image to produce a blue and red pseudocolour display. The blue colour indicated too low a light level, and the red too high a light level. By adjusting the brightness control knob and the condenser diaphragm, the operator could achieve a blue background with slight red breakthrough indicating the optimum brightness level.

The software required the operator to focus at the four corners of the area to be covered during an analysis; this allowed the analyser to adjust automatically for any thickness differences in the microscope slide. The focus was altered to follow the rate of change of thickness over the analysis area. Usually there was little difference. Any large discrepancies were generally because of incorrect slide cradling and required that the slide be re-positioned. Focusing was semi-automatic; a light pen was used to select from an overlaying menu offering fine, coarse or automatic focusing.

To threshold the image the operator selected two greyness levels. Thresholding was the process by which objects of interest were separated from the background using greyness levels. When an image from the microscope was digitised by the image analyser the real colour image was replaced by an image in black, white and shades of grey. The monochrome image was built with many thousands of square elements called pixels; each of these pixels had a grey intensity. These grey intensities were numbered from the lowest at white to the highest at black. Only objects with a greyness level between the two limits were selected. Any pixel in the image with a greyness level outside this range was considered part of the background and ignored. The choice of threshold settings was made on the first field, hence some leeway was included to allow for variation in greyness of the organisms throughout the hundred fields. The operator decided on the greyness levels for thresholding. Once the two threshold values

were entered the analyser would colour all the pixels within the range chosen. The operator then studied the selection and decided if the distinction between organisms and background was acceptable. Once satisfied the operator moved to the next menu. The choice of a threshold range was highly subjective, however the decision had to be as consistent as possible since variation could have a considerable impact on the morphological results for different samples.

The sample control menu did not need revision. At the results file control the operator named the results file and added any other relevant information, for instance, the date, reference number or operator's name.

Figure 8 shows the various menus that allow the operator to exit the program. If the operator made a mistake or wished to abort the run then he continued to the next menu with a quit option.

The programme ran automatically. After each field the number of organisms analysed was printed. The operator chose when to abort the run, for example, after completion of all the fields, after a certain number of organisms have been analysed or after a particular time period. Pressing the space bar during analysis stopped the program at the next field. The operator interrupt menu permitted the program to be aborted, continued, or changed at the execution mode menu.

If the brightness of the microscope lamp was perceived by the analyser to have varied beyond normal fluctuations then the program stopped and sounded an alarm. The operator had to alter the brightness to the desired level and re-commence the run. Often the alarm was triggered by an abnormally large dark object on a field, this disrupted the carefully monitored balance between dark and light pixels even though no change in brightness had actually occurred. If this was the case, the warning was ignored and the run continued immediately.

The results from the analyses were stored in data files; these files have the extension `.data'. Sometimes

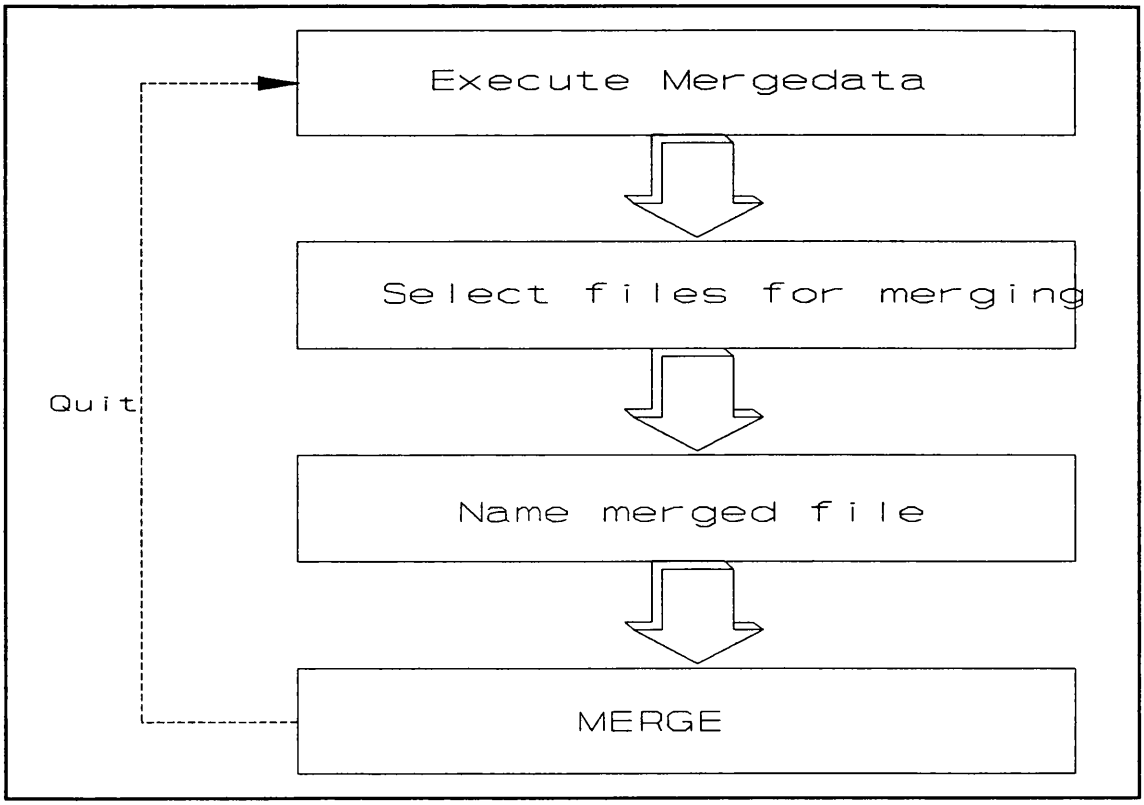

Figure 11: Image analysis file merge.

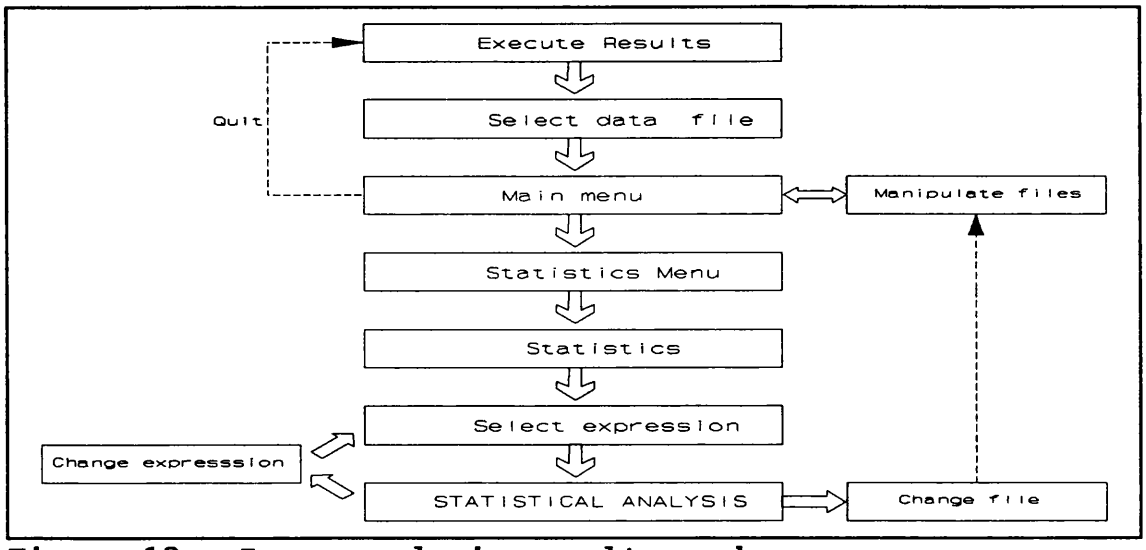

Figure 12: Image analysis results package.

a run was aborted before completion because of time constraints. The sample was then further analysed at a later date and the results stored on a separate data file. The two files were merged and any statistical analysis treated the file as a single run. The programme for merging files was called Mergedata.code. See figure 11.

The statistical analysis programme for the data files

was called Results (see figure 12). The following expressions were measured:

1) The main hyphal length, ML (µm).
2) The total hyphal length including branches, HL (µm).
3) The branch lengths, BL (µm).
4) The number of growth tips, NT (-).
5) The hyphal growth unit length, HGU (µm). (HGU = HL/NT).

For each expression the statistics package produced a mean value and the standard deviation.

2.2.2.2 Microscope operation.

The microscope used for the image analysis work was a Nikon Optiphot Biological Microscope [115], see figure 13. Of the various options available from Nikon, the following optical system was selected for the image analysis system:
The objectives: for low magnification work and initial focusing a Nikon 10X plan achromat was employed. A Nikon 40X plan apochromat objective was used for the image analysis work. This type of lens was designed to produce good definition and image flatness across the field of view, hence it was suitable for photomicrography.
The eyepiece: a Nikon CFW eyepiece was used; it incorporates an optical arrangement to produce a 10X magnification. In addition a Nikon trinocular eyepiece tube type 'T' was used to provide a mount for the video camera.
The condenser: this was a Nikon achromat/aplanat system recommended for use with the chosen objectives.

The microscope controller was turned on. The power on lamp became illuminated on the microscope controller display panel, see figure 14. The microscope lamp button was then turned on. The lamp was warmed up for ten minutes to ensure a steady light output was obtained. The power was turned off to the stage control motors. If the flow of current through the motor coils was not stopped

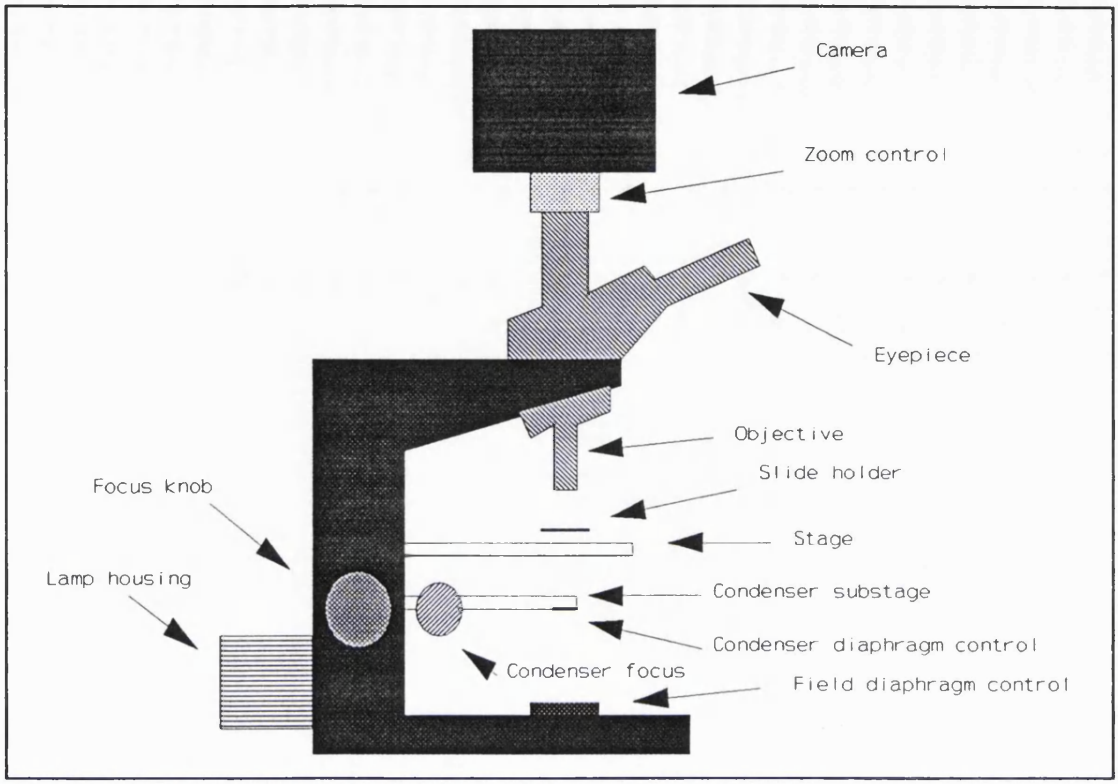

Figure 13: Nikon Optiphot microscope.

then the motors became excessively hot, also manually turning the motors were difficult so the stage could not easily be adjusted. The brightness control knob was adjusted until a reading of approximately four was displayed on the lamp brightness dial. The microscope slide was placed on to the stage. The 10X objective was swung into position and the focus adjusted until a sharp image of the microorganisms was obtained.

The condenser was then centred. The field diaphragm was closed down to its smallest size. The condenser focus knob was turned until a sharp image of the field diaphragm was observed through the microscope. By adjustment of the condenser centring screws the image of the field diaphragm was moved to the middle of the field of view. This centring procedure was only performed at the beginning of an image analysis session. Normally no alterations were required unless another operator had used the system and altered the position of the condenser. The 40X objective was moved into the place of the 10X object glass. The field diaphragm was adjusted so that the image of the

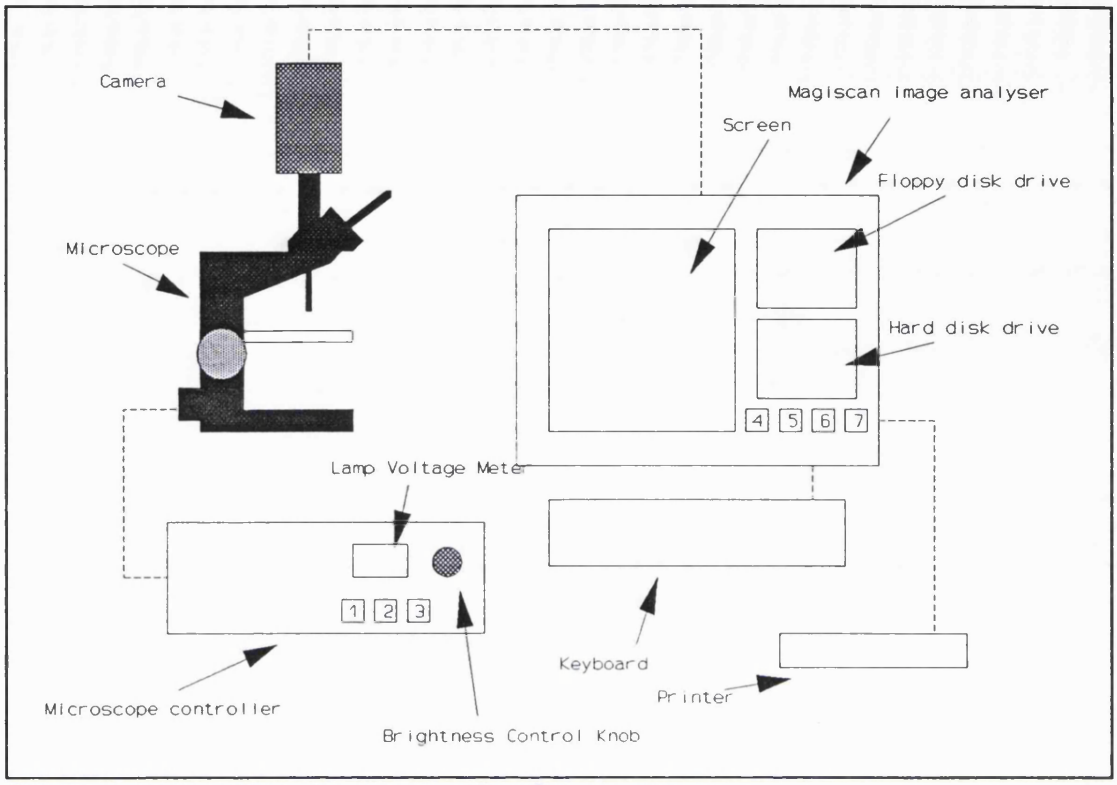

Figure 14: The image analysis system.

diaphragm was only just outside the field of view. This prevented extraneous light entering the field of view and causing image flare and reduced contrast.

The condenser diaphragm controlled the amount of light from the image that reached the observer. This aperture size influenced the resolution, contrast and depth of focus. As recommended by the operating instructions [115] a value of between 70 and 80% of the numerical aperture of the objective was used.

The brightness was adjusted at this stage by the brightness control knob that changed the voltage across the lamp.

The zoom control above the Trinocular eyepiece tube was set to 1.5X. Thus, the magnification of the image reaching the video camera was 40 X 10 X 1.5 = 600 times.

2.3 Fermentation.

The fermentation processes described in the subsequent sections were commercial processes, and hence, highly

confidential. Therefore, the exact media recipes, process run conditions and process times cannot be published. Instead broad outlines of culture conditions are provided.

2.3.1 11 litre fermenters.

Bioengineering fermenters, with an 11L working volume, were used for the majority of the *S. erythraeus* and *A. roseorufa* fermentations, see figure 15. The pressure vessel was constructed from a glass cylinder, a flat stainless steel top plate and a hemispherical bottom plate. Holes were drilled in the top plate, at regular intervals, to enable the attachment of monitoring equipment and feed lines. The bowled bottom section was created from a double skin of stainless steel, thereby forming a chamber to heat or cool the fermenter using pressurised steam or cold water respectively. Agitation of the fermenter contents was achieved using a bottom driven agitator shaft fitted with a pair of Rushton turbines. Baffles were used to minimise production of a vortex around the impeller shaft. All pressure seals in the vessel, except for the carbide seal on the agitator shaft, were achieved using rubber O-rings.

Phox controllers were available to cover most aspects of fermentation control. These were stand-alone units with manually determined set points. For more complex control regimes a Ferranti mini computer could be used to automatically determine the set points from a pre-determined algorithium. The Phox units were used to control pH and temperature, also they monitored dissolved oxygen tension (DOT) and agitation speed. The air flowrate through the fermenter was set manually and monitored using a rotameter, automatic control was also available. A controller for antifoam addition was available but not used.

All fermenter data were passed to the Ferranti for data logging purposes; data were scanned every 30 seconds. The data included all controlled parameters plus the batch

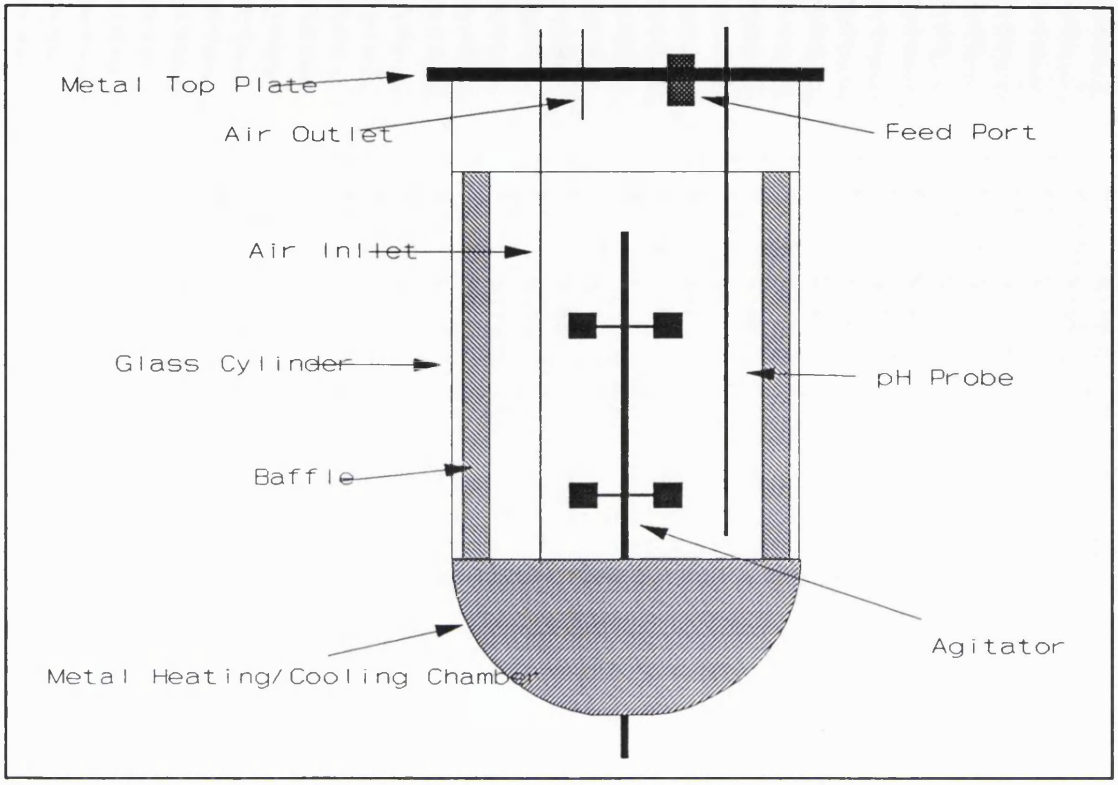

Figure 15: 11 litre Bioengineering fermenter.

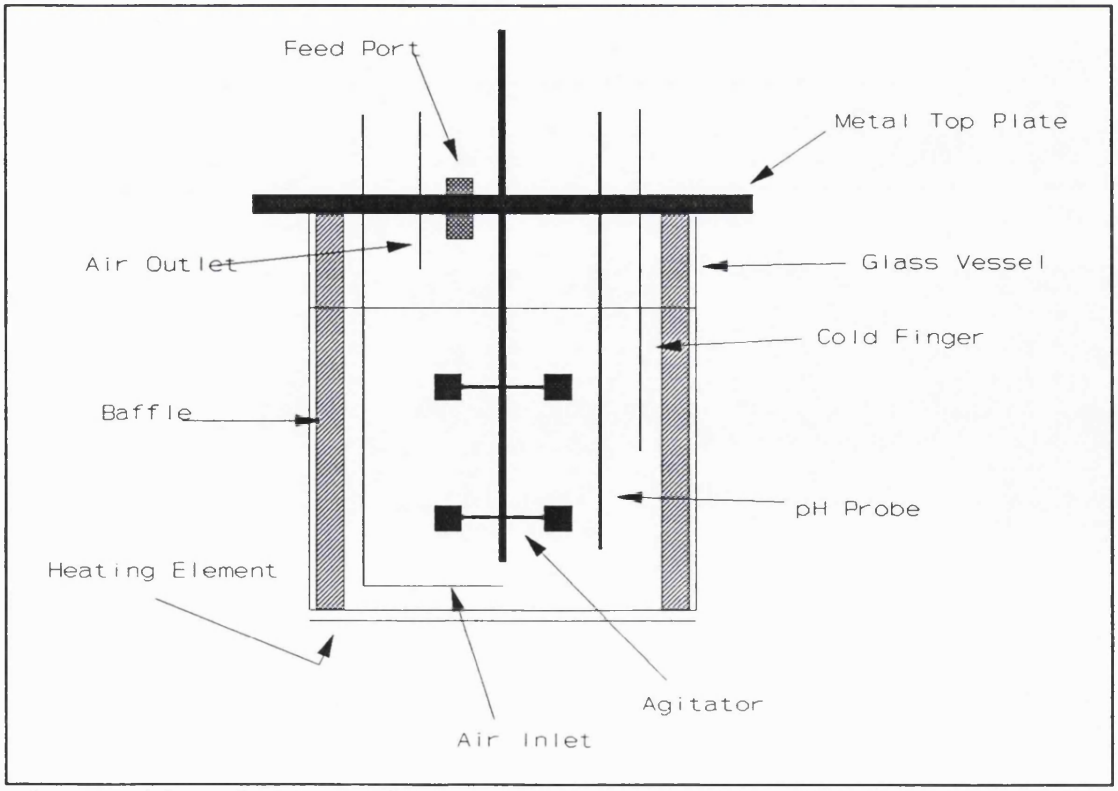

Figure 16: 3 litre fermenter.

weight of the fermenter measured via a load cell. In addition, a continuous sample of off-gas was diverted and pumped to a mass spectrometer. By comparing the composition of the fermenter inlet air against the outlet air more useful information was gleaned about the fermentation; thus values of oxygen uptake rate (OUR), carbon dioxide evolution rate (CER), respiratory quotient (RQ) and K_La were calculated and logged.

The Ferranti data could be reviewed as tables or graphs on the screen or as tabular printouts.

2.3.2 3 litre fermenters.

Some of the work on *S. erythraeus* and *A. roseorufa* was done in 3L working volume fermenters, see figure 16. The pressure vessel was comprised of a glass jar with a flat stainless steel top plate. Ports in the top plate allowed the connection of monitoring equipment and feed lines. The fermenter broth was agitated using a top driven agitator shaft fitted with a pair of Rushton turbines. Baffles were used to prevent vortexing around the agitator shaft. The fermenters were heated by an electrical element below the glass jar and cooled by a cold-finger. All pressure seals in the vessel were achieved using rubber O-rings.

Anglicon controllers were used for all aspects of fermentation control. These were stand-alone units with manually determined set points. The units were used to control pH, temperature, also they monitored dissolved oxygen tension (DOT) and agitation speed. The air flowrate was manually set and monitored using a Rotameter. The monitoring data were then passed to a sophisticated chart recorder. The Siemens unit provided graphical data logging for any variable selected by the operator.

2.3.2.1 Fermentation in parallel.

These fermentations were designed to provide

additional insight into the source of the rheological properties of fermentation broths.

Two three litre fermenters were prepared and run in the manner described above. One of the fermenters was inoculated with a culture in seed medium, the other was not inoculated but sterile seed medium was added to equalise the broth volumes. A far as possible the conditions in each fermenter were kept the same. In place of the nutrient feeds given to the inoculated fermenter, sterile water was supplied to the non-inoculated fermenter to keep broth volumes the same. The fermenters were sampled at the same time and equal volumes of 300 millilitres were removed. The broth samples were rheologically analysed using the Brookfield viscometer and then they were centrifuged to remove the cells and particulates. The centrifugate was decanted off and then rheologically analysed. Hence for a given fermentation time there were four different specimens:

A - sample from inoculated fermentation before centrifugation.

B - the centrifugate of (A).

C - sample from uninoculated fermentation before centrifugation.

D - the centrifugate of (C).

2.3.3 Production fermenters.

All the *S. rimosus* cultures were produced in the production fermenters at the Pfizer site. No information can be provided on these fermenters for reasons of commercial confidentiality.

2.3.4 Sampling and data collection.

Sampling differed depending on the fermenter.

2.3.4.1 11 litre and 3 litre fermenters.

The fermentations were sampled twice daily. A note was made of all fermentation parameters to ensure conditions were within the limits prescribed for the process. In addition, for the 11L fermenters a listing from the Ferranti was printed to show the changes in fermentation parameters at 30 minute intervals for the previous 24 hr.

For complete analysis of the fermentation a sample of at least 250 ml of broth was necessary. Normal boiling tubes had an insufficient capacity, hence these samples were taken using 250 ml quick fit conical flasks. Strong self-adhesive tape was wrapped around the flasks to minimise the dangers of a flask shattering under pressure. The flasks were autoclaved at 121°C for 60 minutes. Boiling tubes were prepared in the same way. Samples were taken under aseptic conditions. The conical flasks were sealed using non-absorbent cotton wool bungs; these were covered with glycine paper which was held in place with an elastic band.

The 11L and 3L fermenters were sampled by pressurising the fermenter. Pinching the fermenter exhaust line caused pressurisation of the vessel and forced broth out through the sample line via a dip tube. The sample line valve had to be open for this sampling procedure and closed immediately afterward.

Initially, the sample line was cleared of stagnant broth by collecting approximately 20 ml of broth in the attached boiling tube. Then the protective glycine paper was removed from a conical flask. The boiling tube on the sample line was loosened to allow rapid switching of sample containers. The cotton-wool bung of the sample flask was then removed and the flask flamed before attachment to the sample line. The flask was swapped for the boiling tube which was then sealed using the flask's bung. These actions were undertaken as rapidly as possible to ensure continuation of aseptic conditions. The sample flask was

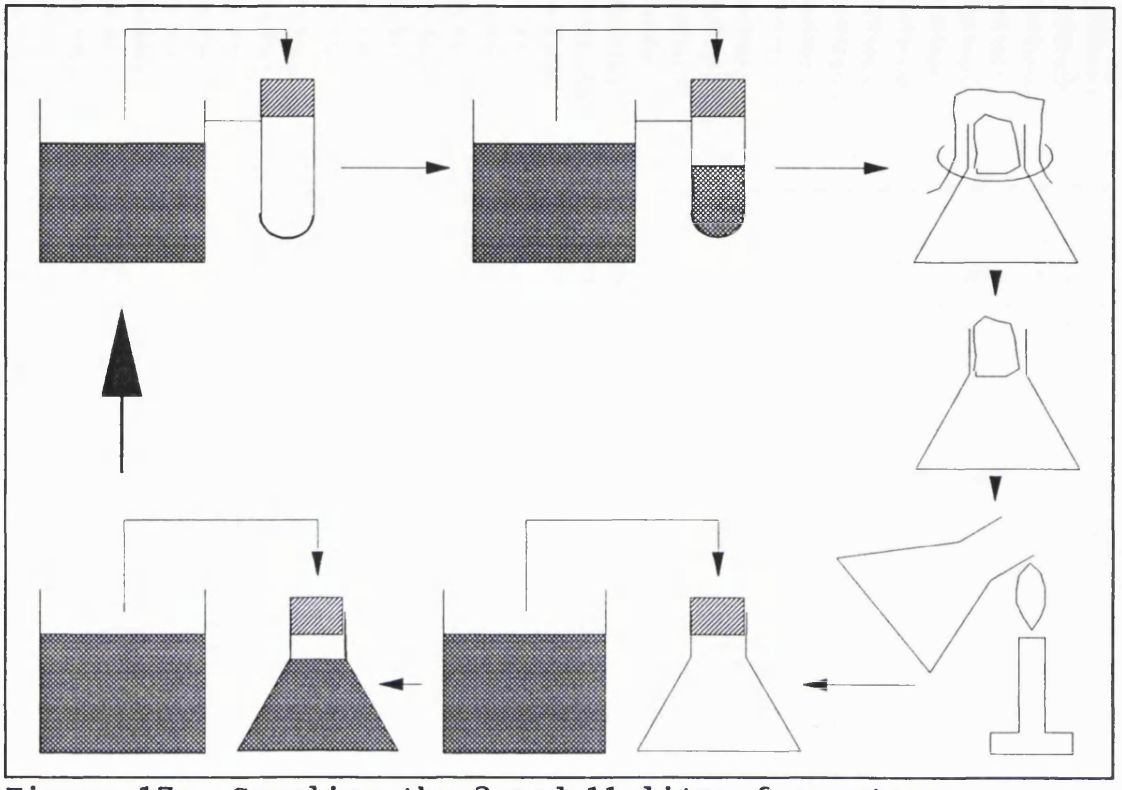

Figure 17: Sampling the 3 and 11 litre fermenters.

then filled to shoulder level with broth. Once a sample had been collected the flask was swapped for a boiling tube as previously described. The weight of broth removed from the fermenter was established. Initially the containers were weighed with broth and then the containers were re-weighed without broth. The complete sampling process is shown in figure 17.

2.3.4.2 3 litre inoculum fermenters and fernbachs.

The fermenters used to produce inoculum were also sampled to allow monitoring of the growth process and to check for contamination. These fermenters do not have a sampling system so a different routine must be used. The fernbach (a squat 5L conical flask) or 3L inoculum fermenter was placed in a laminar flow cabinet. A 20 ml sample was transferred to a sterile boiling tube using a sterile syringe/needle combination. The flask or 3L inoculum fermenter was then returned to the shaker or cradle immediately to prevent oxygen limitation.

2.3.4.3 Production fermenter.

The *S. rimosus* culture was grown in large scale production fermenters. The sampling for these fermenters is shown in figure 18. Figure 18a shows the valve positions before and after sampling, whilst, figure 18b shows the valve positions during sampling. Before and after sampling live steam was passed through valves 2 and 3 where it condensed in the catch-pot and passed down to waste. To sample the fermenter the following valve sequence was used:

1) Close valve 3.
2) Close valve 2.
3) Open valve 1.
4) Crack valve 3 and collect sample.
5) Close valve 3.
6) Close valve 1.
7) Open valve 2.
8) Crack valve 3.

At instruction (4) broth was allowed to flow to waste until the broth from the dead space had been flushed away, only then was a sample taken. Samples were collect in 2L plastic beakers, these were covered in foil to prevent debris or moisture entering the samples during carriage to the laboratory.

2.3.5 Assays.

2.3.5.1 Sterility.

The growth of monoculture fermentations was vital to ensure valid and reproducible observations. Hence, after each inoculum stage and at periodic intervals during the fermentation the broths were checked for contamination. The following methods were used:

a) Plating. In a laminar flow cabinet, a streak of culture was placed on an Emerson's agar plate using a sterile loop. The plate was then incubated at the

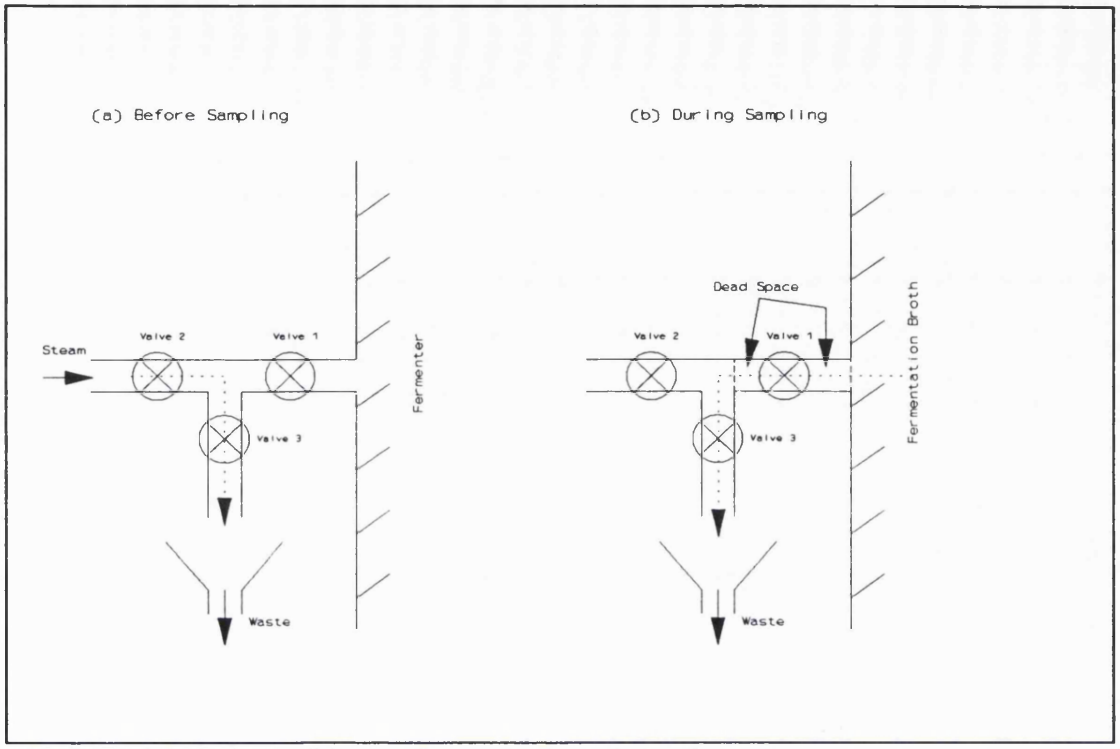

Figure 18: Sampling the production fermenter.

fermentation temperature for several days. Observation of the agar plate displays any contamination.

b) Microscopic observation. In a laminar flow cabinet, a microscopic slide was smeared with a few loopfuls of culture. The broth was heat fixed and Gram stained. The organisms used in this project all stain Gram-positive. Microscopic examination of the slide, at a magnification of 100X, revealed any substantial contamination.

c) Packed cell volume (PCV). A 10 ml sample was decanted into a graduated spin tube, which was spun at 2,000 rpm for 10 minutes.

d) pH. The pH of the culture was measured using a calibrated laboratory electrode.

For each stage of the inoculum train, mean values for PCV and pH from previous fermentations have been derived. By comparing these mean values with the measured ones, the inoculum can be labelled as typical or not.

2.3.5.2 pH assay.

The pH of the broth was checked using a carefully calibrated laboratory pH-meter. The pH-probes used in the fermenters often suffer from the effects of autoclaving and pH-drift. By comparison with an accurate value determined at the bench the differences can be rectified and the appropriate fermentation conditions re-established. Before sampling the fermenter the pH-control was disabled so further additions of acid or alkali could not occur. The difference between the indicated pH of the fermentation broth and the actual pH was then calculated. This difference in pH (ΔpH) was then used to rectify the controller reading. The pH-controller was subsequently re-enabled. By using this technique the problem caused by the pH of the fermentation culture continuously changing was eliminated.

2.3.5.3 Rheology.

To obtain meaningful and reproducible rheological data, not only was the method of rheological measurement followed precisely but so were the procedures for collection and storage of the sample. The previous history of the sample had a significant impact on the rheological characterisation data. Sample collection and storage were designed to minimise shearing of the sample. All pouring was gentle and the samples were carried carefully. The procedures were followed meticulously to ensure every sample was handled consistently before analysis. The sample holders were stored in a water bath at the fermentation temperature until required for analysis. As soon as practicable, 200 ml of the broth were transferred to a 250 ml glass beaker for rheological analysis.

2.3.5.4 Chemical assays.

A 30ml broth sample was filtered to remove biomass and large media particulates. Then a range of methods were used to provide data on residual carbon, nitrogen, phosphate and productivity. These analytical methods included; HPLC, colormetric flow analysis and ion selective electrodes.

2.3.5.5 Morphology.

4g of broth were then weighed out for preparation of the morphological slides.

2.3.5.6 Packed cell volume.

Two 10 ml samples of culture were dispensed into graduated spin tubes; these were centrifuged for 10 minutes at 2,000 rpm. Subsequent observation of the tubes showed the fermentation particulates from the broth were packed down in the tube forming a sharply defined boundary layer; the proportion of the tube filled with solids gave the packed cell volume for the sample.

2.3.5.7 Media feeds.

The media feed bottles were weighed to established the quantity of feed pumped periodically into the fermenter.

2.3.5.8 Dry cell weight.

The DCW assay was used to follow growth during the fermentation. 5 g of broth were weighed into each of two spin tubes. These broth samples were then vigorously agitated with a mixture of reagents and centrifuged. These reagents cause a differential rate of sedimentation between the cells and solids in the fermentation broth. The top layer could then be decanted with a Pasteur

pipette. The middle lighter layer contained the cells. By squirting distilled water onto the layer and using a spatula to break up this layer, these cells could be transferred using the pasteur pipette onto a pre-weighed 12.5 cm Whatman 40 filter. Considerable care was needed to prevent removal of media solids from the bottom layer at the same time. When all the cells had been removed from both tubes, swill any cells remaining in the pasteur pipette onto the filter. The filter paper was placed in a 100°C oven overnight, the following morning the filter was placed in a dessicator, carried to the weighing room and weighed. The first stable reading was noted as the filter will absorb water from the atmosphere fairly rapidly. Tweezers were used to handled the filter paper.

2.3.5.9 Mass spectroscopy.

Fermenter off-gas analysis was used as an analytical tool for monitoring the state of fermentations. By comparison of the gas composition of air entering and exiting the fermenter measures were made of oxygen uptake rate (OUR), carbon dioxide evolution rate (CER), respiratory quotient (RQ) and total oxygen consumption (TOC).

2.3.6 *S. erythraeus* fermentation.

2.3.6.1 Culture.

The culture used for these fermentations was a chemically or photo-mutated form of *S. erythraea*. The mutation work was undertaken to improve the titres of a secondary metabolite, the broad spectrum antibiotic Erythromycin. The stock culture was stored on a frozen agar slope in a boiling tube at -20°C. When required additional sub-cultures on 3 ml frozen slopes of agar were prepared for inoculation of fermentations.

2.3.6.2 Inoculum.

A Fernbach of Fernbach Flask media was prepared and autoclaved. Under aseptic conditions, a syringe was used to transfer approximately 10 ml of the media into the tube containing the frozen agar slope. By scraping the syringe needle against the slope most of the culture was relocated into the liquid media. The liquid medium containing the culture was then transferred back into the Fernbach. The flask was then incubated on an orbital shaker at the required temperature and agitation speed for 24 hours.

The second stage inoculum was grown in a 3L inoculum fermenter. The fermenter containing the inoculum medium was batched and autoclaved. Under aseptic conditions a syringe was used to transfer 120 ml of the primary seed into the fermenter. The vessel was run for 24 hours under the conditions required to give adequate growth.

Sterility checks were made at appropriate periods during the inoculum train.

2.3.6.3 Operation.

The fermentation was a fed-batch process. The production medium used was typical for an aerobic, chemiheterotropic fermentation process. The precise details of the media were confidential, however, the media contained substantial quantities of insoluble, complex sources of carbon and nitrogen. Trace elements and antifoam were also present. Some of the medium constituents were fed at feedrates which were changed throughout out the fermentation to optimise nutrient concentrations.

The Bioengineering fermenter was batched with 10l of Production medium and sterilized in-situ at 121°C for 90 minutes. A 10% by volume inoculum was then transferred into the fermenter from the 3L fermenter.

The actual fermenter run conditions are confidential but conditions were typically in the following ranges:

temperature: 30-35°C.
sparged aeration rate: 0.5-1.5 vvm.
agitation speed: 800 rpm.

pH was controlled to within the range 6.9 and 7.3; additions of 10% by weight sodium hydroxide and 10% sulphuric acid solutions were used to maintain these limits.

2.3.7 *A. roseorufa* fermentation.

2.3.7.1 Culture.

A. roseorufa was a novel species from the genus Actinomadura isolated by Pfizer and held in their culture collection. The organism has undergone considerable mutation by mutagenic agents to enhance production of one of a secondary metabolites, a polyether antibiotic. The sub-species used for this fermentation work was known as M5129.

The organism was stored at -20°C on agar slopes for sub-culturing to liquid media when required.

2.3.7.2 Inoculum.

A Fernbach containing 500ml of inoculum medium was prepared and then autoclaved for 45 minutes at 121°C. The medium contains a carbon source, several nitrogen sources, a pH buffer, trace elements and antifoam. The pH was adjusted to the desired level using sodium hydroxide before sterilisation.

Using a sterile syringe approximately 5 ml of media was transferred into the boiling tube accommodating the agar slope. The needle was used to dislodge the surface culture form the agar to the liquid media, then the media was transferred back to the Fernbach. The Fernbach was placed on an orbital shaker at a prescribed temperature for 9 days.

The second stage of the inoculum train involved the

transfer of 50 ml of first stage broth to a Fernbach containing a litre of sterilised medium. The transfer was completed in a laminar flow cabinet using a 50 ml glass syringe. This medium was similar to the production medium as it contained similar complex carbon and nitrogen sources. The Fernbach was incubated on a shaker for 4 days at the desired temperature and speed.

Sterility of the inoculum train was checked regularly.

2.3.7.3 Operation.

This fermentation was a fed-batch process. The actual medium used is a commercial secret, however a high concentration of insoluble complex carbon and nitrogen sources were used. In addition trace elements and antifoam were added. Some of the medium constituents were fed. It was necessary to control feed rates within strict limits to maintain nutrients at optimal levels.

The 11L fermenter was initially batched with medium components for 11 litres of broth but only diluted up to 10 litres. The production medium was sterilized in-situ for 1 hour at 121°C. One litre (10% by volume) of second stage inoculum was then added from a Fernbach.

The fermenter run conditions were within the following ranges:

temperature: 30-35°C.
sparged aeration rate: 0.5 to 1.5 vvm.
agitation speed: 800 rpm.

The pH was maintained at a level between 6.8 and 7.2 by additions of 10% by weight sodium hydroxide or 10% sulphuric acid.

2.3.8 *S. rimosus* fermentation.

The culture used for this work was originally isolated by Pfizer. The organism has been mutated to improve the yield of Oxytetracycline (OTC).

The inoculum process and operation of the fermenter are commercially sensitive and so cannot be discussed.

3 The control experiments.

Initially a series of experiments under standard operating conditions was carried out in order to establish morphological and rheological properties of the fermentation system. The results from these runs formed the basis on which all subsequent experiments were carried out and analysed.

A highly reproducible procedure was developed for measuring the viscosity of fermentation broths. The method provided an excellent starting point for altering experimental parameters and assessing the resultant effects. The procedures used in these experiments are outlined in the Materials and Methods section, any deviations from these methods are clearly described in the individual experimental reports.

3.1 The Contraves viscometer.

The viscometer used initially in this project was a Contraves Rheomat 115 coupled to the 145 cup and bob measuring head. This particular measuring head was preferred to the other sizes available because it gave the highest torque response for a typical *S. rimosus* fermentation broth without going over-scale. The apparatus was set up and operated as described in section 2.1.1, with an equilibration time of thirty seconds.

Figure 1 shows the straightline produced when plotting log shear stress, τ, (Pa) against log shear rate, γ, (1/s) for a 1000 cP Silicone fluid. The point scatter at the beginning of the straightline was because of the insensitivity of the viscometer. At these low shear rates the change in shear stress was too small to be registered by the viscometer. After ignoring these erroneous data points, regression analysis (the method of least squares) was used to fit a straightline through the remaining data points. The equation of this straightline is equivalent to the Power law equation (see section 1.3.3) and allows

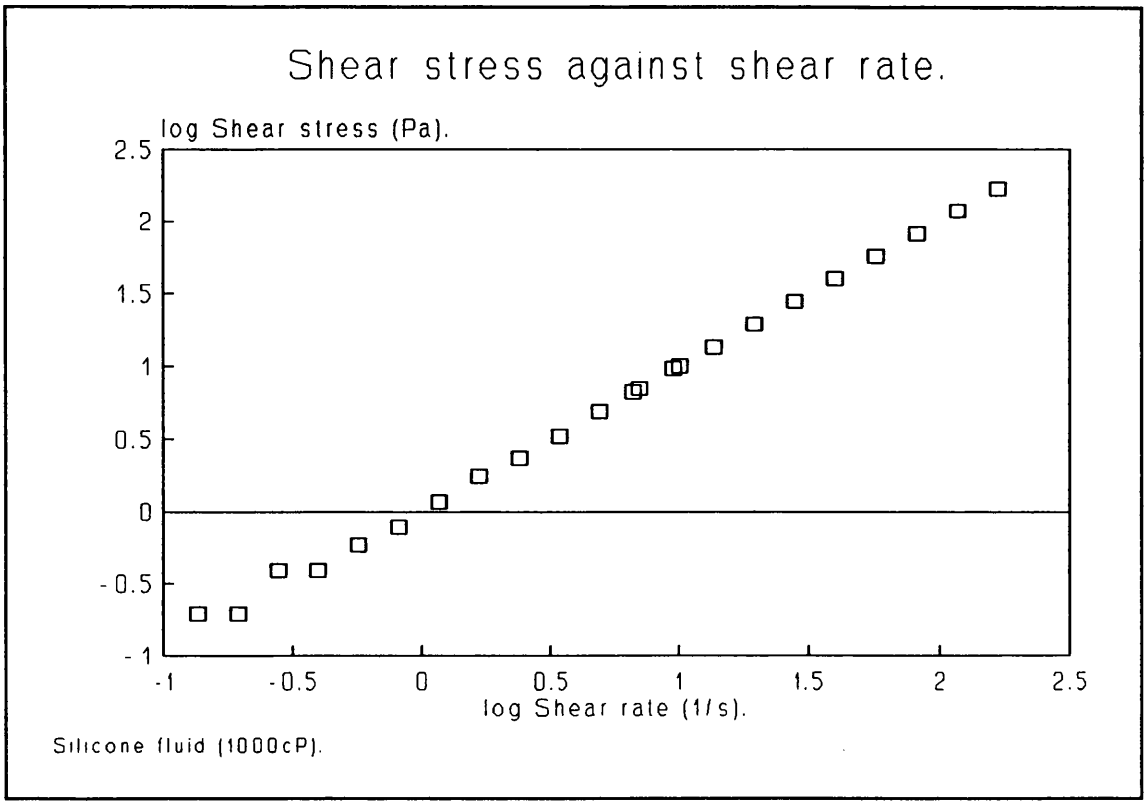

Figure 1

the determination of the Power law index, n, (no units) and the consistency coefficient, K, ($Pa.s^n$). The values obtained were 1.001 and 0.994 $Pa.s^n$, respectively. The Silicone fluid is a calibration liquid which is known to be Newtonian (a value of, n, equal to one) and to have a viscosity of 1 Pa.s; therefore, it may be concluded that the Contraves viscometer was functioning correctly.

Frequent calibration checks, at least once a week, were made on the Contraves using the Silicone fluid. If any significant measurement deviation was noted then the trial was repeated with fresh Silicone fluid. Both the Power law index and the consistency coefficient never varied more than ±1% for the actual value. This level of variation is within the specified tolerances of the Contraves viscometer [112].

Figures 2 and 3 show typical plots of log shear stress against log shear rate for *S. rimosus* fermentation broths. Even though the fermentation broths had entirely different apparent viscosities of 700 cP and 1140 cP (on the single point system), the plots show the same characteristics.

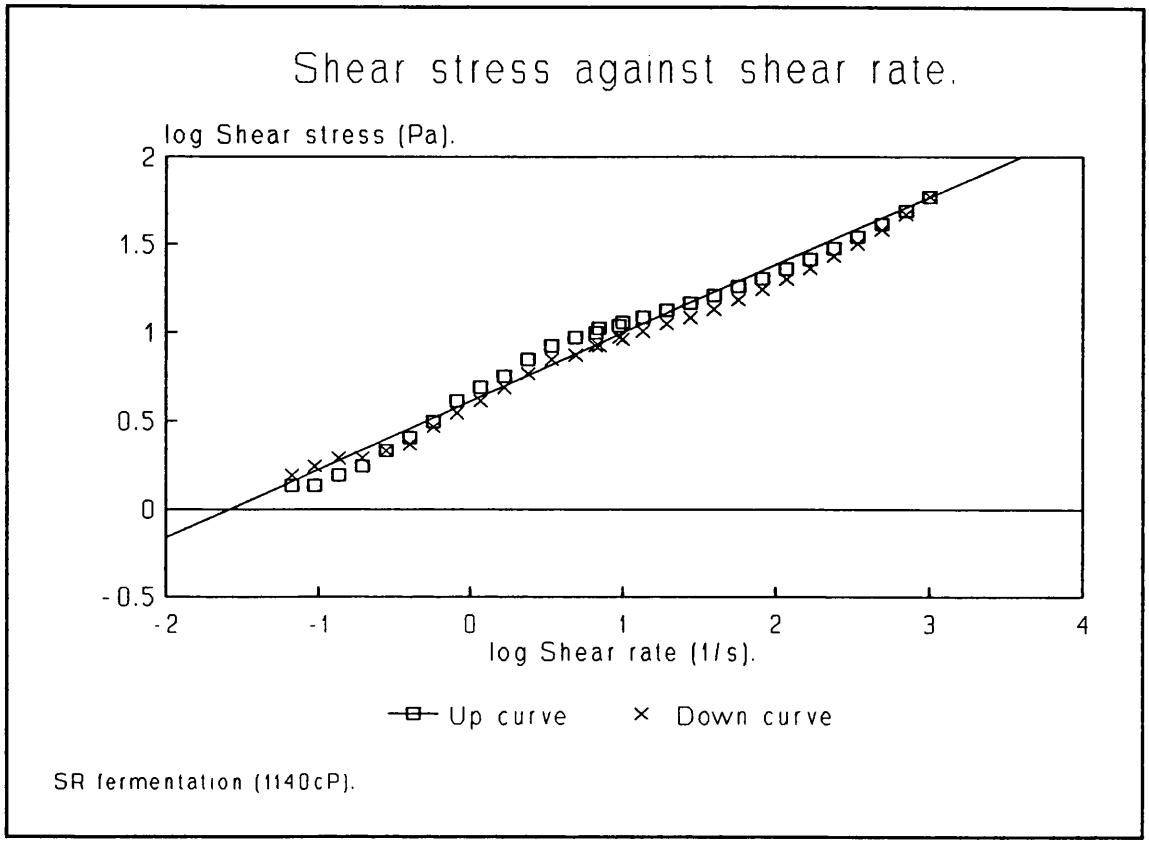

Figure 2

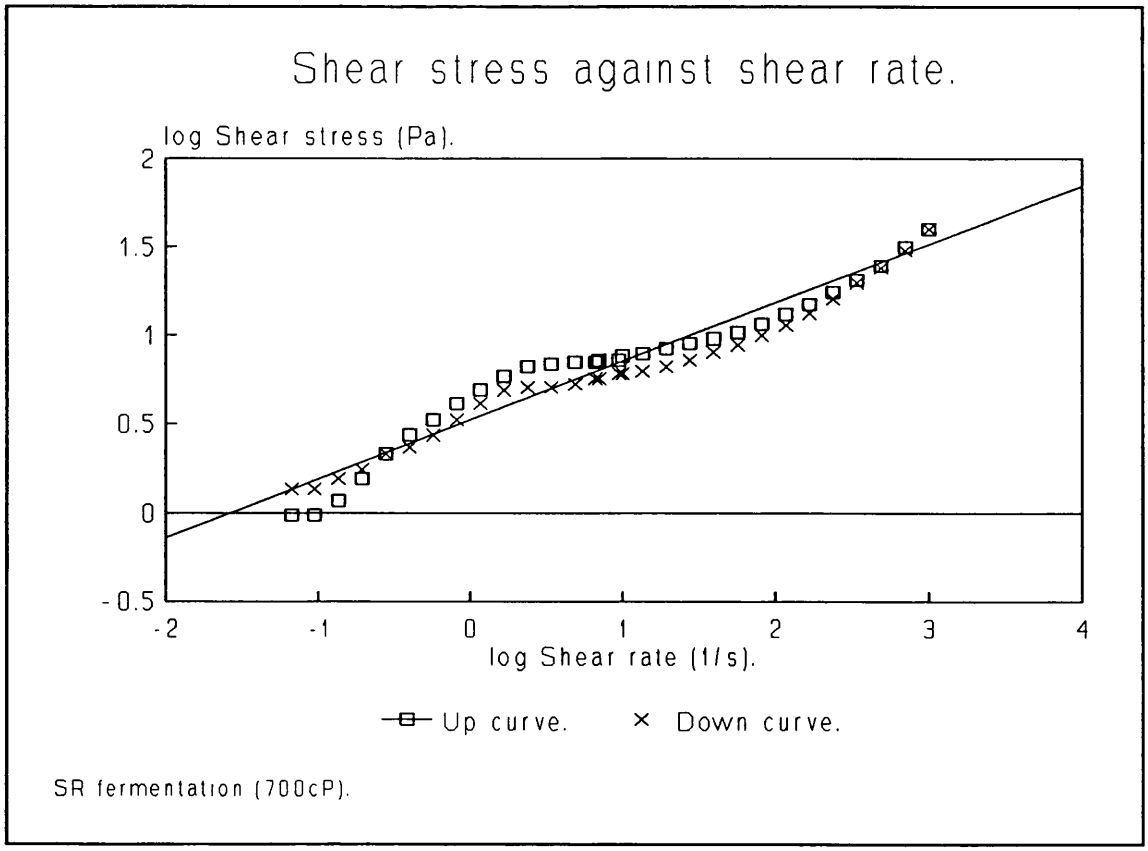

Figure 3

Initially the data points curve upwards, then they plateau and finally they resume an upward curve. Despite this characteristic curved behaviour a straightline was forced through the up-curve data points using linear regression analysis, thereby permitting the use of the Power law. This action can be ratified by examination of figures 2 and 3 which show the up-curve data points to be reasonably close to the straightline throughout the shear rate range. The application of the Power law means that quantitative rheological data which is independent of shear rate can be determined for the fermentation broths. When attempting to correlate broth rheology with the morphology of filamentous microorganisms in the fermentation, a shear rate-independent rheological parameter must be used otherwise the value of the rheological parameter would change with the shear rate and make establishing a correlation impossible. A number of rheological models, other than the Power law, were fitted on to the *S. rimosus* data, but none of them modelled the data as closely.

In both figures 2 and 3 the up-curves display higher shear stresses for a given shear rate than the down-curves, except at low shear rates when this rule was reversed. The resulting hysteresis effect is characteristic of thixotropic fluids (see section 1.3.2.2). From figures 2 and 3 it can be observed that the thixotropic nature of the *S. rimosus* had an inconsequential effect on the fitting of the data to the Power law model. Henceforth, it was decided to use only up-curve data for calculating rheological characteristics. The down-curve data was rejected because it required specific pre-shearing which could result in erroneous data. The possibility of averaging the up-curve and down-curve data for a given shear rate was rejected because when the two sets of rheological data were determined by the Mitschka method [113] they did not have the same shear rates and so could not be averaged.

There is an overlap between the two shear rate ranges of the Contraves viscometer. The shear stress values in

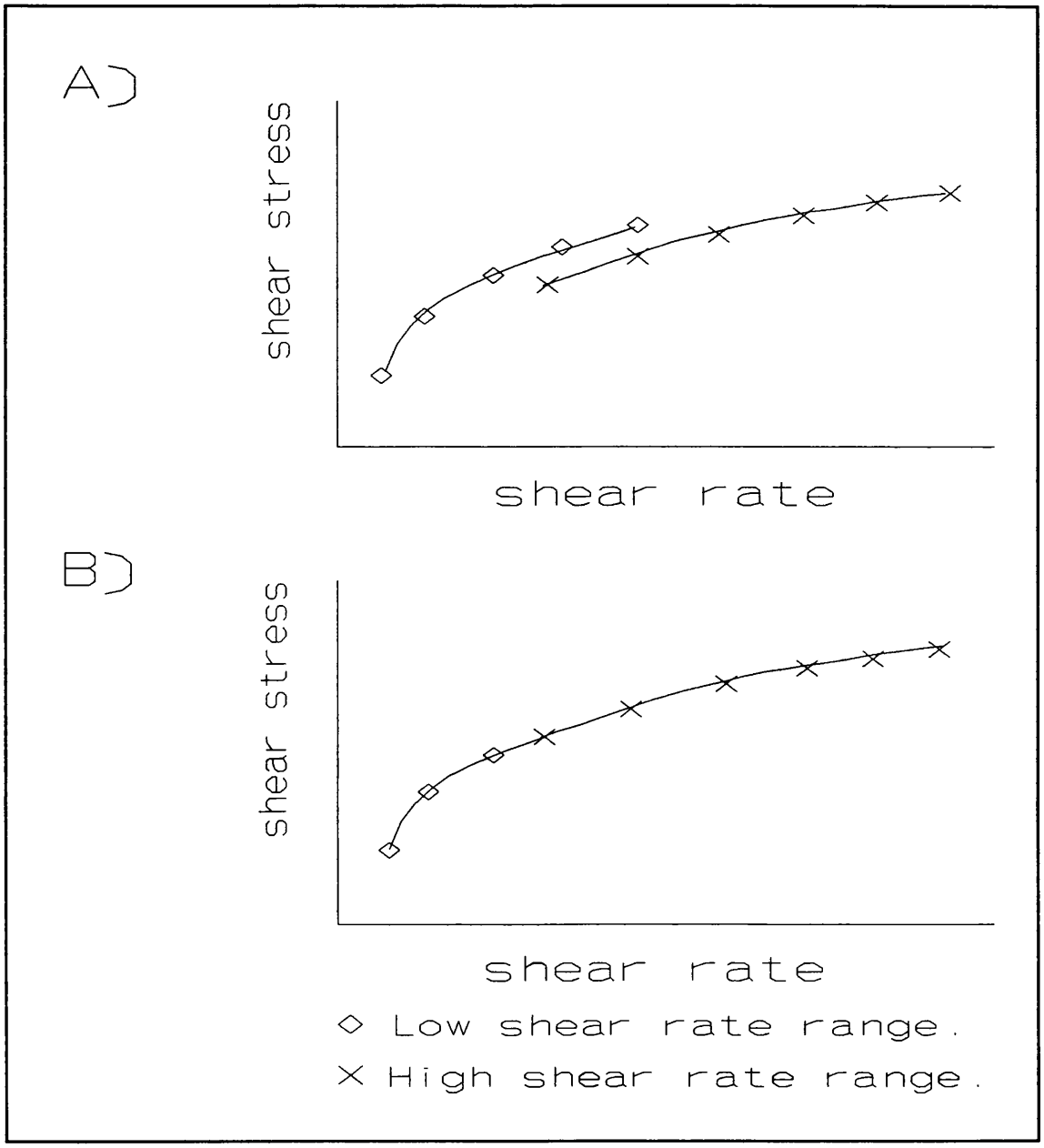

Figure 4: The overlap in the shear rate range of the Contraves viscometer.

this overlapping section do not coincide as theory would predict. If a thixotropic fluid is sheared at a low shear rate, then at a higher rate and finally back at the lower rate, the shear stress from this second reading will be lower than the equivalent shear rate for the first. Such a sequence took place in an analysis by the Contraves viscometer, see figure 4a (top). The final shear rate of the lower shear rate range was $\approx 10\ s^{-1}$, but the initial shear rate of the upper shear rate range is only $\approx 6\ s^{-1}$.

To overcome this problem the analysis was stopped at a shear rate of ≈5 s^{-1} in the lower range then the upper range could begin at ≈10 s^{-1} without the overlap taking place, see figure 4b (bottom). This region of the Contraves analysis was further complicated by the necessity to stop the viscometer's motor in order to switch the gearbox to the alternative shear rate range, however, this appeared to have little influence on the rheological data.

3.1.1 The Contraves viscometer equilibration time.

As described in section 2.1.1.2, the equilibration time (ET) was the period of time allowed for the measuring head to turn at a given speed before the reading was recorded and the speed changed. This time interval enabled the reading to stabilise.

A sample of *S. rimosus* fermentation broth was removed from a fermenter, split into three specimens and these were analysed consecutively using the Contraves viscometer.

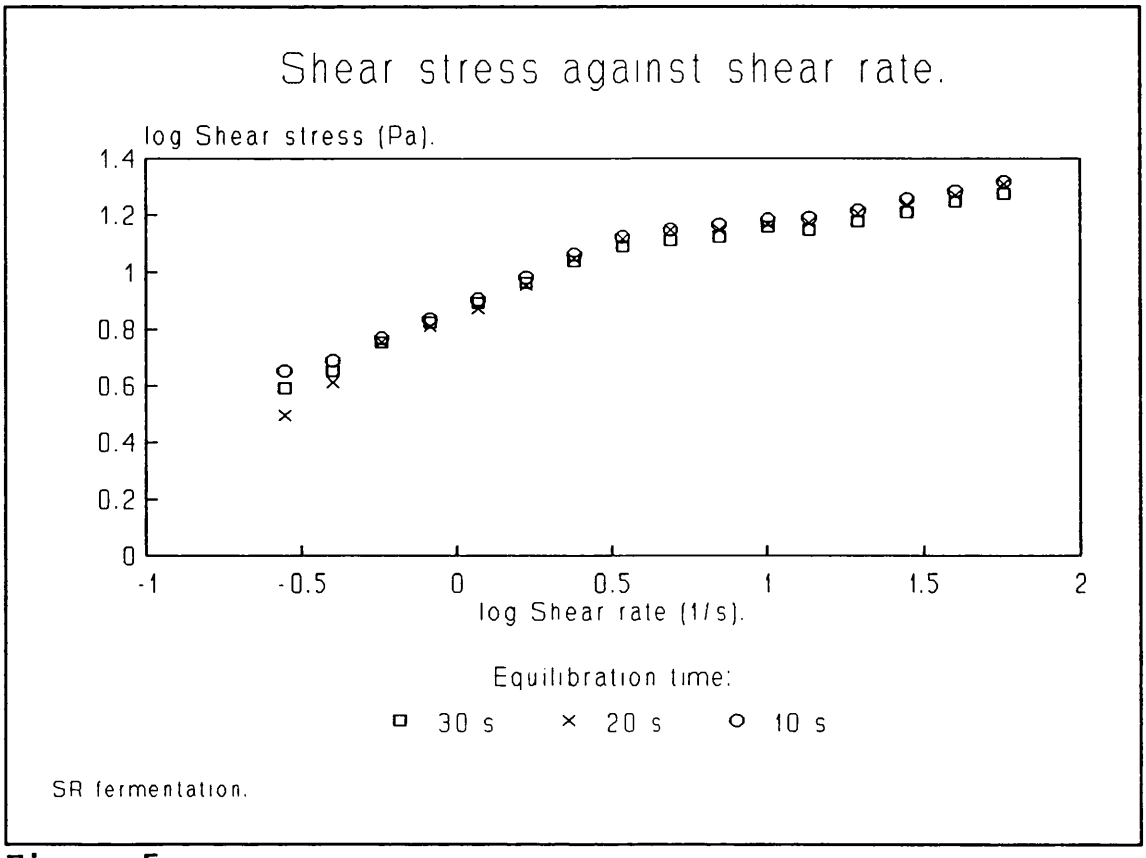

Figure 5

Equilibration times of 10, 20 and 30 seconds were used for each analysis. Figure 5 shows a plot of log shear stress against log shear rate for the three different equilibration times. The figure shows a reduction in shear stress for a given shear rate as the equilibration time increases. This was to be expected because of the thixotropic nature of the fermentation broth. Since the rheograms all exhibit the same shape and are closely grouped there appear to be no advantages in terms of data accuracy from an extended equilibration time. As the employment of a shorter equilibration time meant the overall analysis time was reduced, an equilibration time of fifteen seconds was chosen.

3.2 The Brookfield viscometer.

All data acquired with the Brookfield viscometer was obtained using the Brookfield 2HA DVII.

The data from the Brookfield viscometer were analysed

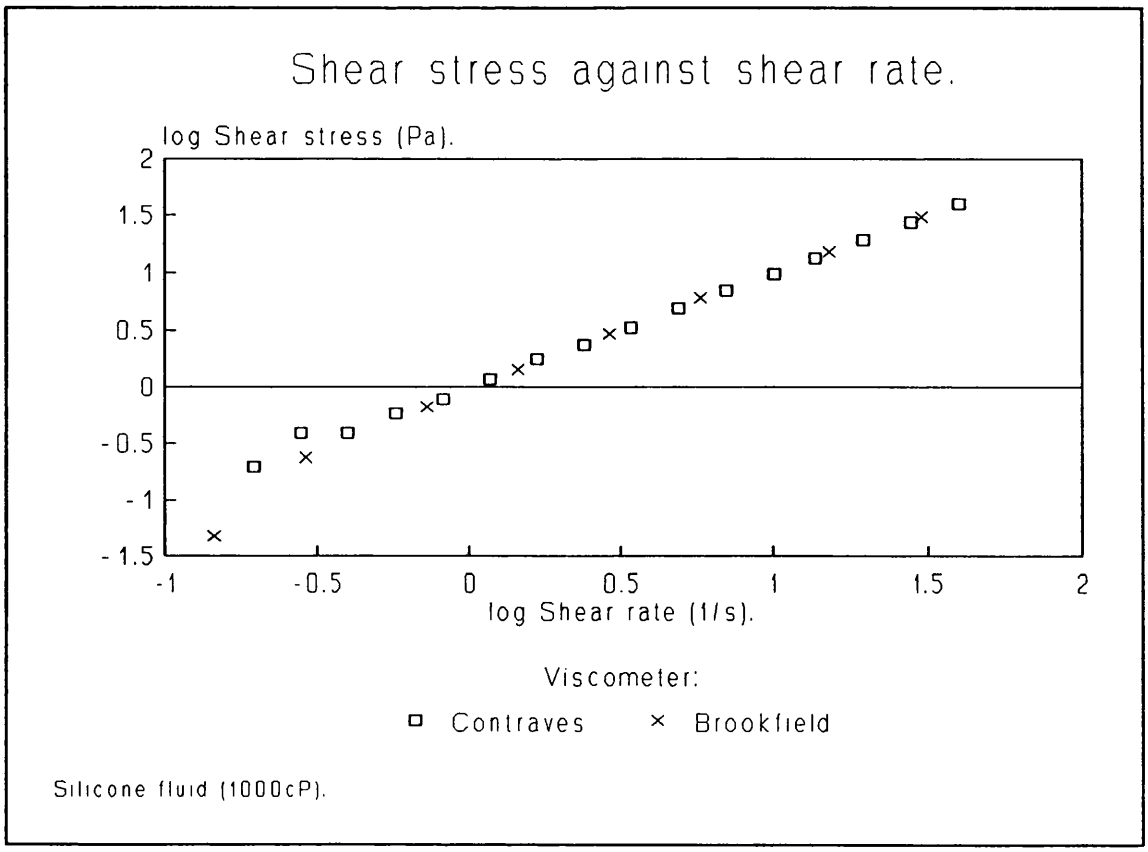

Figure 6

using a novel procedure devised by Mitschka [113] to calculate shear stresses and shear rates (see appendix). The paper by Mitschka has had little collaborative data in other research literature so the method was assessed for accuracy and reproducibility by direct comparison with the Contraves viscometer. Figure 6 shows a plot of log shear stress against log shear rate for the two viscometers using a 1000 cP Silicone fluid. The two straightline plots correspond almost precisely, except at the lowest shear rates where instrument insensitivity causes some data point scatter. By using linear regression analysis the equation for a straightline through each group of data was determined (some of the erroneous low shear rate data was ignored). From these equations the Power law parameters were (table 1):

Table 1. Rheological measurements for Silicone fluid.

Viscometer	Power law index,n	K
Contraves	0.998±0.007	0.991±0.028
Brookfield	1.019±0.021	0.968±0.027

A procedure in Kennedy and Neville [116] describes how the 95% confidence limits, shown in the table, were calculated for these constants. Table 1 shows the excellent correlation between the two viscometer systems, the Power law indices and the consistency coefficients are statistically equivalent when the 95% confidence limits are taken into account.

The Power law index and the consistency coefficient obtained from the Brookfield viscometer agree closely with the Silicone fluid's known values of 1.000 and 1 Pa.s, respectively. The Brookfield was regularly calibrated using the Silicone fluid; the Power law index and the consistency coefficient obtained were always equivalent to the Silicone fluid's known values when the 95% confidence limits were taken into consideration.

Figures 7, 8 and 9 show plots of log shear stress

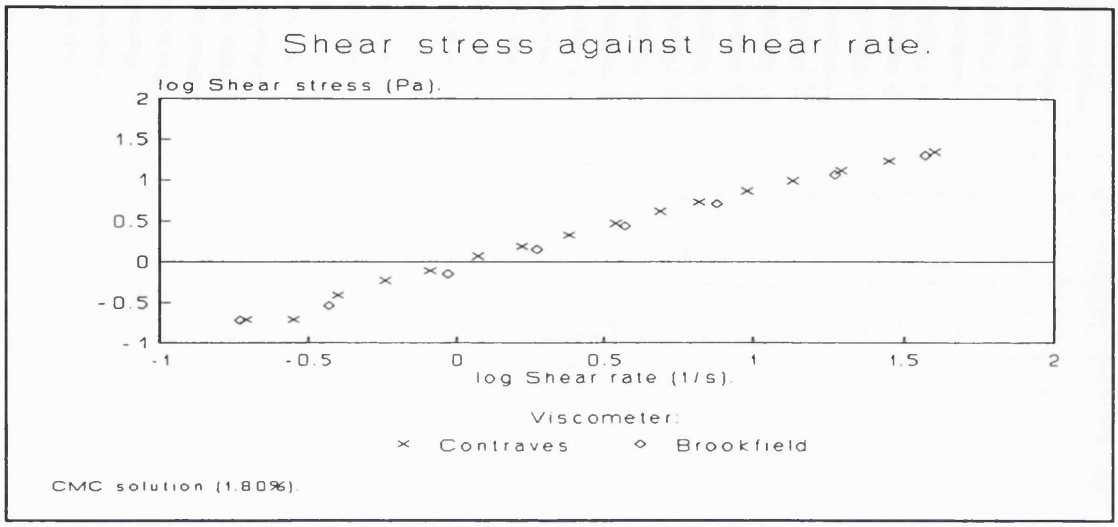

Figure 7

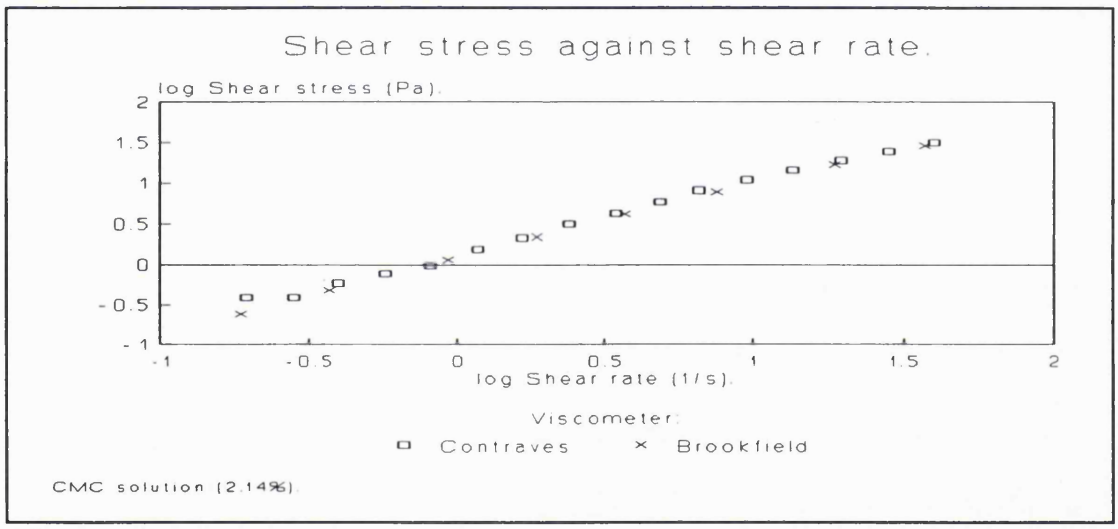

Figure 8

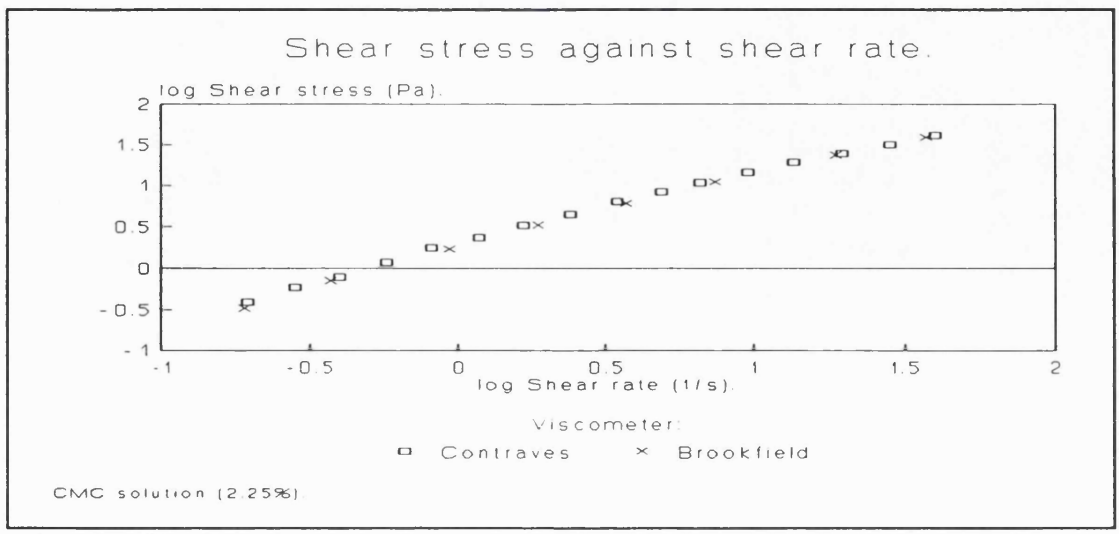

Figure 9

against log shear rate for the two viscometer systems using three different concentrations of carboxy methyl cellulose (CMC) solution. CMC is a polymer capable of producing a highly viscous pseudoplastic and homogeneous solution. From the figures it can be observed that the Brookfield data displays a close similarity to the Contraves data, although the Brookfield's data appears to indicate marginally lower shear stresses for a given shear rate than those of the Contraves. By the use of linear regression analysis the equations for straightlines through the Brookfield and Contraves data were determined. These equations allow the calculation of the Power law parameters (see table 2).

Table 2. Rheological measurements for CMC.

CMC soln (%wt)	Power law index		log Consistency Coefficient	
	Contraves	Brookfield	Contraves	Brookfield
1.80	0.905±0.018	0.905±0.018	0.046±0.040	0.120±0.033
2.14	0.899±0.010	0.910±0.015	0.121±0.022	0.071±0.028
2.25	0.860±0.013	0.897±0.025	0.295±0.028	0.237±0.045

Close examination of table 2 shows that, with the exception of the Consistency Coefficient for the 1.80%wt solution, all the remaining associated Contraves and Brookfield parameters were statistically equivalent when the 95% confidence limits were considered.

Figures 10, 11 and 12 show plots of log shear stress against log shear rate for the two rheological systems using three different *S. rimosus* fermentation broths. The Brookfield data exhibited a reasonably close resemblance to the Contraves data, although figure 11 shows some inconsistencies. By using regression analysis a straightline can be plotted through both groups of data. The equations for these straightlines allow Power law parameters for the fermentation broths to be determined. The following table shows a comparison of these parameters:

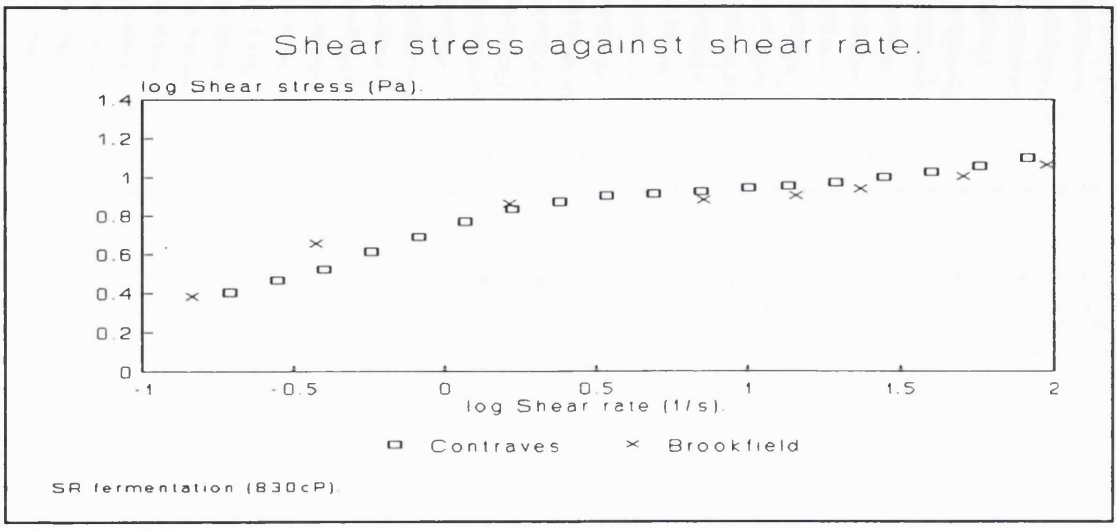

Figure 10

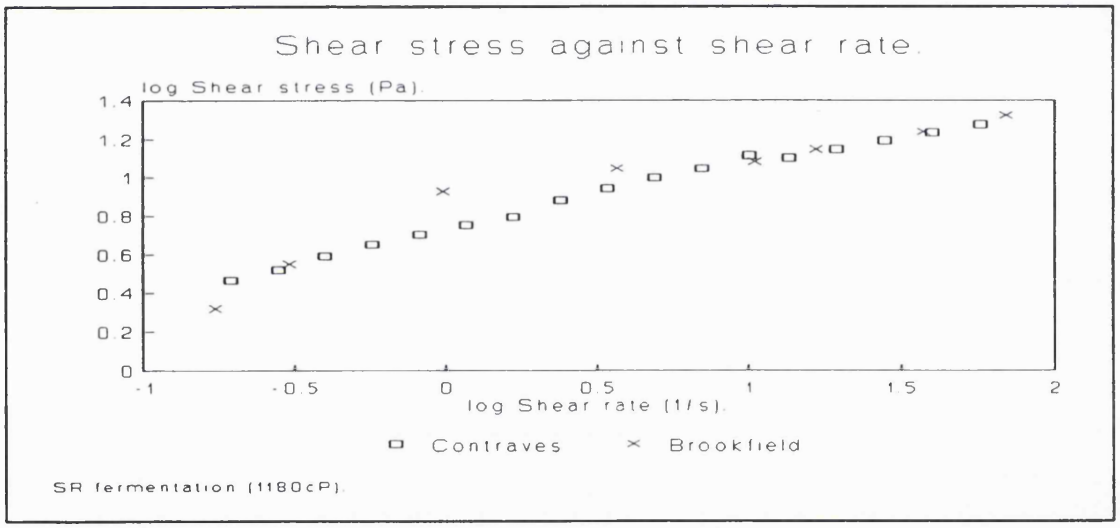

Figure 11

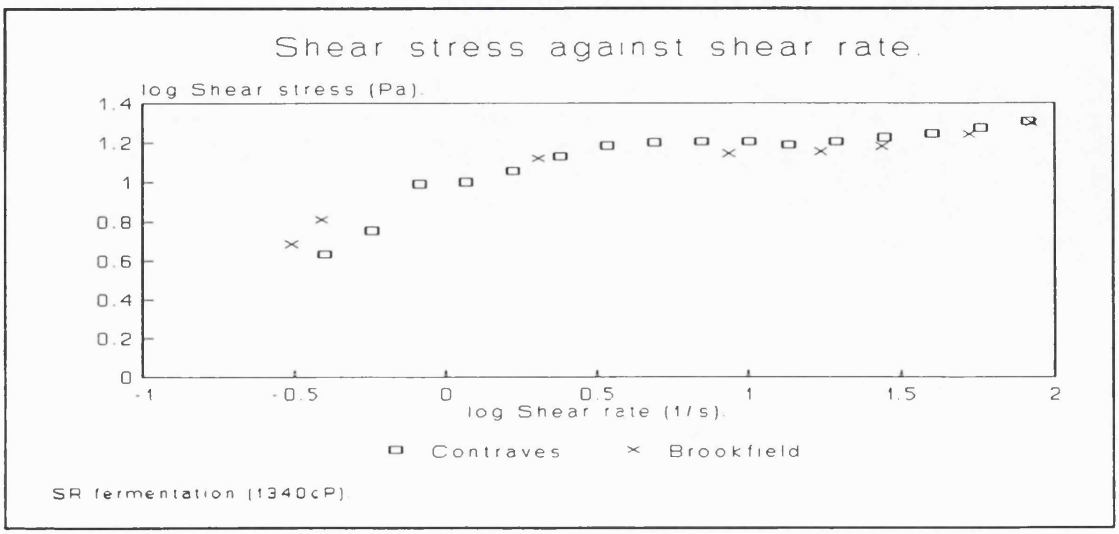

Figure 12

Table 3. *S. rimosus* rheological measurements.

Broth (cP)	Power law index, n		log K	
	Contraves	Brookfield	Contraves	Brookfield
1340	0.222±0.026	0.215±0.032	0.943±0.076	0.901±0.096
1180	0.333±0.006	0.343±0.043	0.732±0.017	0.745±0.120
830	0.241±0.012	0.202±0.028	0.685±0.041	0.685±0.091

Table 3 indicates that the associated Brookfield and Contraves figures are statistically equivalent when the 95% confidence limits are considered.

3.2.1 The Brookfield viscometer equilibration time.

The equilibration time for the Brookfield viscometer was determined by examining the traces produced by an attached chart recorder. Figures 13 shows the type of trace produced when a pseudoplastic fluid was analysed; as a new speed was selected the torque reading moves rapidly to a new value and remained steadfastly at this reading. Figure 14 shows the type of trace obtained when the *S. rimosus* fermentation broth was analysed; the torque value changed fairly rapidly as a different speed was selected but during the up-curve the reading fell continuously for the entire equilibration period. A comparison of figure 14 and figure 15 shows remarkable similarities, according to Walters [54] this figure represents a typical trace for a thixotropic fluid. Also, a comparison of figure 14 with figure 22 (in chapter one) indicates thixotropic properties. A period of thirty seconds was chosen as the equilibration time for the Brookfield viscometer. This interval allowed the readings to become more stable and meant that the complete Brookfield analysis did not take too long. The Brookfield viscometer used a soft torque measuring system compared to the stiff torque measuring system used by the Contraves, therefore the longer ET for the Brookfield was appropriate.

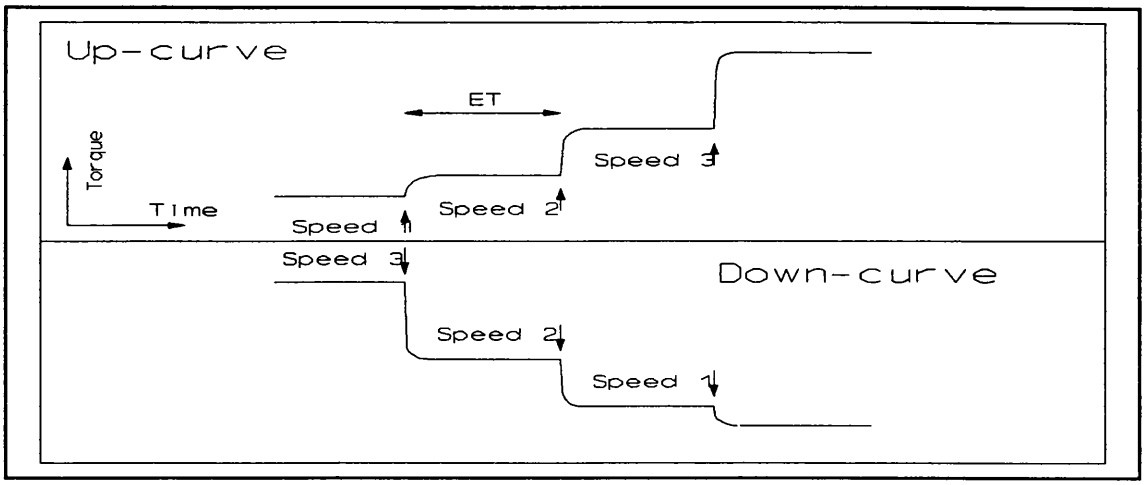

Figure 13: Typical chart recorder trace for pseudoplastic fluid.

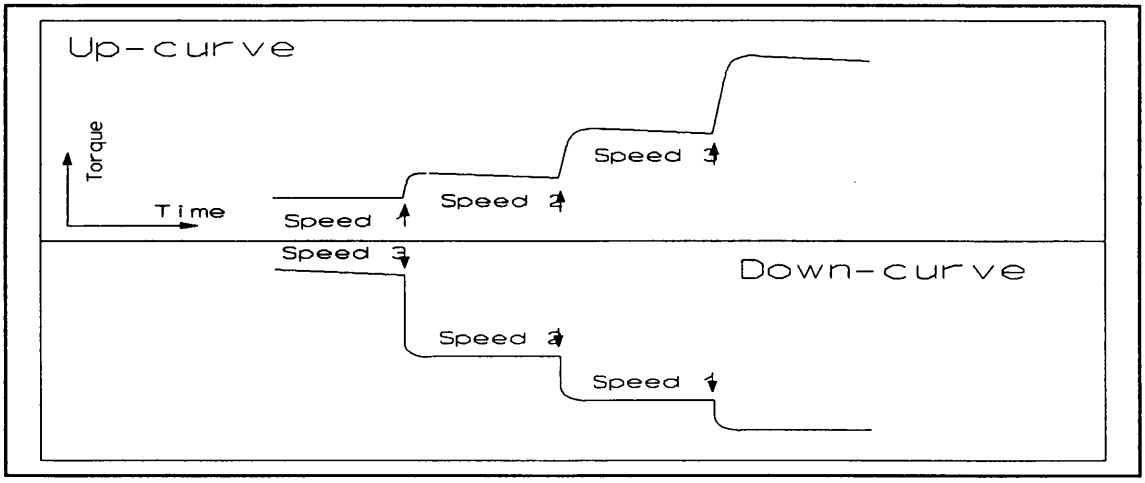

Figure 14: A typical chart recorder trace for the *S. rimosus* fermentation broth.

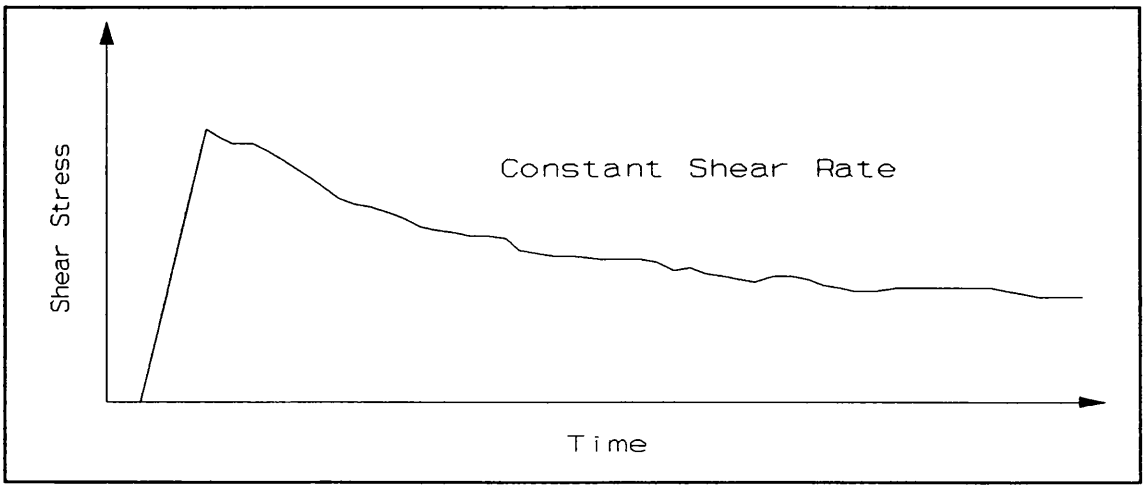

Figure 15: A typical trace for a thixotropic fluid.

3.3 The physical properties of fermentation broths.

The next experiments were used to determine the physical properties of the *S. rimosus* fermentation broth.

3.3.1 Fermentation broth reproducibility.

At the beginning it was necessary to demonstrate that two samples from a single fermenter source would produce comparable results. The fermentation broth may be so heterogeneous that reproducible results are not possible. A sample was removed from a fermenter, split into two specimens and these were analysed consecutively using the Contraves viscometer. Figures 16 and 17 show comparisons of the data from these specimens for two different *S. rimosus* fermentation broths. The plots display good reproducibility between the data from the specimens, although the data at low shear rates demonstrated small discrepancies. This disparity may result from the heterogeneous nature of the fermentation broths. At low shear rates, insufficient mixing meant that any localised regions of heterogeneity were exposed and caused anomalous results. At a later stage this experiment was repeated using both *S. erythraeus* and *A. roseorufa* cultures to prove that these broths also produced highly reproducible data.

3.3.2 Fermentation broth ageing.

Leaving samples to stand before analysis may result in significant changes to the rheological properties of the fermentation broth. On standing the fermentation broth may chemically react or de-aerate and cause a critical change in the broth rheology to take place. A sample was removed from a fermenter, split into four specimens and stored for periods of zero, one, two and four hours before analysis with the Contraves viscometer. Figure 18 displays a plot of log shear stress against log shear rate for these specimens. The figure indicates that storage

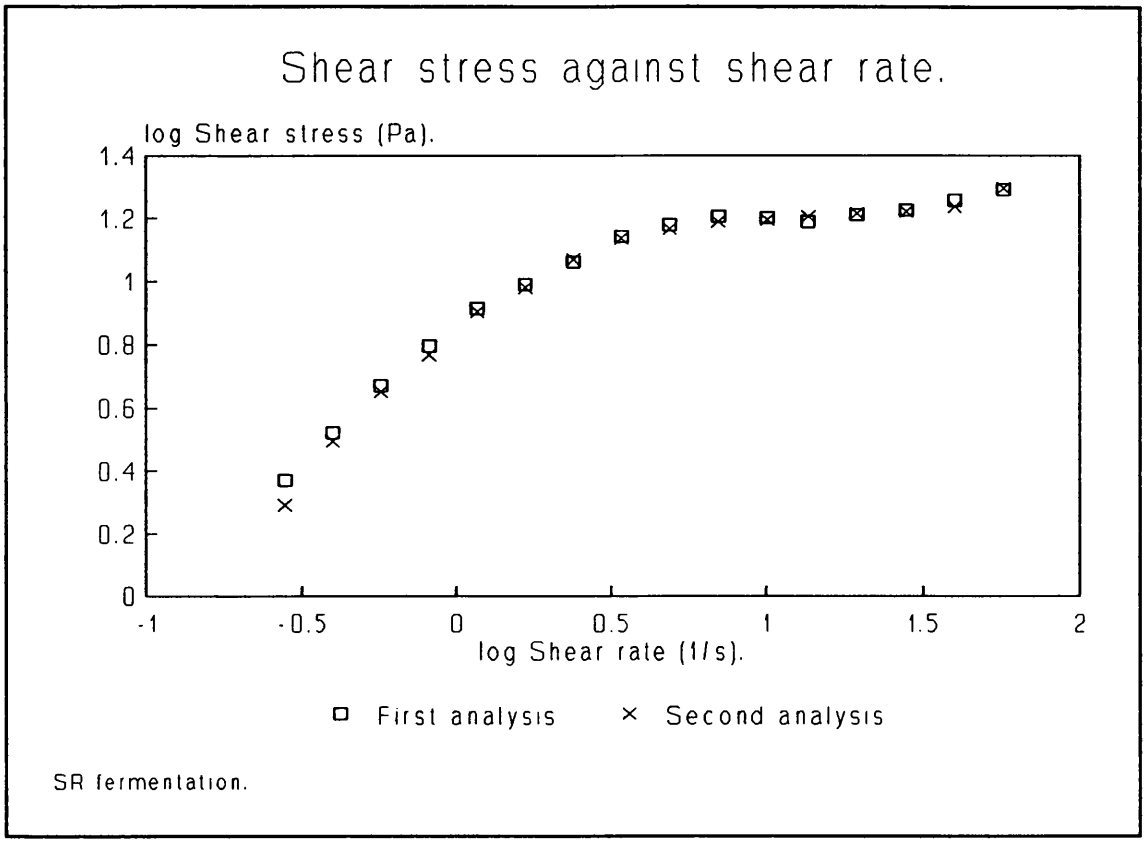

Figure 16

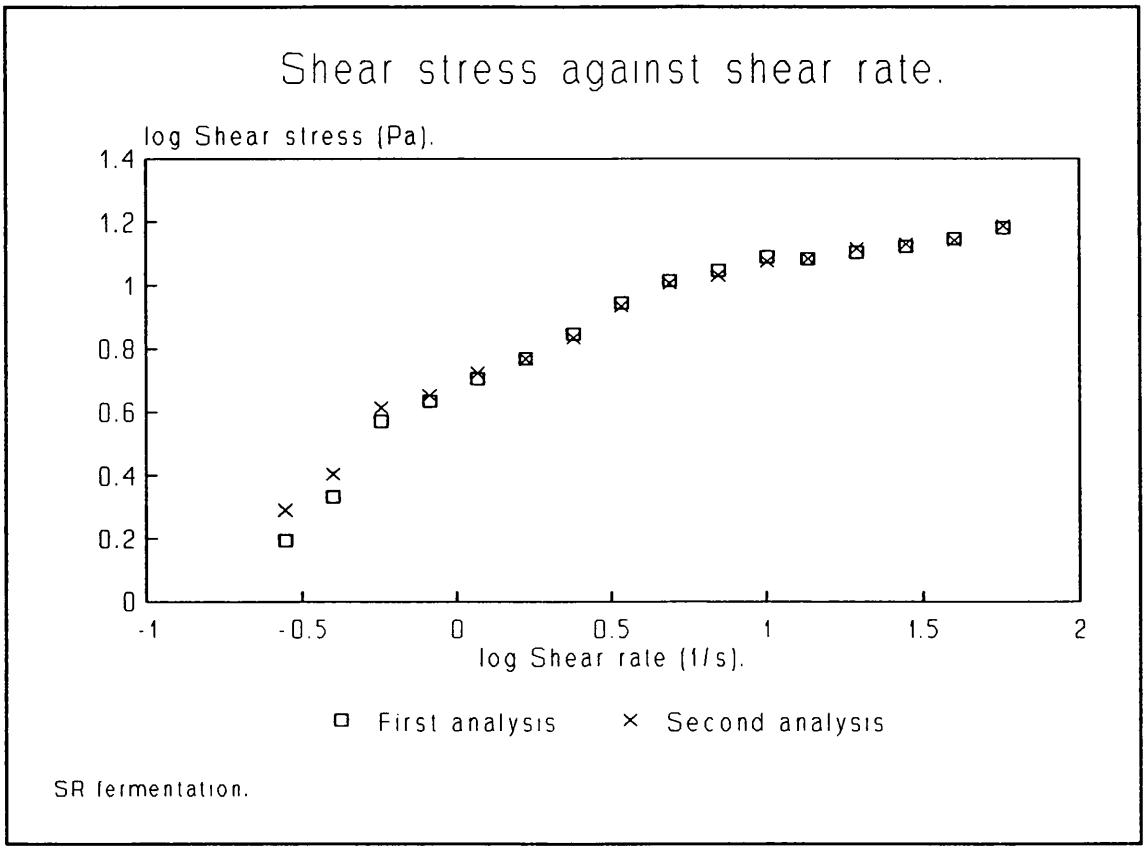

Figure 17

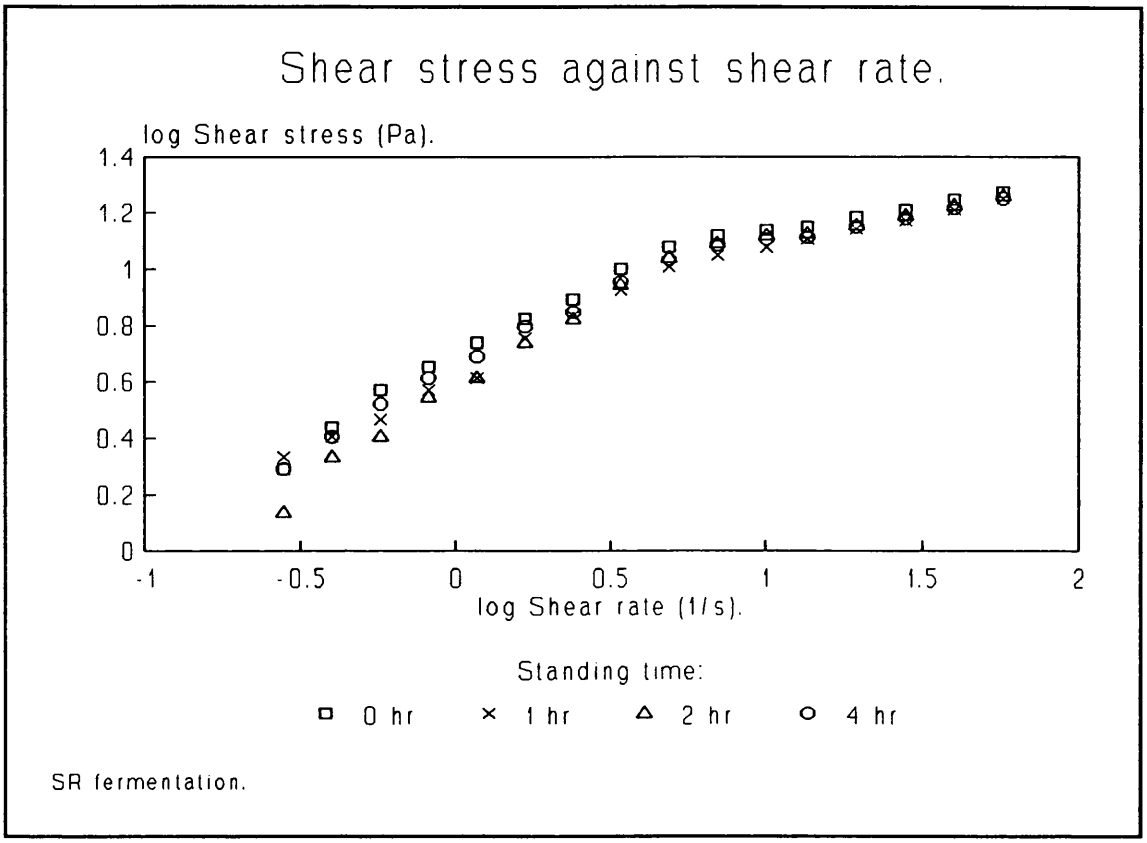

Figure 18

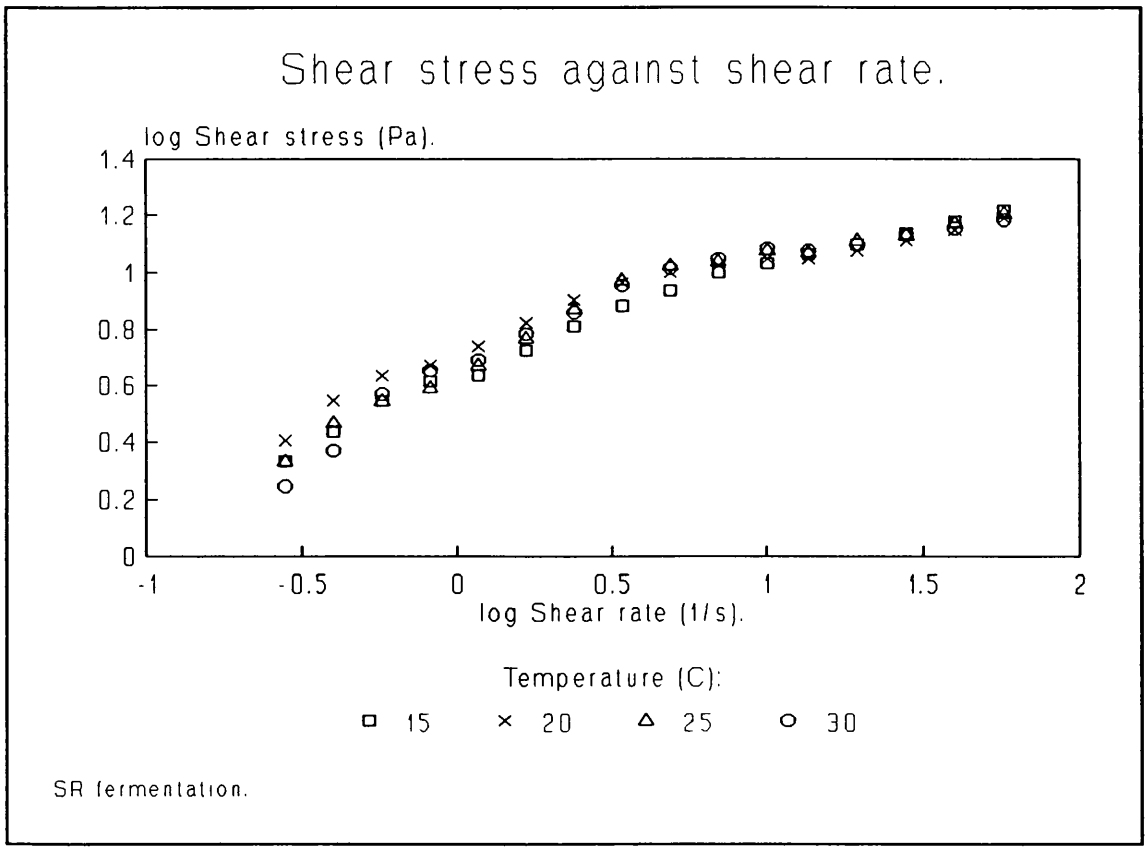

Figure 19

did have some effect on the rheological properties of broth. However, no obvious trend could be detected in the data. This experiment was repeated using *S. erythraeus* and *A. roseorufa* broths, once again a trend could not be distinguished in the ageing data.

3.3.3 Fermentation broth temperature.

Viscosities of liquids are generally temperature dependent; normally they show a decrease in viscosity with an increase in temperature. A sample was removed from a fermenter, split into four specimens and stored at temperatures of 15, 20, 25 and 30°C before analysis with the Contraves viscometer. As each specimen was initially at the same temperature a sufficient period was allowed for the desired temperature of all the specimens to be reached. The viscous nature of the broth means that a long period of cooling was required to ensure a stable temperature throughout the sample. During the rheological analysis the specimen temperatures were maintained by circulating water at the desired analysis temperature through the heating/cooling chamber of the Contraves. Figure 19 shows a plot of log shear stress against log shear rate for the samples at different temperatures. The figure indicates that these temperature differences had a minimal effect on the rheological properties of the fermentation broths. Since the changes show no obvious pattern it must be concluded that other more influential factors were present.

3.3.4 Fermentation broth de-aeration.

The *S. rimosus* fermentation broth contains large quantities of trapped air-bubbles. The de-aeration of the broth could have given novel rheological characteristics. A sample of fermentation broth was removed from a fermenter and split into three specimens. Two of the specimens were de-aerated by subjecting the broth to a vacuum for an hour and then one of these broths was re-aerated by air sparging

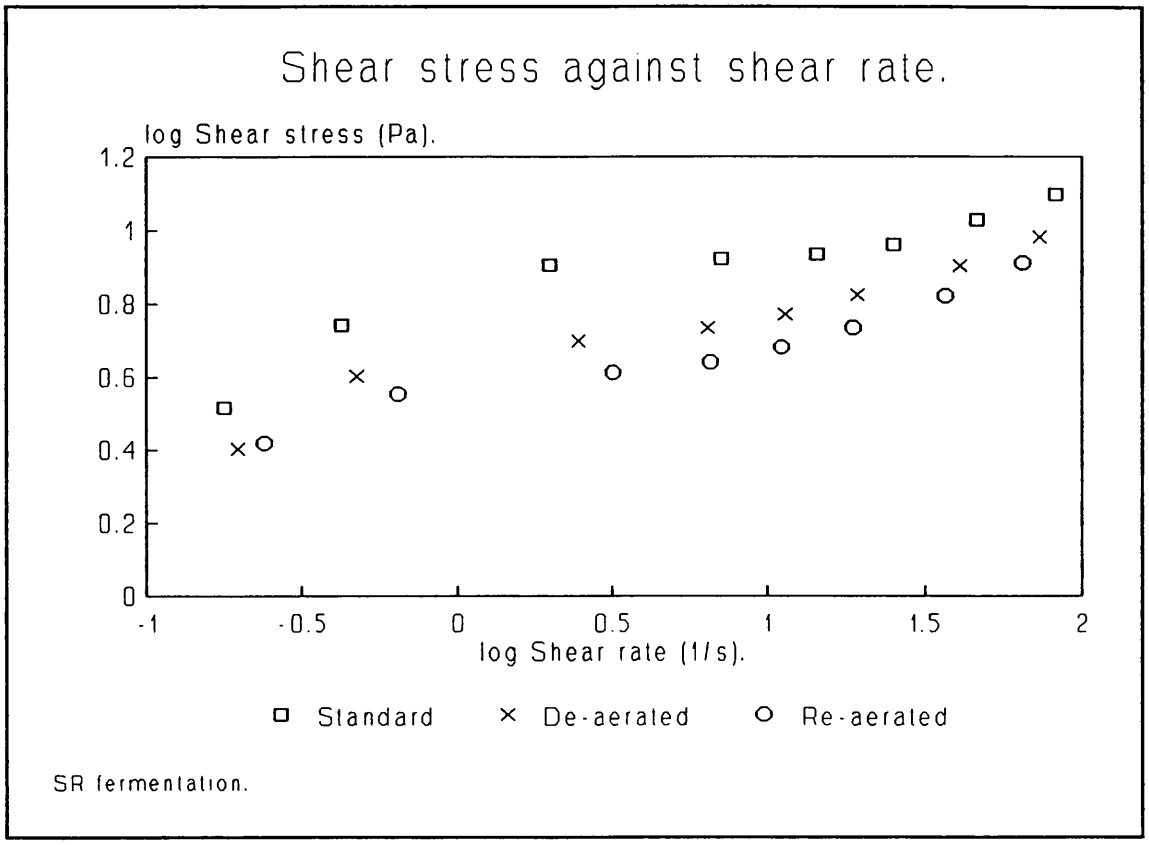

Figure 20

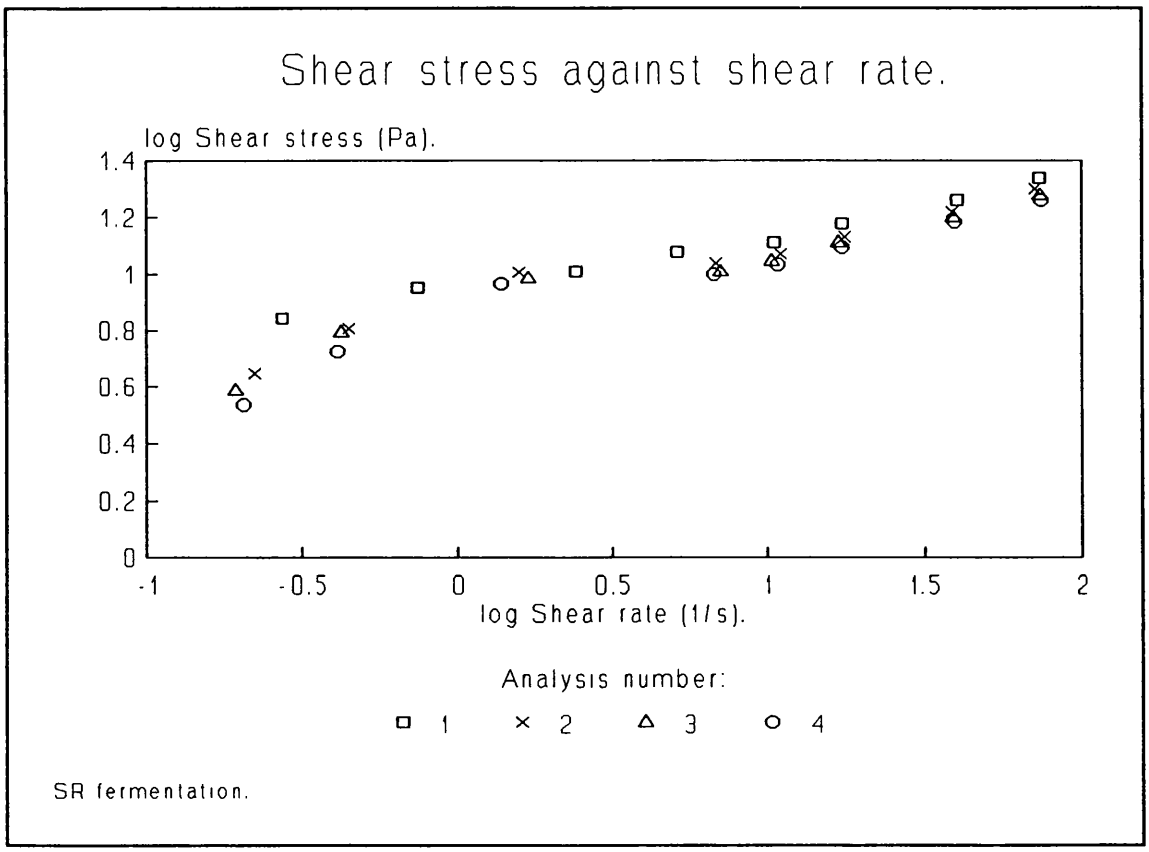

Figure 21

for an hour. Next, the three specimens were analysed consecutively using a Brookfield viscometer. Figure 20 shows a plot of log shear stress against log shear rate for these three specimens. The figure indicates that each specimen has similar rheological characteristics because the shapes of the curves remain the same. However, the apparent viscosity of the standard broth is higher than the de-aerated broth which is higher than the re-aerated broth. The initial supposition might be that the removal of the air-bubbles had reduced the apparent viscosity of the broth, but this cannot be correct as the re-aerated broth was even less viscous than the de-aerated broth. A plausible theory is that the actions of de-aeration and re-aeration caused considerable shearing of the broth and resulted in a reduction in the apparent viscosity because of the thixotropic nature of the broth. Since de-aeration of the broth without the vacuum cannot be achieved in a reasonable period of time no further investigation in this direction was deemed beneficial.

3.3.5 Fermentation broth hysteresis.

The *S. rimosus* fermentation broth has been shown to be thixotropic by the characteristic hysteresis effect produced when plotting the shear stresses at various shear rates from the up-curve and the down-curve data, see figures 2 and 3. Figure 21 shows the up-curve data for a plot of log shear stress against log shear rate for an *S. rimosus* fermentation broth when analysed four times consecutively. Only the up-curve data have been shown for reasons of clarity, however the curves clearly show that the shear stresses, for a given shear rate, reduced with each subsequent analysis.

3.4 Image analysis.

3.4.1 Dilution of the broth samples.

The most accurate image analysis results were obtained when the optimum concentration of filamentous organisms were on the microscope slide. The best conditions occurred when at least five organisms were present in each image analysis field, but not too many organisms to cause excessive hyphal overlap. To ensure a good concentration of organisms several microscopic slides were prepared using a range of broth dilutions. Four slides were prepared at dilutions of 1/50, 1/100, 1/250 and 1/500 of the original broth concentration. Studying these slides using the microscope revealed that the 1/250 slide produced the best results.

3.4.2 Number of organisms analysed.

Using the ANOVA method explained by Kennedy and Neville [116], more than five hundred and fifty organisms must be analysed to detect a significant difference between the mean mycelial lengths that are measured over the length of the fermentation.

3.4.3 Software Modification.

The software program by Adams and Thomas [41] and Packer and Thomas [42] was developed for making morphological measurements on any filamentous microorganism. However, certain sections of the program had to be microorganism-specific for optimum automatic operation. Since development work was undertaken using an isolate of *S. clavuligerus* some areas of the programme had to be modified for use with other organisms, in this case, *S. rimosus, S.erythraeus and A. roseorufa.* The regions of the programme that required attention were:

1) Debris removal.

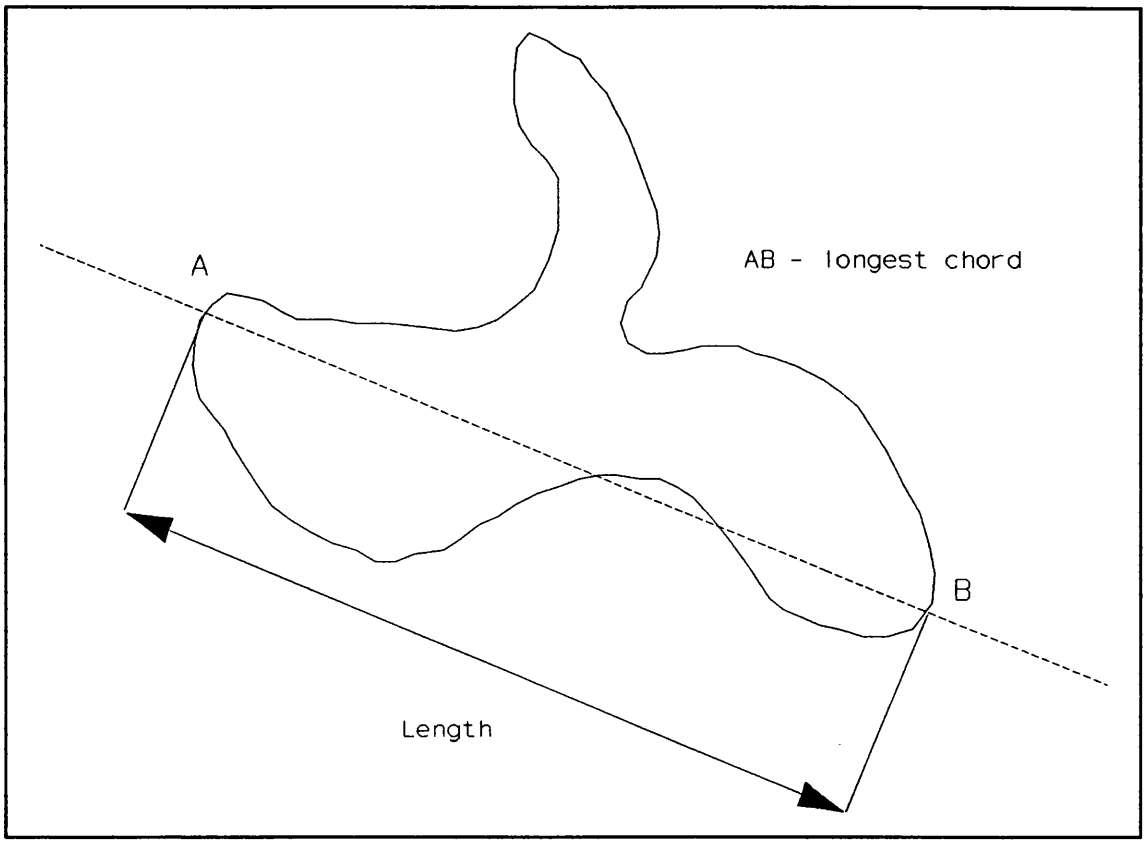

Figure 22: The length of an object.

2) Noise removal.

After thresholding, see sections 1.2.2.2 and 2.2.2.1, all objects in the chosen range of greyness intensity became selected whilst all others were rejected as background. The selected objects consist of microorganisms in the main, but inevitably a few foreign objects were also included. These foreign objects consisted of media particulates, dye crystals, and dust. Debris Removal was the section of the program that differentiates between these pieces of debris and the microorganisms. Three parameters were used in the selection process [49]:

1) Length.
2) Area.
3) Circularity.

The program measured a particular object by moving a chord from position A, see figure 22, to all other points on the perimeter of the object. At the position AB shown,

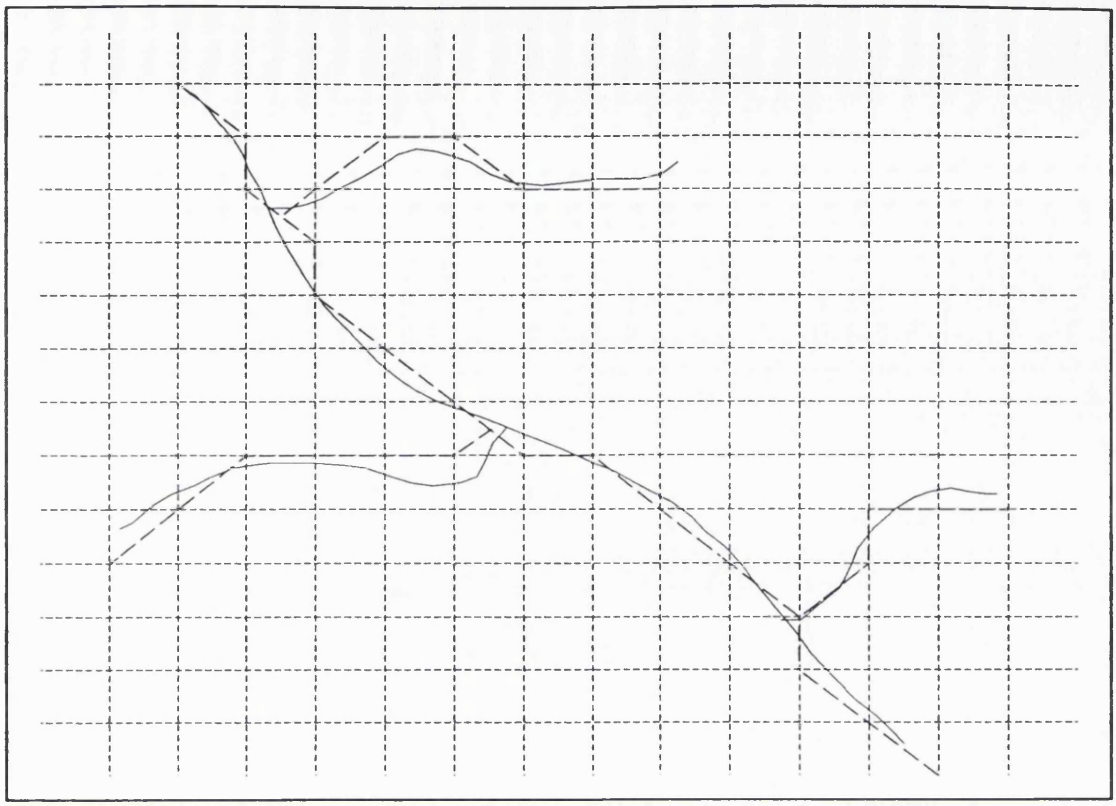

Figure 23: Measurement of the perimeter of a object.

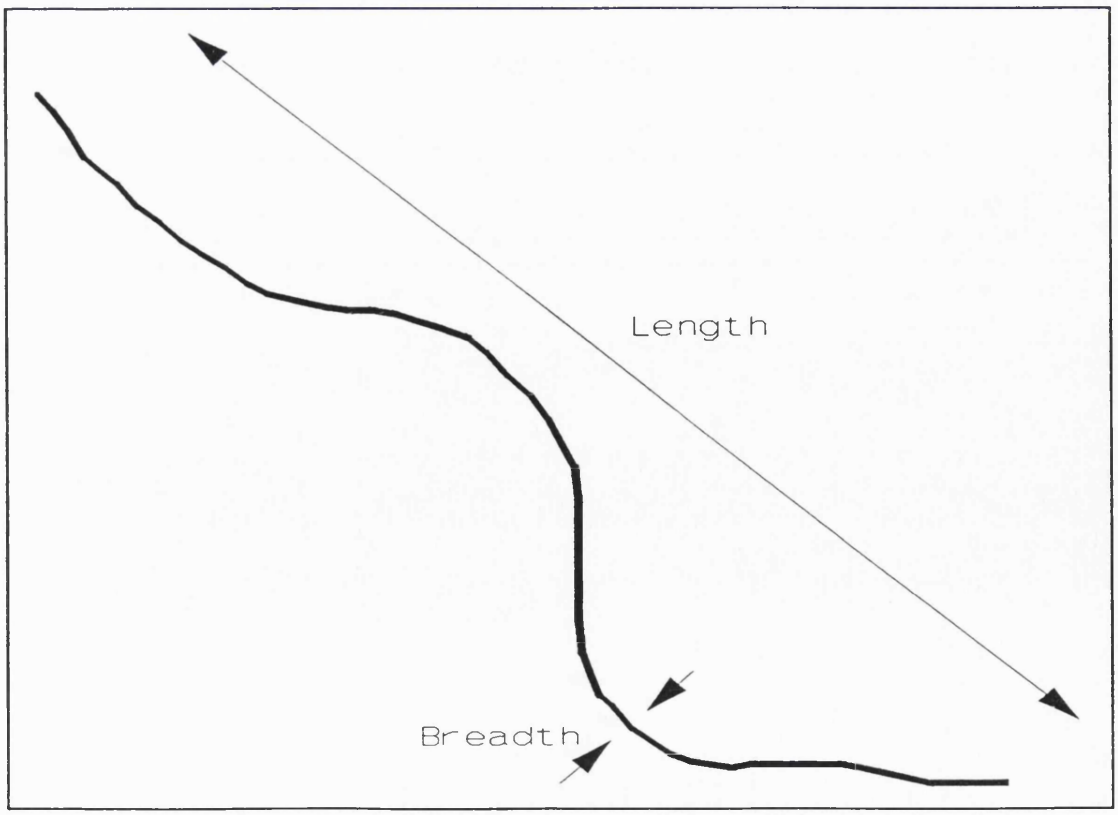

Figure 24: The high length to breadth ratio of filamentous microorganisms.

this chord is at maximum length; hence, the distance from A to B became known as the length of the object. The Area of an object was calculated using a calculus procedure that integrated along the boundary of the object. The Circularity parameter is a measure of how closely the object under scrutiny resembled a circle. The parameter can have a value between one and zero with unity denoting a circle.

$$Circularity = \frac{4 \cdot \pi \cdot Area}{(Perimeter)^2} \qquad (1)$$

The perimeter was measured using the procedure shown in figure 23. Filamentous microorganisms have a high length to breadth ratio, see figure 24. Hence, the typical shape of these filamentous microorganisms was completely different from most debris which tended to be circular. The circularity parameter took advantage of this difference. Using these three parameters it was possible, for a specific group of microorganisms in a given fermentation, to find a value for each parameter that ensured the optimum distinction and hence solution between the microorganisms and debris. Some debris was indistinguishable from the microorganisms even for the machine operator. The results caused by such deceptions were erroneous, but given the large number of microorganisms examined and the small number of foreign objects defying the rejection procedure the consequences of such data were negligible. In order that values could be determined for these parameters, it was necessary to make a preliminary study of several slides from these particular fermentations. The slides and microscope were prepared as normal, see section 2.2.2.1 and 2.2.2.2 respectively. The image analyser was run on a manual basis by using the object editor. After the field had been thresholded the operator pointed to objects of interest using a light pen. The measurements taken from each body were of length, area and perimeter. The operator selected pieces of debris

from a slide; the objects were measured and the results placed in a file. Then, in a second file the measurements of microorganisms from the same slide were stored. By comparison of the population distributions for length, area and circularity, see figures 25-30, it was possible to devise an algorithm that differentiates between debris and microorganisms. The circularity values shown in the figures 29-30 would appear to contradict the statement made earlier that suggested circularity could only vary between zero and one. Values of greater than unity were recorded because the image analyser was incapable of measuring accurately areas and perimeters for very small objects. Since only particles of debris were affected, the problem was considered unimportant in terms of morphological analysis and disregarded.

The data shown in the histograms were from the different *S. rimosus* fermentations at various fermentation times. For an object to be selected it had to conform to the following rules:

1) Length greater than 9 pixels.
2) Area greater than 28 pixels.
3) Circularity less than 0.84.

By reassessing data collected on the debris and the microorganisms with these rules it was possible to determine the effectiveness of the algorithm. The measurements of six hundred *S. rimosus* organisms and six hundred pieces of debris from the fermentation were stored in a data file. By comparing these measurements with the algorithm rules then the number of organisms mistaken for debris and the amount of debris mistaken for an organism could be assessed. The figures are shown in table 5.

It should be remembered when looking at these figures that often the machine operator for some objects could only just distinguish between the two groups. Given the highly fragmented nature of this fermentation the figures seemed reasonable.

To include this algorithm in the main program a piece of code was written in Pascal. This modification was

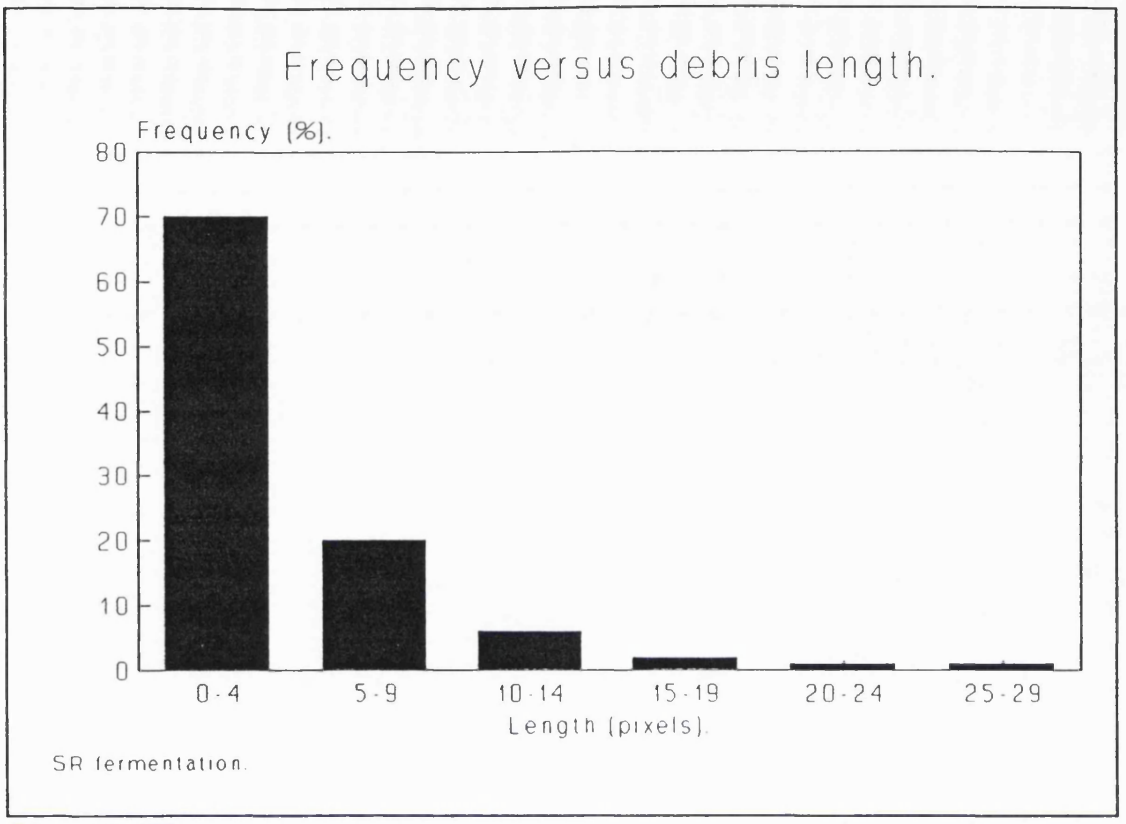

Figure 25

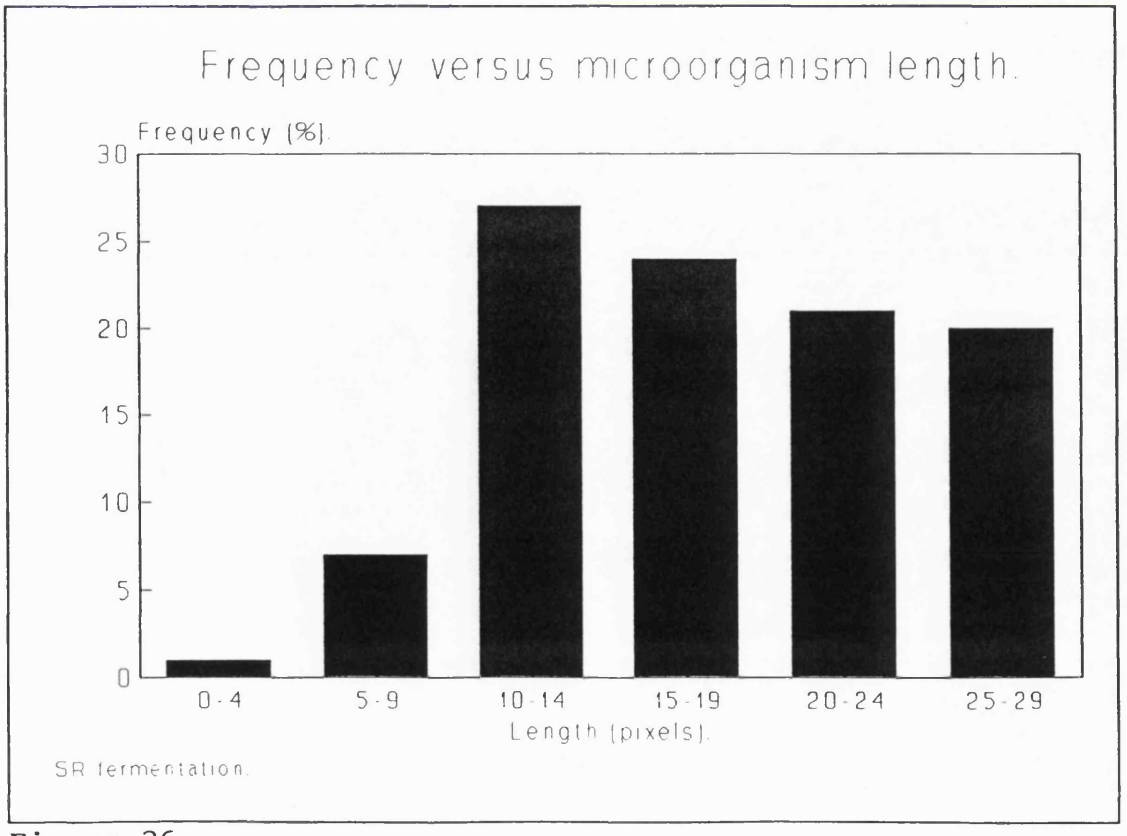

Figure 26

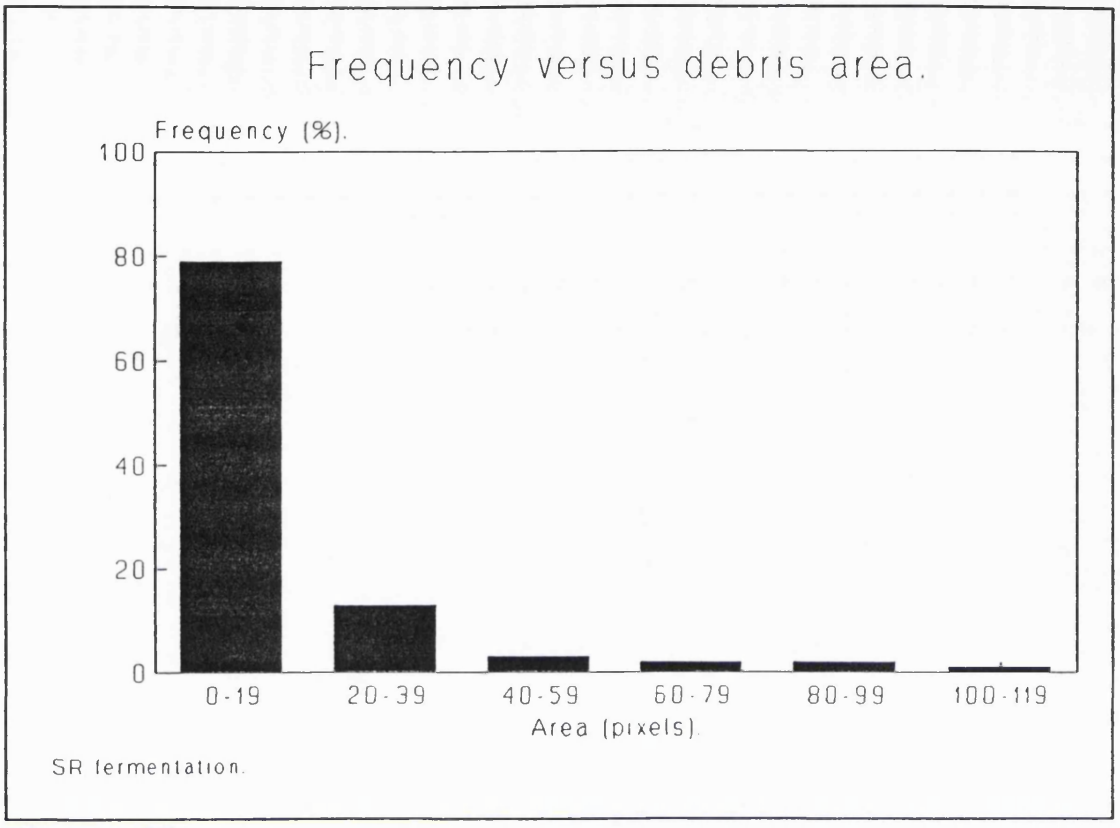

Figure 27

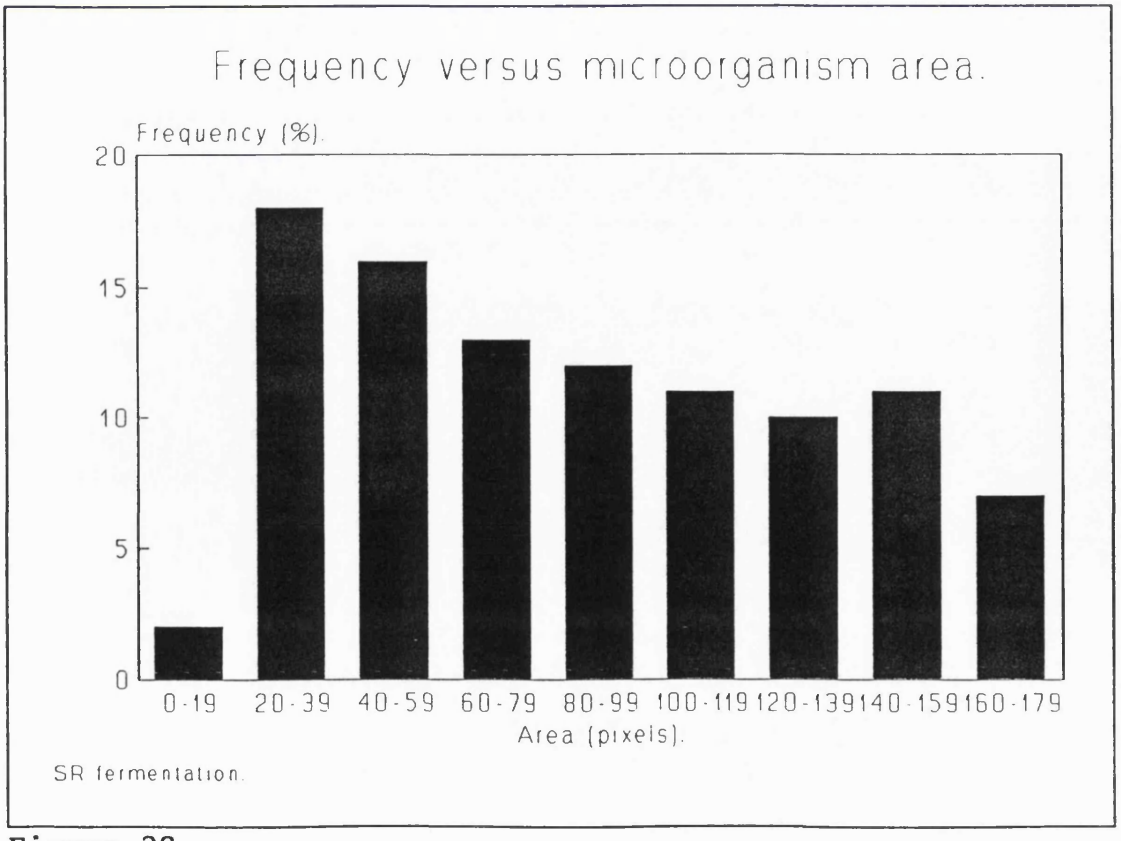

Figure 28

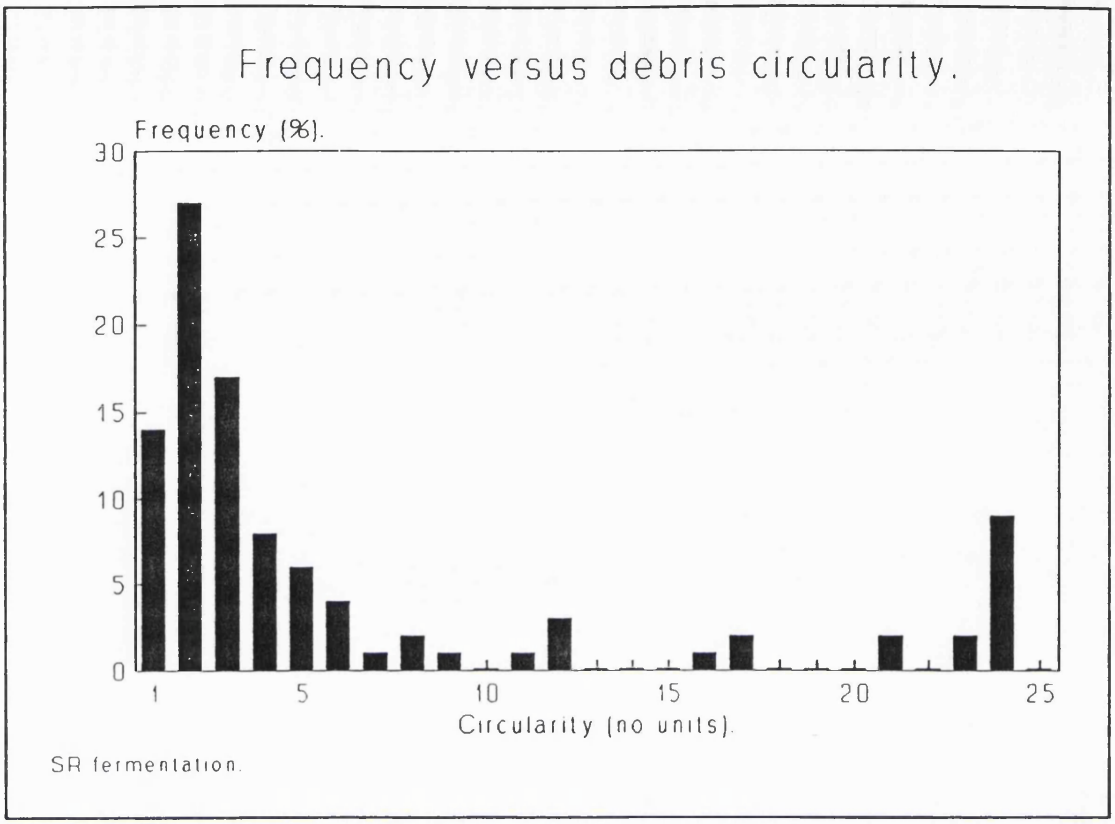

Figure 29

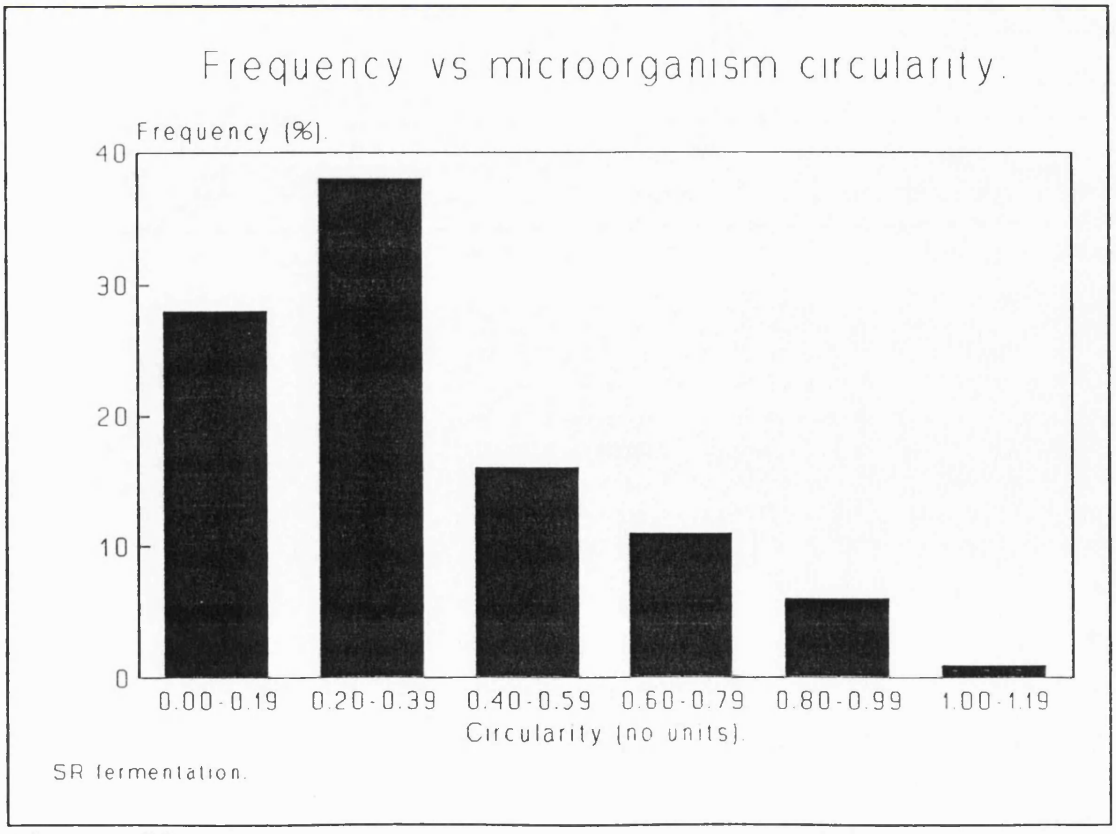

Figure 30

extremely complex and time consuming, hence no further alterations were made for analysing *S. erythraeus* and *A. roserufa* organisms even though these organisms have a slightly different morphology. However, the effectiveness of the modifications for the selection of these organisms was examined using the procedure outlined above. The following table shows the results of these examinations:

Table 4. Organism and debris selection rates.

Organism	Organisms rejected	Debris selected
S. rimosus	10%	2%
S. erythraeus	3%	3%
A.roseorufa	7%	2.5%

In comparison with the figures for the *S. rimosus* organisms, these values show less microorganisms are rejected and a similar number of pieces of debris are selected. This is because both the *A. roseorufa* and the *S. erythraeus* organisms are on average longer than the *S. rimosus* organisms and therefore less likely to be mistaken for debris. In any complex media fermentation the quantity of debris will mean that some will be mistaken

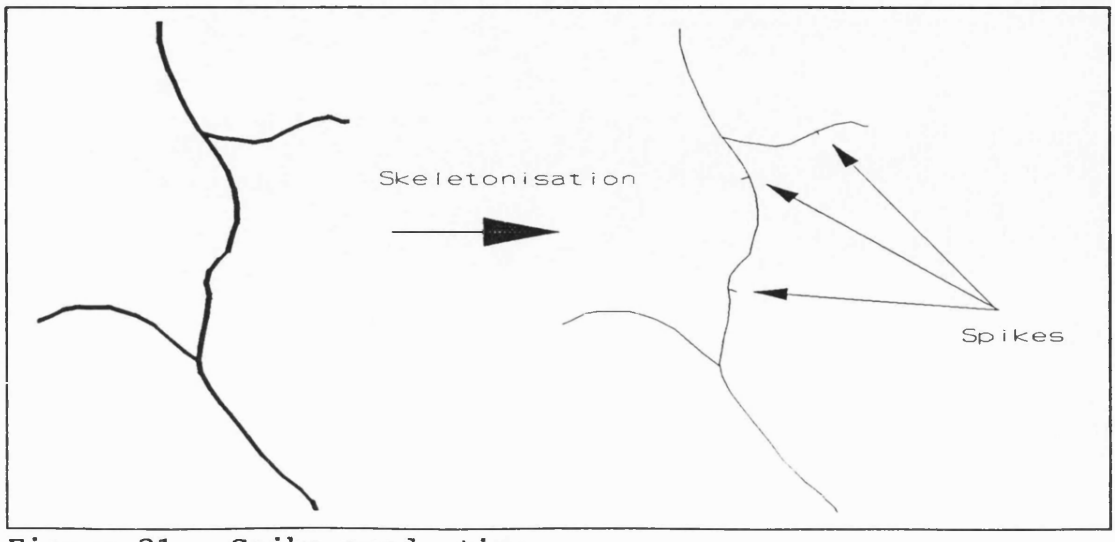

Figure 31: Spike production.

for the organism, but the levels of only 2-3% are not a significant problem. Although alteration of the selection parameters might reduce the amount of debris selected, the reduction in errors would be small and the time consumed to make the changes would be too great.

An unfortunate side-effect of the skeletonisation process was the production of spurious spikes known as noise, see figure 31. The noise removal section of the image analysis software studies all skeletonised objects and removes these spikes. The difference between a spike and a skeletonised branch were indistinguishable. Thus a decision was made to define a spike as any branch less than 1µm long, since this was the mean length of spikes produced.

3.4.4 Image analysis reproducibility.

This project aimed to show that a change in the rheology of the fermentation broth correlated to a transformation in the morphology of the fermentation microorganisms. To prove a difference in morphology had taken place, the image analysis system had to be capable of achieving reproducible results; the mean measurements of microorganisms from duplicates of a single sample must be statistically equivalent.

A sample of *S. rimosus* fermentation broth was removed from a fermenter and split into duplicate specimens. These specimens were smeared onto separate microscope slides (slide A and slide B), see section 2.2.1 for a detailed description of the process. The image analyser was used to measure over six hundred *S. rimosus* organisms on each of the slides using the procedure discussed in section 2.2.2. The following table gives a comparison of mean mycelial lengths for many different samples:

Table 5. Mean main mycelial lengths for *S. rimosus*

Sample number	Slide A		Slide B	
	mean (μm)	95% CL (μm)	mean (μm)	95% CL (μm)
1	8.521	1.405	8.690	1.409
2	9.062	1.631	8.889	1.495
3	9.325	1.531	9.150	1.660
4	9.865	1.717	11.369	1.601
5	10.090	1.499	9.548	1.652
6	10.256	1.991	12.419	1.684
7	10.670	1.768	11.125	2.042
8	11.168	2.140	10.832	1.987
9	11.489	1.925	13.025	2.087
10	12.233	2.244	10.538	2.35
11	12.295	2.287	12.131	2.272
12	12.465	2.446	11.145	2.395
13	12.736	2.272	11.099	2.376
14	13.323	2.332	15.634	2.155
15	13.355	2.415	13.662	2.711
16	13.607	1.962	11.255	2.301
17	14.106	2.468	14.166	2.540
18	14.676	2.407	15.178	2.568
19	14.958	2.358	13.692	2.185
20	15.102	2.648	15.564	2.585
21	15.388	2.289	15.328	2.511

In every case the mean mycelial lengths for the duplicates can be considered statistically equivalent since they lie within the 95% confidence limits of each other.

4 The *Streptomyces erythraeus* fermentation results.

The rheological and fermentation data for *S. erythraeus* are presented in figures 1 to 8. Rheological data are presented in terms of the two power law parameters K and n.

Figures 1 to 4 are entitled Fermentation Profile (part one) and display data for fermentations SE1, SE2, SE3 and SE4 respectively. These plots show the consistency coefficient, K, ($Pa.s^n$) and total oxygen consumption, TOC, (moles) against fermentation time (hours). Additionally, figures 2, 3 and 4 show plots of dry cell weight, DCW, ($g.l^{-1}$) as function of fermentation time.

The plots of consistency coefficient in figures 1 and 3 show close similarities. Both plots of the K data rise over the first 50-70 hours, plateau until approximately 120 hours and then decrease for the remainder of the fermentation. In comparison, the profiles of K in figures 2 and 4 show a different type of pattern. These plots show the K data peaking earlier at ≈70 hours, then decreasing to almost zero by ≈120 hours and remaining at this low level for the remainder of the fermentation.

There was an excellent agreement between the TOC profiles for all the *S. erythraeus* fermentations and this was a reflection of the controlled nutrient feeding occurring during the fermentation. The plots of TOC rose at a fairly constant rate over the duration of the fermentation. Fermentation SE2 shows the highest values of TOC followed by SE4 and then SE1 and SE3 have the lowest values.

The DCW data in figures 1 and 3 indicate that the cell concentration rose to a peak at ≈100-110 hours and then fell throughout the remainder of the fermentation. However, figures 2 and 4 show the DCW peaking at ≈70-80 hours. All the DCW plots show considerable scatter because of the difficulties involved in measuring dry cell weight accurately.

The DCW data and the TOC data indicate that

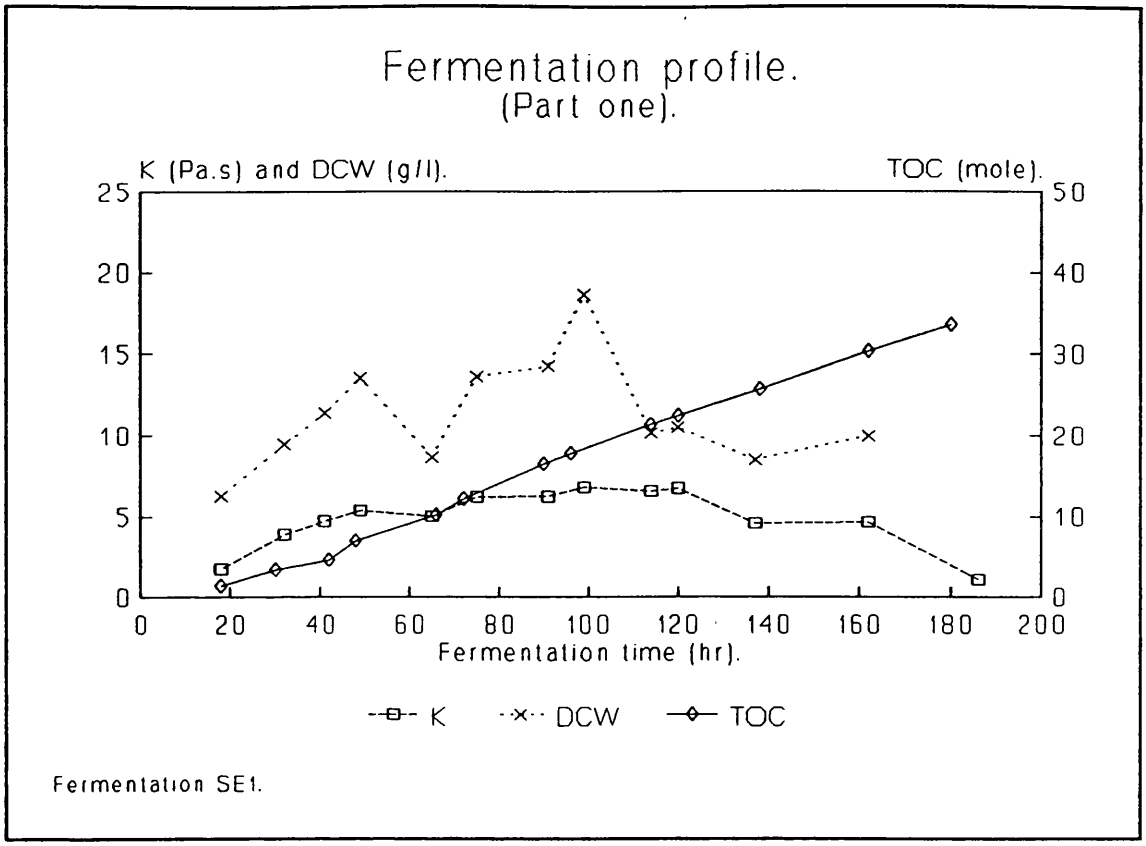

Figure 1

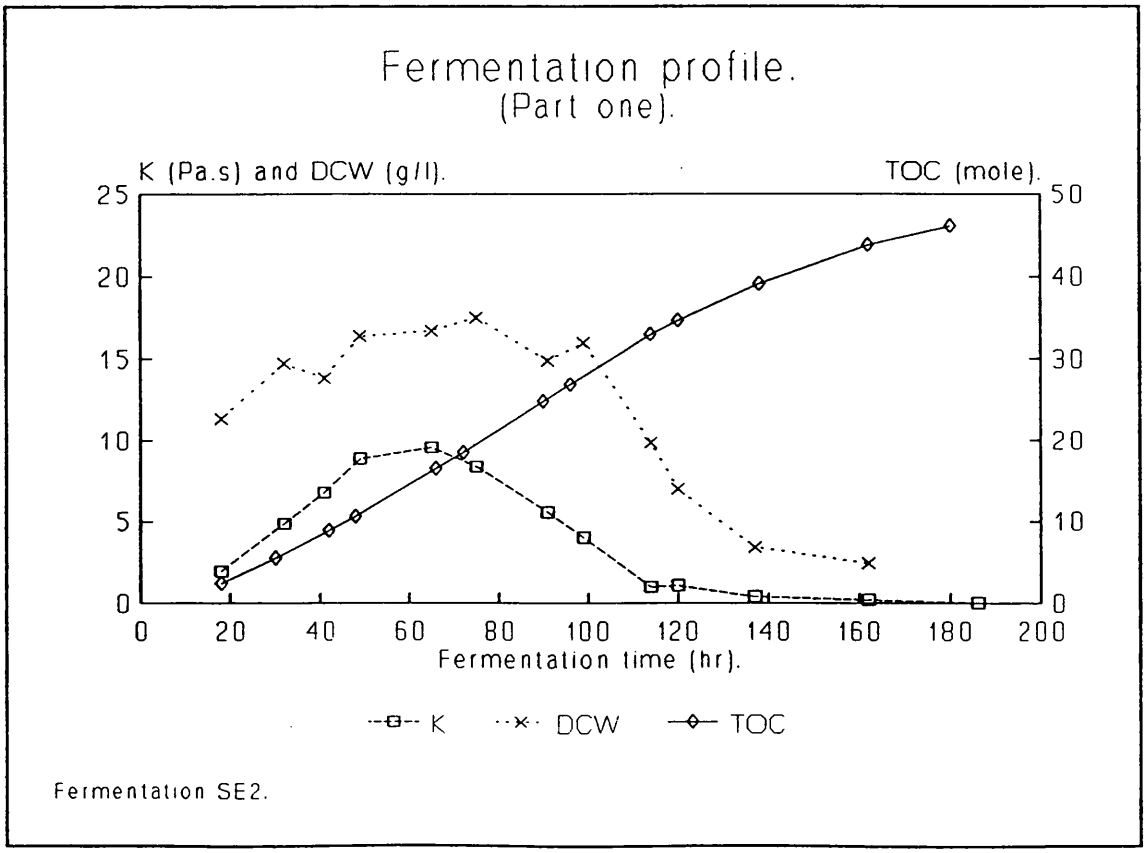

Figure 2

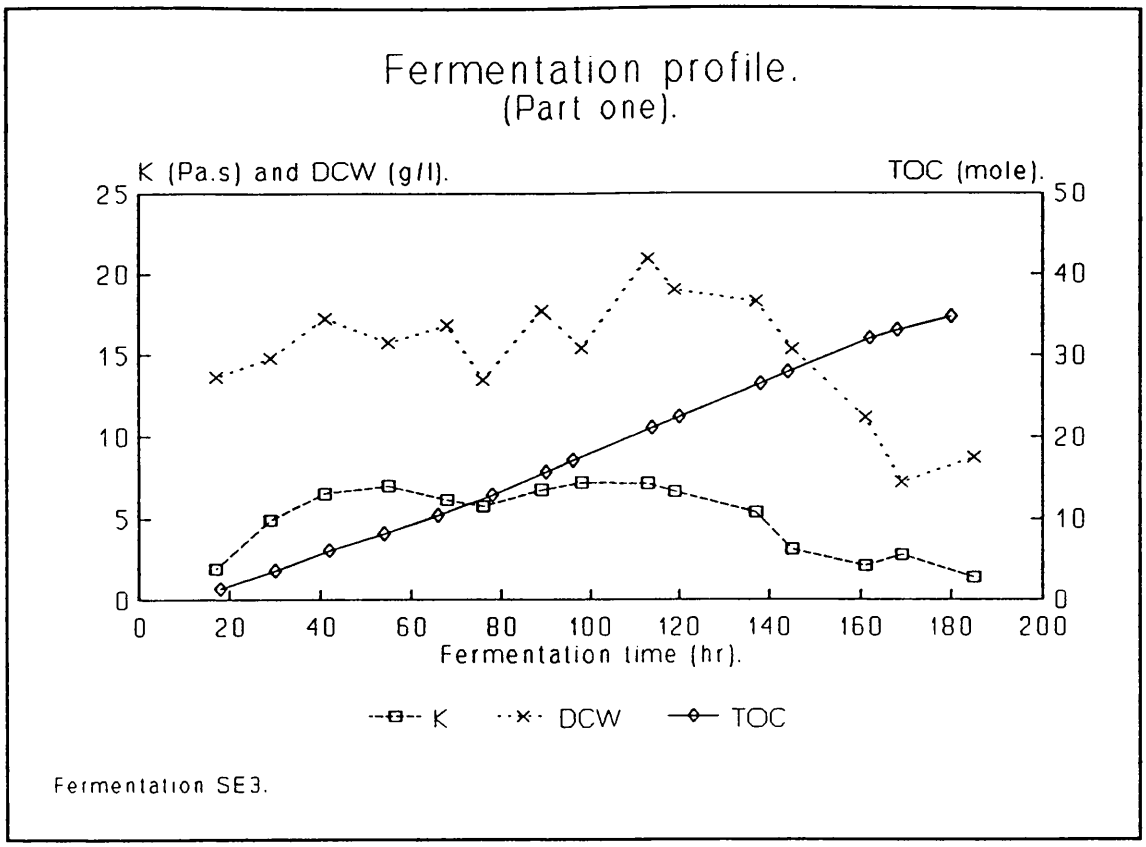

Figure 3

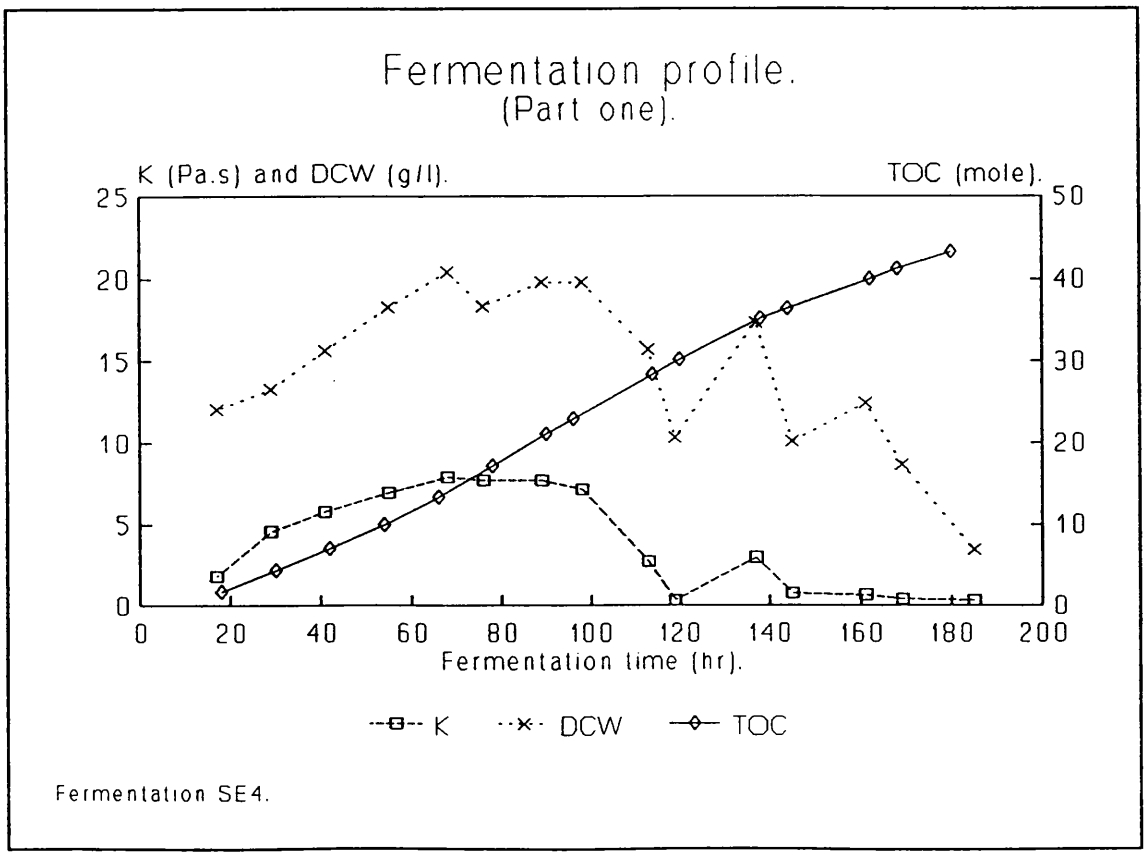

Figure 4

fermentations SE2 and SE4 grew faster during the early stages of the fermentation process than SE1 and SE3. Possibly as a consequence of this fast growth fermentations SE2 and SE4 displayed a sharp reduction in DCW by ≈100 hours whereas fermentation SE3 did not show a decrease in cell concentration until ≈140 hours. The K profiles showed marked similarities with the DCW profiles, which suggests a correlation exists between K and DCW and such a correlation is investigated later on in this chapter.

Figures 5-8 are entitled Fermentation Profile (part two) and show the oxygen uptake rate or OUR (moles/l.hr), the dissolved oxygen tension or DOT (%) and the respiratory quotient or RQ (no units) for fermentations SE1-SE4.

The plots for the respiratory quotient all follow a similar pattern. The values for RQ decreased initially, then rose slightly and ultimately levelled off for the remainder of the fermentation process. The RQ seems to stabilised at a value of approximately 0.75. Such an RQ value indicates a typical profile for an oil utilizing fermentation with no substantial change in metabolism over the duration of the fermentation.

The OUR data plots can be divided into two groups: figures 5 and 7 show the values of OUR remaining reasonably constant over the duration of the fermentation, whereas figures 6 and 8 show the values of OUR rising until ≈70 hours, levelling off and slowly decreasing for the remainder of the fermentation.

Figures 6 and 8 show the DOT profiles for fermentations SE2 and SE4 are similar. Both DOT plots fall sharply to approximately 15% (air saturation), remain there for a short while and then rise to about 80-90% at the end of the fermentation.

Figure 5 shows a plot of DOT that also decreases rapidly but stabilises at a level of 25% until almost the end of the fermentation. In contrast, the DOT plot in figure 7 shows a slow descent to 10% at 110 hours and then a sharp recovery to about 60% where it remains until the end of the fermentation.

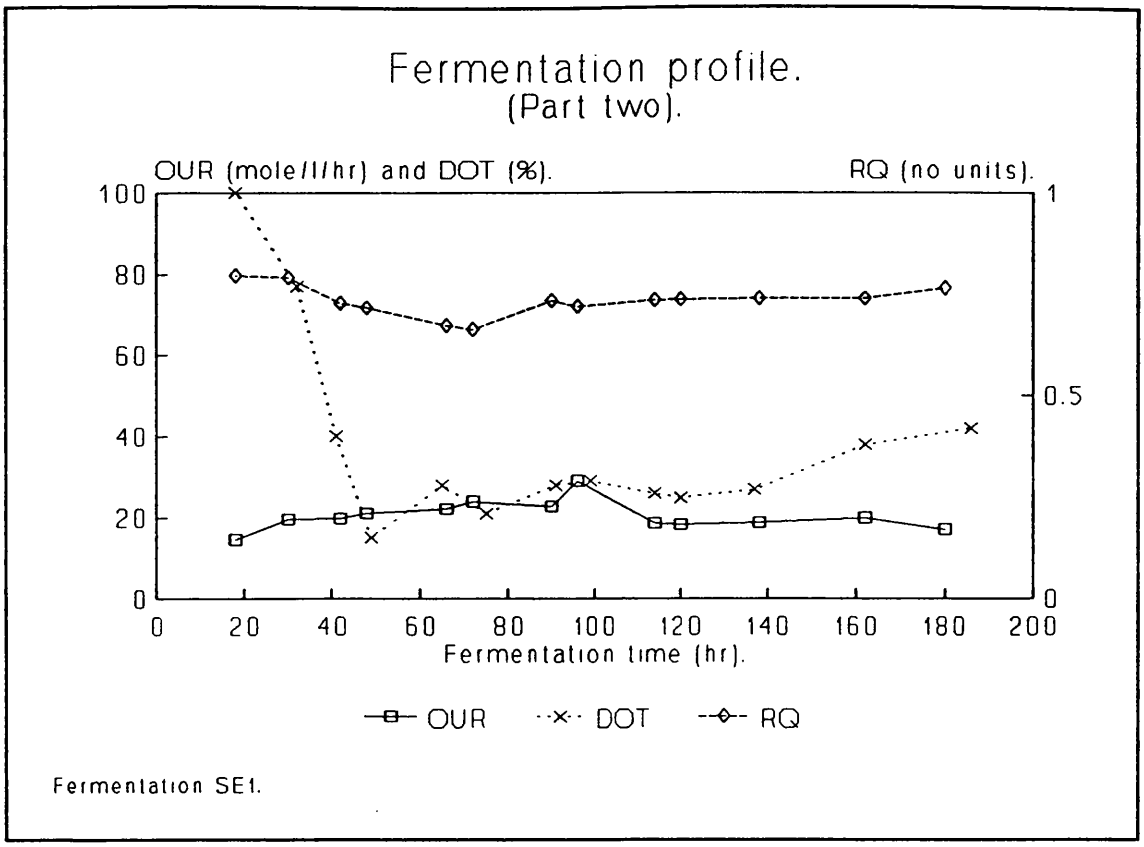

Figure 5

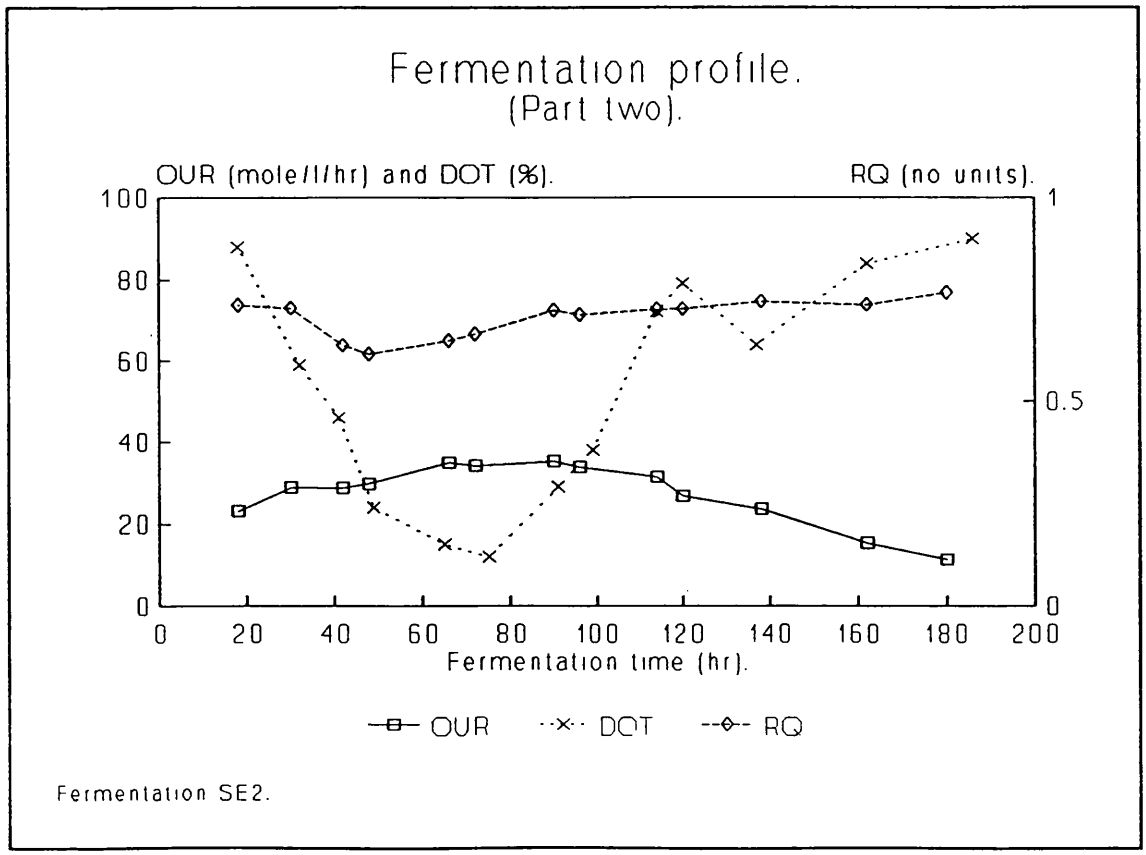

Figure 6

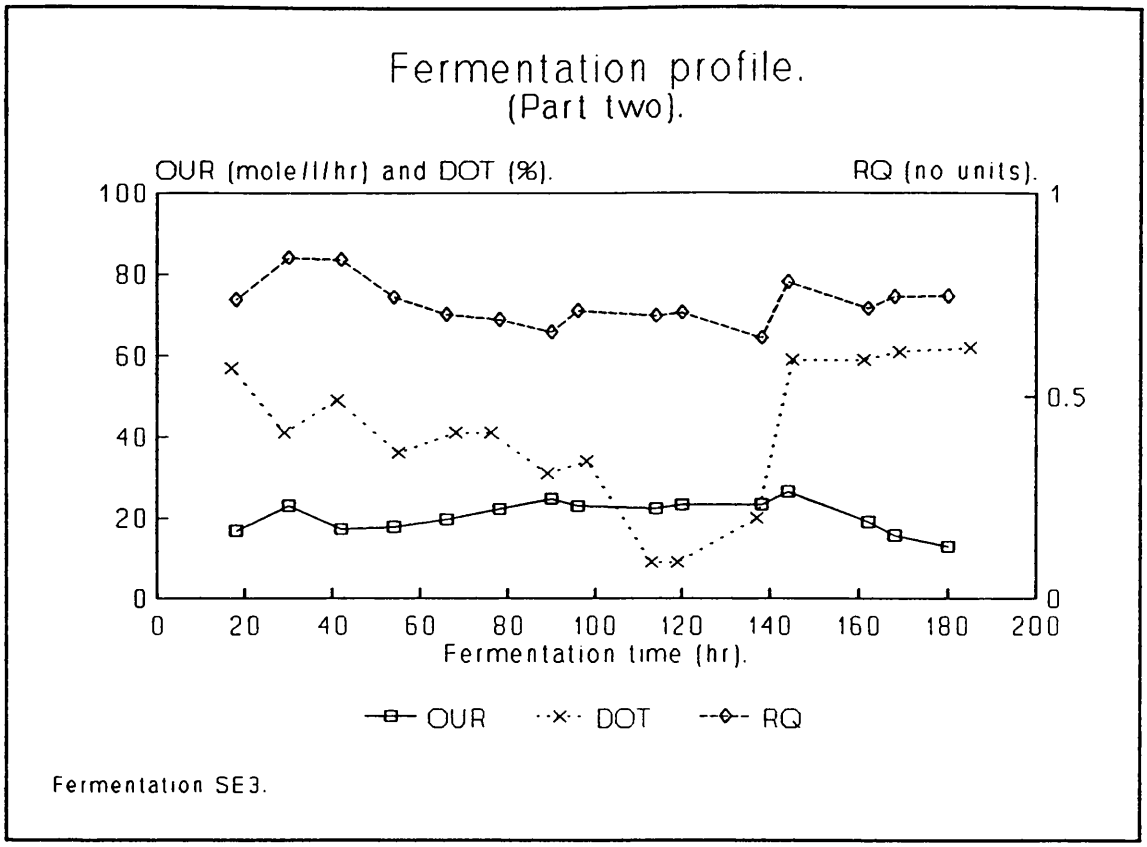

Figure 7

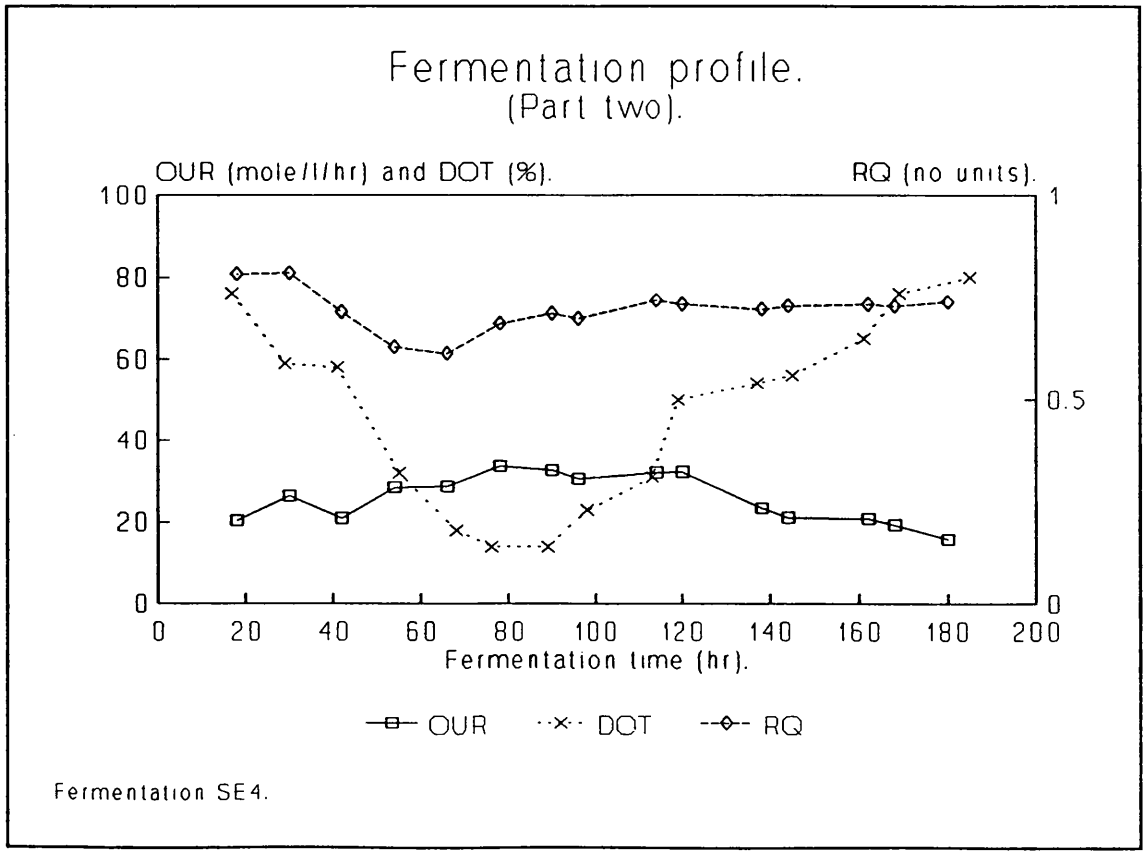

Figure 8

In fermentations SE2 and SE4 the decrease in DOT (%) had some detrimental effect on the oxygen uptake rate, OUR (moles/l/hr). When the DOT reached a nadir, the corresponding OUR profile ceased rising and either levelled off or dropped. This deficiency in dissolved oxygen may have caused the oxygen uptake rate to stop increasing or it could be due to consumption of readily utilisable carbon source.

Despite good agreement in the fermentation data between fermentations SE1 and SE3 and also fermentations SE2 and SE4, the differences in the OUR data, K data, TOC data and DCW data between these two groups indicates that the fermentations were not identical. Since, the fermentations were prepared and run in precisely the same way, the differences could be caused by variation in the condition of the inoculum. Although the same inoculum medium and the same procedure to inoculate the medium were used, it seems likely that the inocula were at different stages of growth when transferred to the fermentation and this resulted in the variation between fermentations. Possibly the differences between the inocula resulted from variation in the quantity or quality of seed culture.

Figures 9 and 10 describe the rheological characteristics of the fermentation broths at various stages of the fermentation process. Only three of the broth samples are shown for reasons of clarity. During this project it has been assumed that a straightline relationship (the Power law) exists between the log shear stress and the log shear rate of a fermentation broth. Figures 9 and 10 show the best and an average example of this straightline relationship, respectively. Linear regression analysis (the method of least squares) was used to calculate the equation of the best fit straightline through the data. Figures 9 and 10 show the excellent fit of these straightline plots in relation to the data points. By comparing the Power law equation with the equation for the straightline, values for the Power law index,n (no units) and the consistency coefficient, K ($Pa.s^n$) was

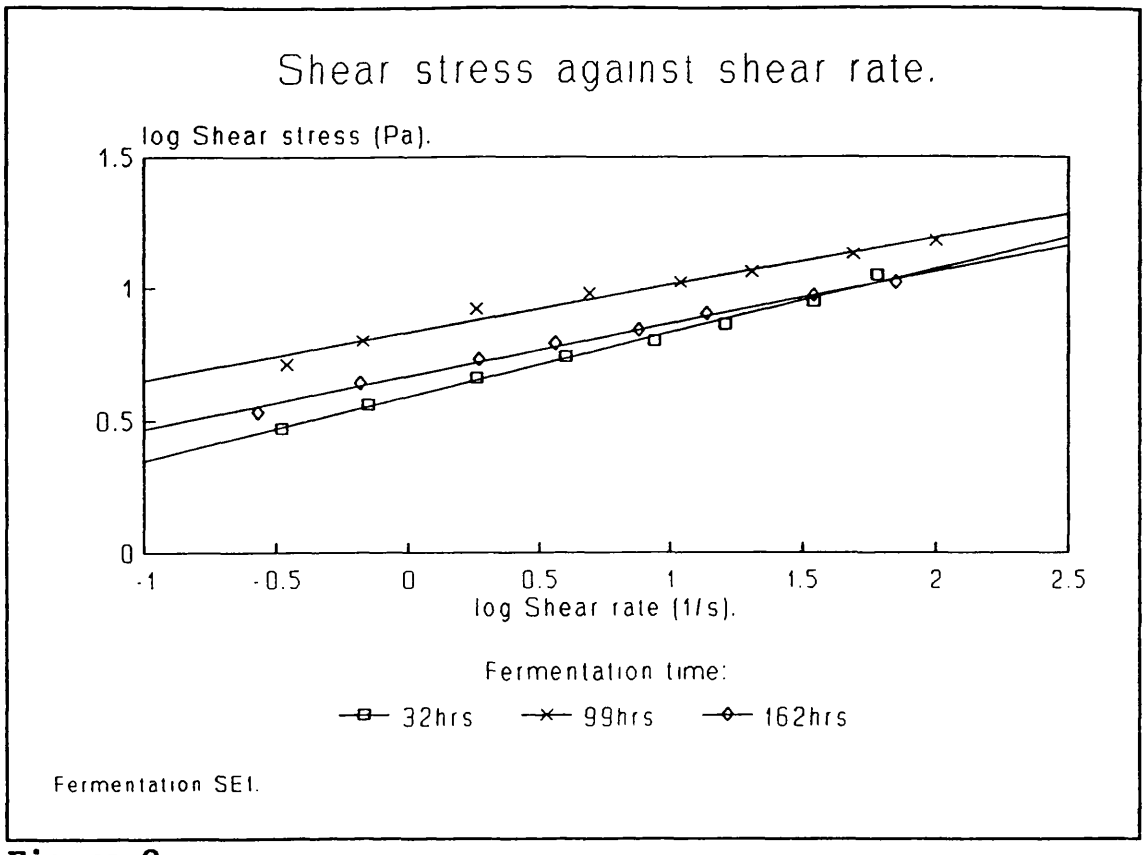

Figure 9

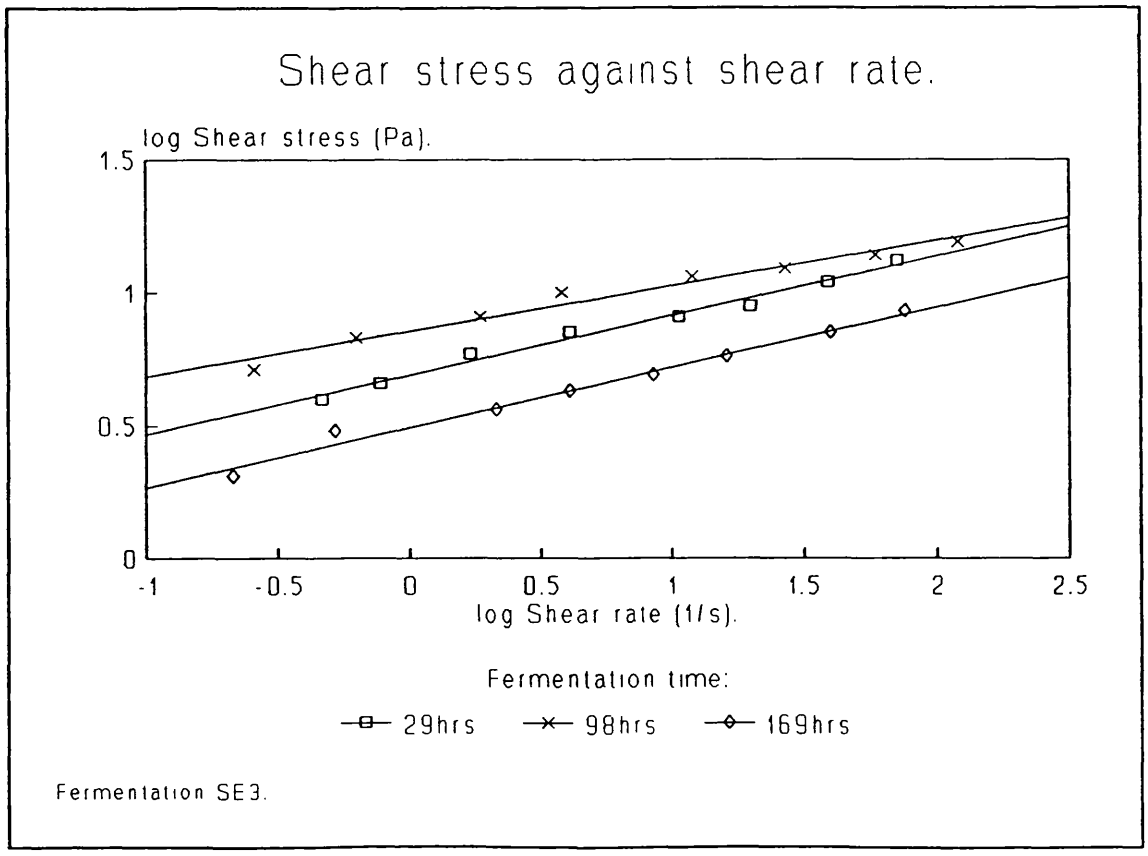

Figure 10

deduced for a broth sample at any given time during the fermentation. The changes in the values of n and K were established by analysing the fermentation broth at regular intervals throughout the length of the fermentation.

Figure 11 indicates the change in consistency coefficient, K (pascal-seconds) with fermentation time (hours) for the fermentations SE1 to SE4. The figure highlights the earlier discussion of these data which suggested there were two distinct groups of profiles.

Figure 12 shows the change in the Power law index, n (no units) over the duration of the fermentation; data from all four fermentations are shown. At 20 hrs the Power law index was at approximately 0.2. The values remained around this level until 110 hrs when the data became more erratic. The plot for SE1 and SE3 shows the values of n remaining at about 0.2-0.3, whilst the values of n for SE2 and SE4 increased over the remainder of the fermentation.

A comparison of figures 11 and 12 shows that the values of the Power index became erratic when the values of the consistency coefficient were low; this can be seen in fermentations SE2 and SE4 from 120 hr onwards. The torque response of the Brookfield viscometer became insensitive when the apparent viscosity of the fermentation broths was low. This instrument insensitivity appeared to have a more pronounced effect on the values of n than the values of K.

A paper by Tuffile and Pinho [55] shows similar profiles for n and K with a viscous *S. aureofaciens* fermentation. Although, the early part of the profiles (up to 50 hr) show significant differences due to the influence of the rheological properties of a medium constituent, once these effects had subsided the profiles were similar. The Power law index remained in the range 0.2 to 0.4 throughout the fermentation and the consistency coefficient rises during the fermentation to a peak of 9 Pa.s at 170 hr.

Another paper by Buckland et al [122] provides a Power law equation for a *S. avermitilis* fermentation:

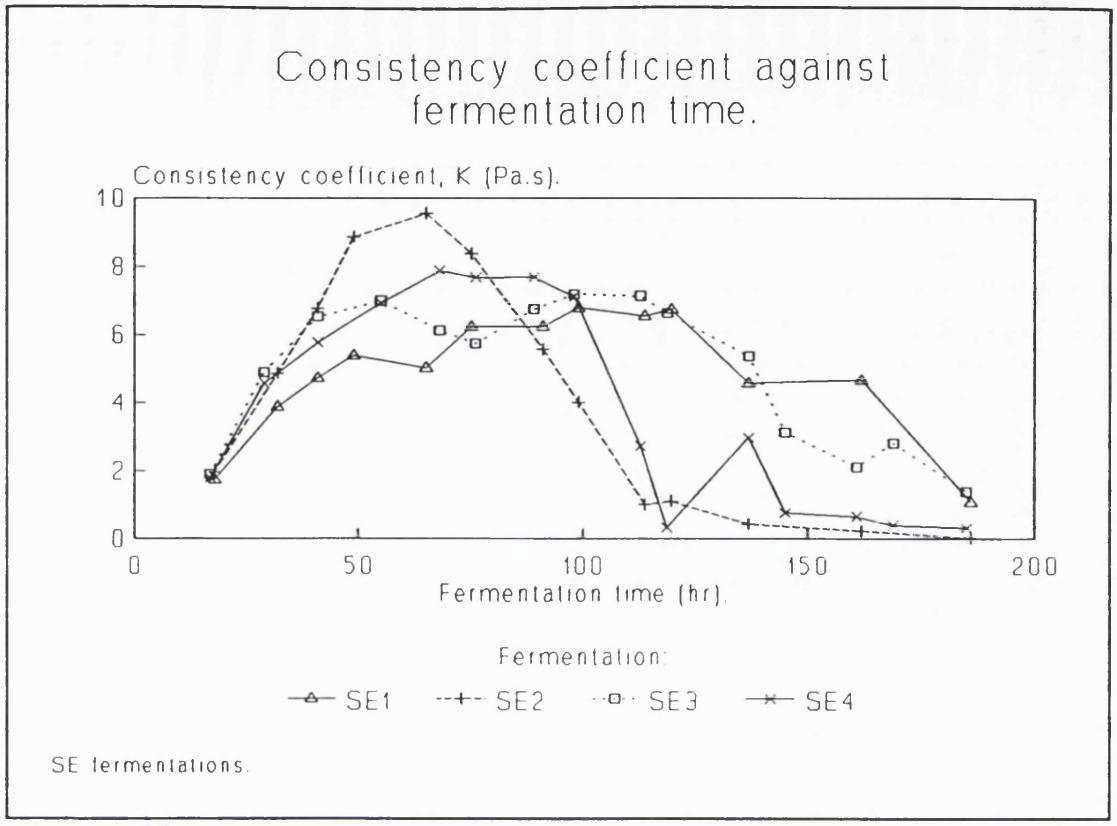

Figure 11

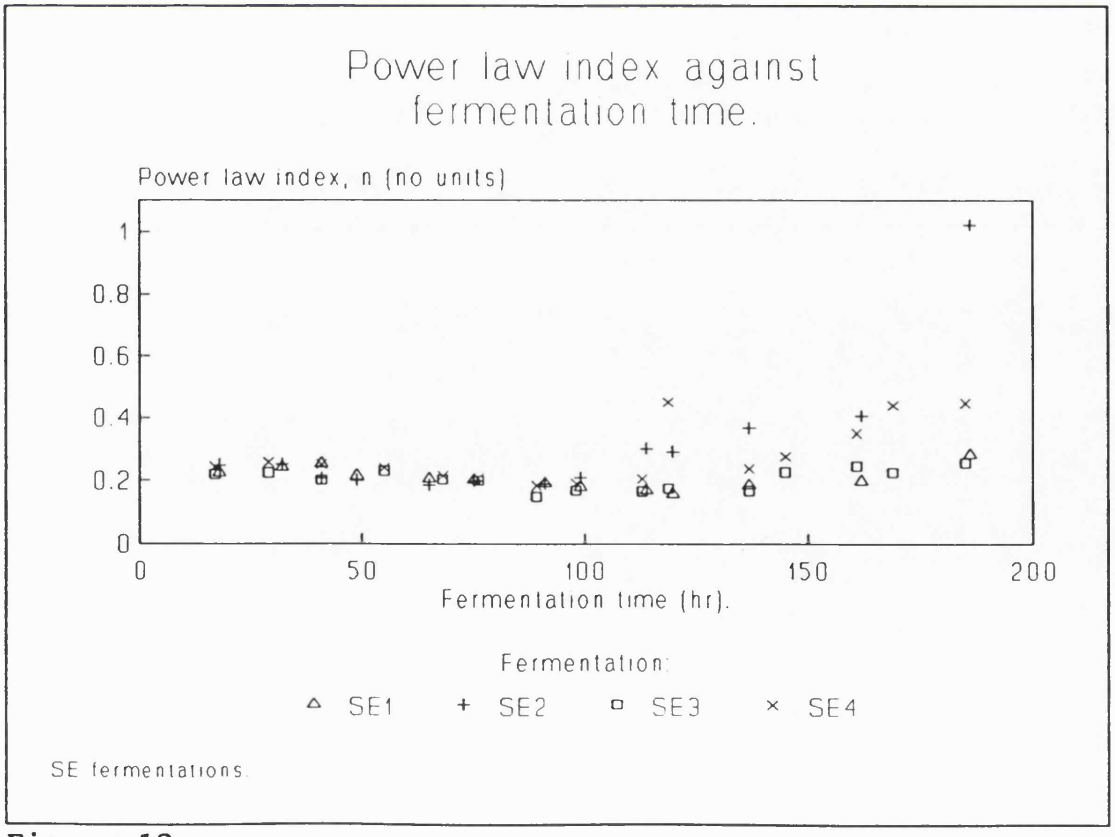

Figure 12

$$\tau = 0.43 \cdot \dot{\gamma}^{0.27} \qquad (1)$$

Similar values of K and n were determined for the *S. erythraeus* fermentation in the early stages.

In a paper by Gbewonyo et al [121] the authors show a correlation between cell concentration and the total oxygen consumption during the active growth stage of a *S. avermitilis* fermentation. Close observation of the dry cell weight data and the total oxygen consumed data of the *S. erythraeus* fermentations indicates the existence of a similar correlation, see figures 2, 3 and 4.

The period during which active growth took place in the *S. erythraeus* fermentations was calculated by assuming that the active growth period occurred whilst the oxygen uptake rate increased. For fermentations SE1 and SE2, see figures 5 and 6, the OUR values peaked at 72 and 66 hours respectively. Unfortunately, in fermentations SE3 and SE4, figures 7 and 8, the OUR initially peaked at 30 hours and therefore they provided few data points with which to demonstrate a correlation. Examination of the OUR plot for fermentation SE4, see figure 8, reveals that the value at 42 hours may be suspect. By ignoring this point, peak OUR was not reached until 78 hours into the SE4 fermentation.

Figure 13 shows a plot of log total oxygen consumed against log dry cell weight of the fermentation broth , for the period of increasing oxygen uptake rate (OUR). Fermentations SE1, SE2, SE3 and SE4 show a straightline relationship between increasing log TOC and increasing log DCW. The limited number of data points for SE3 means that statements regarding any trend must be qualified, but since the data points show the same trend as the other fermentations it is a reasonable assumption to suggest that the same straightline relationship exists in this fermentation. Therefore a non-linear relationship exists between cell concentration and total oxygen consumption for *S. erythraeus* fermentations and infers that a smaller

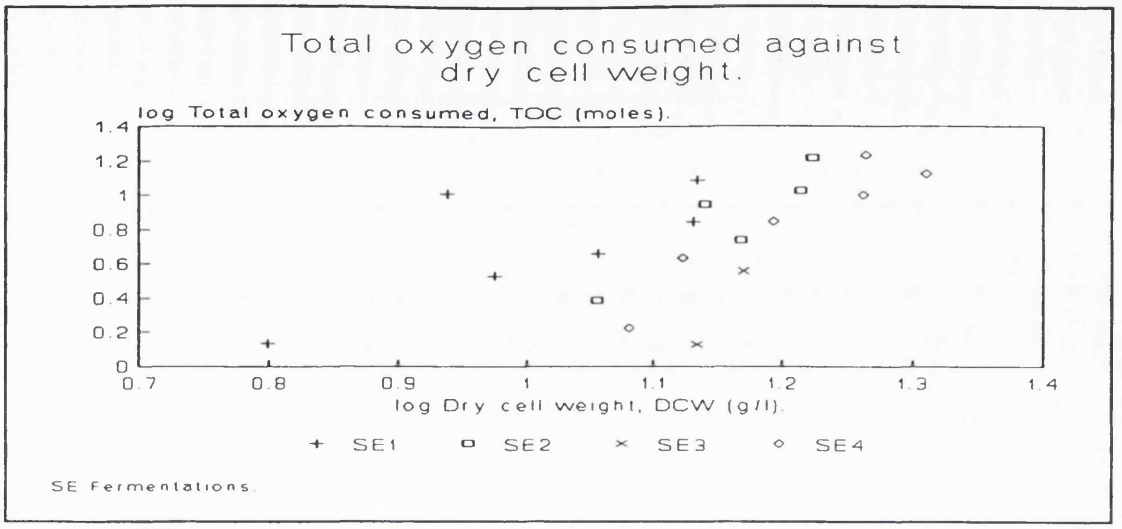

Figure 13

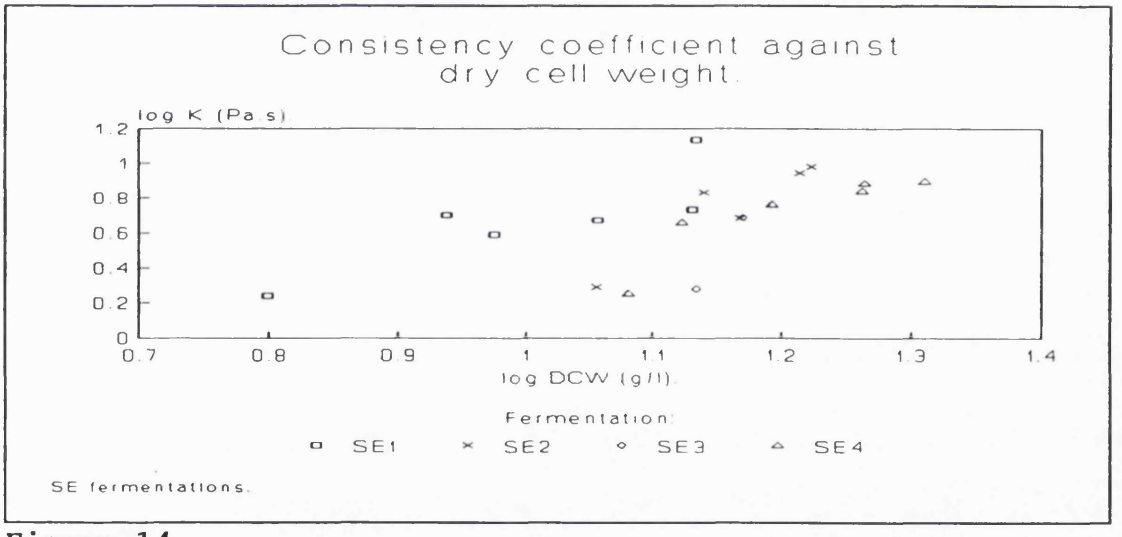

Figure 14

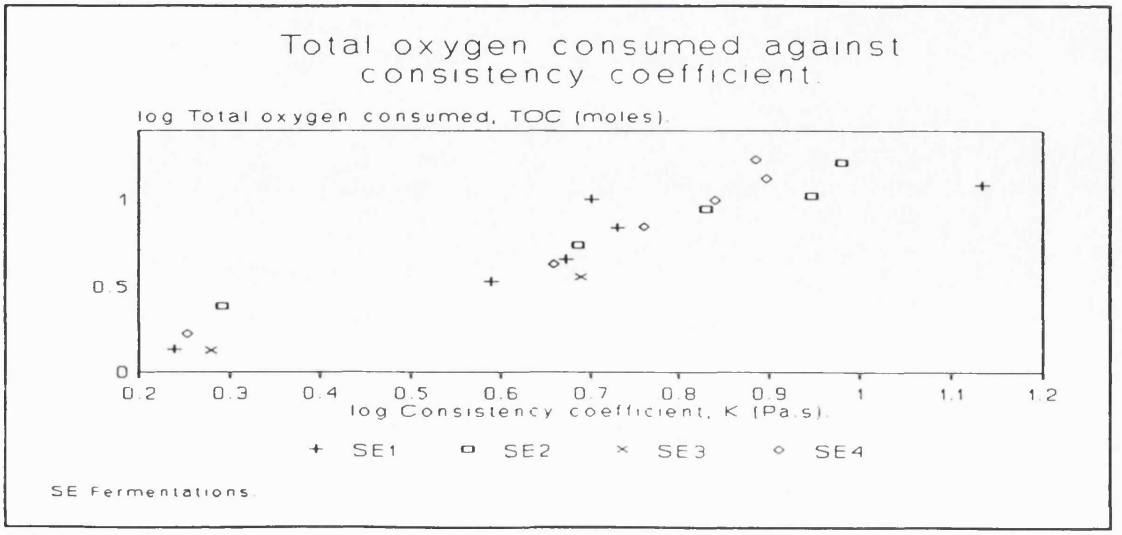

Figure 15

proportion of the organic carbon used is incorporated into biomass.

From figures 1 to 4 it can be observed that for a given *S. erythraeus* fermentation the dry cell weight profiles and the consistency coefficient profiles follow each other closely during the period of increasing OUR (see figures 5 to 8). Figure 14 shows a plot of log consistency coefficient, K (Pa.s) against log dry cell weight, DCW (g/l) for the fermentations SE1 to SE4. Although the data points show considerable scatter, there appears to be a non-linear relationship between increasing values of DCW and increasing values of K. The scatter is probably caused by the difficulties encountered in trying to obtain accurate dry cell weight data.

Next a plot was prepared of total oxygen consumed or TOC (moles) against Power law consistency coefficient or K ($Pa.s^n$), see figure 15. The plots for SE1, SE2 and SE4 indicates a straightline relationship between log TOC and log K for the initial period. Fermentations SE3 has only two points in its plot, unfortunately the period of peak OUR occurred so quickly that only two samples had been taken. Although it is difficult to draw conclusions concerning a plot with such limited data, the fermentation shows that as log TOC rises log K also increases. This pattern follows precisely that shown in fermentation SE1, SE2 and SE4. Hence, for all four fermentations a non-linear relationship exists between TOC and K.

Although a correlation has been established between log TOC and log K for a given fermentation, no single correlation can be found that applies to all four fermentations. Thus some fermentation-specific factor must influence the correlation.

A parallel fermentation was run to provide further insight into the rheological properties of the *S. erythraeus* fermentation broth (see section 2.3.2.1 for an explanation of the procedure). Two fermentations were prepared and run in exactly the same way except that one of the fermentations was inoculated with *S. erythraeus* and the

other was not . The samples taken from these fermentations were initially rheologically analysed and then centrifuged to remove the *S. erythraeus* cells and/or medium particulates and finally the centrifugate was re-analysed. Figure 16 shows several plots of log consistency coefficient, K, ($Pa.s^n$) and a plot of dry cell weight for the inoculated fermentation against fermentation time for an *S. erythraeus* fermentation broth (SE5). The key for figures 16 and 17 is:

A - sample from inoculated fermentation before centrifugation.

B - the centrifugate of (A).

C - sample from uninoculated fermentation before centrifugation.

D - the centrifugate of (C).

Figure 16 shows that the consistency coefficient for (A) increases to a peak of 6 $Pa.s^n$ at ≈40 hr and then begins to decrease. The consistency coefficient for (C) remains fairly constant at a level of less than 0.02 Pa.s. Both the consistency coefficients for (B) and (D) remain constant at values of less than 0.007 Pa.s. The plot for the dry cell weight of the inoculated fermentation appears to follow closely the consistency coefficient data for (A).

Figure 17 shows several plots of Power law index and a dry cell weight plot for the inoculated fermentation against fermentation time for the same *S. erythraeus* fermentation (SE5). The figure shows (A) decreasing from a high value of ≈0.9 at ≈1 hr to a low value of ≈0.3 from ≈20 hr onwards. The other samples (B), (C) and (D) all remain at approximately unity for the entire length of the fermentation. The plot of dry cell weight seems to show an inverse relationship to the Power law index plot for sample (A). However, no similar relationships were found in fermentations SE1 to SE4.

A comparison of (A) with (B) gives an indication of the effect of *S. erythraeus* biomass on the rheology of the fermentation broth. The removal of the cells by centrifugation caused the consistency coefficient of the

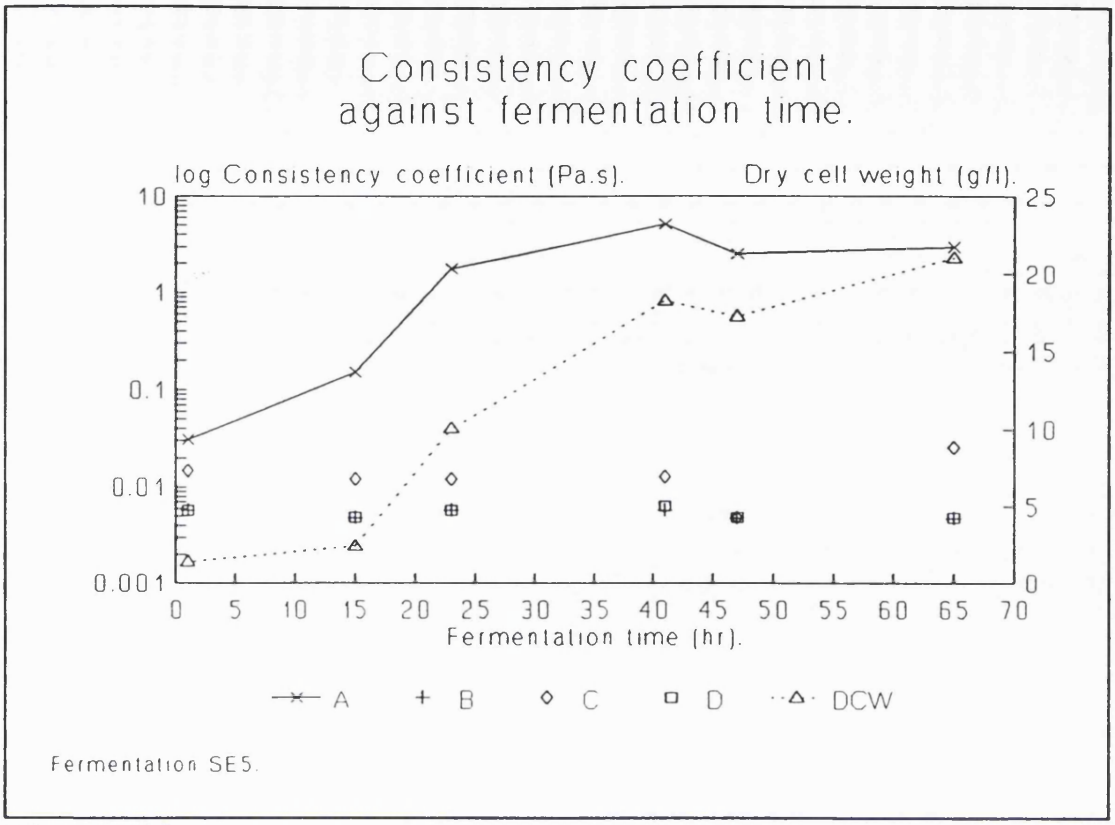

Figure 16

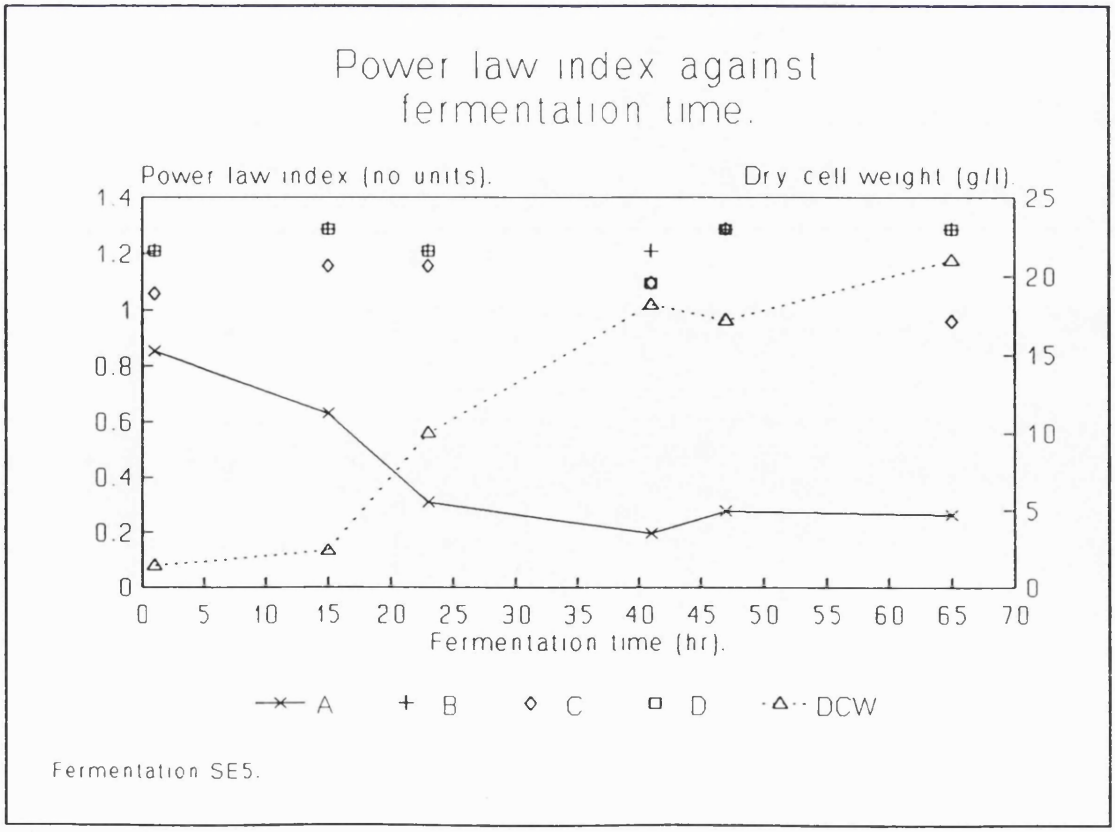

Figure 17

broth to decrease and the Power law index to increase. Thus the highly viscous pseudoplastic broth at a fermentation time of 42 hr with an n of ≈0.2 and a K of 6 Pa.s became a Newtonian, low viscosity fluid with an n of ≈1.2 and a K of 0.007 Pa.s when the *S. erythraeus* cells were removed. The high apparent viscosity of the fermentation broth was dependent on the presence of *S. erythraeus* organisms.

The Newtonian characteristics and non-viscous nature of (C) indicates that the high apparent viscosity was not caused by the presence of solids or a chemical reaction between the substrates in the fermentation broth. The slight reduction in K and the small increase in n for (D) compared with (C) suggests that the solid particulates present in the broth did have a small, but almost negligible, influence on the rheological characteristics of the fermentation.

The considerable point scatter for the data points at low consistency coefficients or high Power law indices is because of the insensitivity of the viscometer when analysing low viscosity fluids.

Figures 18 to 21 show the relationship between the morphology of the filamentous microorganisms and the rheology of the fermentation broth. The plots show mean main mycelial length and consistency coefficient or K against fermentation time (hours). The width of the plotted line indicates the 95% confidence limits for data. Each of the figures shows that no correlation can be found between the mean main mycelial length (the morphology parameter) and the consistency coefficient (the rheology parameter).

Figures 18 to 21 show that the mean main mycelial length, ML, changed considerably over the duration of a fermentation (from 9 up to 30μm), however the change in ML for the *S. erythraeus* organisms did not show any particular trend.

Using linear regression analysis the correlation coefficients, r, for log ML against log K were calculated

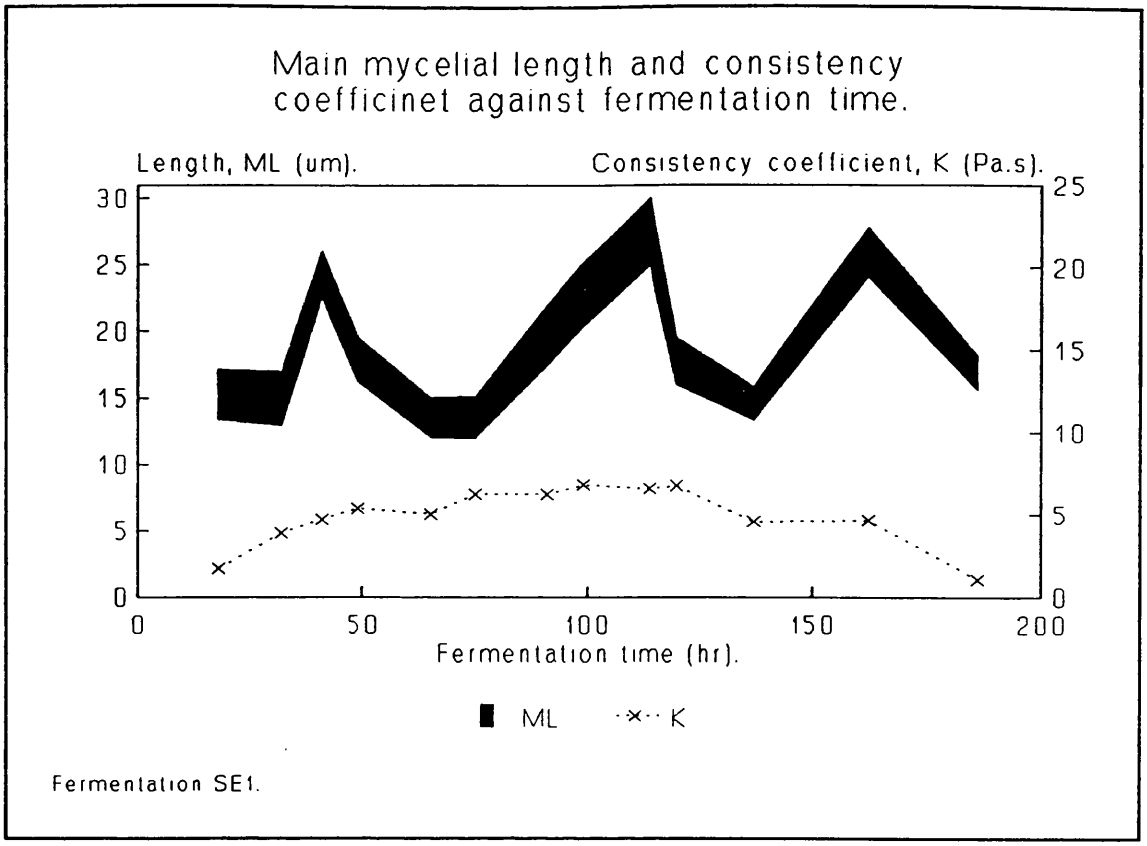

Figure 18

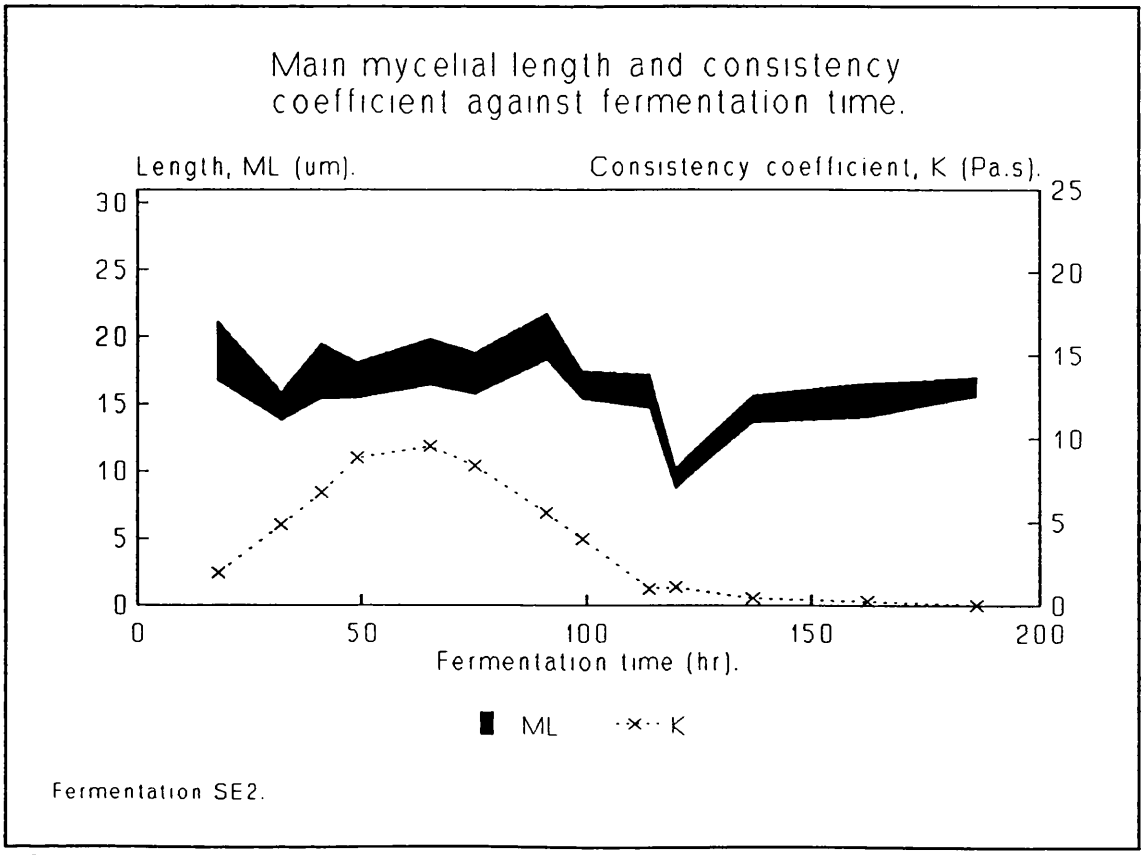

Figure 19

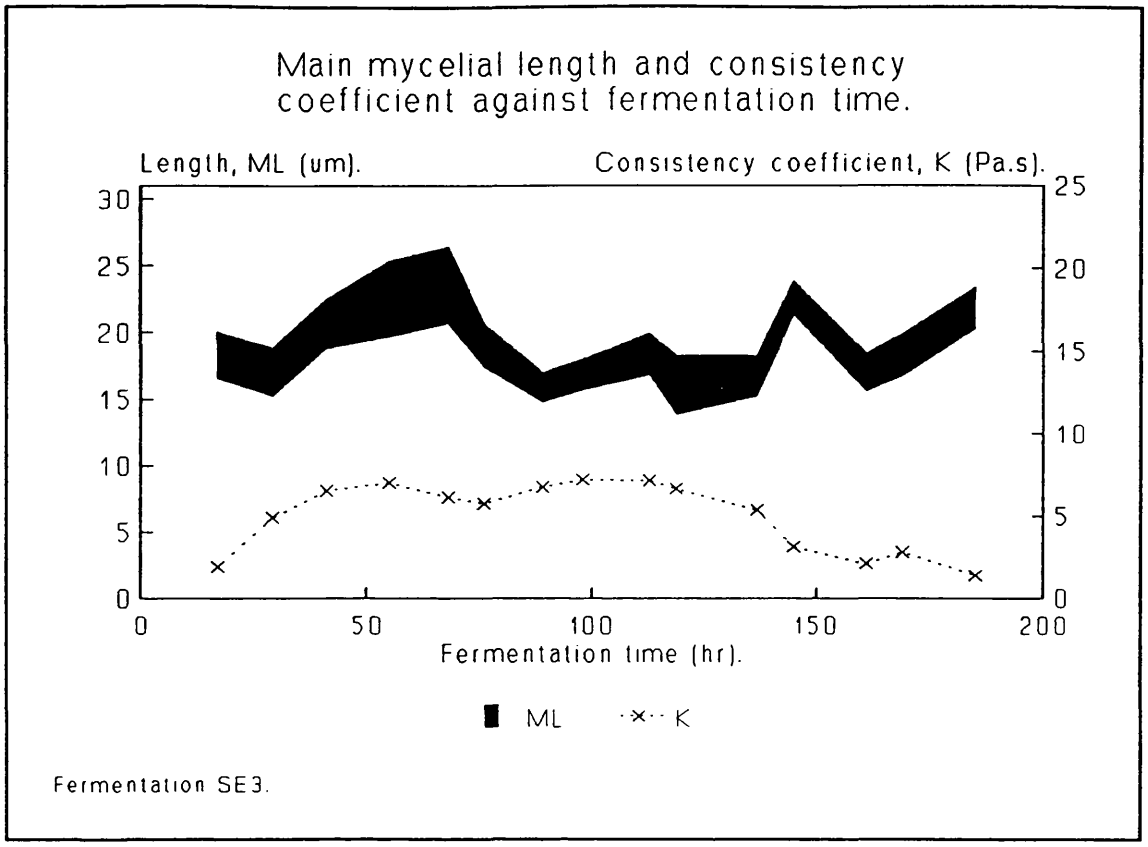

Figure 20

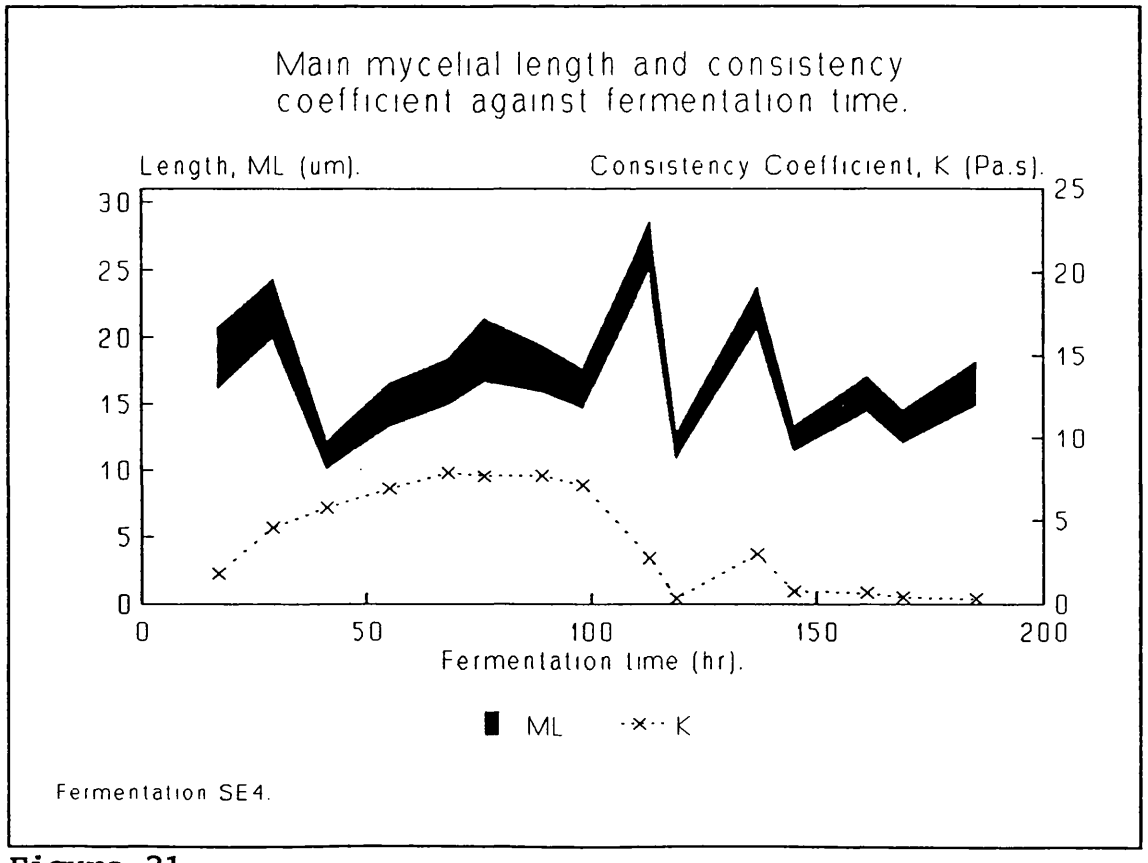

Figure 21

for each fermentation. By following a procedure in Kennedy and Neville [116] the calculated correlation coefficients were compared with critical tabulated values of r (at a 1% level of significance) and found to be lower, which indicates statistically that no correlation exists between ML and K.

5 The *Actinomadura roseorufa* fermentation results.

Figures 1, 2 and 3 (entitled Fermentation Profile (part one)) show data from fermentations AR1, AR2 and AR3 respectively. These plots show consistency coefficient and total oxygen consumed against fermentation time. In addition figures 2 and 3 show a plot of product (% of maximum) and dry cell weight concentration. It is worth noting that DCW value could no longer be assayed after ~70 hr of fermentation time. All of these fermentations had a similar profile for the TOC data, with an initial slow rate of total oxygen consumption followed by, at ≈45 hours, a sharp rise in rate. The reason for this unexpected increase was the connection of a carbon source feed to the fermentation at 45 hours. The TOC values for fermentation AR1 were similar in magnitude to fermentation AR3 and both are higher than fermentation AR2.

The profiles for the consistency coefficient also showed similarities between AR1 and AR3. Figures 1 and 3 show the consistency coefficient increased rapidly from 40 hours to a peak at 90 and 65 hours respectively. The values of K then decreased for the remainder of the fermentation only showing some recovery at the end of the process. The fermentations AR1 and AR3 peaked at K values of 14 and 10 Pa.s respectively. In contrast, figure 2 shows the consistency coefficient data increased rapidly from 40 to 60 hours, the values of K then remained at a constant level of ≈8 Pa.s and did not begin to decrease until the end of the process. Between 90 and 100 hours into the fermentation process the antifoam feed was removed and another feed was connected and as a result the K data profiles for each of the fermentations rose.

For fermentations AR2 and AR3 the DCW profiles are similar; the DCW values increased over the first 70hrs of the fermentation. No DCW data were collected for fermentation AR1.

The product yield plots for fermentations AR2 and AR3 followed the same pattern. The product concentration

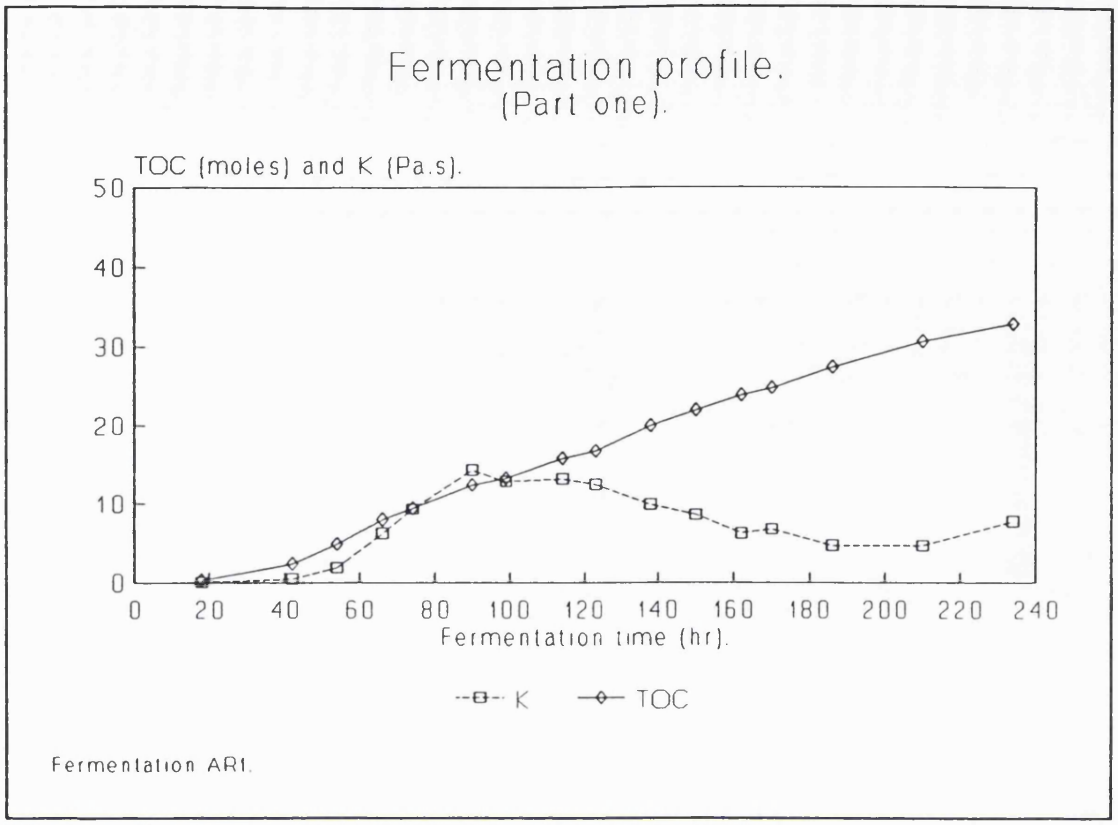

Figure 1

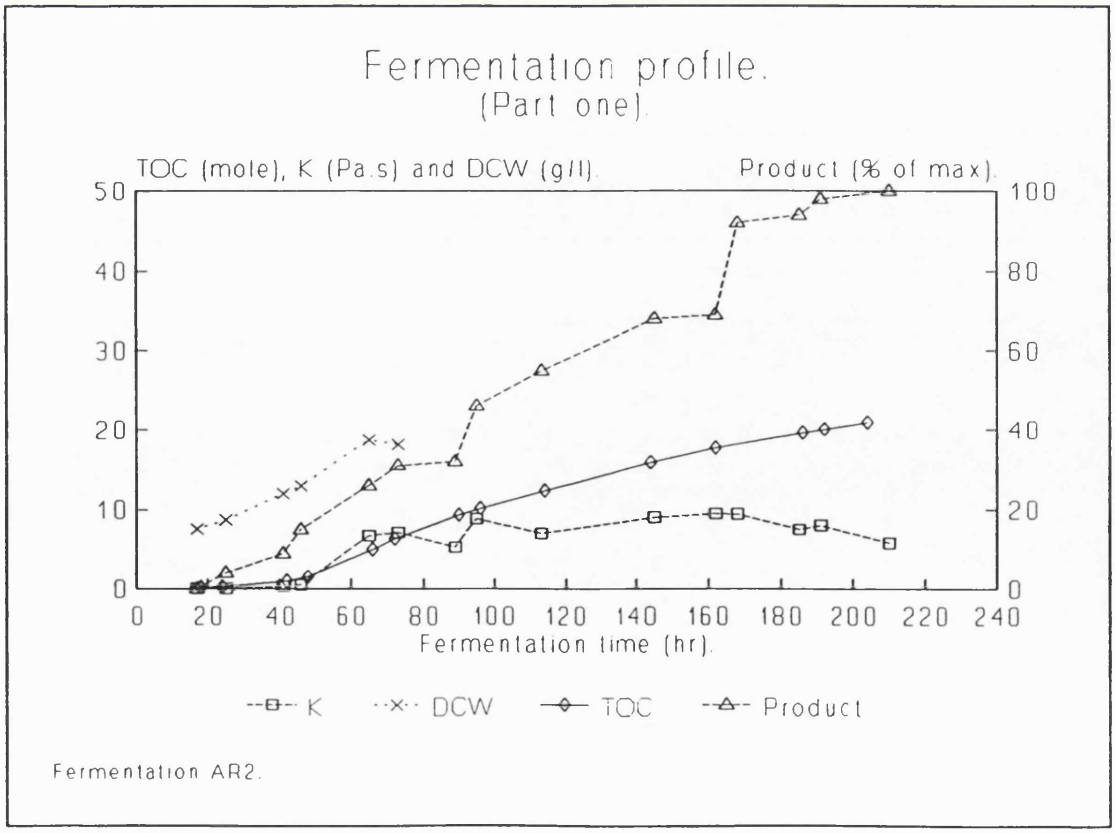

Figure 2

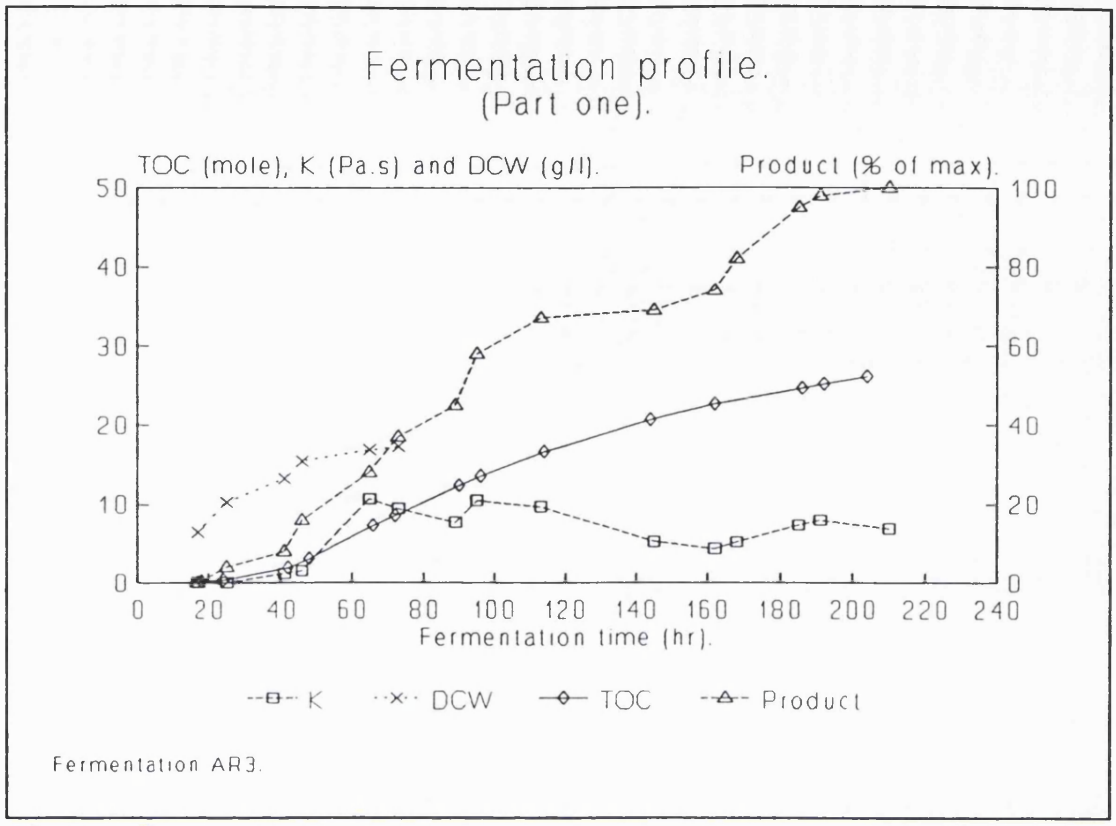

Figure 3

increased in a step-wise fashion over the length of the fermentation. The AR3 fermentation yielded almost 10% more product than the AR2 fermentation. The TOC data suggest that the AR3 fermentation produced a higher cell concentration than fermentation AR2 and this biomass difference could explain the higher product yield. The fermentation product began to be produced in substantial quantities after ≈45 hr possibly due to the connection of the carbon source feed.

Figures 4, 5 and 6 describe the data from AR1, AR2 and AR3 respectively. These show the oxygen uptake rate, DOT and the respiratory quotient or RQ (no units) against fermentation time. The figures show that the RQ values for the fermentations were similar, remaining constant at around unity throughout the fermentations. This RQ profile suggests a typical sugar utilizing fermentation which does not undergo a change in metabolism during the fermentation process.

The OUR profiles for the three fermentations were reasonably consistent. In the case of fermentation AR2 the OUR rose to a peak at 50-65hrs and the OUR values then decreased for the remainder of the fermentation. Fermentations AR1 and AR3 followed the same profile except AR3 remained at a stable value of OUR for ≈40 hours after peaking and AR1 showed a second smaller peak at ≈150 hours.

The DOT profiles for fermentations AR2 and AR3 showed close similarities. The DOT dropped quickly from 90% to 0% by ≈65 hours and then AR2 remained at this level for the rest of the fermentation whilst AR3 showed some recovery in the DOT after 140 hours. Whereas the DOT profile for fermentation AR1 decreased slowly from 90% to 0% by 150 hours and no recovery in DOT was observed during the remainder of the fermentation.

In each of the fermentations the decrease of DOT to zero caused the OUR profile to cease rising and either level off or, in the case of fermentation AR3, fall.

The data for the *A. roseorufa* fermentations show many similarities, however a few marked differences suggest that the process was not completely reproducible. The low values in the TOC data for fermentation AR2 implies that the growth rate was slower than the other fermentation, but the DCW data do not collaborate this hypothesis. The lower growth rate could also explain the differences seen in the K data. Like the *S. erythraeus* fermentations, the variation in growth rate could be caused by a disparity in the stage of growth of the inoculum when it was transferred to the fermenter.

Figures 7 and 8 describe the rheological characteristics of the fermentation broths at various stages of the process. Only three of the fermentation broth samples are drawn for reasons of clarity. During the project it has been assumed that a straightline relationship (the Power law) exists between the logarithm of shear stress (Pascals) and the logarithm of shear rate (reciprocal seconds) for a fermentation broth. Figures 7 and 8 show the best and an average example of this

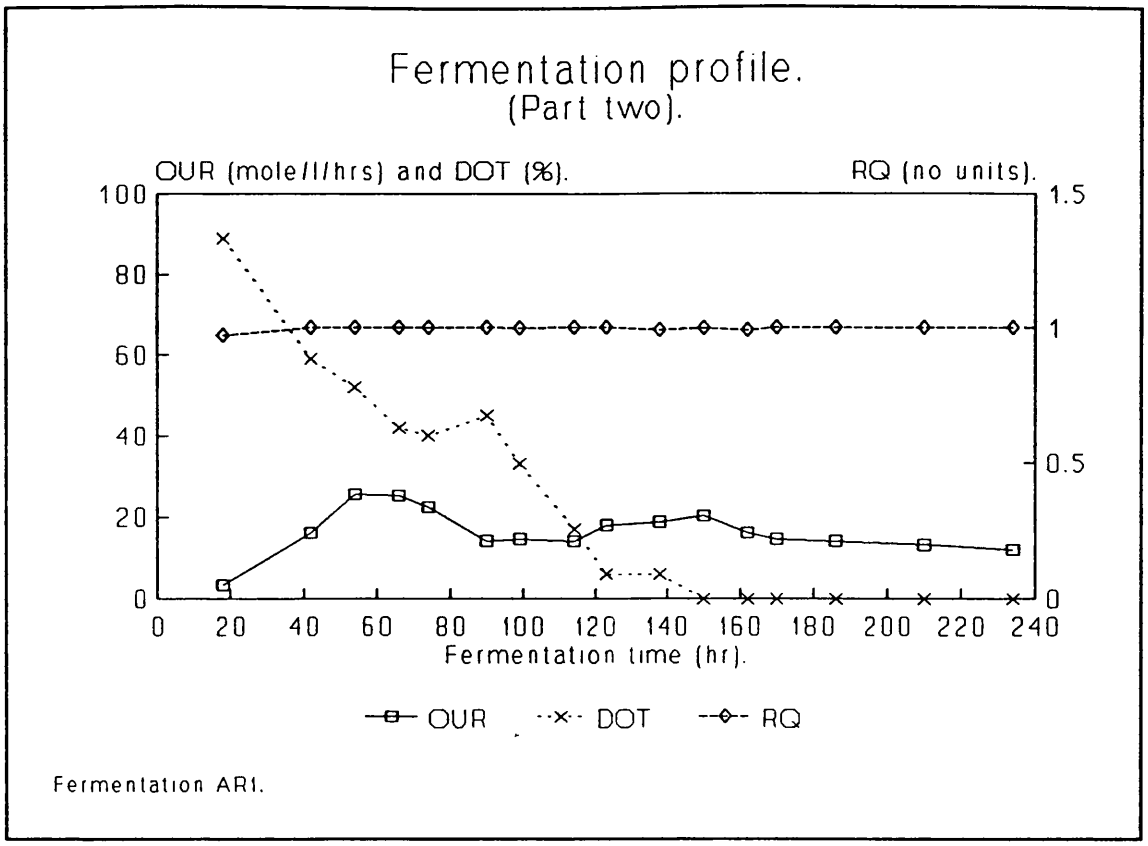

Figure 4

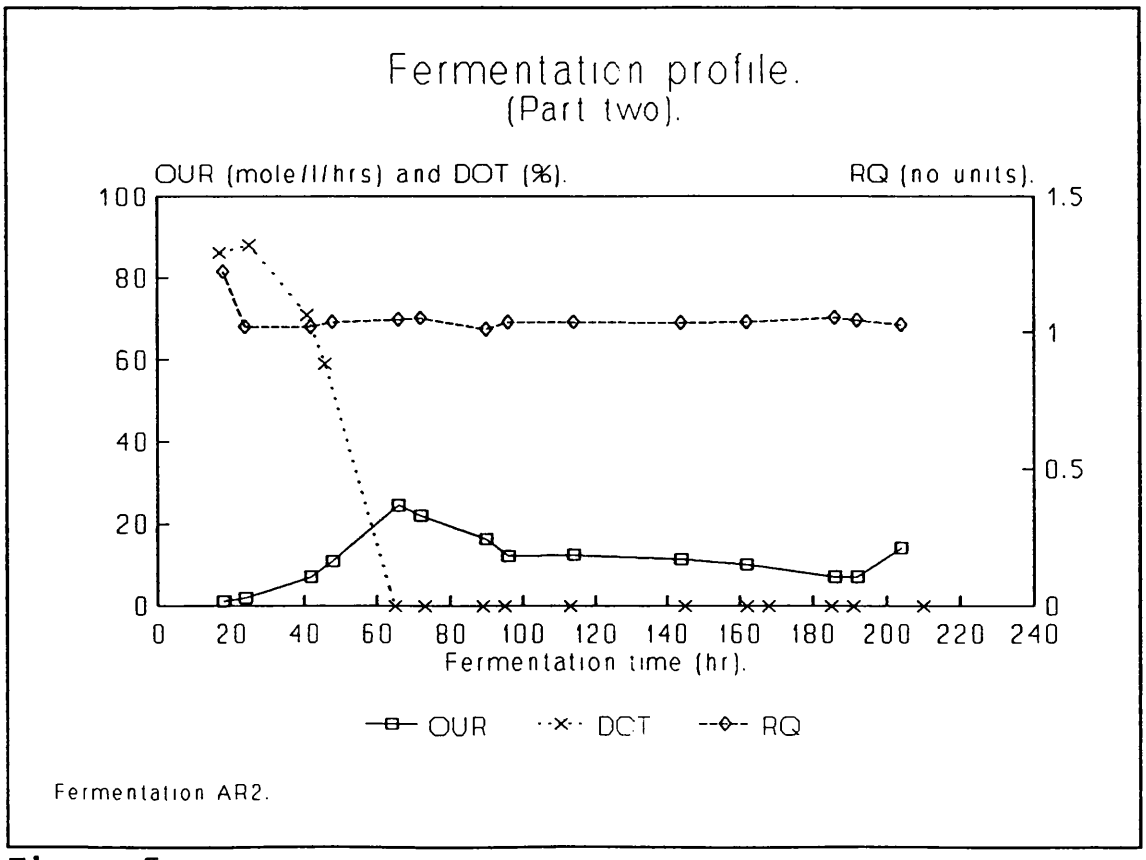

Figure 5

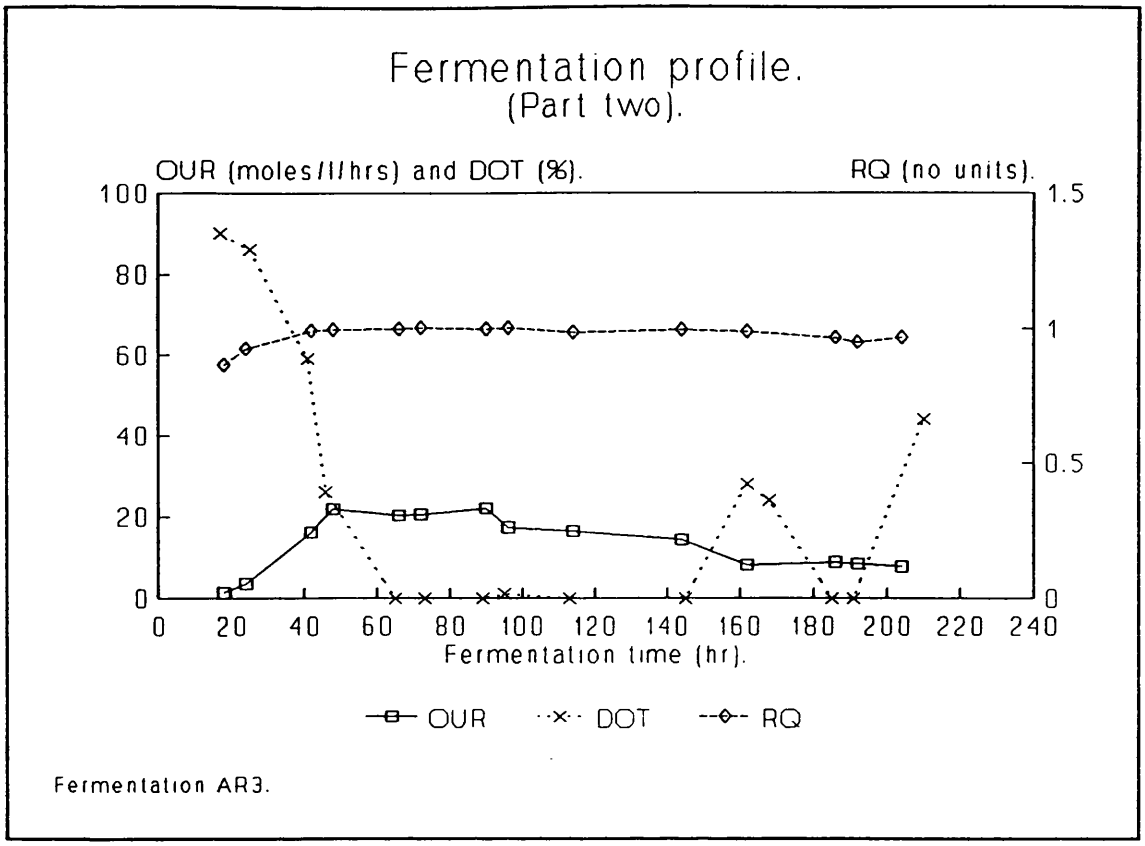

Figure 6

straightline relationship, respectively. Linear regression analysis (the method of least squares) was used to calculate the equation for the best fit straightline through the sample data. Figures 7 and 8 show the excellent fit of the calculated straightline in relation to the actual data points. By comparing the Power law formula with these straightline equations, values for the Power law index, n (no units) and the consistency coefficient, K can be calculated for a broth sample at any given time during the fermentation. By analysing the fermentation broth at regular intervals the changes in n and K can be established throughout the length of the fermentation.

Figure 9 indicates the change in consistency coefficient against fermentation time for the fermentations AR1, AR2 and AR3. The figure shows some variation between the three profiles as has previously been described.

Figure 10 shows the change in the Power law index over

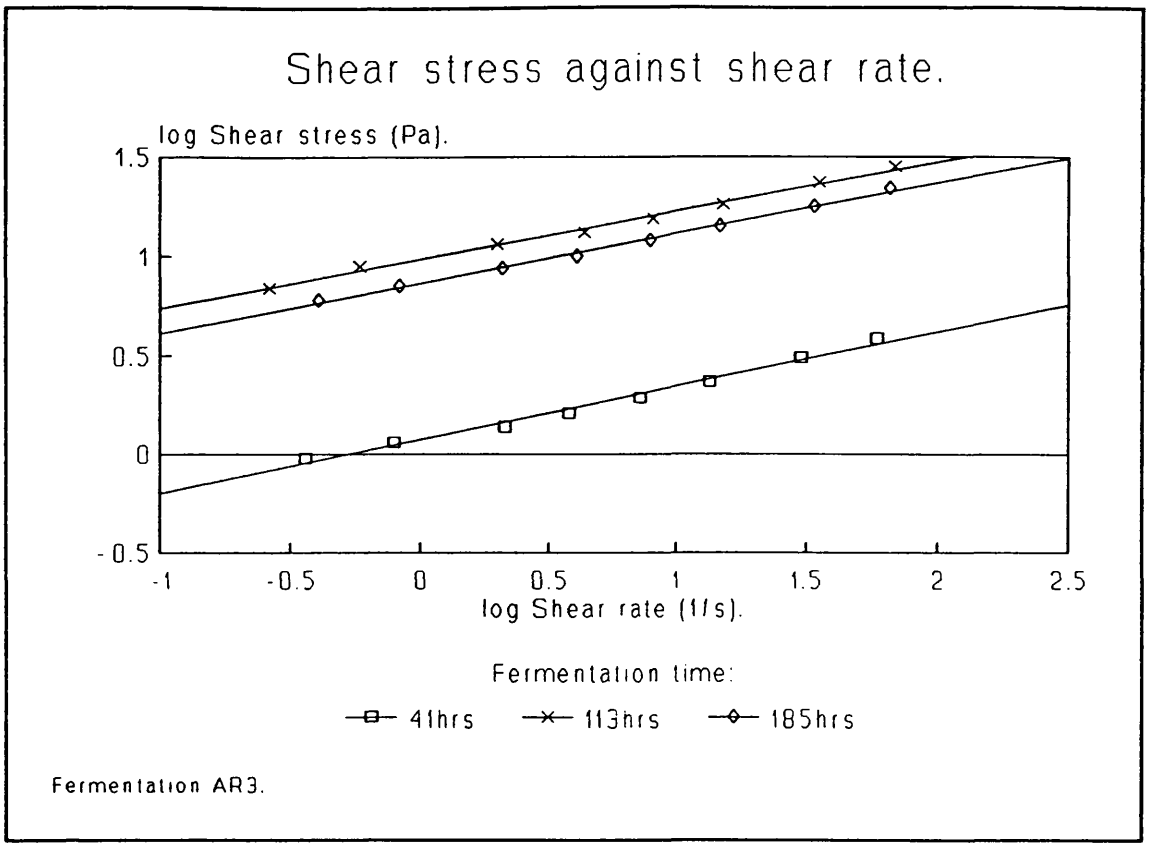

Figure 7

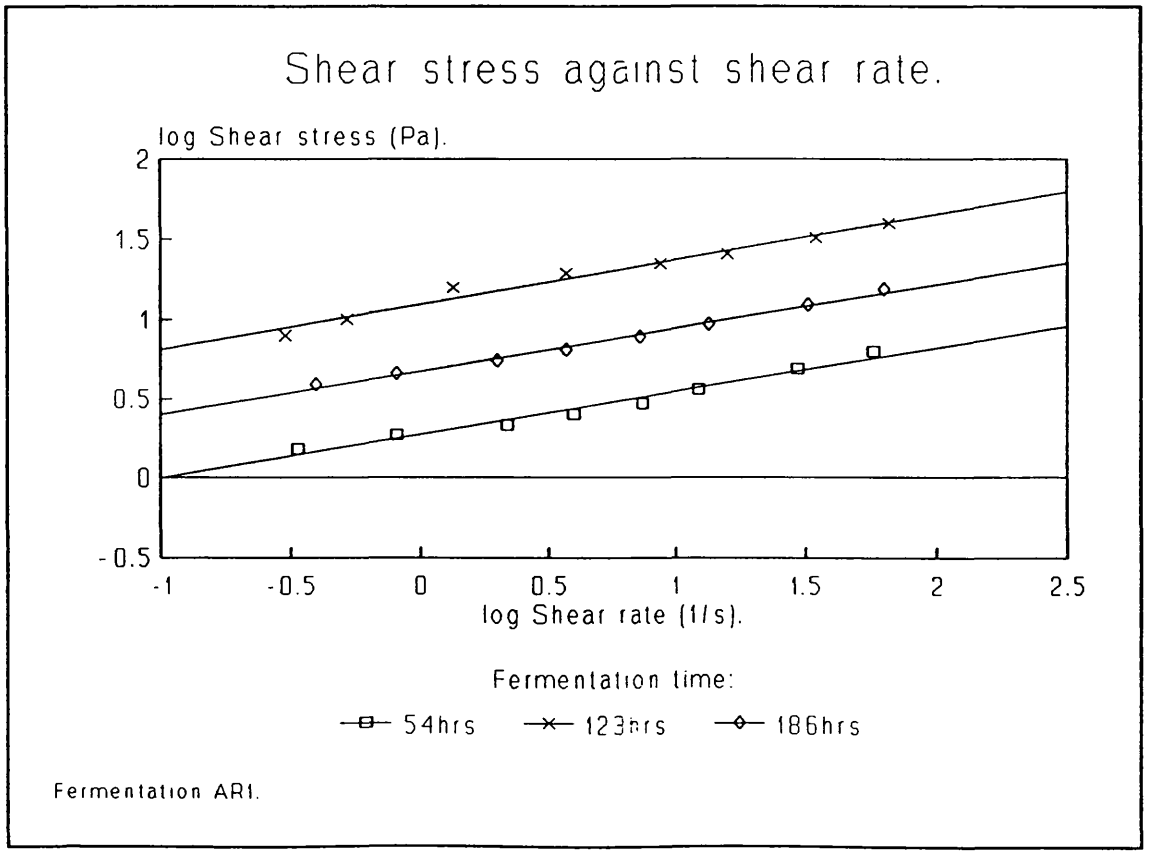

Figure 8

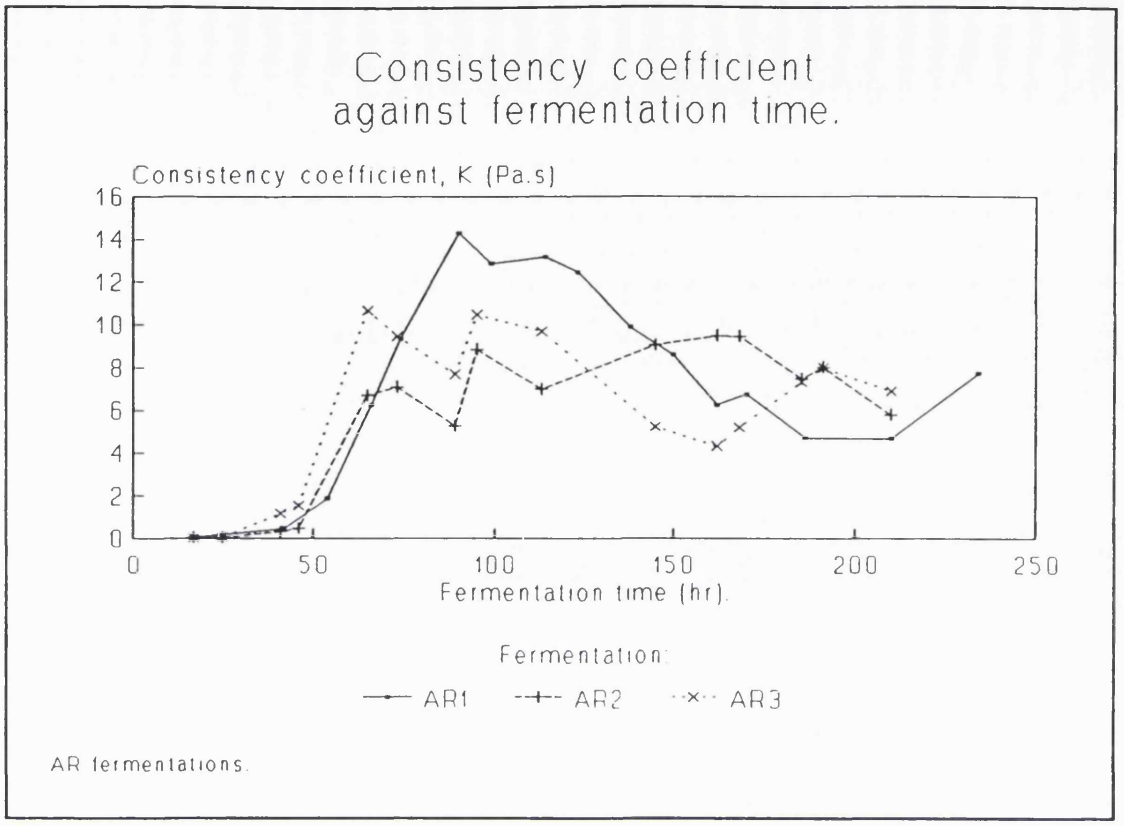

Figure 9

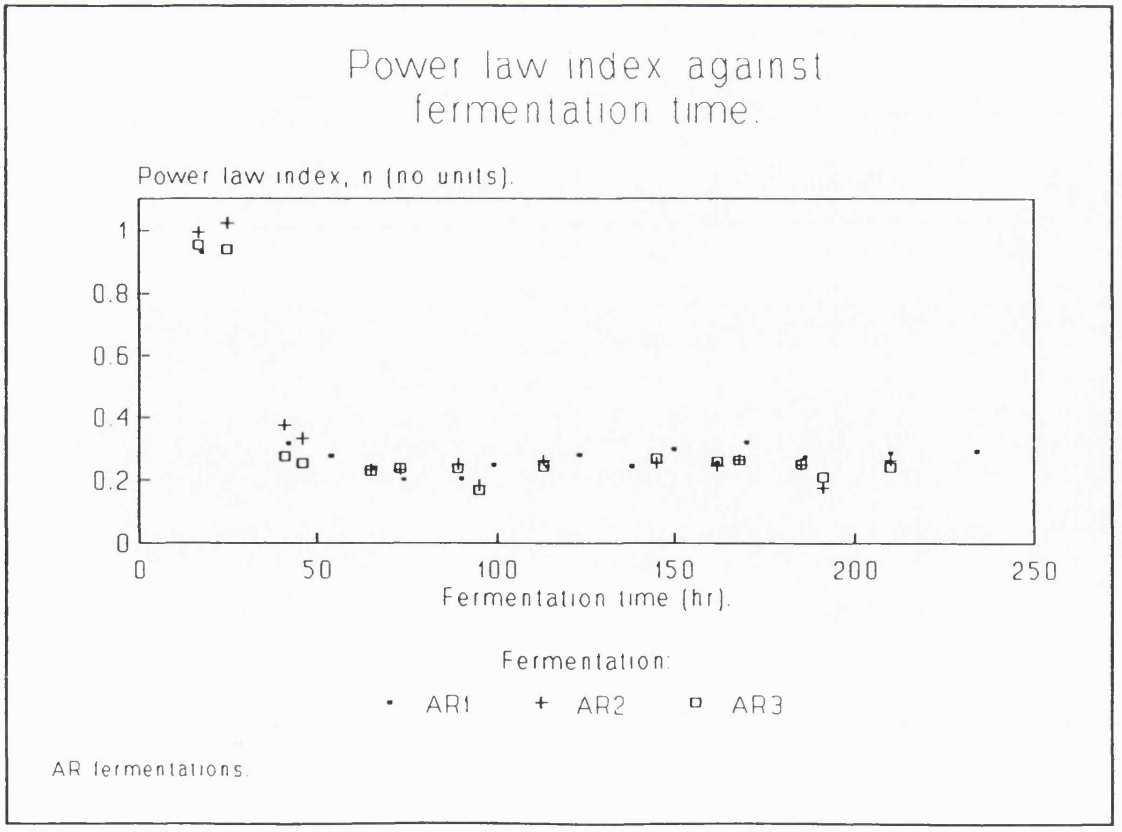

Figure 10

the duration of fermentations AR1, AR2 and AR3. All the fermentations closely follow the same profile. Initially the Power law index had a value of approximately unity, but by 40 hrs the n values had declined to between 0.3 and 0.15. The n values remain at this level for the remainder of the fermentation time course. Thus the fermentation broth stays Newtonian (with an n value of unity) up to ≈25 hr and then rapidly becomes highly pseudoplastic by ≈40 hr.

Stimulated by the paper of Gbewonyo et al [121], an attempt was made to establish a relationship between the TOC and the DCW for the *A. roseorufa* fermentation during the active phase.

Figure 11 shows a plot of log total oxygen consumed against log dry cell weight for fermentations AR2 and AR3 during the active growth phase. Dry cell weight values for the fermentation AR1 were not measured. The plots for both fermentations show a straightline relationship between increasing log TOC and increasing log DCW. Thus a non-linear relationship exists between TOC and DCW. The data from the two fermentations appear to fit the same straightline correlation.

As with the *S. erythraeus* fermentations the active growth phase of the fermentations was defined as the period of the fermentation during which the oxygen uptake rate was increasing (figures 4, 5 and 6).

During an *A. roseorufa* fermentation the dry cell weight profiles and the consistency coefficient profiles follow each other closely, figures 2 and 3. Figure 12 shows a plot of log K against log DCW for fermentations AR2 and AR3 during the active growth phase. The plot shows a non-linear correlation between increasing DCW and increasing K. In comparison with the equivalent relationship for the *S. erythraeus* fermentation, the *A. roseorufa* relationship appears much more distinct, this is possibly because the dry cell weight data were more reproducible. Although there was no dry cell weight data for fermentation AR1, the same relationship can be assumed

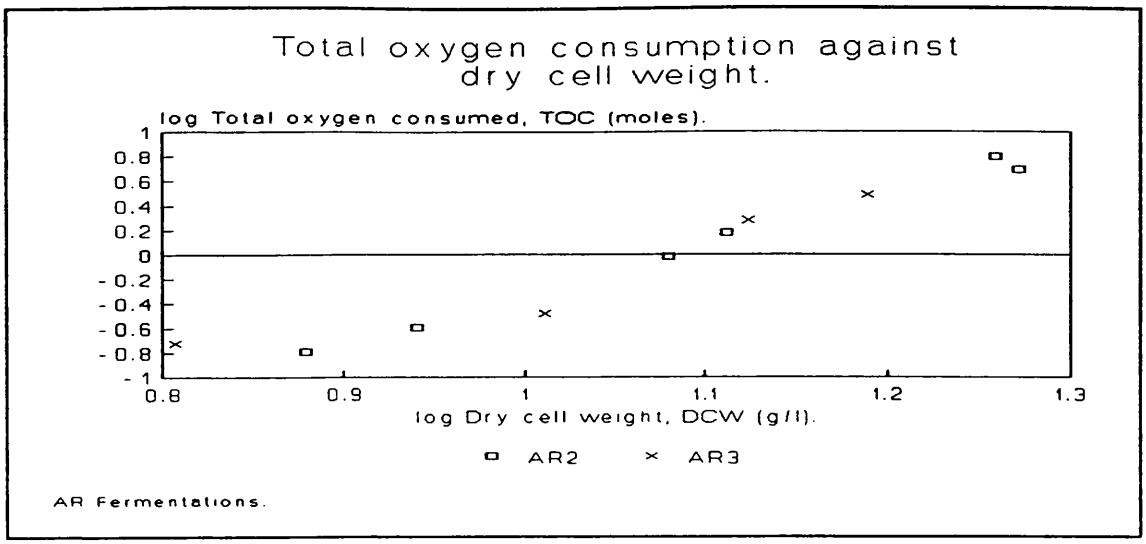

Figure 11

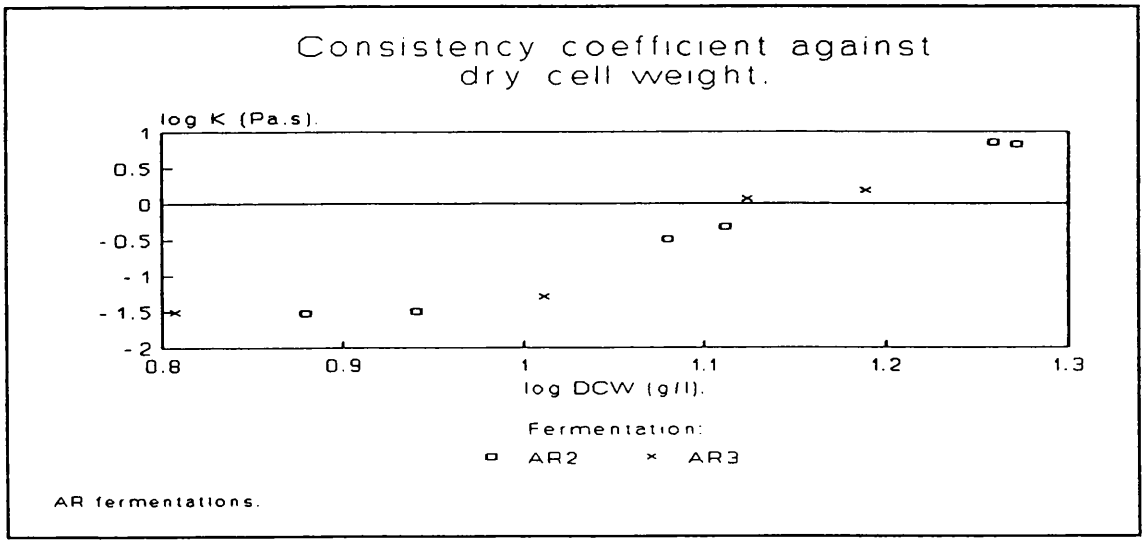

Figure 12

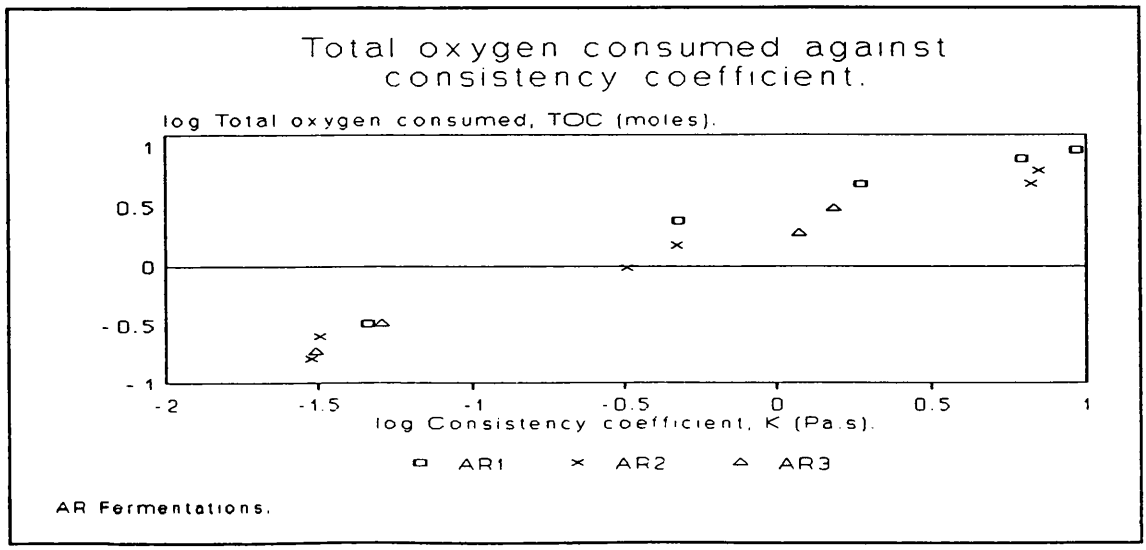

Figure 13

to exist.

Figure 13 shows a plot of log total oxygen consumed against log consistency coefficient for the fermentations AR1, AR2 and AR3. The plots for AR1, AR2 and AR3 show a straightline relationship between the increasing values of log TOC with increasing values of log K during the active growth phase of the fermentation. Therefore a relationship exists between TOC and K.

A parallel fermentation was run to provide further insight into the rheological properties of the *A. roseorufa* fermentation broth (see section 2.3.1.1 for explanation of procedure). Two fermentations were prepared and run in exactly the same way except one fermentation was inoculated with *A. roseorufa*, whilst the other was not. The samples from these fermentations were rheologically analysed and then centrifuged to remove any *A. roseorufa* cells and/or medium particulates and finally the centrifugate was re-analysed. Figure 14 shows several plots of log consistency coefficient and a plot of dry cell weight against fermentation time for an *A. roseorufa* fermentation (AR4). The key for figures 14 and 15 is as follows:

A - sample from inoculated fermentation before centrifugation.

B - the centrifugate of (A).

C - sample from uninoculated fermentation before centrifugation.

D - the centrifugate of (C).

Figure 14 shows that the consistency coefficient for (A) increases over the duration of the fermentation and so does the dry cell weight for the inoculated fermentation. The consistency coefficient for (C) remains at a constant level of ≈ 0.02 Pa.s^n. The consistency coefficient for the centrifugates (B) and (D) also remain constant but at a K value of less than 0.01 Pa.s^n.

Figure 15 shows several plots of Power law index, n, and a plot of dry cell weight for the inoculated fermentation against fermentation time for an *A. roseorufa*

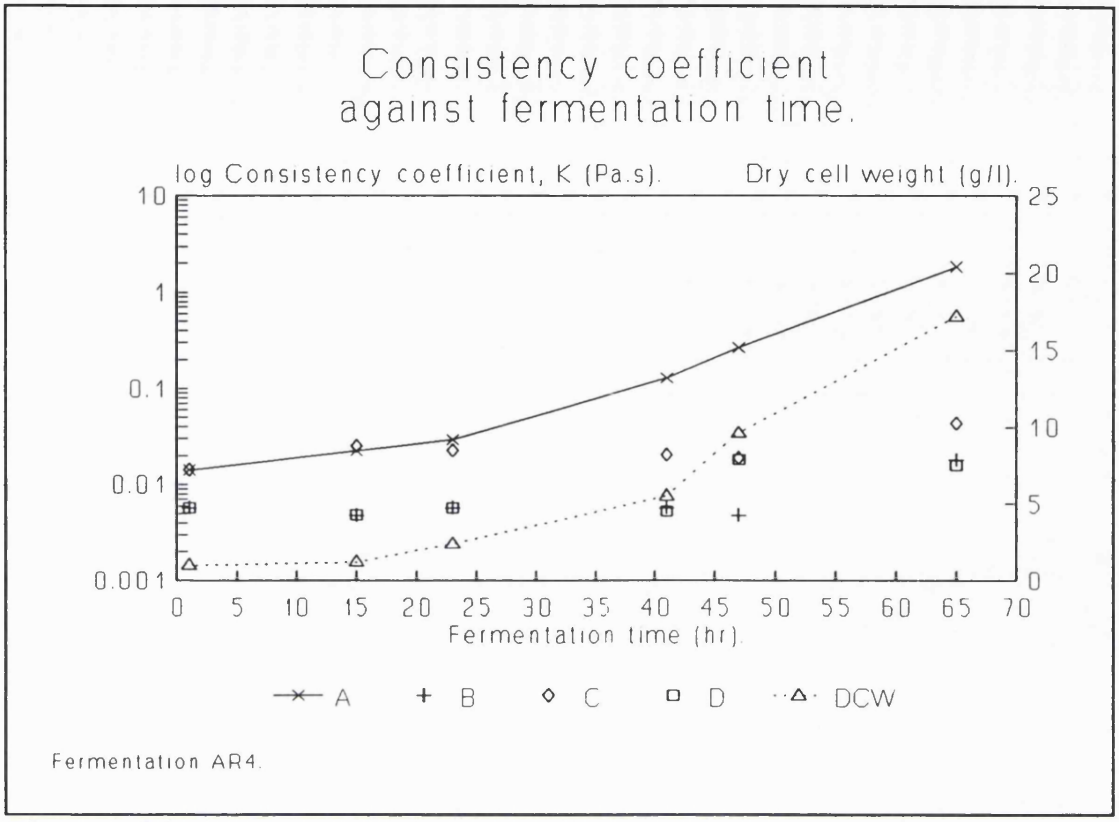

Figure 14

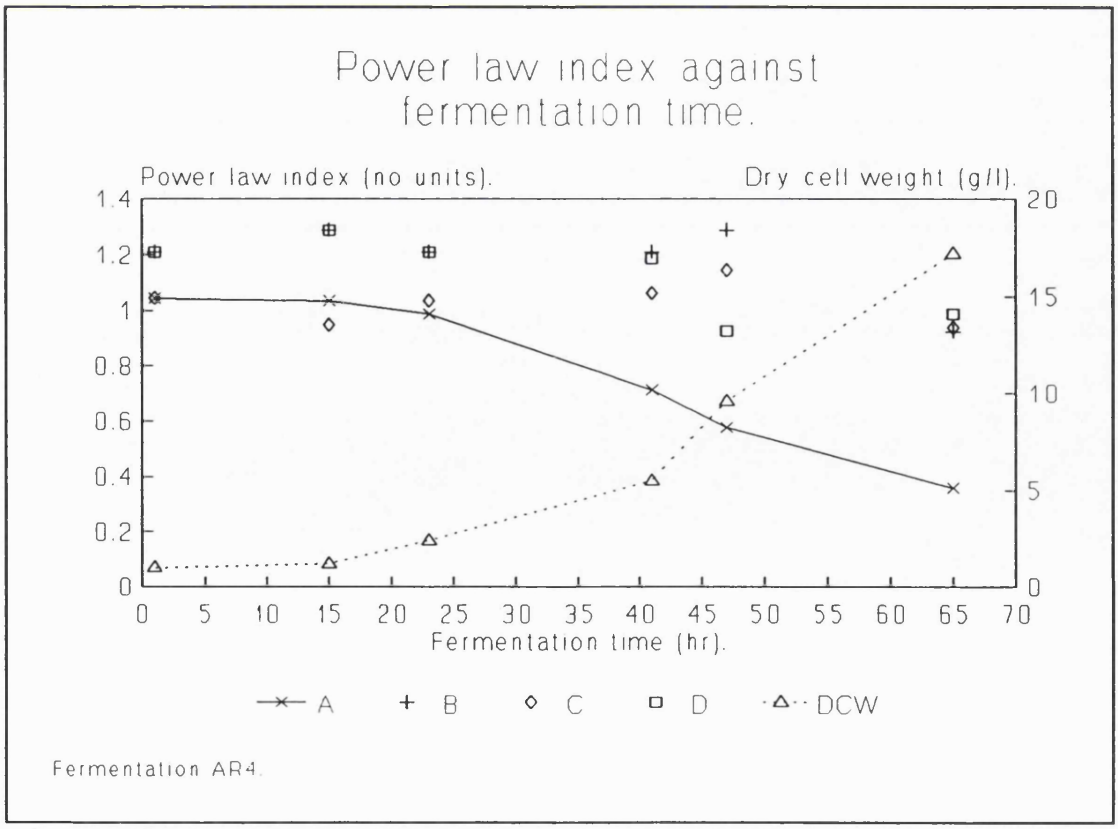

Figure 15

fermentation (AR4). The figure shows the Power law index for (A) decreasing from a value of ≈1 at 1 hr to ≈0.4 at the end of the fermentation. The Power law index for (B), (C) and (D) remain at ≈1 until the end of the fermentation.

A comparison of (A) with (B) gives a clear indication that the removal of the *A. roseorufa* organisms by centrifugation causes the consistency index of the broth to decrease and the Power law index to increase. A specific example helps to explain the implications of such changes: at 65 hr the AR4 fermentation broth is highly pseudoplastic and viscous with an n of 0.4 and a K of 2 $Pa.s^n$, but when the *A. roseorufa* cells are removed by centrifugation the broth becomes Newtonian and non-viscous with an n of ≈0.95 and a K of ≈0.02 Pa.s. Hence, the presence of the *A. roseorufa* organisms are necessary for the high apparent viscosities of the fermentation broth.

The Newtonian and non-viscous nature of (C) indicates that the viscosity of (A) is not caused by the presence of solids or any chemical reaction between the substrates in the fermentation medium. A slight reduction in K and a small increase in n when (C) was centrifuged to produce (D) suggests that the solids present in the fermentation medium had some effect on the rheological characteristics, but the influence was tiny when compared with the effect caused by the presence of the organisms. These results are similar to those obtained for the *S. erythraeus* fermentation.

For fermentation AR1 the plot of the dry cell weight appears to follow an inverse relationship to the Power law index plot for (A). However, this relationship was not present in fermentations AR2 and AR3.

The considerable amount of point scatter evident at low values of K and high values of n were due to the insensitivity of the Brookfield viscometer when analysing such low viscosity fluids.

Figures 16, 17 and 18 show the relationship between the morphology of the filamentous microorganisms and the rheology of the fermentation broth. The plots show mean

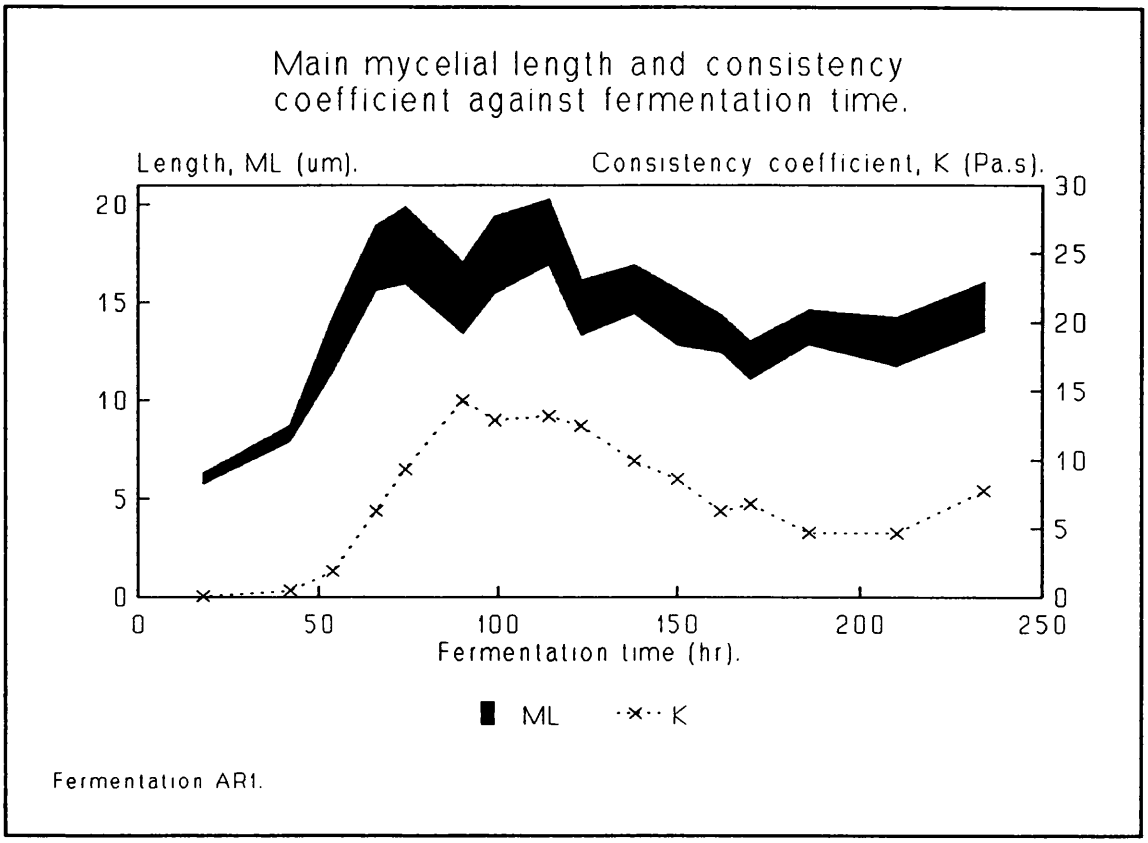

Figure 16

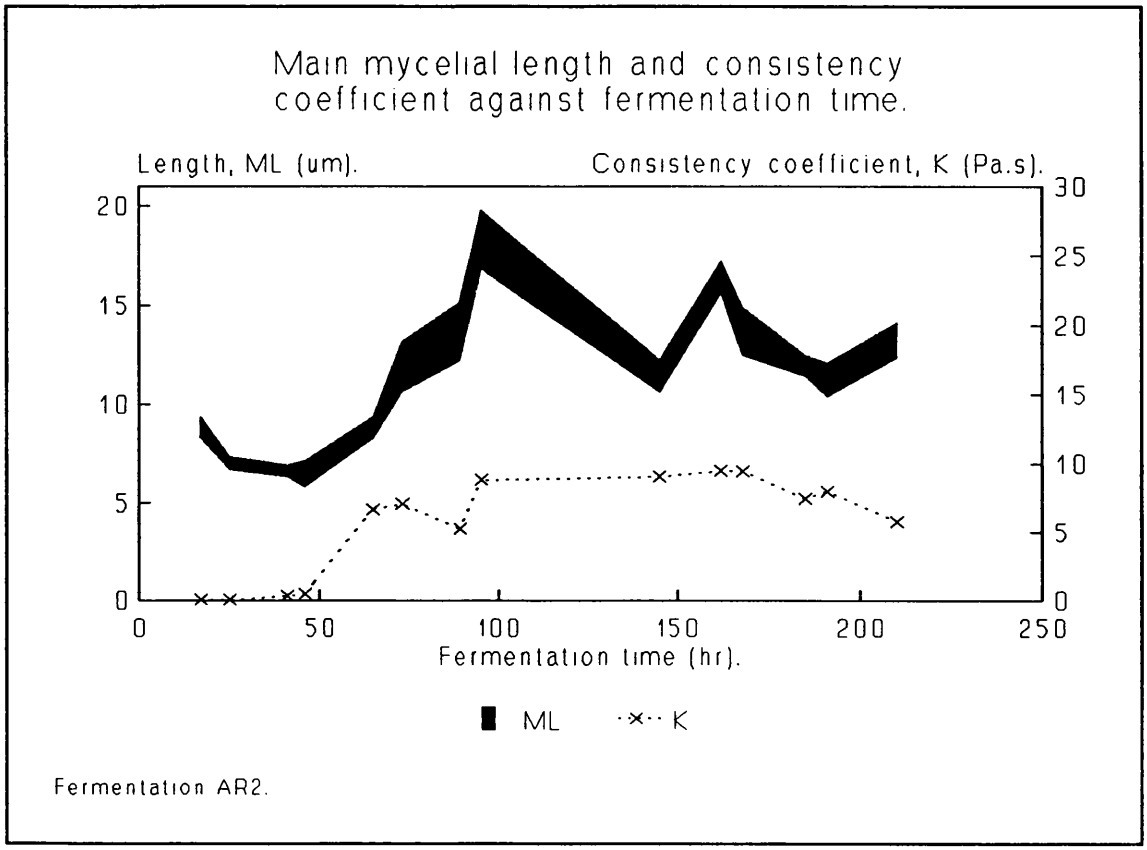

Figure 17

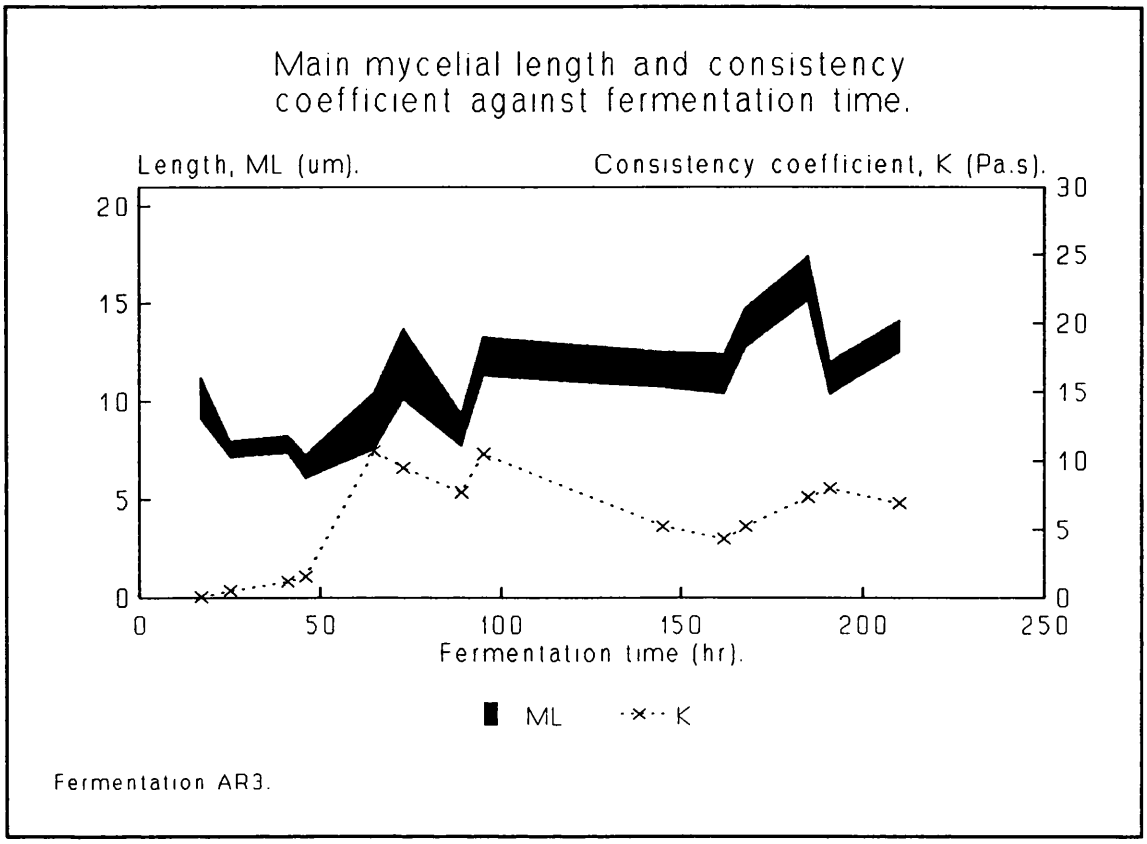

Figure 18

main mycelial length and consistency coefficient against fermentation time. The width of the plotted line indicates the 95% confidence limit for the data. The figures show that no correlation exists between the morphology parameter (ML) and the rheology parameter (K).

Figures 16 to 18 show the wide range of mean main mycelial length, ML, over the duration of the fermentation. In AR1 and AR2 there is an increase in ML from 6 to almost 20μm during the initial growth phase and then a gradual decline. In AR3 ML did not rise to the same extent.

Using linear regression analysis the correlation coefficients, r, for log ML against log K were calculated for each fermentation using the same procedure as described in chapter 4 and showed that in statistical terms no relationship exists between ML and K.

6 The *Streptomyces rimosus* fermentation results.

Figures 1, 2 and 3 are entitled Fermentation Profile (part one) and show data from fermentations SR1, SR2 and SR3 respectively. These figures show the consistency coefficient and the total oxygen uptake against the fermentation time. Figures 1 and 3 show a close match between the TOC profiles; there was an initially fast and constant rate of increase in TOC which then slowed at approximately 40hrs, this slower constant rate then continued for the remainder of the fermentation. No TOC data is displayed in figure 2 because the OUR data for fermentation SR2 was found to be erroneous.

The consistency coefficients for all three fermentations showed a similar pattern. The value increased with time until the 140-170hrs region when the value reduces. In each case there was a subsequent recovery in the value. The saw-tooth profile of the K data probably resulted from the many adjustments to the rate of nutrient feed to the fermenters.

No dry cell weight data were collected for these fermentations because of commercial confidentiality problems.

Figures 4, 5 and 6 give the oxygen uptake rate, dissolved oxygen tension and respiratory quotient against fermentation time for fermentations SR1, SR2 and SR3, respectively.. The profiles for the respiratory quotient show a close resemblance in the three fermentations. There was a fairly constant value of approximately 0.65 for the duration of the fermentation, which is typical for an oil utilizing fermentation which displays no metabolic changes during the process.

The OUR values initially rose, and then rapidly fell over the next 20hrs, see figures 4 and 5. This was followed by a slow decline in OUR over the remainder of the fermentation.

After examination of the OUR values for fermentation SR2 it was decided that they were false, for some unknown

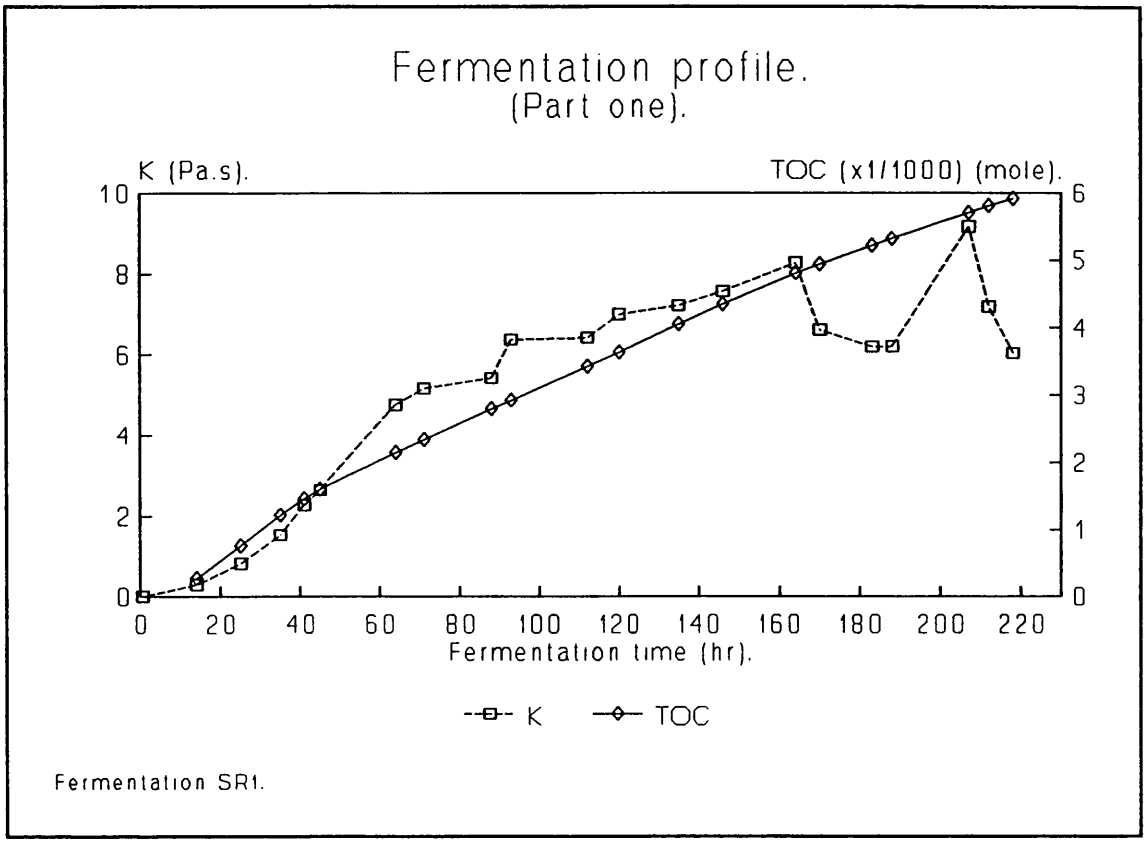

Figure 1

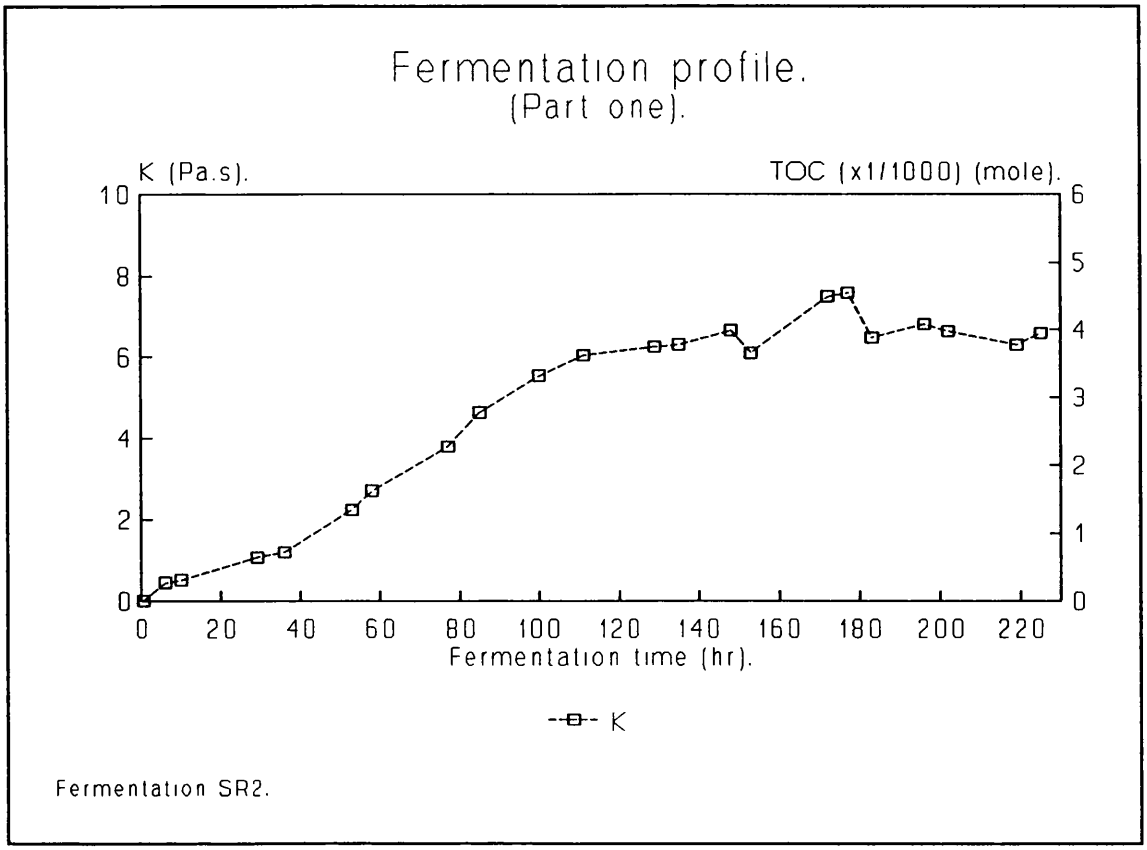

Figure 2

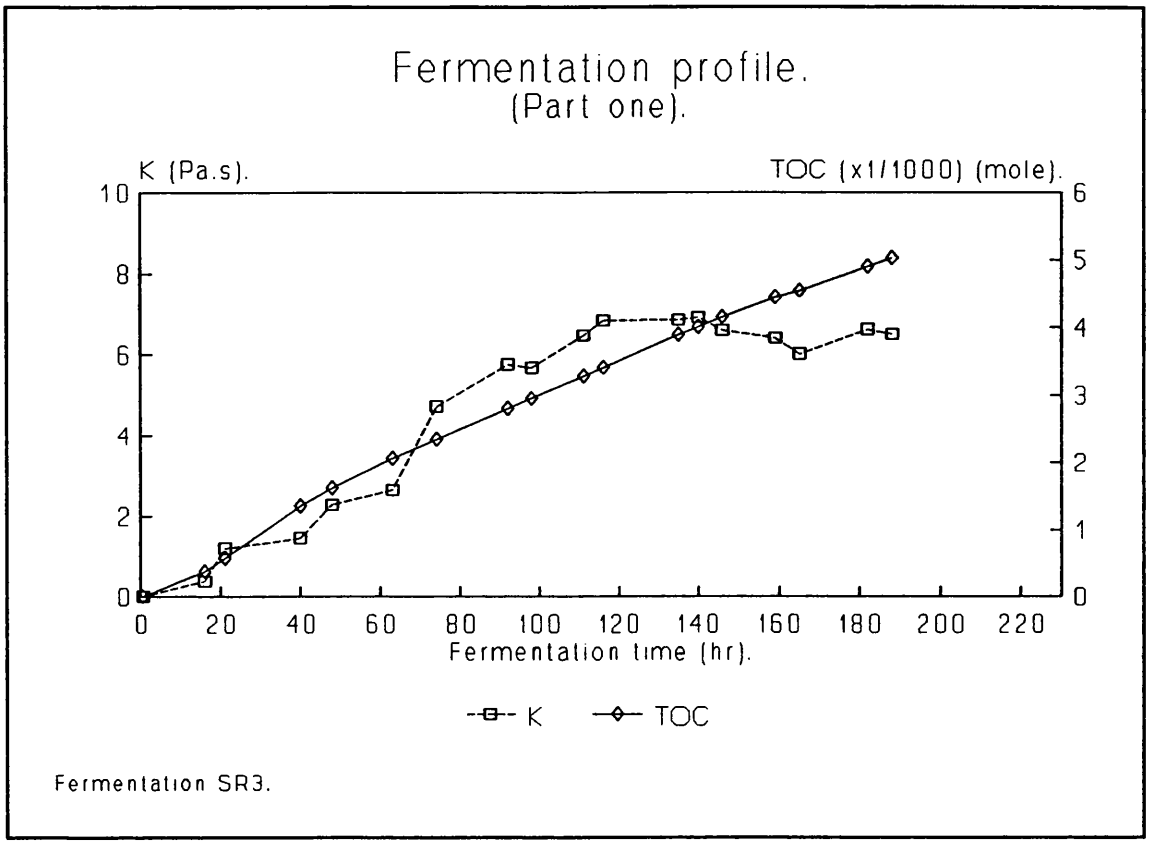

Figure 3

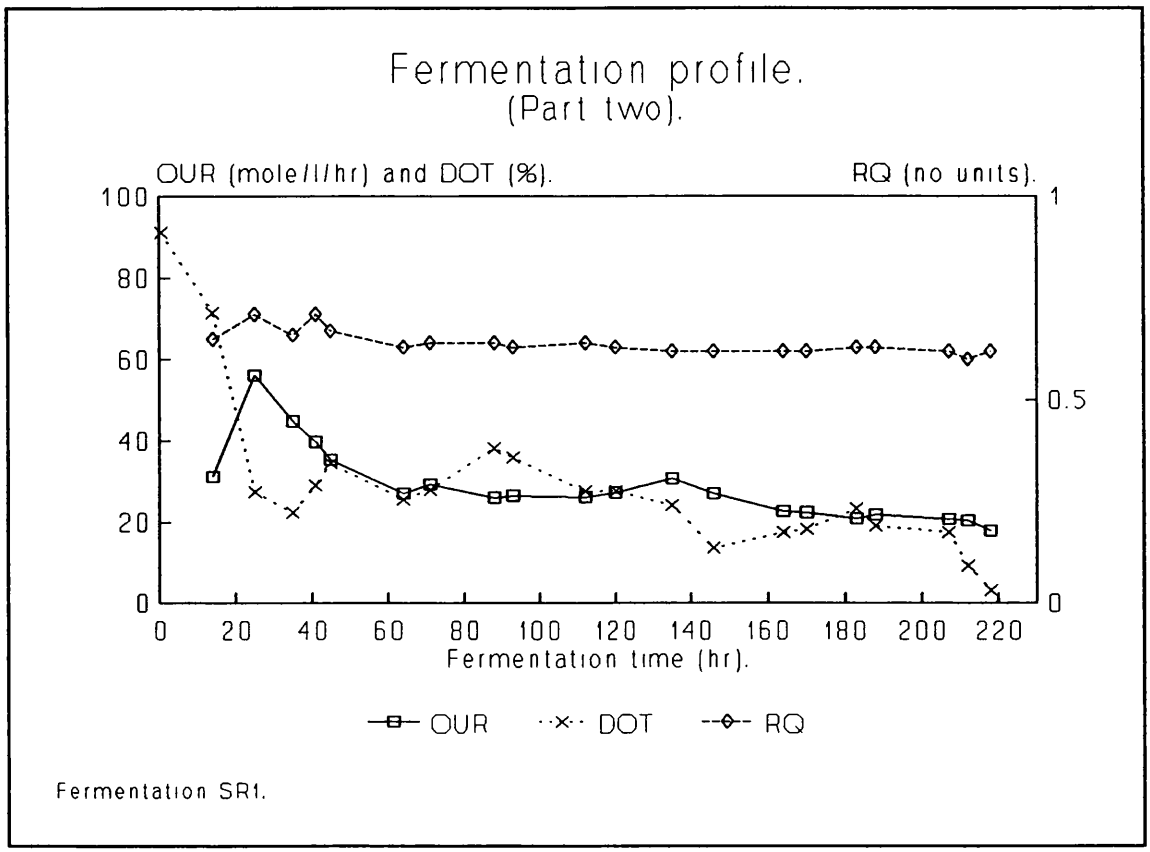

Figure 4

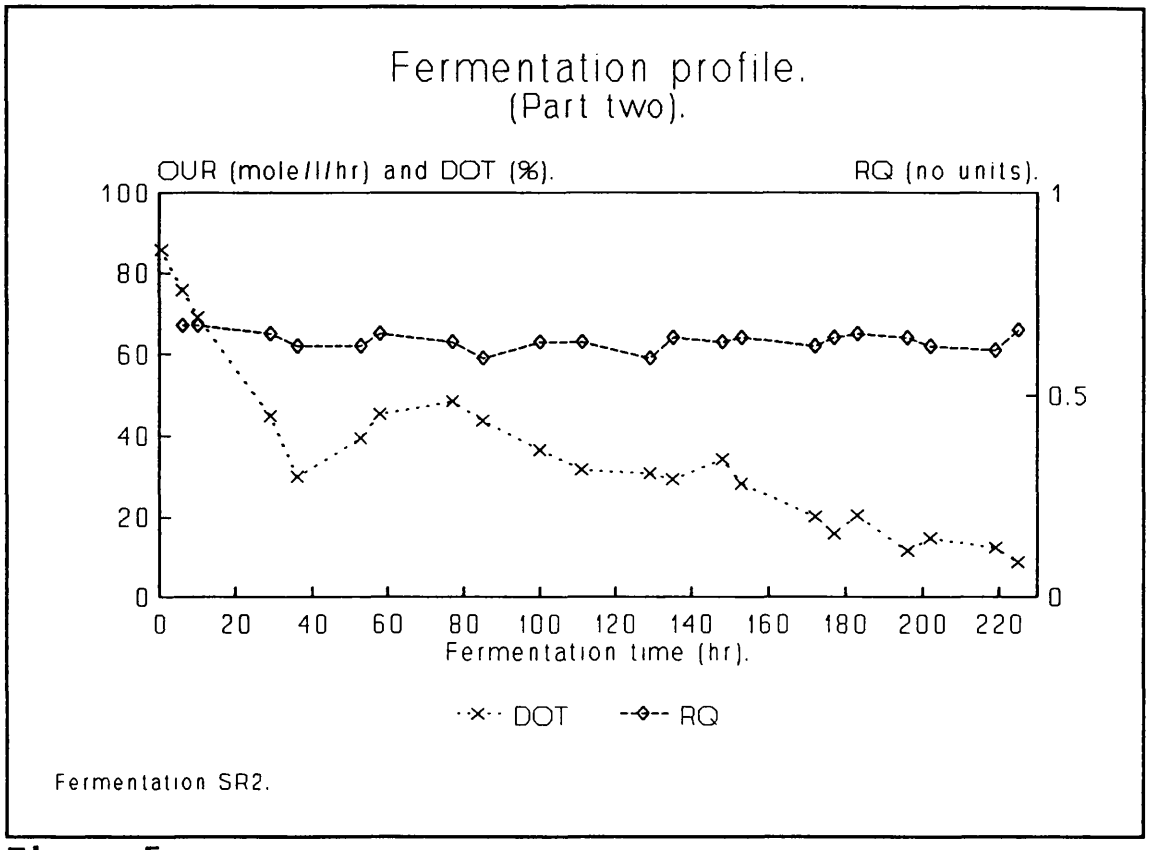

Figure 5

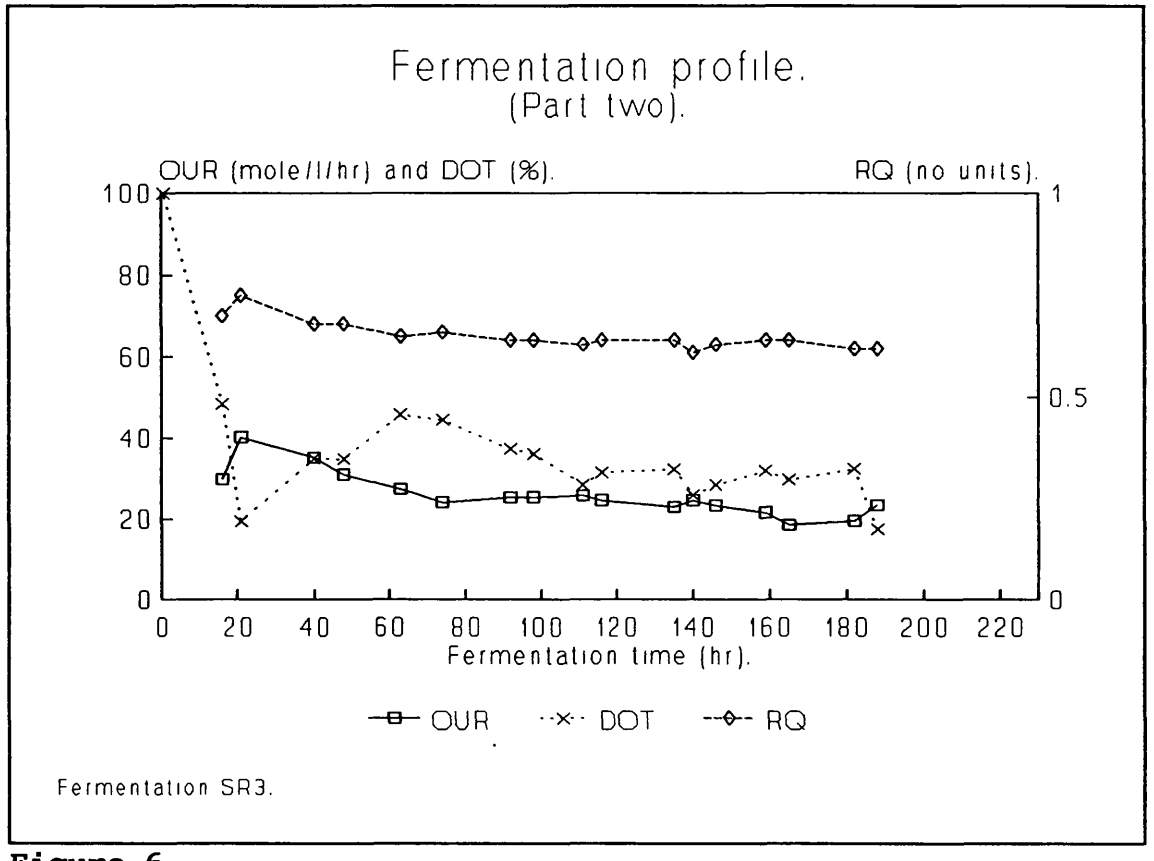

Figure 6

reason the data logger had recorded spurious information. Therefore, the OUR and the TOC data for fermentation SR2 have been omitted.

The plots of DOT for the three fermentations show a consistent pattern. The DOT dropped rapidly to between 20 and 30%, then it increased to a peak and finally decreases for the remainder of the fermentation. The initial fall in DOT to a nadir corresponds with the initial peak in the OUR plot.

In fermentations SR1 and SR3 the decrease in DOT caused the OUR profile, which was increasing, to peak and fall. As would be expected, a lack of dissolved oxygen prevented the oxygen uptake rate from rising further.

Figures 7 and 8 display the rheological characteristics of the fermentation broths at various stages of the fermentation process. Only three of the broth samples are shown for reasons of clarity. The plots show log shear stress against log shear rate at various fermentation times for fermentations SR1, SR2 and SR3. During this project it has been assumed that a straightline relationship (the Power law) exists between the logarithm of shear stress and the logarithm of shear rate for any fermentation broth. These figures show the best (figure 7) and an average (figure 8) examples of these straightline relationships. Linear regression analysis (the method of least squares) was used to calculate the equation of the best fit line through the sample data. Figures 7 and 8 show how closely these straightlines fit the rheological data points. By comparing the Power law with the equations for the best fit lines, values for the Power law index, n (no units) and the consistency coefficient, K was determined for a broth sample at any particular time in the fermentation. By analysing the fermentation broth at regular intervals the changes in n and K throughout the fermentation were established.

Figure 9 indicates the change in consistency coefficient against fermentation time for fermentations SR1, SR2 and SR3. This figure highlights the similarity

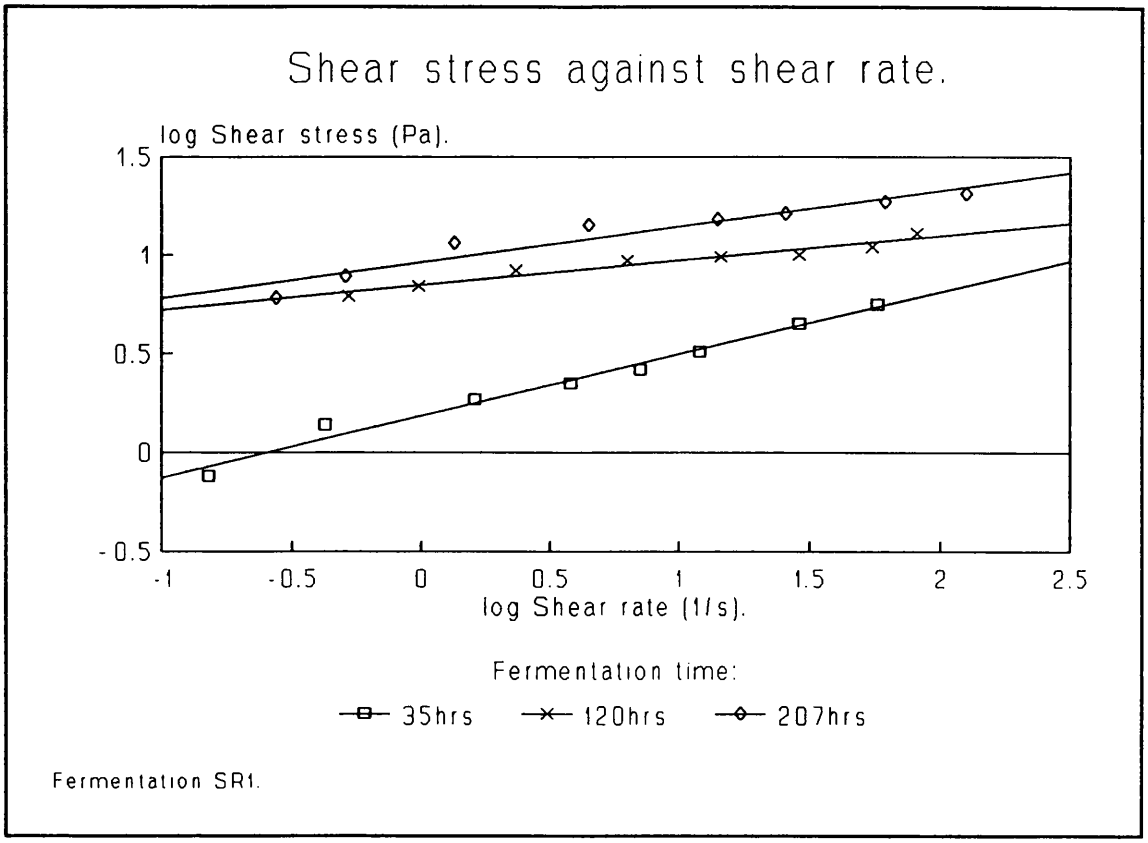

Figure 7

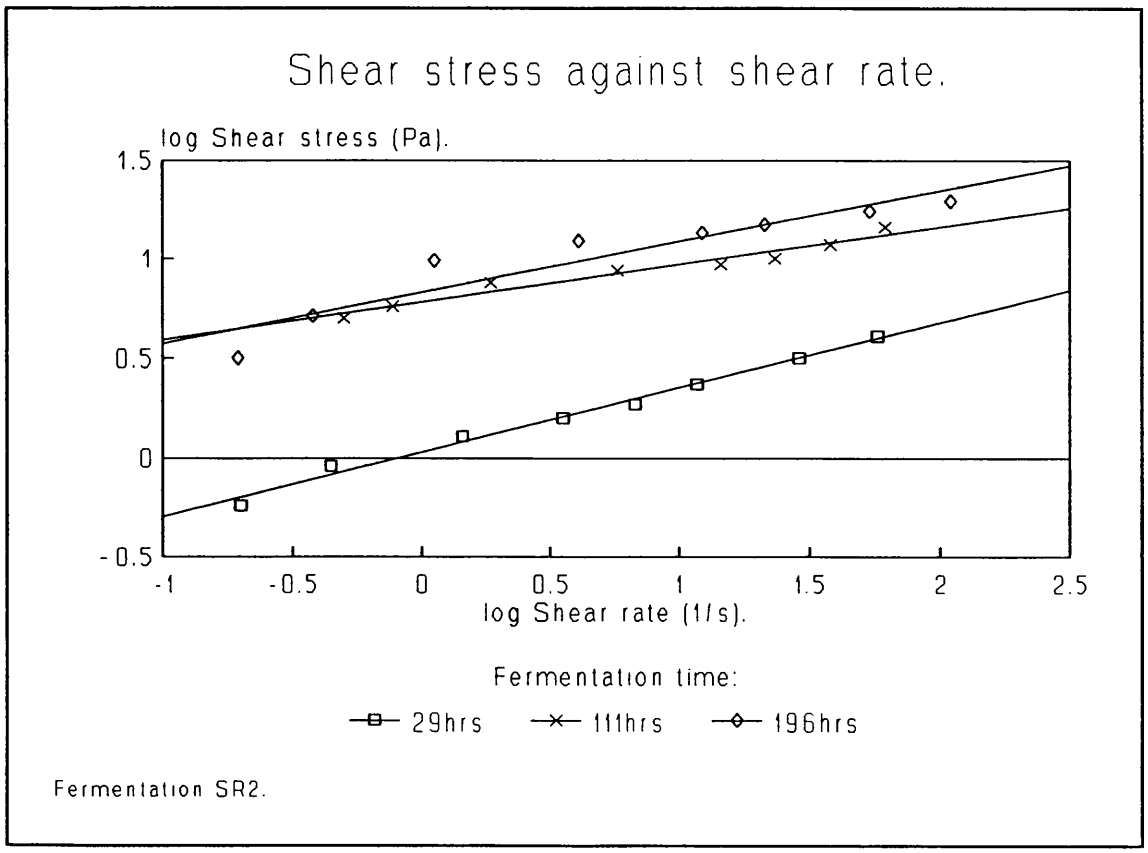

Figure 8

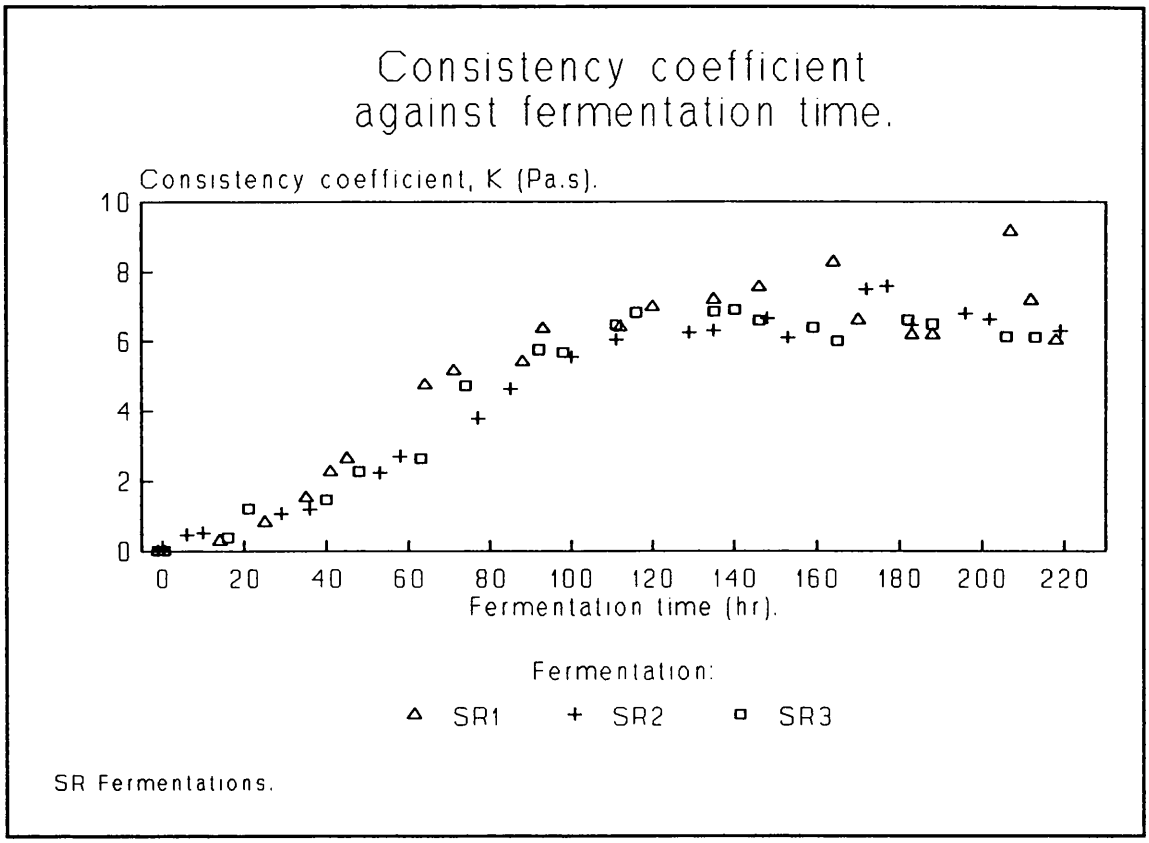

Figure 9

of the K data for all three fermentations.

Figure 10 shows the change in the Power law index over the duration of the fermentation. Data from all three fermentations are shown. At 0hrs the index had a value of between 1.2 and 1.4, but by 10hrs this value had decreased to approximately 0.3. The values stayed between 0.4 and 0.15 for the remainder of the fermentation; within this range the values dropped slowly until 100hrs, plateaued for 70hrs and began to rise slightly over the remaining 50hrs. Thus the fermentation broth remained Newtonian for only a few hours before becoming highly pseudoplastic for the remainder of the fermentation. Similar results were seen in the other Actinomycete fermentations.

During the control experiments (see chapter 3), the *S. rimosus* fermentation broth was shown to be thixotropic. This behaviour probably resulted from the alignment of particles and the destruction of interparticular bonds during the sustained shearing.

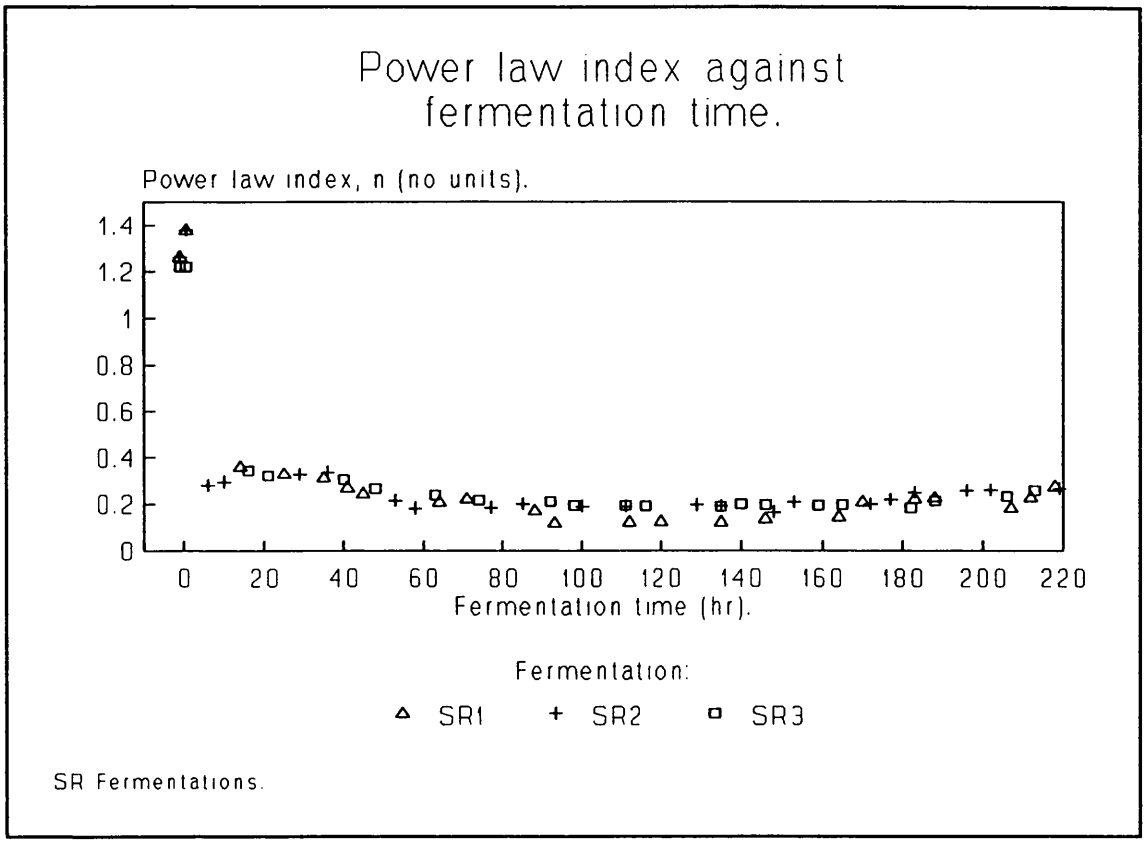

Figure 10

The work conducted by Gbewonyo et al [121] and the observations made in the *A. roseorufa* and *S. erythraeus* fermentations suggest that there is a relationship between TOC and K during the active part of Actinomycete fermentations. This statement is reinforced by the graphical evidence shown in figures 1 to 3, which indicates that the plots of TOC and K have similar profiles. Figure 11 shows a plot of log TOC against log K over the active growth phase of fermentations SR1 to SR3; the plot shows a straightline relationship between increasing log TOC and increasing log K for each of the fermentations. After establishing this non-linear relationship it was reasonable to assume that there was also a non-linear correlation between K and DCW as was found in the *A. roseorufa* and *S. erythraeus* fermentations.

The active growth phase was defined as the region during which the rate of change of oxygen uptake rate was greater than 2.6 moles of oxygen per litre per hour [2].

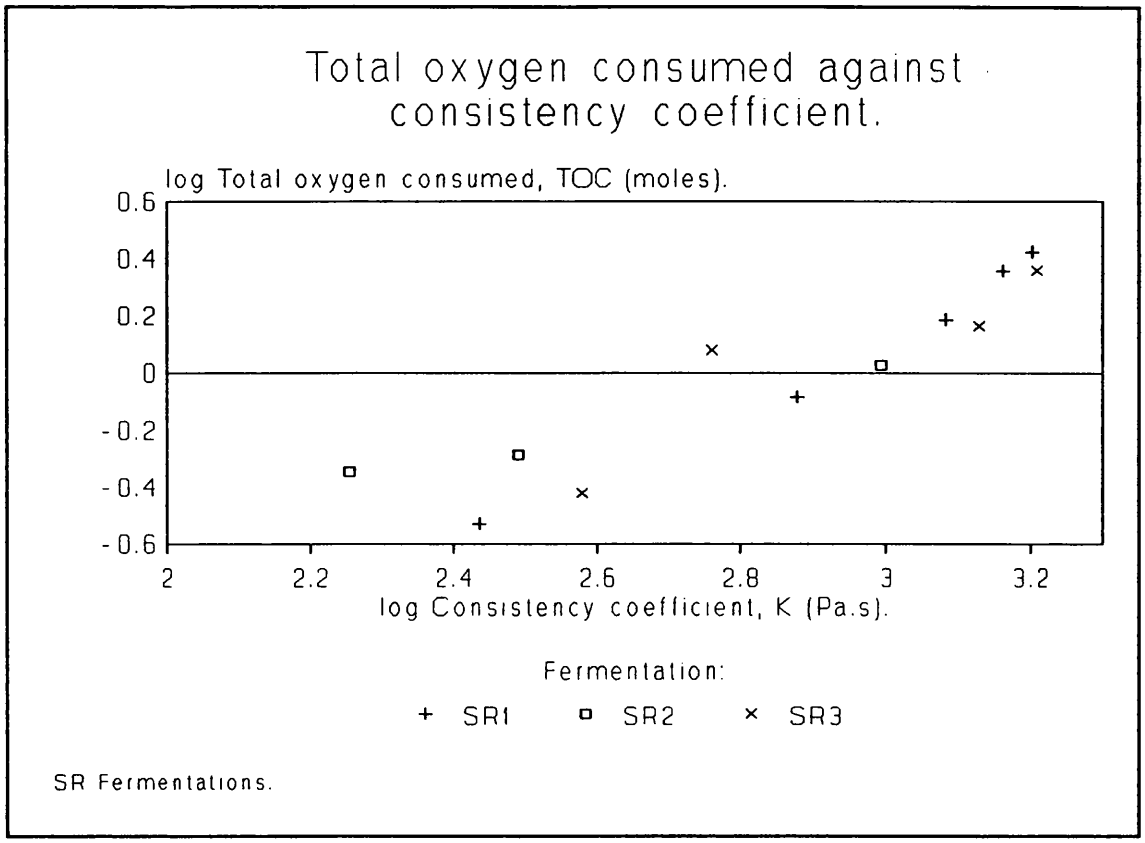

Figure 11

The definition used in the other Actinomycete fermentations could not be used because in this fermentation the OUR peaked extremely early, before the active growth phase could possibly be complete.

Figures 12 and 13 show the relationship between the morphology of the filamentous microorganisms and the rheology of the fermentation broth. The plots show mean main mycelial length and consistency coefficient against fermentation time. The width of the plotted line indicates the 95% confidence limit for the data. In both cases it should be noted that there is little correlation between the morphology parameter (ML) and the rheology parameter (K) for the fermentation broths. Figures 12 and 13 show the value of ML ranging from 7 to 18μm over the duration of the fermentation. Neither of the morphology profiles show any particular trend in the changing values of ML with respect to time.

Using linear regression analysis the correlation

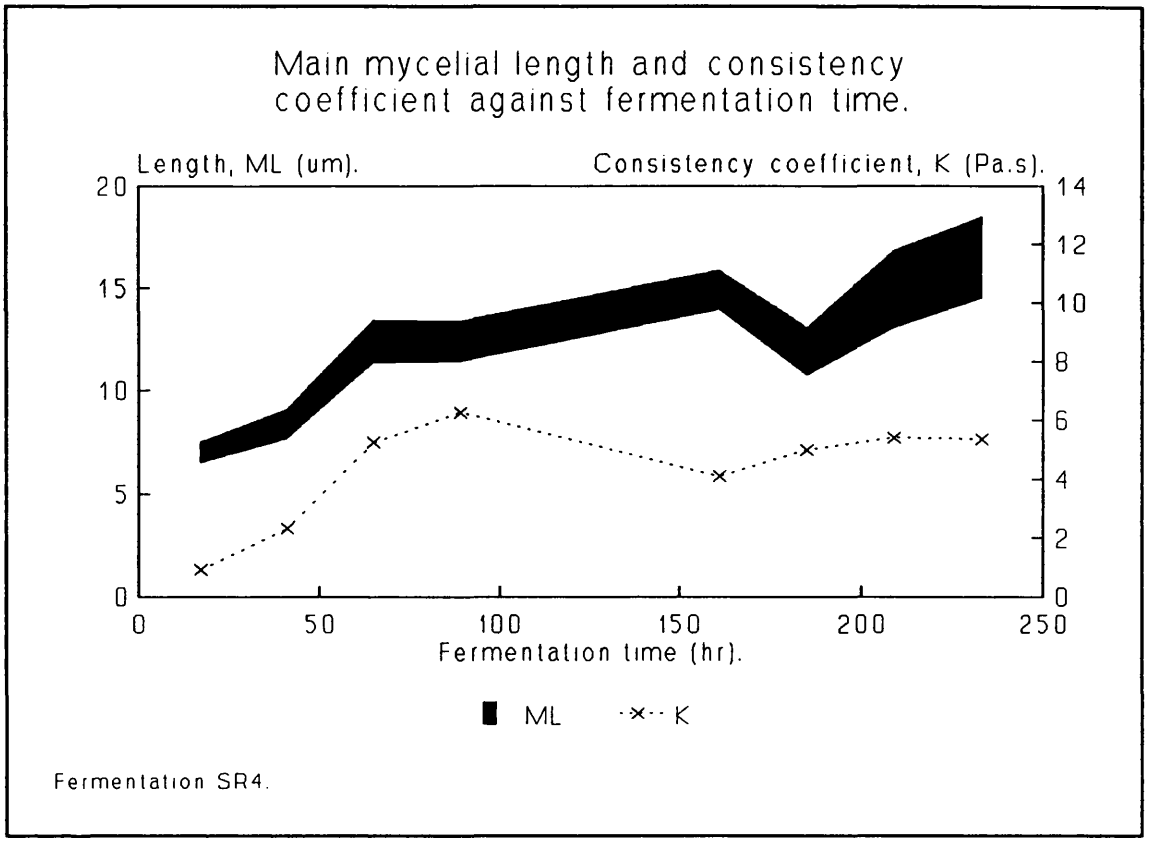

Figure 12

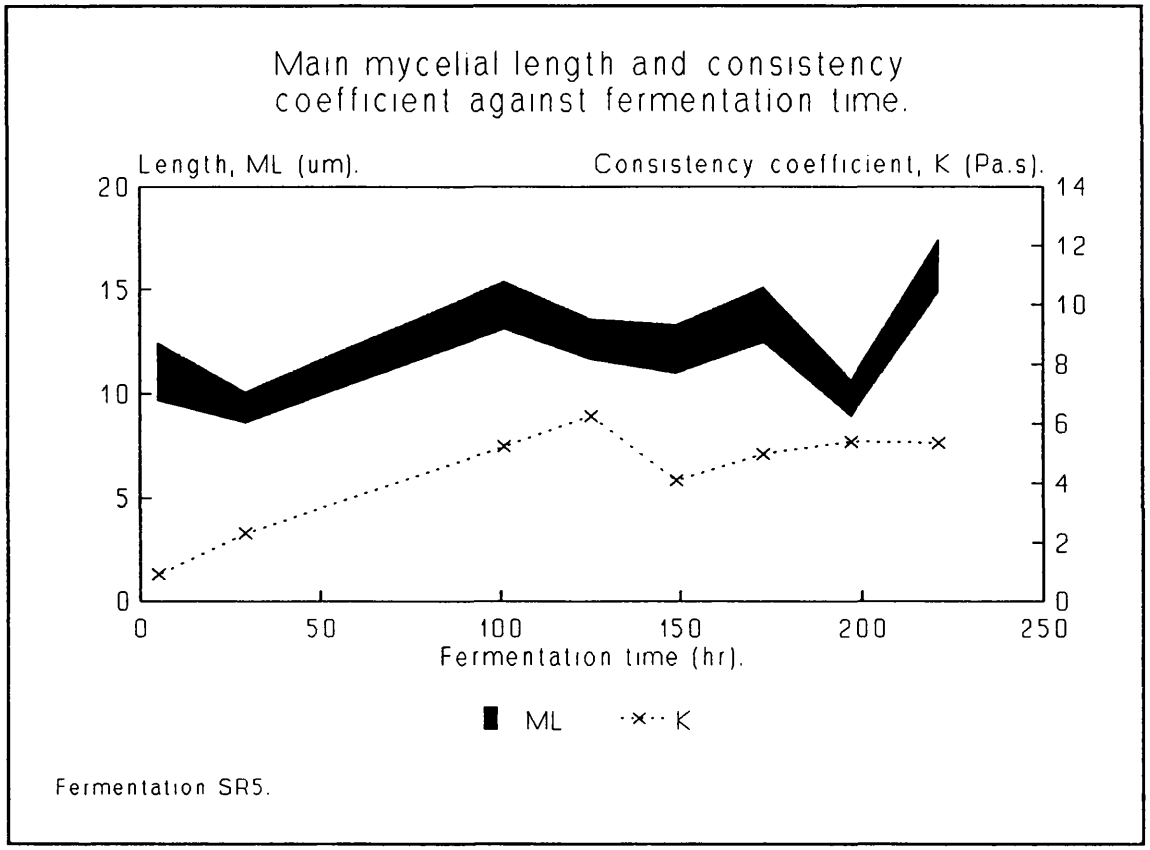

Figure 13

coefficient, r, for log ML against log K was calculated for each of the fermentations. A procedure described in chapters 4 and 5 shows that the determined correlation coefficients were below critical values and therefore prove statistically that there is no relationship between ML and K.

7 Additional results.

7.1 The effect of pH on the broth rheology.

A series of experiments were carried out to assess the effects of a change in pH on the rheology of *S. rimosus* fermentation broth. A large sample of *S. rimosus* fermentation broth was removed from a fermenter and divided into several specimens. Using concentrated hydrochloric acid and concentrated sodium hydroxide (60% by weight) the pH of each broth specimen was altered to cover the range pH10 to pH3 in 0.5 pH unit increments. Care was taken to ensure that each specimen received a similar amount of shear whilst the acid or alkali was mixed into the broth. Each specimen was then rheologically analysed using the standard Brookfield system.

Figure 2 shows a plot of the consistency coefficient or K (Pascals-seconds)^n against pH of two different *S. rimosus* fermentation broths labelled A and B. Both broths A and B follow the same general pattern; as the pH of the fermentation broth falls, the value of K increases to a peak at a pH of 5.5 and then the value of K decreases. Figure 3 displays Power law index, n, (no units) against pH for these same fermentation broths (A and B). As the pH of the broth sample is reduced, the value of n rises to a peak at 5.5 and then the value falls.

Figure 2 indicates that pH has a highly significant effect on the apparent viscosity of the *S. rimosus* fermentation broths. The influence of pH tends to suggest that some form of interparticular force exists between the organisms and that a change in pH causes a change in the magnitude of these interparticular forces. There is little experimental information on the effect of pH on the rheology of fermentation broths and there is hardly any information on the nature and magnitude of surface charges on the microorganisms. Considerable work has been done on other concentrated colloidal dispersions and excellent

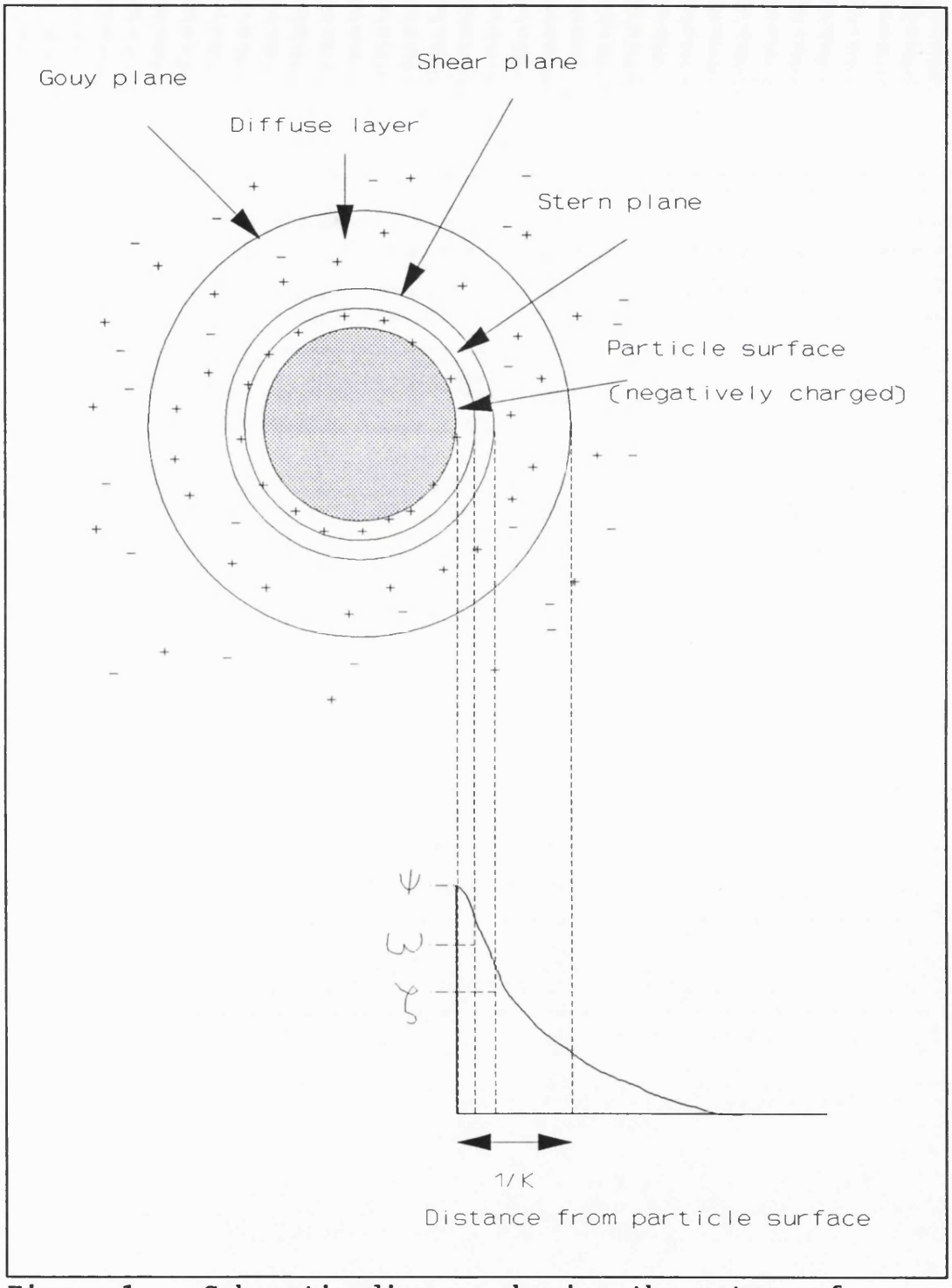

Figure 1. Schematic diagram showing the nature of electrical forces around a particle in bulk solution.

reviews are available.[125 and 126]

According to the well established theory of colloidal stability net interaction force between two similar

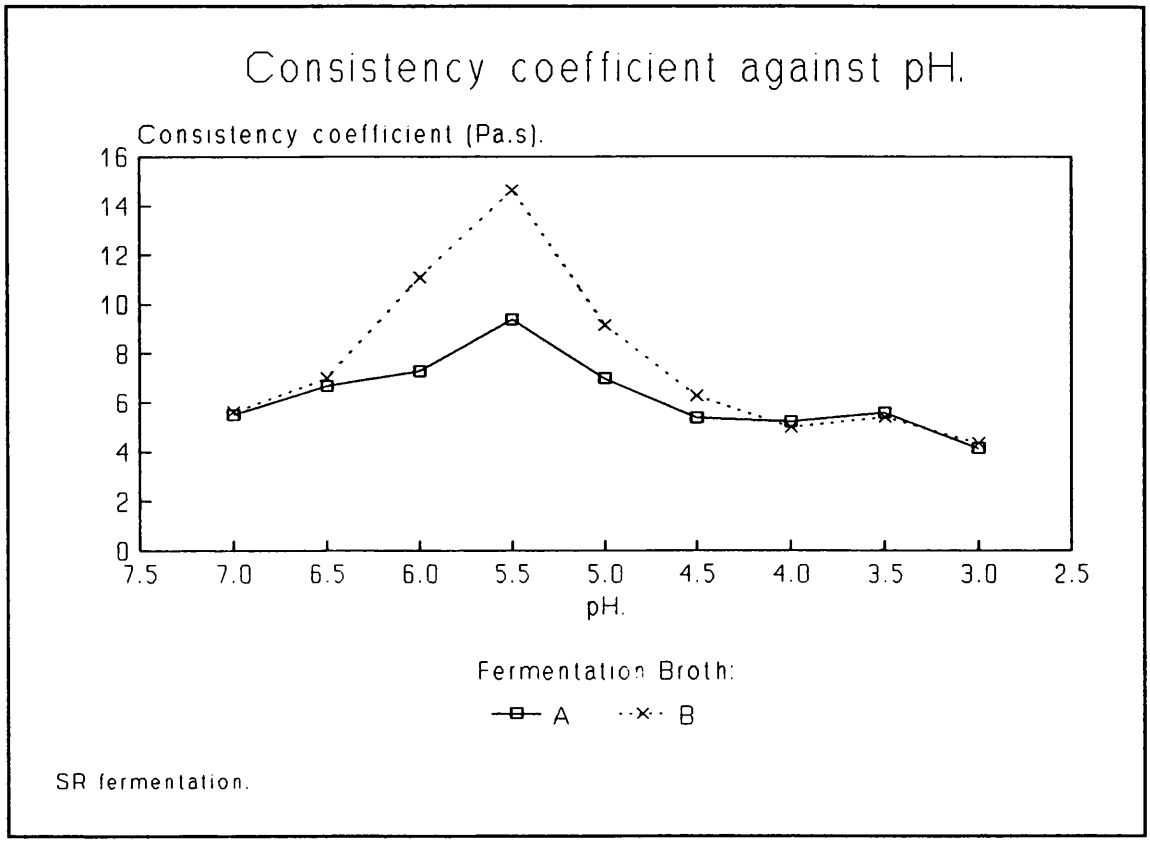

Figure 2

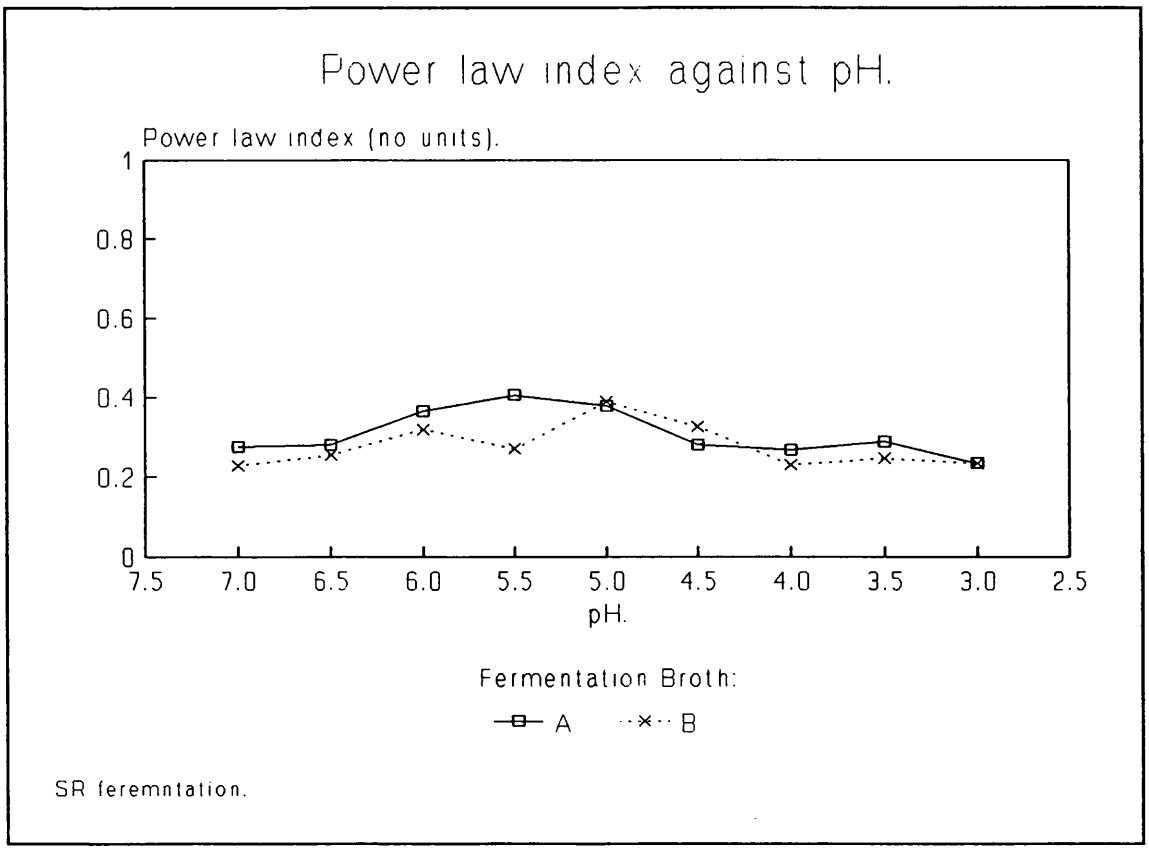

Figure 3

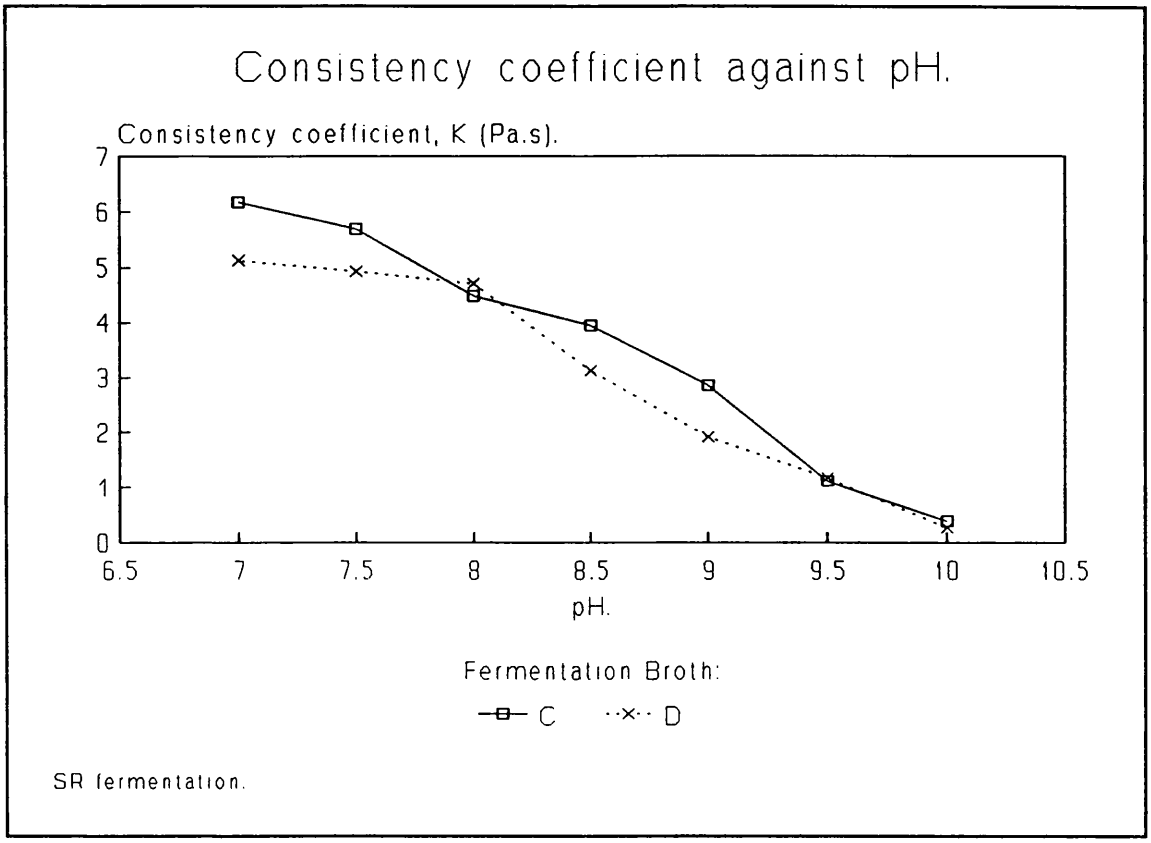

Figure 4

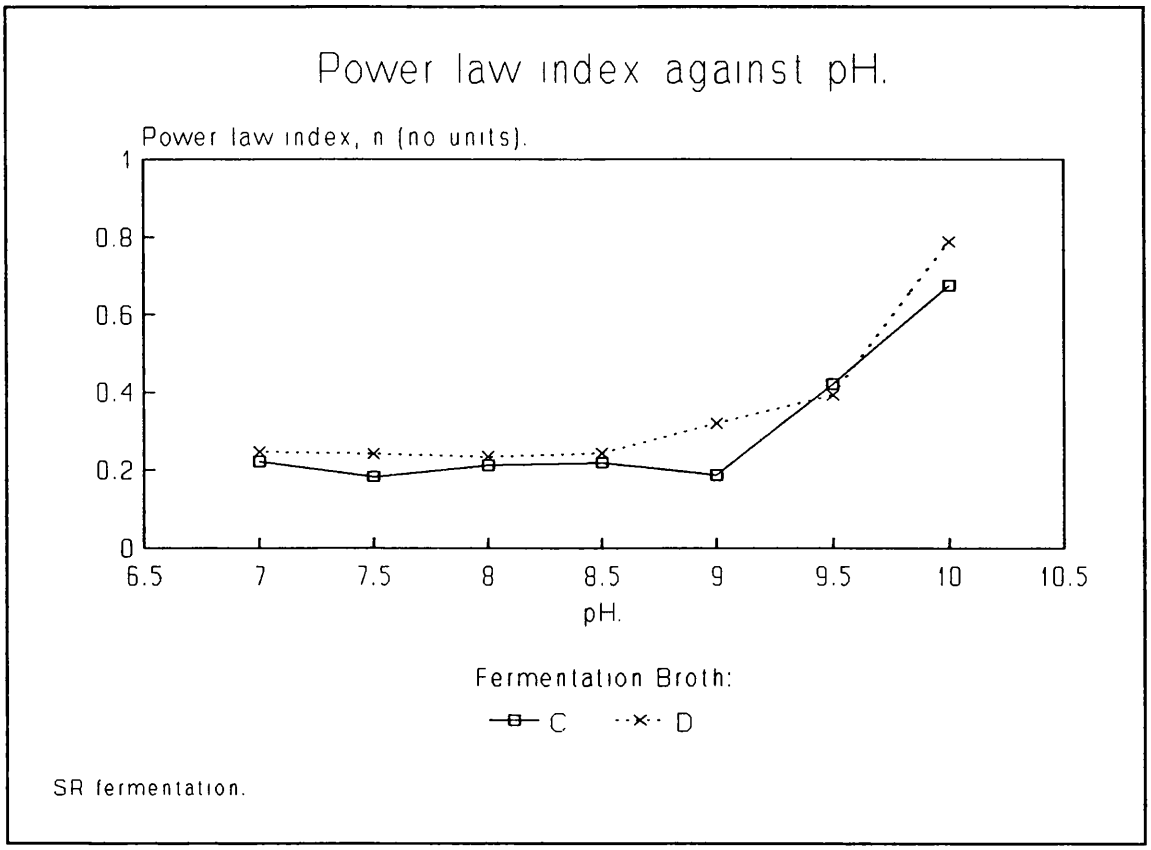

Figure 5

particles is due to the attractive van der Waals forces and the repulsive double layer forces which originate from surface charges on the particles in solution, see figure 1. The charge on the surface of a particle tends to attract a cloud of oppositely charged ions which form an electric layer around the particle. When two similar particles are sufficiently close to one another the interaction of the electric layers form the double layer repulsive force between them.

Several expressions are available for the estimation of the magnitude of the electric double layer force, F_R, including the following equation:[125]

$$F_R = \frac{\kappa.\xi.d_p.e^{-\kappa.H}}{4(1-3^{-2.\kappa.H})}[\zeta^2(e^{-\kappa.H}-1)] \qquad (1)$$

where:

$$\kappa = \frac{8.E^2.I}{\xi.k.T} \qquad (2)$$

κ - Debye-Hückel reciprocal thickness (1/m).
k - Boltzmann's constant ($J.K^{-1}$).
I - ionic strength of medium ($g.mol.l^{-1}$).
E - electronic charge ($4.774x10^{-10}$ ecu).
T - absolute temperature (K).
ξ - permittivity of liquid ($C^2.N.m^2$).
ζ - zeta potential (V).
F_R - electric double layer force (N).
H - separation distance between particles (m).
d_p - particle diameter (m).

In equation (2) I is the ionic strength and in equation (1) ζ is the particle zeta potential a function of particle roughness, liquid viscosity, pH and the ionic strength of the solution[128].

Equation (1) suggests that if the ionic strength of the solution is raised, for example by adding an acid, then the double layer is compressed, the maximum energy barrier is lowered and the repulsive forces decrease. The overall

effect is an increase in the net force of attraction and consequently a higher probability of aggregation of particles.

Experiments were carried out with *S. rimosus* in which the pH of the solution was changed by the addition of concentrated hydrochloric acid. If it is assumed that the microorganisms carry a surface charge then the addition of the acid will be expected to alter the magnitude of the electric double layer charge between the microorganisms. The net effect is a change in the characteristics of the suspension culminating in a change in viscosity which was clearly observed during the experiments, see figures (2) and (3).

These experiments revealed that the viscosity of the suspension increased initially as the pH changed from a neutral value of 7 to 5.5 and then decreased beyond that pH as the pH was reduced to 3 (figure 2 and 3).

In another series of experiments with the same fermentation broth (*S. rimosus*) the pH of the suspension was increased by the addition of sodium hydroxide. The resulting change in rheological properties (K and n) are shown in figures (4) and (5) and are consistent with the trends shown in figures (2) and (3).

All these experiments strongly suggest the existence of surface charges around the microorganisms and indicate that the rheology of the fermentation broth is critically dependent on the surface properties of the microorganism. It would be valuable to measure the magnitude and the change in surface charges on the microorganisms (e.g. zeta potential) as a function of pH in order to confirm these observations. This could form part of any future investigation in this area.

7.2 The effect of pH on organism morphology.

This is an experiment to assess the effect of a change in pH on the morphology of *S. rimosus* organisms in

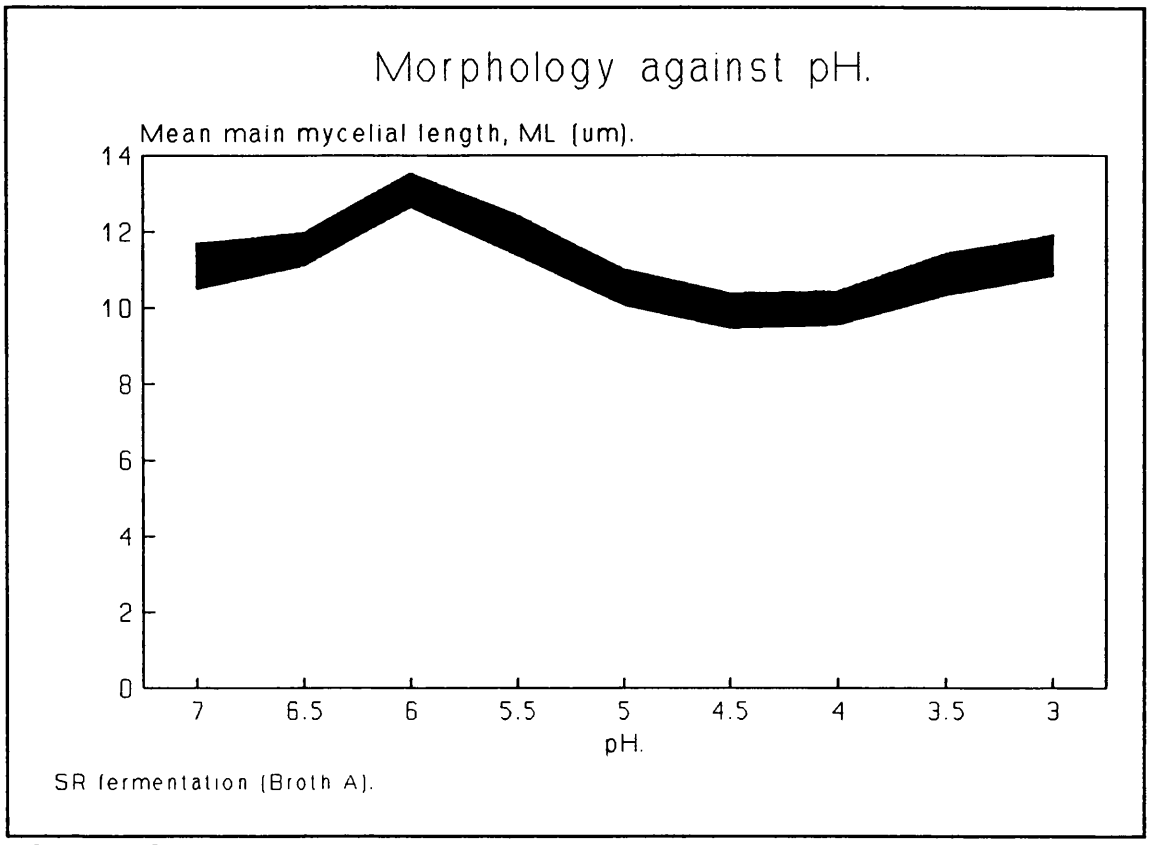

Figure 6

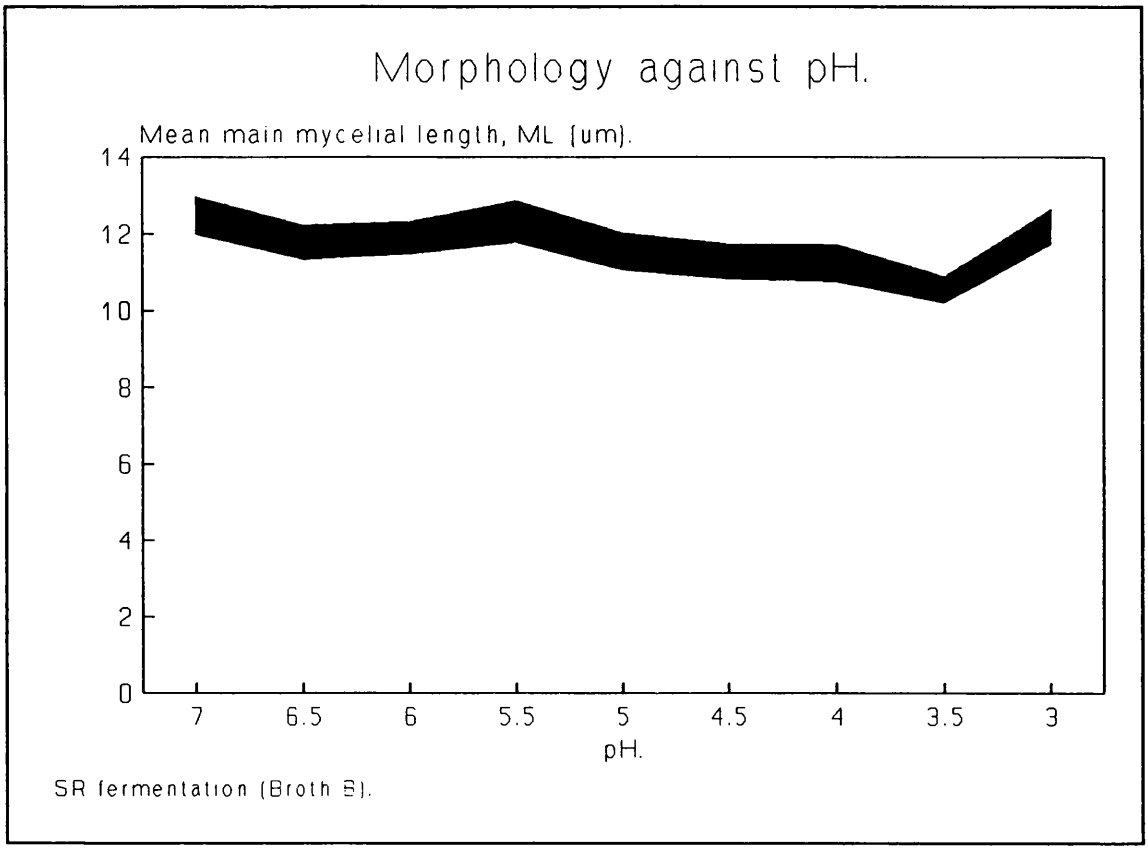

Figure 7

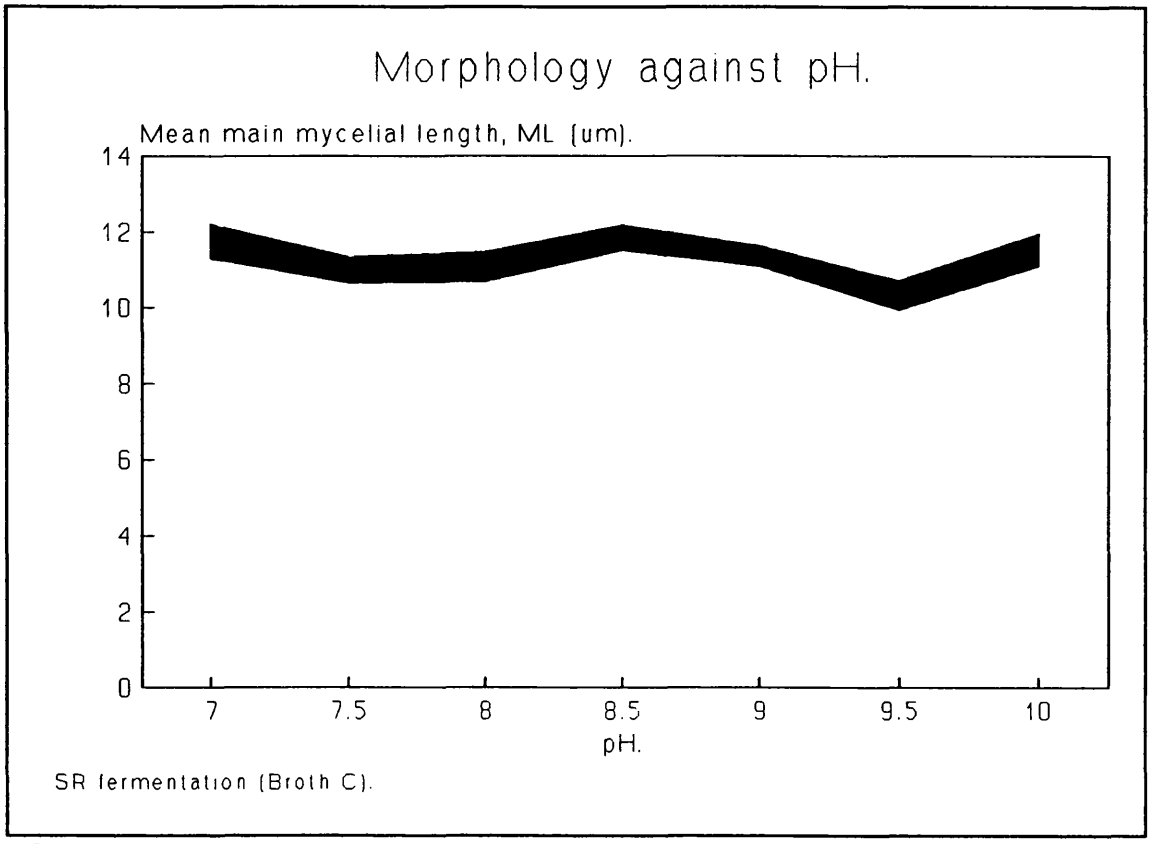

Figure 8

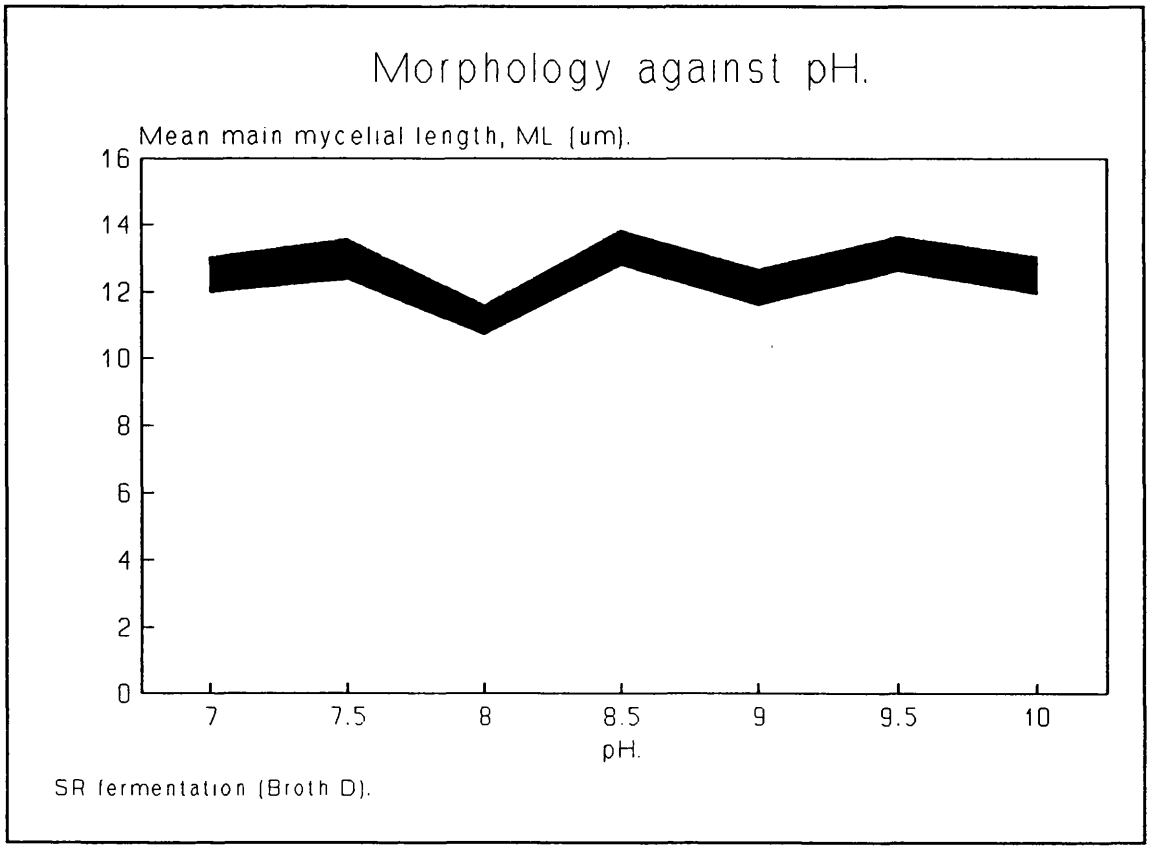

Figure 9

fermentation broth. After the preparation of the rheological specimens a small sample was taken, diluted and plated onto a microscope slide. These slides were then morphologically examined using the image analyser.

Figures 6 to 9 show a plot of mean main mycelial length against pH for the broths A, B, C and D, respectively. The line thickness of the plots indicates the span of the 95% confidence limits for each ML data point. Despite a couple of probably erroneous ML data points, the figures show that a change in pH to the fermentation broth has no effect on the morphology of the *S. rimosus* organisms.

This experiment was devised in order to eliminate the possibility of a change in pH causing the morphology of the organisms to alter and thereby change the rheology of the broth. Figures 6 to 9 give no indication of any significant change in morphology.

All rheological measurements were taken at the operating pH of the fermentation broth unless otherwise stated. As all similar fermentations were controlled to the same pH set point the influence of changing pH on the rheological characteristics of the broth were avoided.

7.3 The effect of dilution on rheology.

Figure 10 shows apparent viscosity (centipoise) against dilution (% by weight). An *S. rimosus* fermentation broth was steadily diluted by the addition of de-mineralised water. The plot shows that as the dilution increases the apparent viscosity of the broth at a shear rate of 10 1/seconds reduces. The plot appears to follow a straightline relationship. Figure 11 provides more detail of the results shown in figure 10. It plots consistency coefficient and Power law index against dilution. As the dilution increases the value of K can be seen to decrease in an apparent straightline relationship. However, the value of n remains constant as the dilution increases.

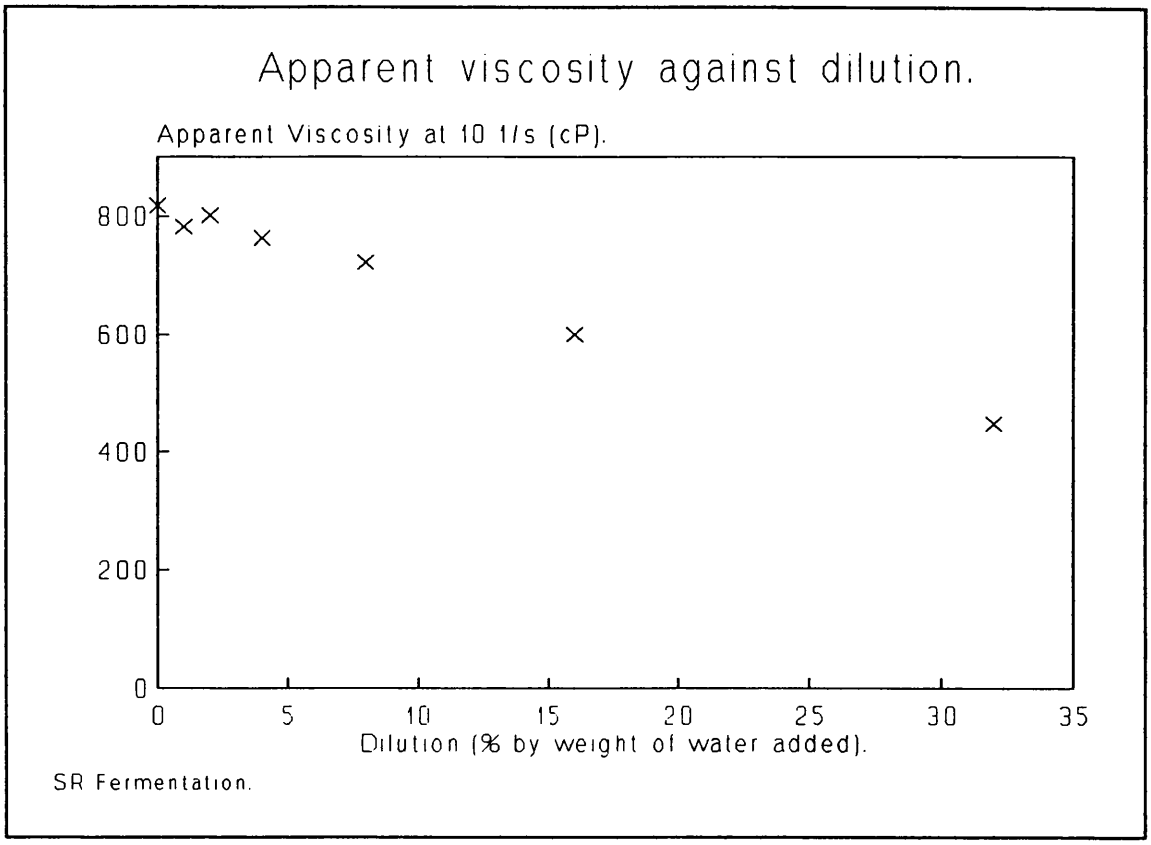

Figure 10

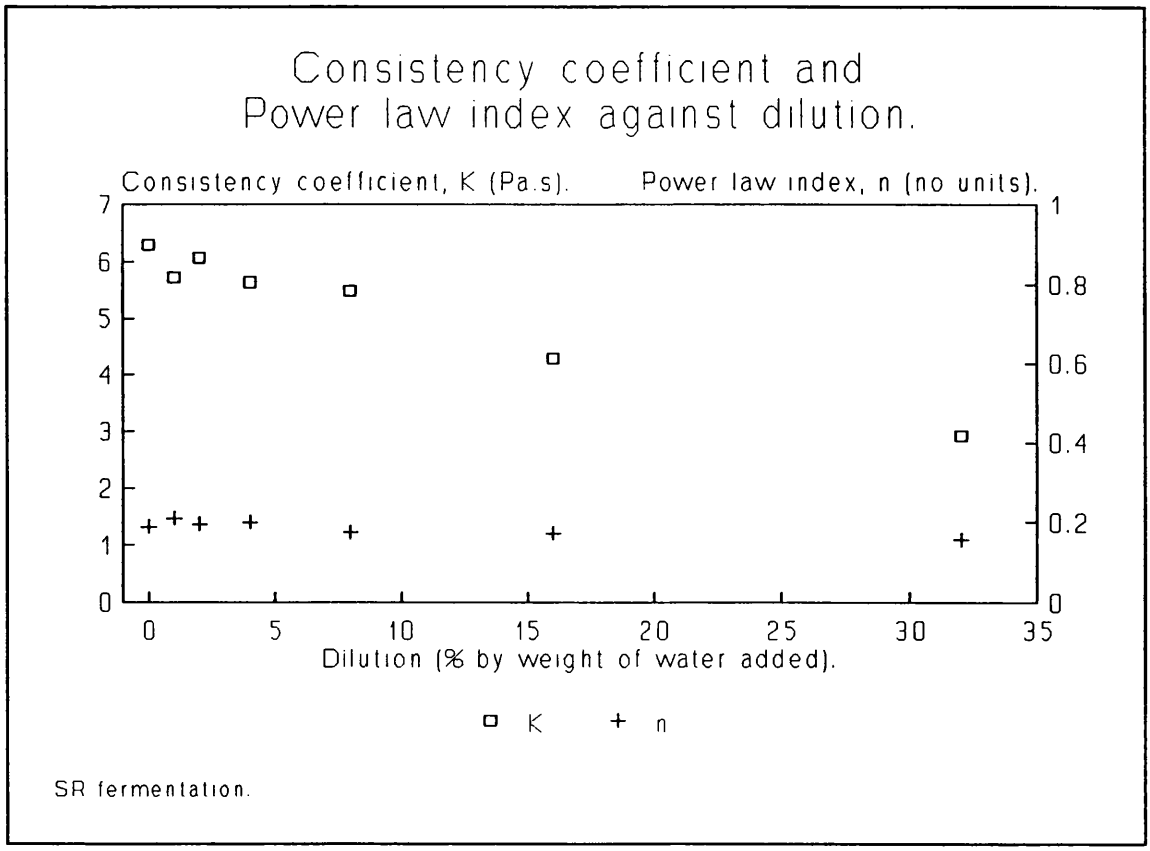

Figure 11

The combination of reducing the concentration of cells present and altering the ionic composition of the fermentation broth means that dilution has a significant effect on the rheology of the fermentation broth.

8 The turbine viscometer.

8.1 The Contraves turbines.

In the introduction to this project, considerable time was given to the subject of impeller viscometers because they appear to overcome the problems encountered when using more conventional viscometry systems to measure non-homogenous fermentation broths (see section 1.3.7.4). In this chapter, the procedures described by Kemblowski and Kristiansen [73] and outlined in chapter one are used to evaluate the performance of several turbine systems compared with more typical viscometer designs. By experimenting with a variety of impeller designs it may be possible to establish an optimal design for rheological measurement.

Figures 1 to 5 show the designs for the five different impellers. Figures 1 to 4 show impellers with two, four, six and eight vanes respectively and figure 5 shows a helical ribbon impeller (HRI). The coupling that connects the impellers to the Contraves viscometer is shown in figure 6.

The design of the impellers was based around the sample holder; the holder was the cup from the Contraves 145 cup and bob system. Figure 7a shows that the cup has a fairly complex internal design thus careful calculation was needed to find the optimum dimensions for the impellers. Initially, some rules were established for the turbine design:

a) The impeller employed must be large i.e. it must have a diameter no less than 90% of the diameter of the vessel in order to eliminate stagnant zones in the cup and to provide a reasonably sensitive instrument.

b) The turbine must be completely submerged in fluid during analysis.

In the design of the impellers used in the present study a clearance of 2mm between the blade and the sample holder

was used. Also the length of the impeller was chosen so that the impeller would be 5mm below the surface of the liquid in the cup. From figure 7a it can be seen that the inner diameter at the top of the cup is 48.5mm, thus allowing 2mm on either side of the cup gives an impeller diameter of 44.5mm. However, at the bottom of the cup the diameter reduces to 43 mm and so the impeller was terminated at a point where the convergent section of the cup began. The height of the impeller, l, and its position in the cup were chosen so that the gap between the edge of the impeller and the converging section of the cup was 1mm (see figure 7b). This gives an impeller length of 112mm for all impellers used.

The Contraves has a wide range of rotational speeds up to 780 rpm, but the Kemblowski and Kristiensen approach is only applicable in the laminar flow regime. This means that the Reynolds number for the impellers (equation (37) in chapter one) must be less than 10 [117].

Figure 8 shows a typical *S. rimosus* fermentation broth rheogram. The broth had a single point apparent viscosity (see section 2.1.3 for definition) of 1200 cP and as such was considered highly viscous. In table 1 the Reynolds number for mixing has been calculated for given rotational speeds (the density of the fermentation broth was 1050 kg/m^3). The Reynolds numbers show that the fluid remains laminar until the rotational speed exceeds 90 rpm. The speeds to be used in the impeller experiments range from 0.218 to 44.3 rpm (similar to the range offered by the Brookfield viscometer).

Table 1. Reynolds numbers at a given rotational speed.

Rotational Speed (rpm)	Reynolds number (-)
0.074	0.00125
7.8	0.249
44.3	2.15
780	138

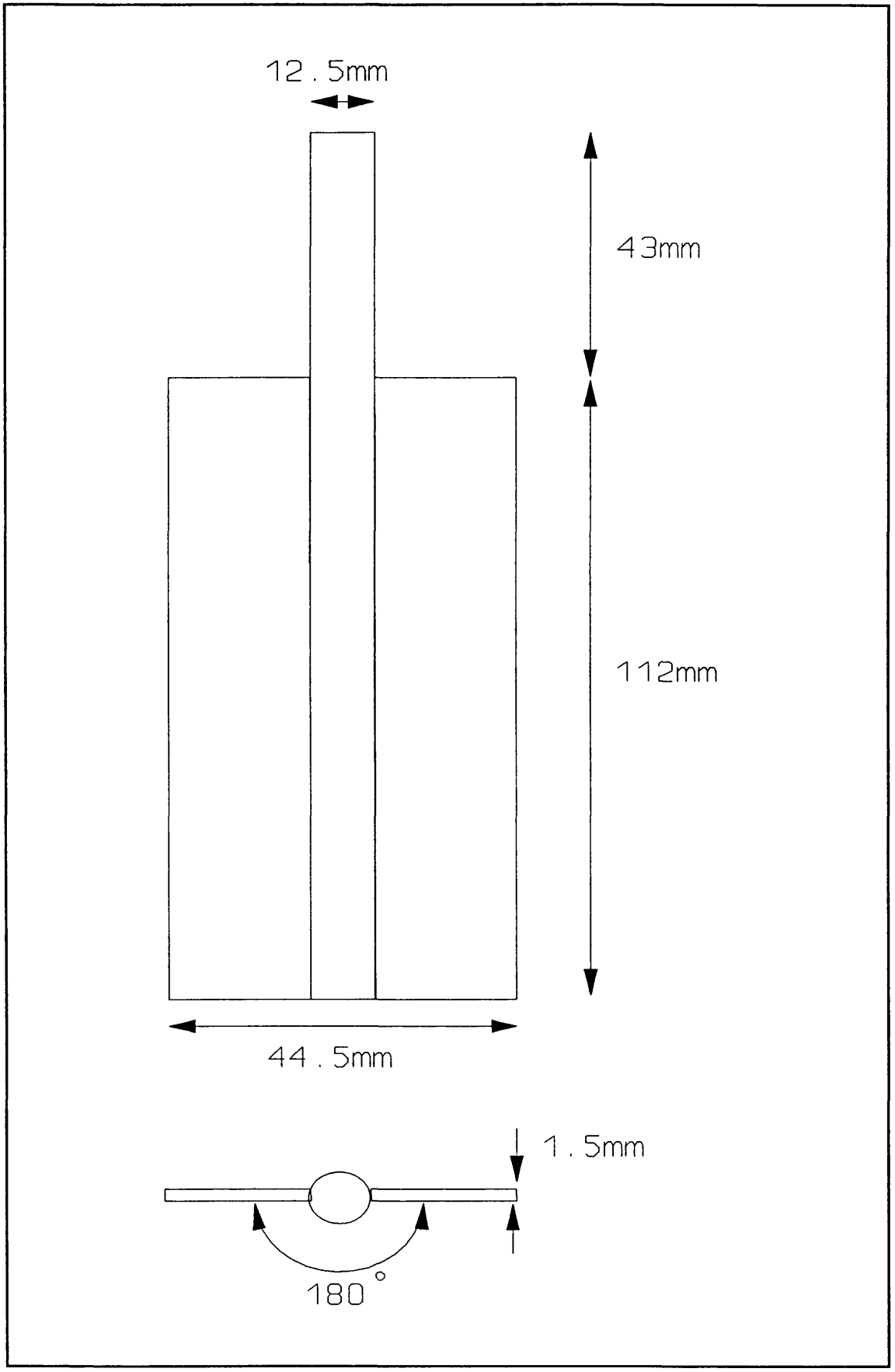

Figure 1: Two vane turbine.

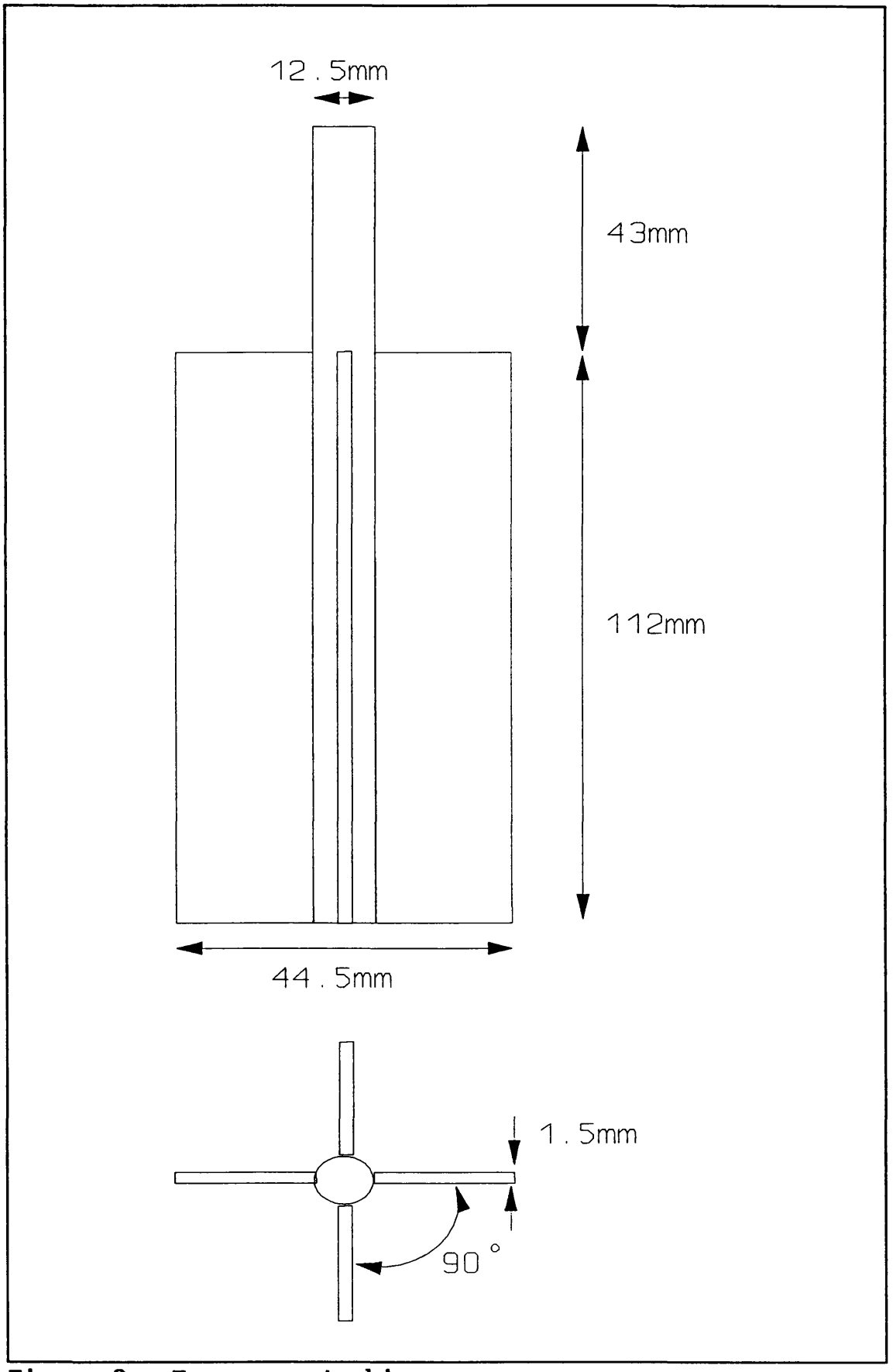

Figure 2: Four vane turbine.

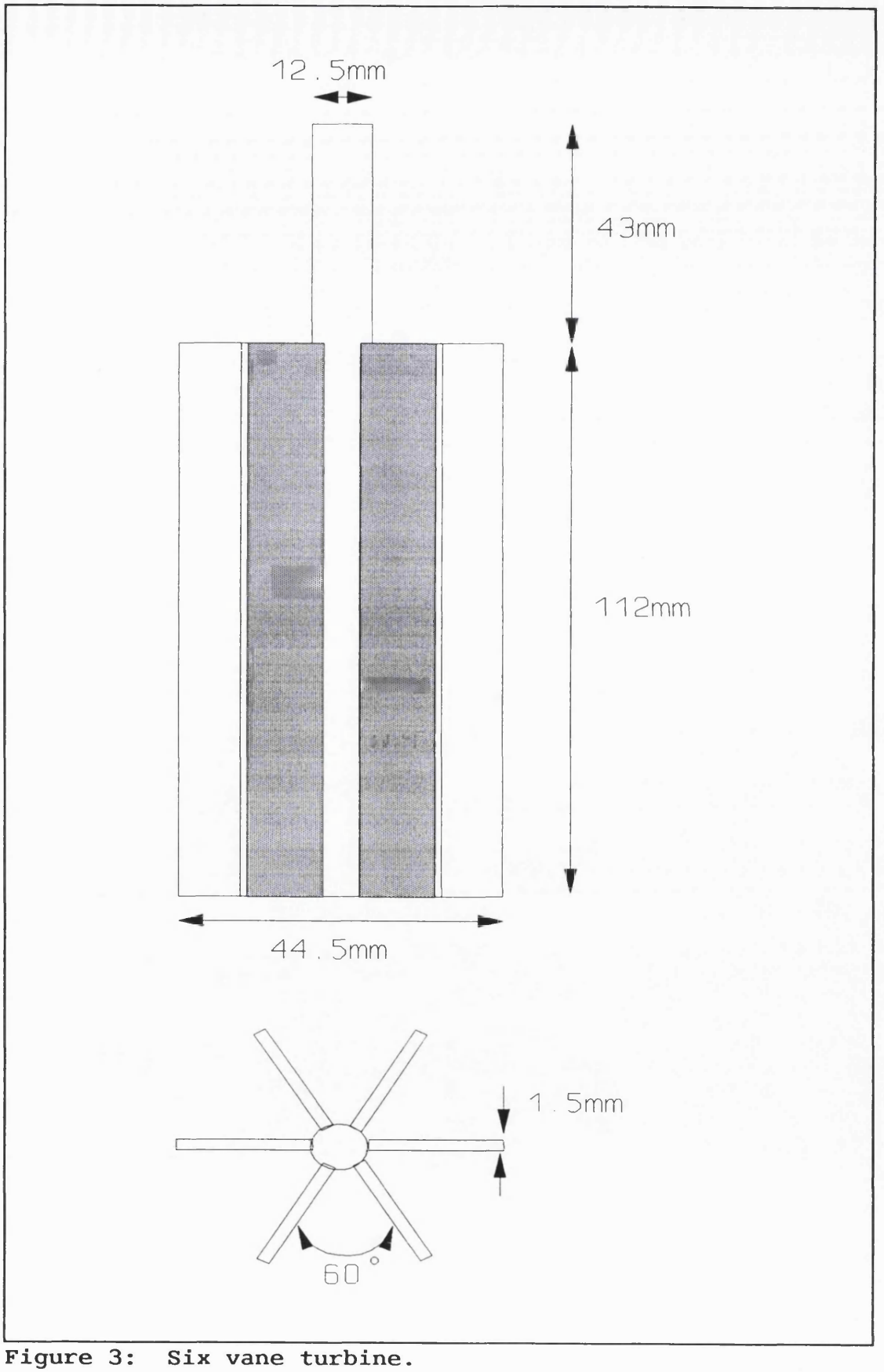

Figure 3: Six vane turbine.

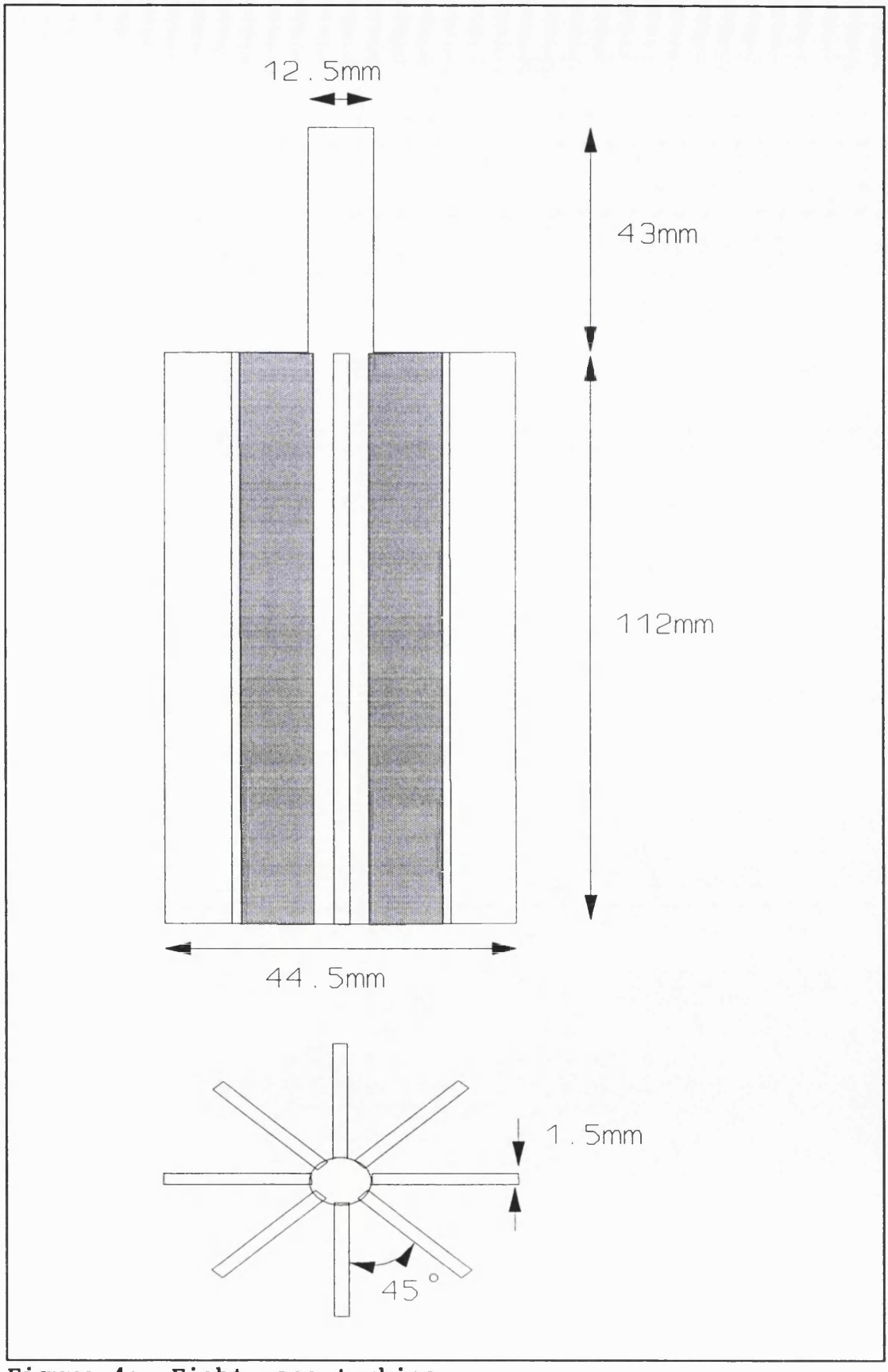

Figure 4: Eight vane turbine.

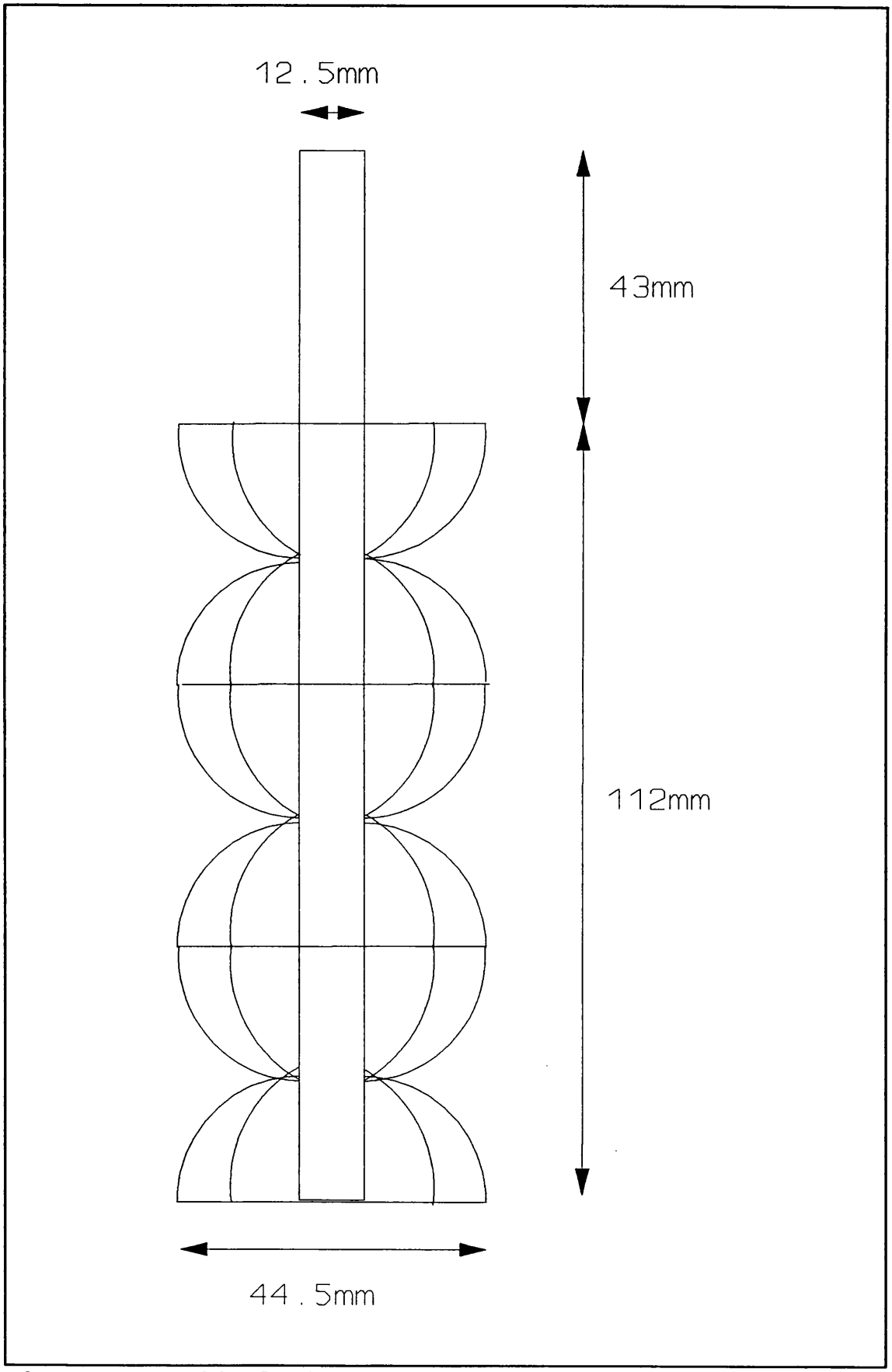

Figure 5: Helical ribbon impeller.

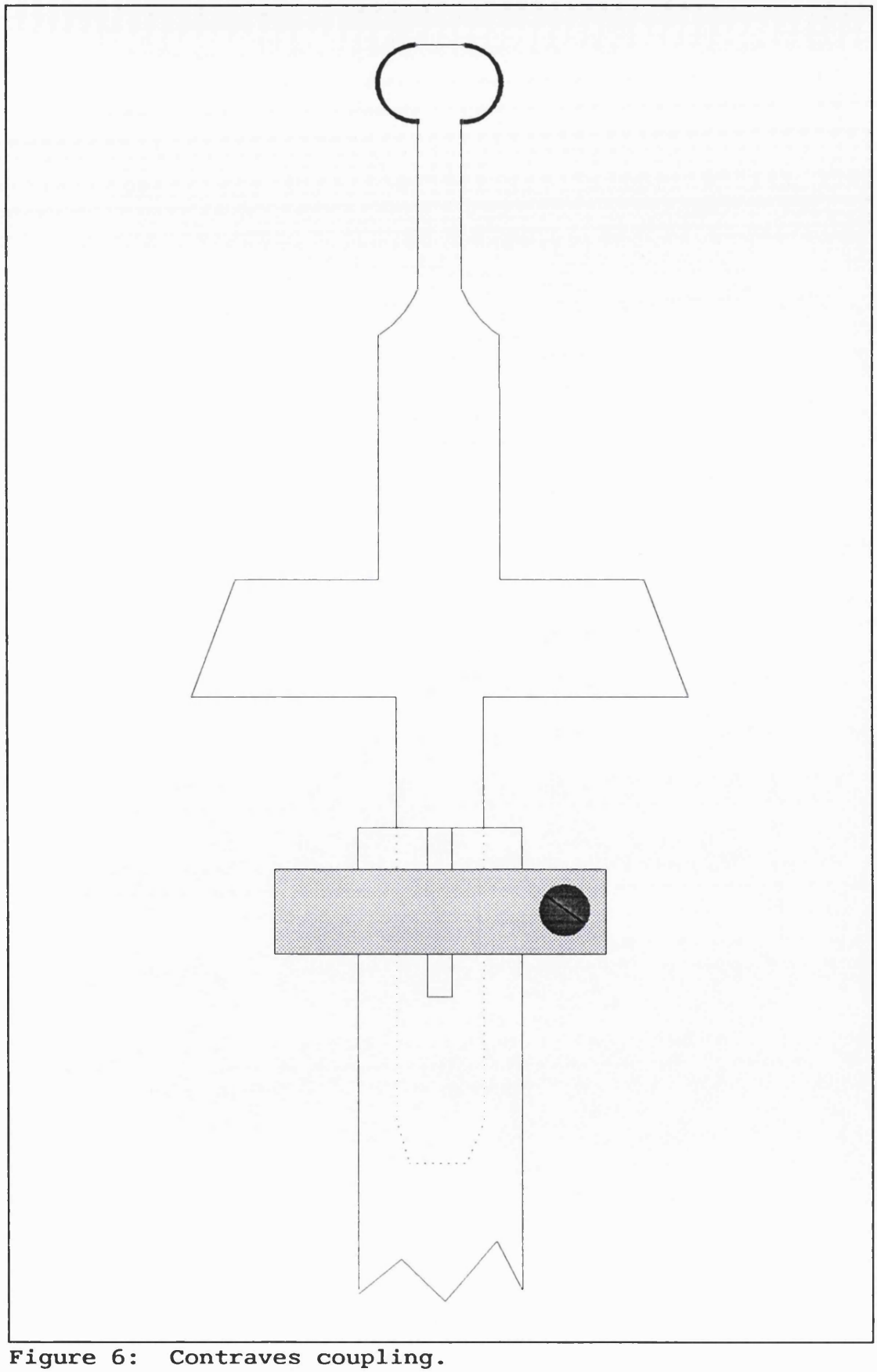

Figure 6: Contraves coupling.

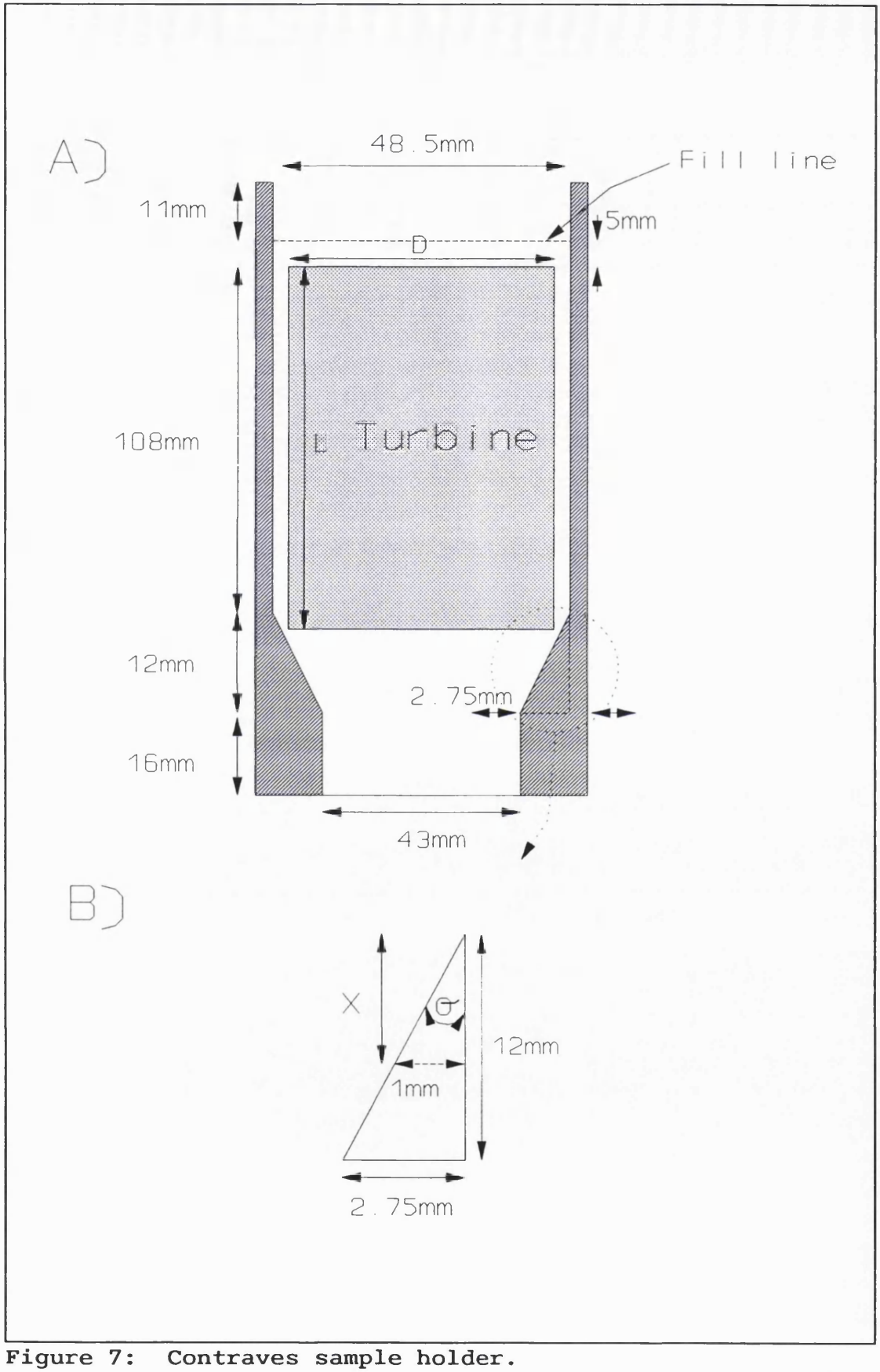

Figure 7: Contraves sample holder.

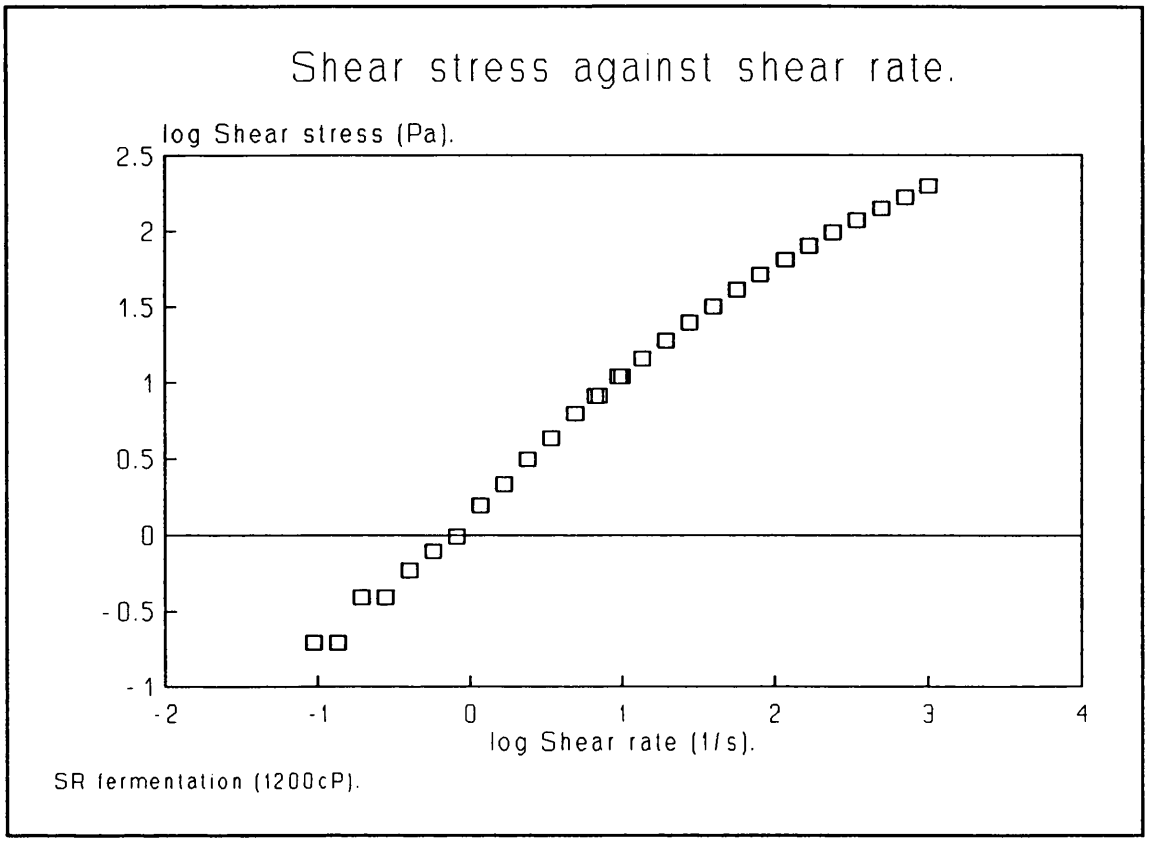

Figure 8

All the impeller designs used had the same overall dimensions. The vane thickness was chosen to prevent any flexing during use. All impellers used in this investigation had a shaft diameter of 12.5mm. This allowed up to a maximum of eight vanes to be attached to the shaft as shown in figure 9.

The helical ribbon impeller (HRI) design also had the same overall dimensions of the vane impellers but had a more detailed structure. The pitch ratio of an HRI has a significant impact on the power consumption and mixing efficiency of the impeller. According to Patterson et al [118], as the pitch ratio increases, the power consumption decreases and the mixing efficiency decreases. Since a high torque response is desirable, a low pitch ratio of 0.5 was chosen. Other examples of HRI design are given in Reuss [102], Kim [108], Mitard [119] and Takahashi [120].

From the Patterson et al paper the following design details were used for the helical ribbon impeller, see

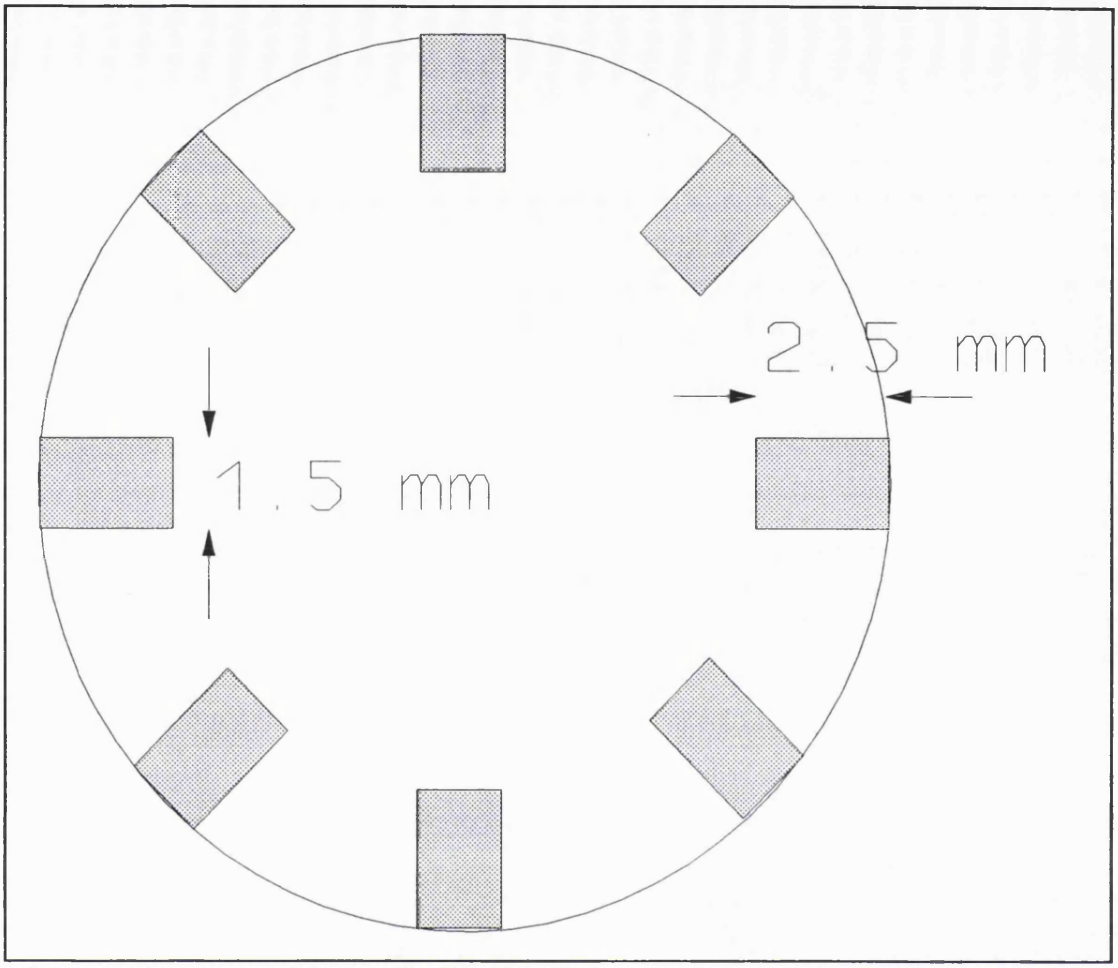

Figure 9: Impeller shaft design.

figure 10:

$$n_b = 1 \text{ or } 2 \quad (1)$$

n_b - number of blades.

$$1.11 < \frac{D}{d} < 1.37 \quad (2)$$

D - sample holder diameter (m).
d - impeller diameter (m).

$$3 < \frac{l}{d} < 4.75 \quad (3)$$

l - impeller length (m).

$$0.072 < \frac{w}{d} < 0.195 \qquad (4)$$

w - impeller blade width (m).

$$0.69 < \frac{p}{d} < 1.048 \qquad (5)$$

p - pitch length (m).

The helical ribbon impeller used in this investigation had the following design specification:

$$n_b = 2$$

$$\frac{l}{d} = \frac{112}{44.5} = 2.5$$

$$\frac{D}{d} = \frac{48.5}{44.5} = 1.09$$

$$\frac{w}{d} = \frac{5}{44.5} = 0.11$$

$$\frac{P}{d} = \frac{56}{44.5} = 1.26$$

Since all the values are close to those used by Patterson the theory he demonstrated in his paper should apply to this turbine. However, the model does not hold for blade inclination angles, α, of less than 15°. From figure 11, the angle can be calculated as follows:

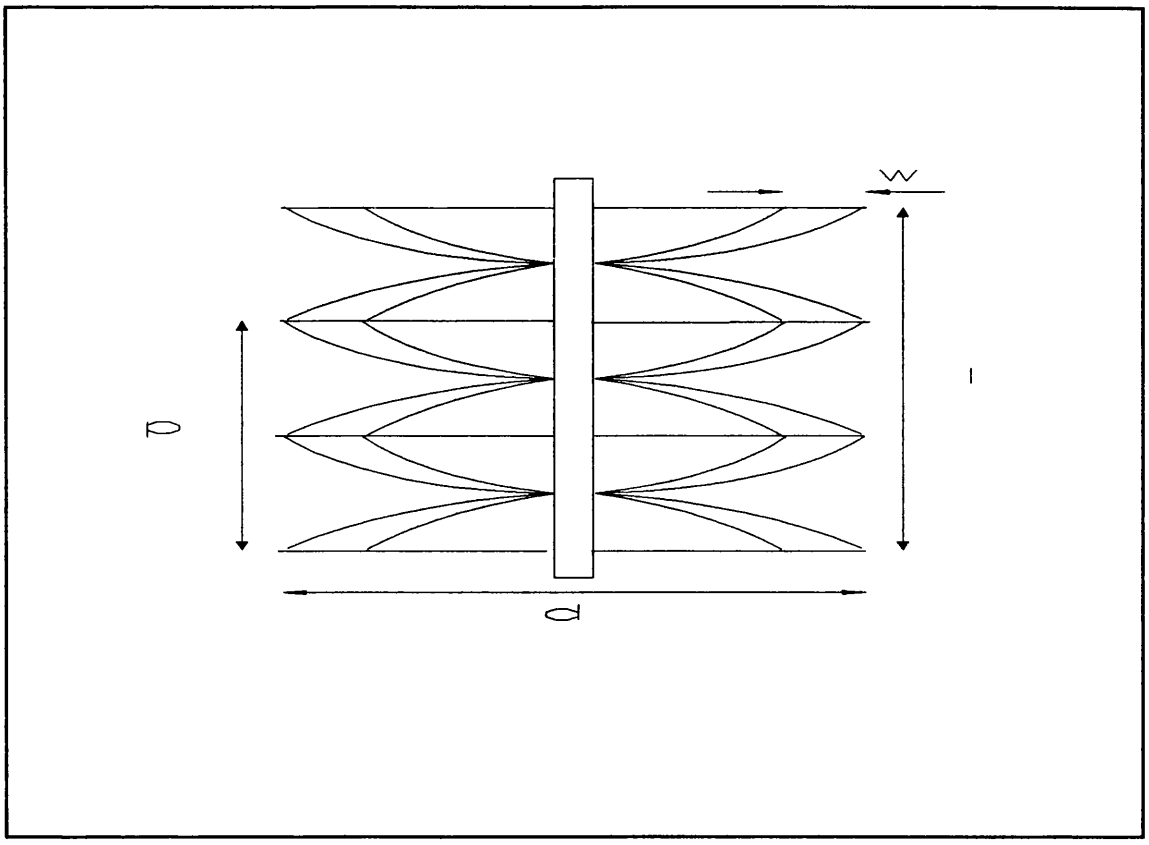

Figure 10: Critical dimensions for the HRI.

Since, the blade inclination angle, α, is ≥15°, the theory can be used on this HRI.

$$\alpha \approx 17\ ^{\circ}$$

At the design stage the power consumption of the HRI was calculated using a slightly modified form of equation (39) suggested by Patterson et al:

$$K_p = 24.n_b\ (\frac{d}{D})^{0.91}\ (\frac{l}{d})^{1.23} \qquad (8)$$

where;

$$P_o = \frac{K_p}{Re^{0.93}} \qquad (14)$$

The operating conditions of the HRI ensured that for all measurements the flow remained in the laminar flow regime.

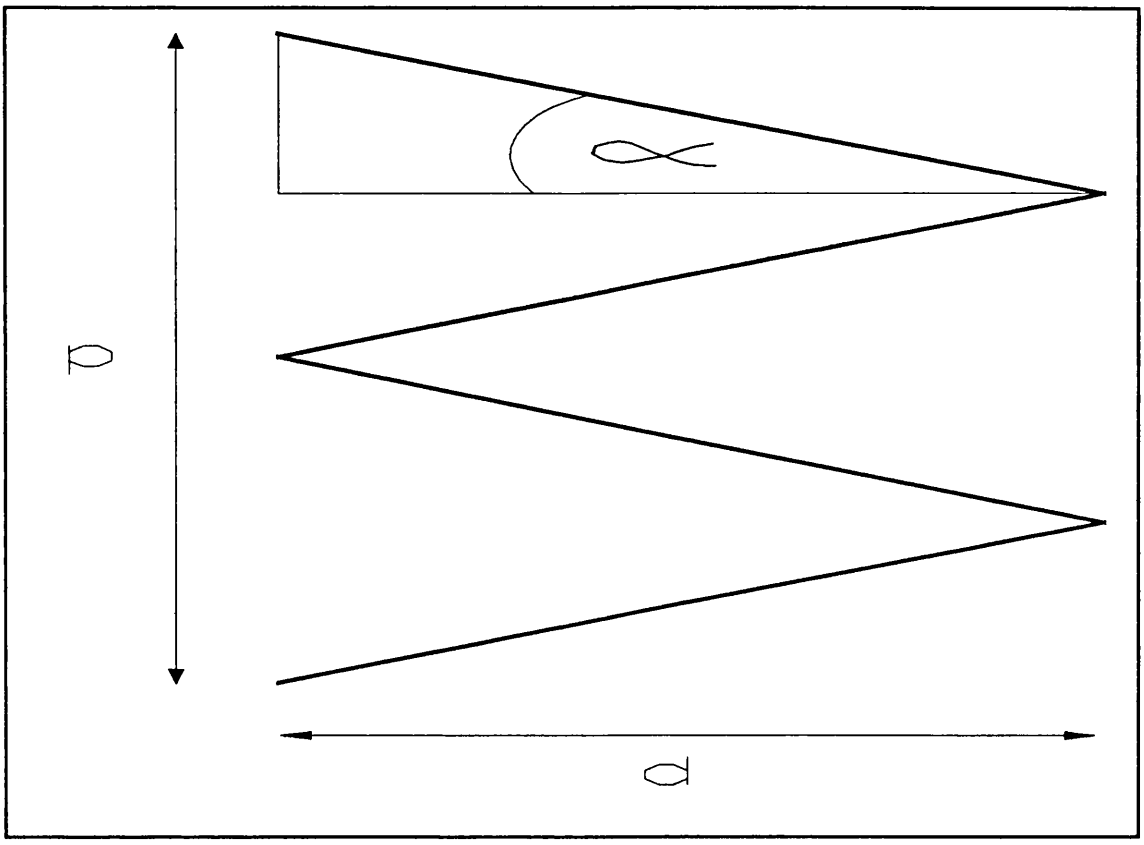

Figure 11: Calculating the angle of the HRI.

To couple the turbines to the Contraves viscometer, a male connection piece was manufactured by copying the connection on the Contraves' standard systems, see figure 6. The distance between the top of the turbine and the top of the connector was critical to ensure the turbine was the prescribed 5mm below the fill line. Therefore, before a different turbine analysis this distance was measured and adjusted to 75 mm. Adjustment of the length was achieved by loosening the screw on the fixing collar, pushing or pulling the connector to the correct length and then re-tightening the fixing collar.

8.2 The Brookfield turbine.

The Brookfield turbine was manufactured to be dimensionally similar to the Contraves system. The reduction ratio was based upon the ratio of the cup (sample holder) diameters; the $D_{Brookfield}$ and the $D_{Contraves}$ are 27.5

and 48.5 mm, respectively.
The reduction ratio, α, is given by:

$$\alpha = \frac{D_{Brookfield}}{D_{Contraves}} \qquad (11)$$

Hence, the diameter of the Brookfield turbine can be calculated:

$$d_{Brookfield} = \frac{d_{Contraves}}{\alpha} \qquad (12)$$

Thus, the turbine diameter was calculated to be 25.2 mm, and was manufactured with a diameter of 25 mm; the precise figure was rounded down. Hence the length will be:

$$l_{Brookfield} = \frac{d_{Brookfield}}{d_{Contraves}} \cdot l_{Contraves} \qquad (13)$$

The length of the Brookfield turbine was calculated to be 62.9 mm, but was manufactured to 63 mm. The stem diameter was calculated using a similar equation. The vane thickness should have been equal to ≈ 8.5 mm, but only 9 mm material was available. Figure 12 shows the full design of the turbine.

The requirement for a narrow gap system remains satisfied; there is a gap of 1.25 mm either side of the turbine and this equates to 10% of the turbine radius as required. The turbine was manufactured using aluminium. The use of this metal ensured the weight of the turbine remained below the heaviest Brookfield disc spindle, hence, no damage should be incurred by the bearings due to excess weight.

The turbine was attached to the Brookfield viscometer by means of a female-threaded coupling in the stem.

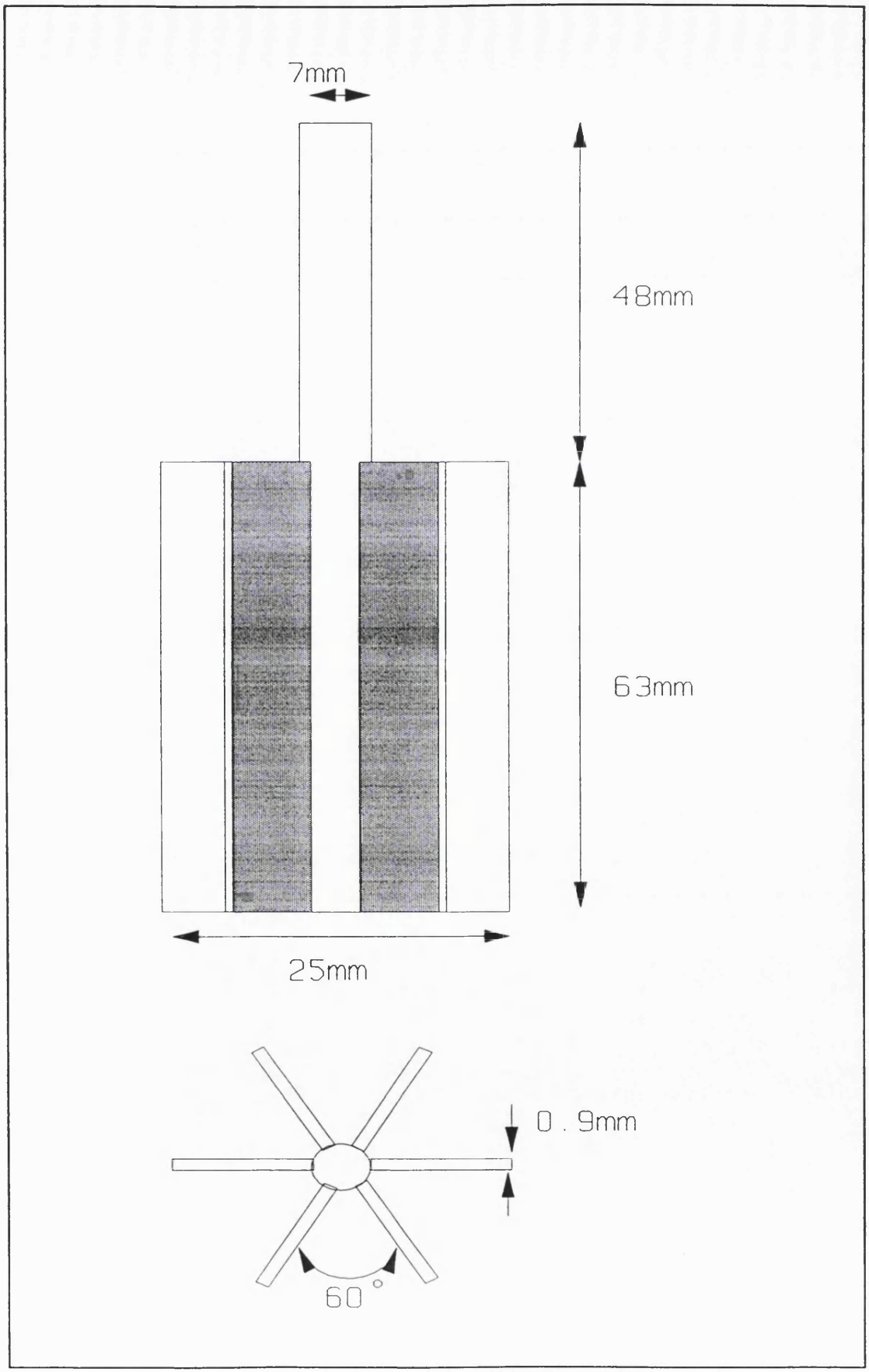

Figure 12: Six vane turbine for the Brookfield viscometer.

8.3 The turbine experiments.

The calibration procedure outlined by Kemblowski and Kristiensen was followed. The Contraves turbines were analysed using a 1000 cP Silicone fluid (a Newtonian fluid) provided by Dow-Corning and a solution of 0.8% Xanthum Gum (a highly pseudoplastic fluid). The calibration fluids were chosen because they had similar viscosities to those of a typical fermentation broth. The viscosity of these broths vary between 200 and 1500 cP on the Pfizer single point system. The Silicone fluid had a viscosity of 1000 cP and the 0.8% solution of Xanthum Gum had a viscosity of ≈900 cP.

The results for each turbine, including the standard geometry (145 cup and bob system), were plotted on graphs of log torque (Newton-metres) against log rotational speed (rpm) for both calibration fluids, see figures 13 to 16. Figure 13 shows the plots for the eight vane turbine, the four vane turbine and the standard geometry when analysed in Silicone fluid. The figure shows each measuring head producing a similar shaped plot, however, as would be expected, the torques produced by the heads are disparate for a given rotational speed. Similarly, figure 14 shows the plots for the same measuring heads, but in this case analysed in the Xanthum Gum solution. Once again the figure shows the measuring heads producing comparable plots. Figure 15 plots the results for the six vane turbine, the two vane turbine, the HRI and the standard geometry when analysed in Silicone fluid. The data presented in figure 15 suggests that within the experimental accuracy of the technique any of the three turbine heads can be used in conjunction with the Contraves to obtain the rheological characteristics of the broth. Figure 16 displays results for a non-Newtonian Xanthum Gum solution using the same heads and confirms observations made in figure 15.

In figures 13 to 16 there is some point scatter at the lowest rotational speeds possibly because of the low values

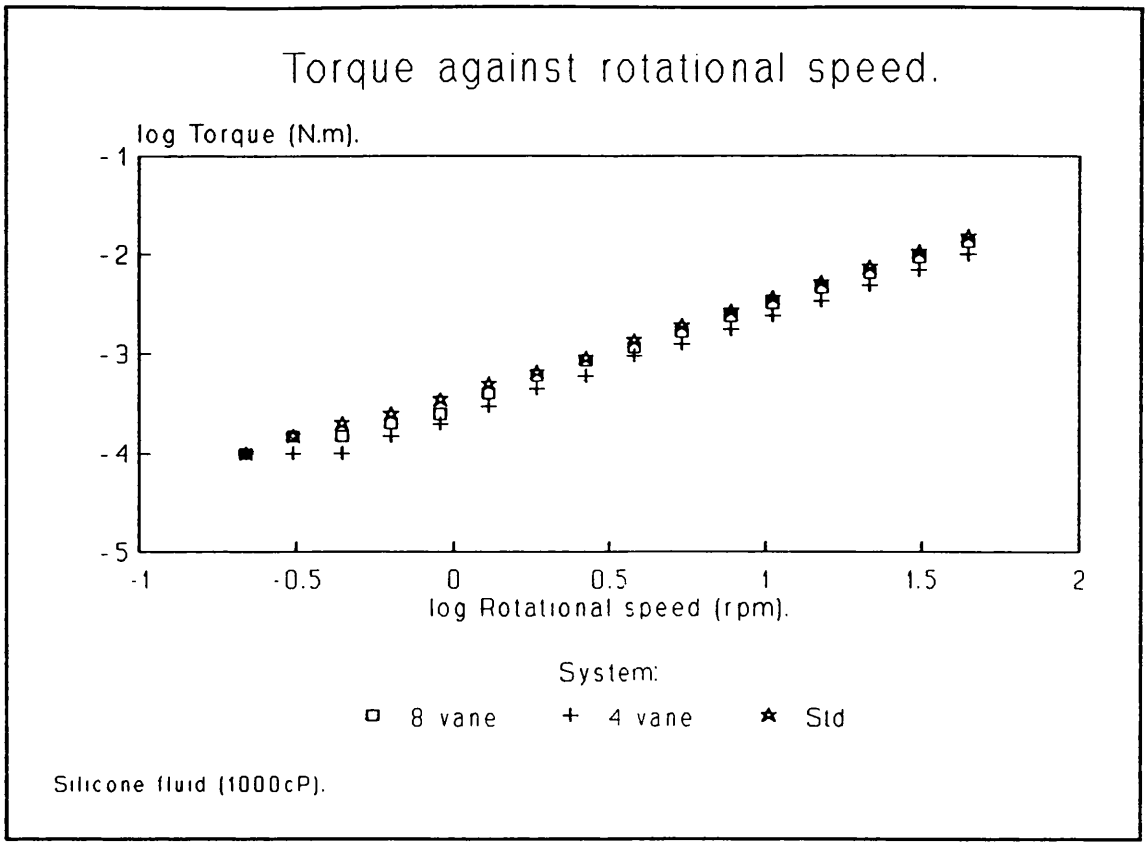

Figure 13

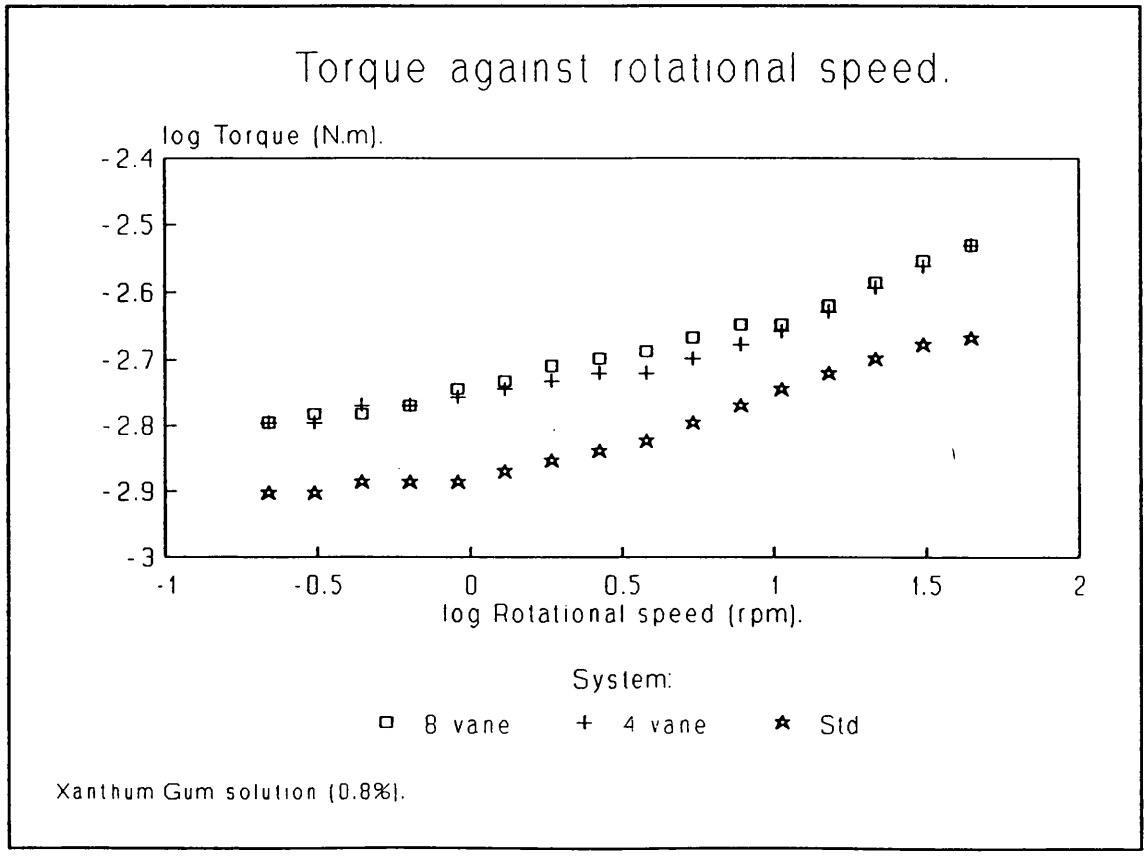

Figure 14

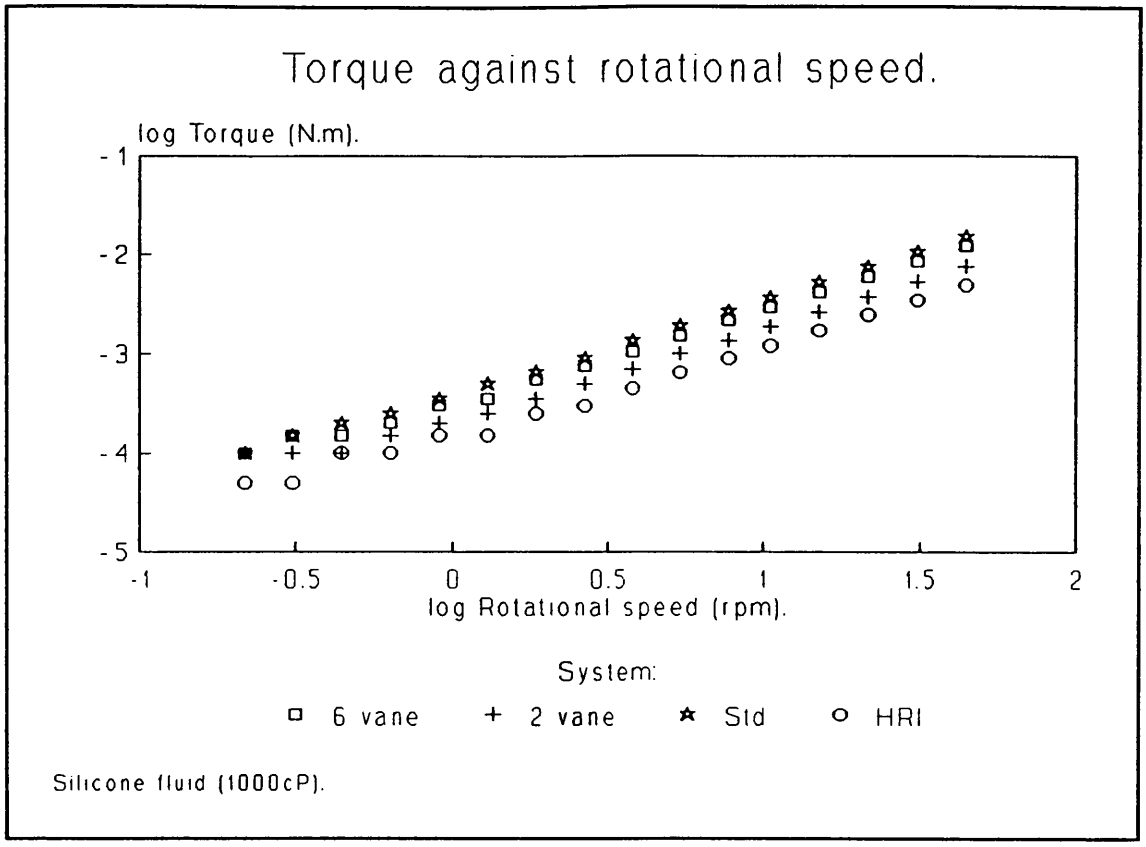

Figure 15

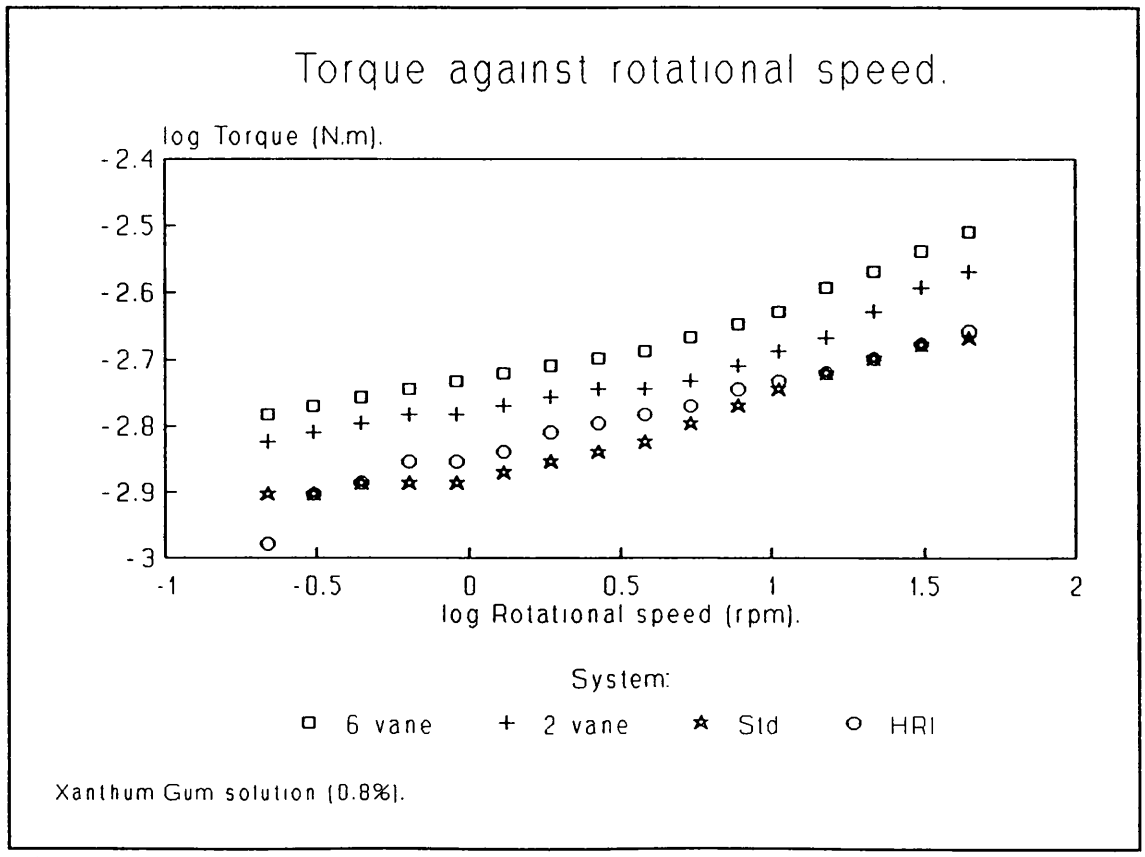

Figure 16

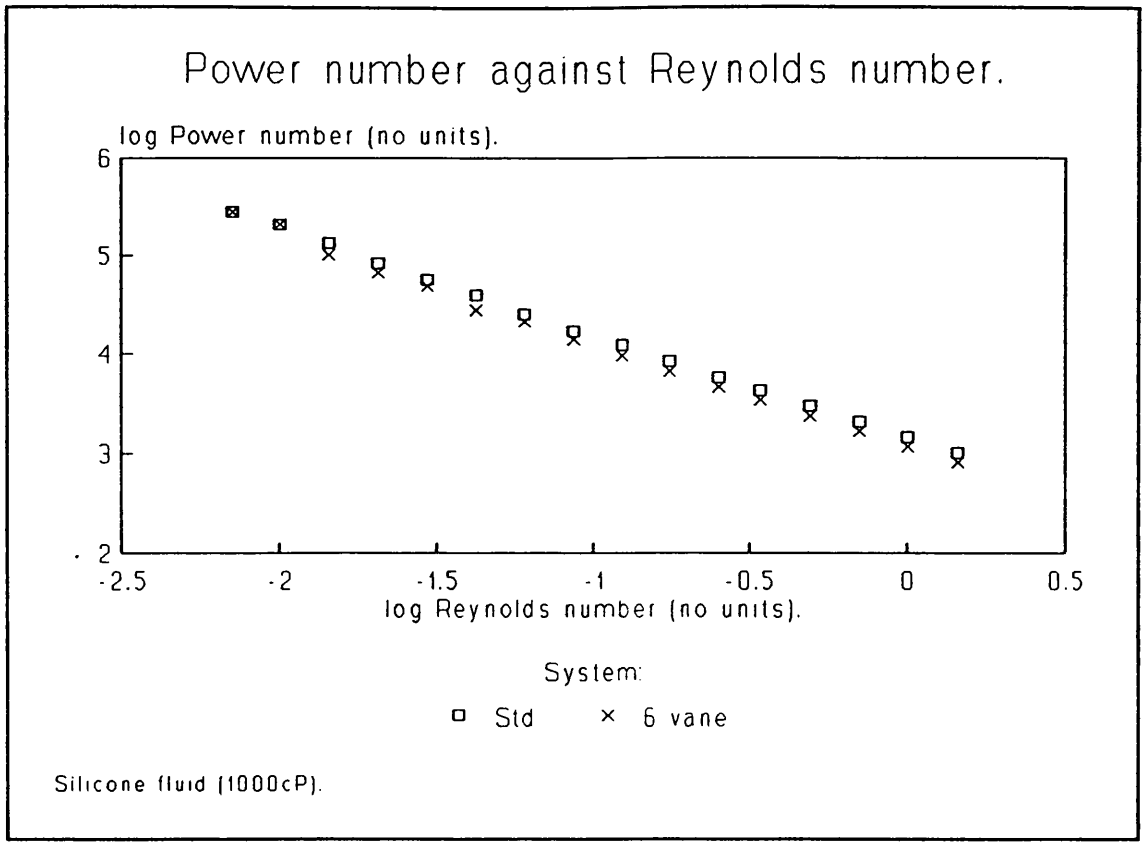

Figure 17

of torque which are close to the sensitivity limits of the instrument. The reason for this spread was the inability of the Contraves to determine a difference in the readings for consecutive speeds at these low rotational speeds.

After examination of figures 13 to 16 it was decided to continue the investigation using just the six vane turbine and the Contraves' standard geometry. The other vane turbines were rejected because the results produced would probably be similar to the six vane turbine and the additional work required was wasteful. The HRI did not produce the same torque response curve as the turbines and the standard geometry, so further work was deemed superfluous.

The procedure for calibration of turbines, as developed by Kemblowski and Kristiensen and described in chapter one, was followed for the six vane impeller and the standard geometry. A plot of log Power number, P_o, against log Reynolds number, Re, for the two measuring

heads is shown for Silicone fluid, in figure 17. Using linear regression analysis on the data gives the following values for β and K_p were calculated as in equation (38).

Table 2. Calculated values for the systems.

System head	β	K_p
Standard geometry	-1.06	1378.3
Six vane turbine	-1.08	1075.0

To obtain the k_s values for the impellers used a non-Newtonian fluid was analysed, in this case the fluid chosen was Xanthum Gum. A graph of log torque against log rotational speed was plotted for the measuring heads using the Xanthum Gum. Figure 18 indicates that both the six vane head and the standard head produce an approximately straightline plot. Equation 51 defines the properties of A and n.

Table 3. Calculated values for the systems.

System head	n	A
Standard geometry	0.112	2.16×10^{-3}
Six vane turbine	0.113	2.97×10^{-3}

Finally the rheological properties of the 0.8% solution of Xanthum Gum were determined. This information was ascertained by analysis of the fluid using the Contraves with the standard rheological geometry (145 cup and bob system). Figure 19 shows a plot of log shear stress, τ, (Pascals) against log shear rate, γ, (1/seconds) for the solution. By fitting a straightline through the data points, using linear regression analysis the Power law parameters K and n were obtained for this fluid.

$$\tau = 5.2\dot{\gamma}^{0.11} \qquad (16)$$

Equation 52 allowed the determination of values for

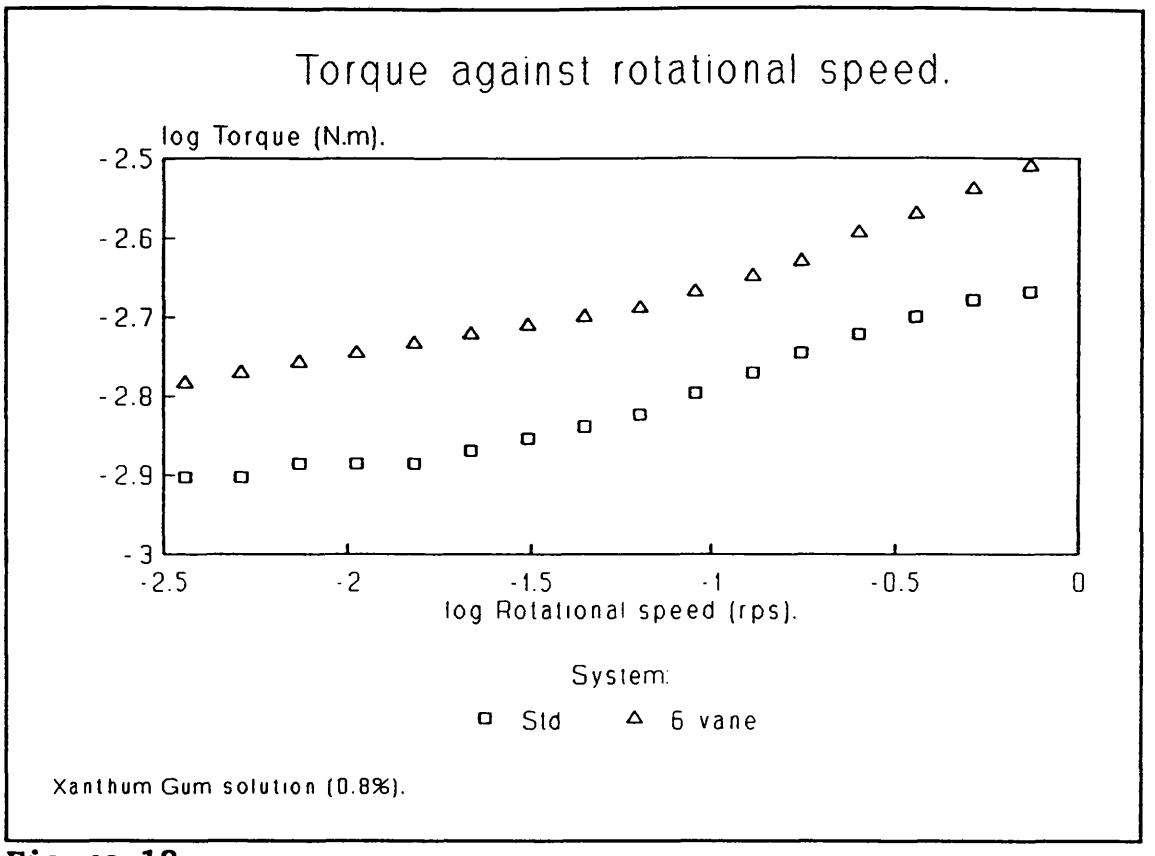

Figure 18

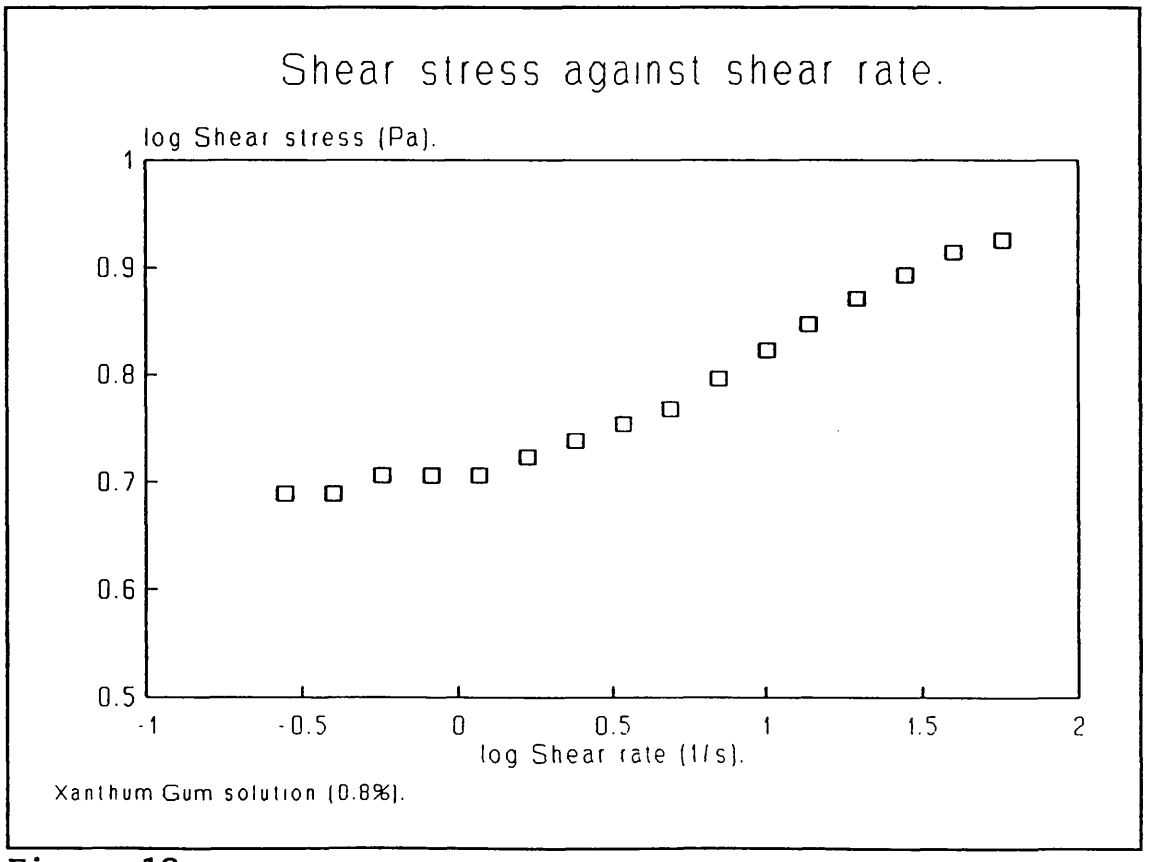

Figure 19

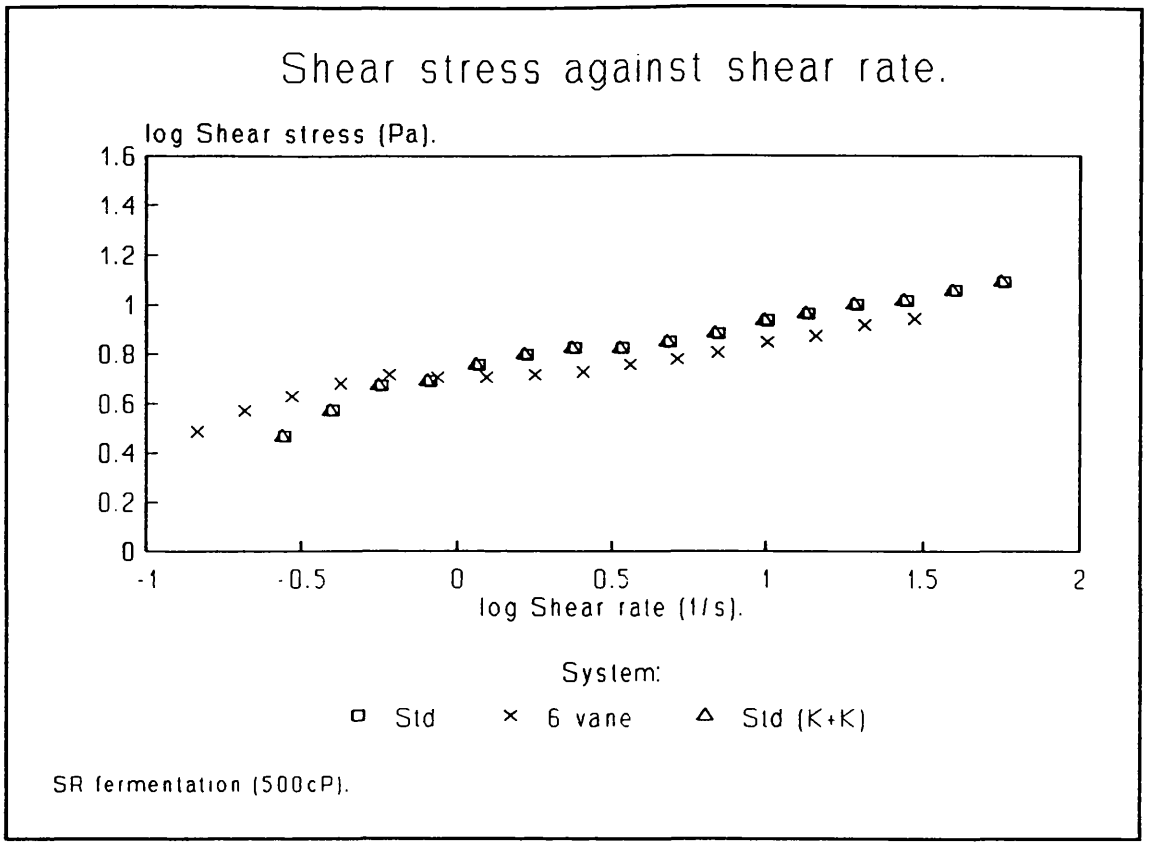

Figure 20

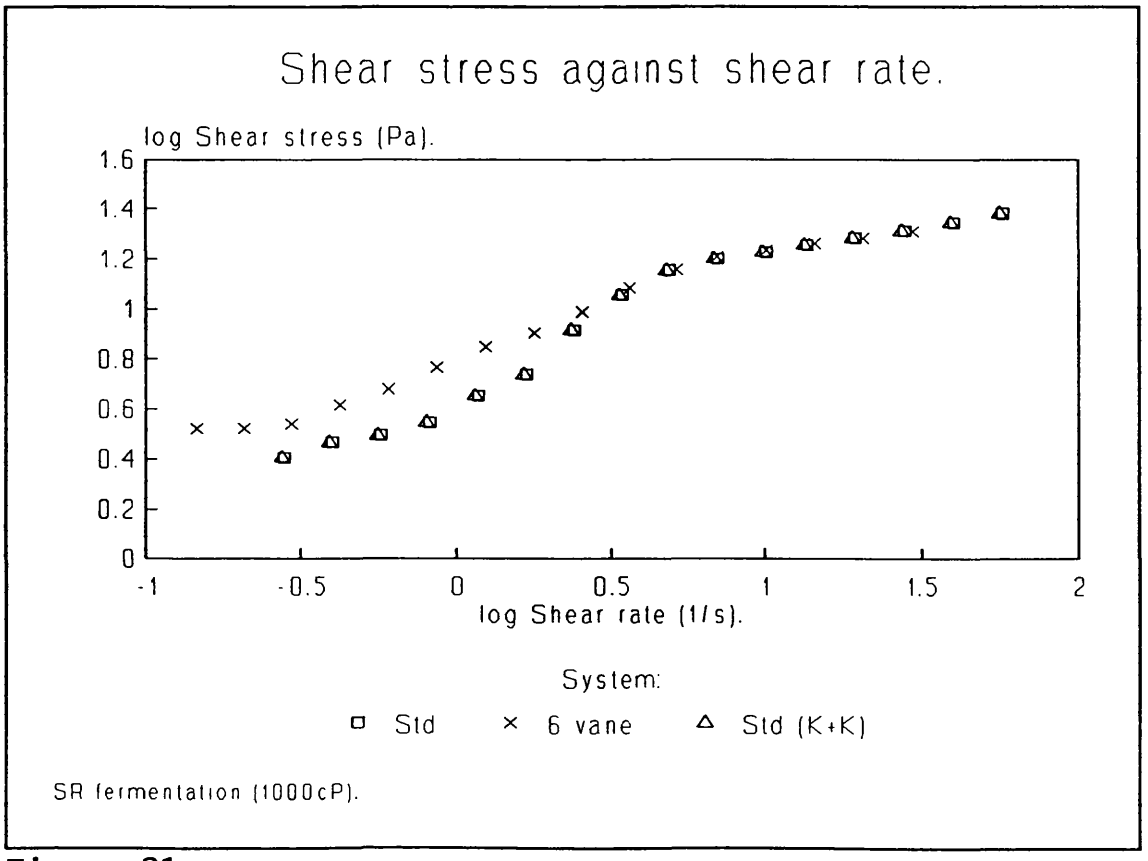

Figure 21

k_s.

By using the constant k_s values for the average shear stress, τ_{av}, (Pa) and the average shear rate, γ_{av}, (1/s) were calculated from torque, M, (Nm) and rotational speed, N, (1/s) data for any test fluid. Using equations 42 and 45.

Table 4 gives the values of k_s obtained for both measuring heads:

Table 4. Calculated values for the systems.

System	k_s
Standard geometry	75.7
Six vane turbine	40.0

A comparison of the six vane impeller data obtained in this thesis and the data obtained by Kemblowski and Kristiensen for their six vane turbine reveals the values to be almost identical, which was to be expected when considering the similarities in shape and dimensions of the two systems.

Figures 20 and 21 show a comparison of rheological data for the measuring heads, using the Kemblowski and Kristiensen method, with rheological data for the standard rheological procedure for this project (see section 2.1.1). The plots show log shear stress (Pascals) against log shear rate (reciprocal seconds) for two different *S. rimosus* production broths; the broths had single point viscosities of 500 and 1000 Cp. Both figures 20 and 21 show close fits between the three plots shown, unfortunately, at the lower shear rates the resemblance begins to break down.

These figures show the similarity between the data from the standard viscometer system (std) and the data obtained by applying the Kemblowski and Kristiensen procedure to the standard system (std K+K). In obtaining the data for the standard system (std K+K) the bob was treated as an impeller and an equivalent k_s value was

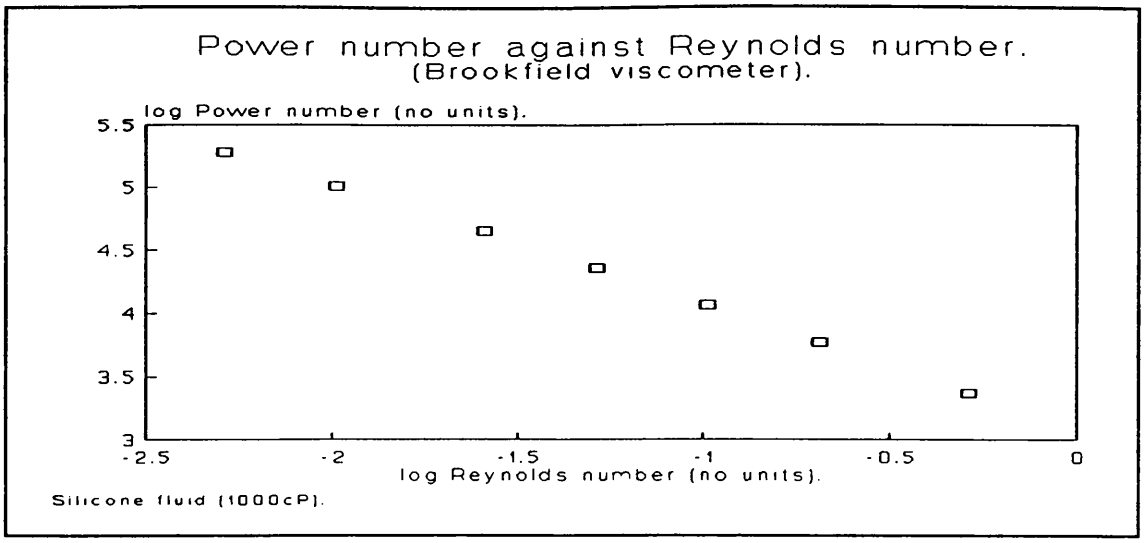

Figure 22

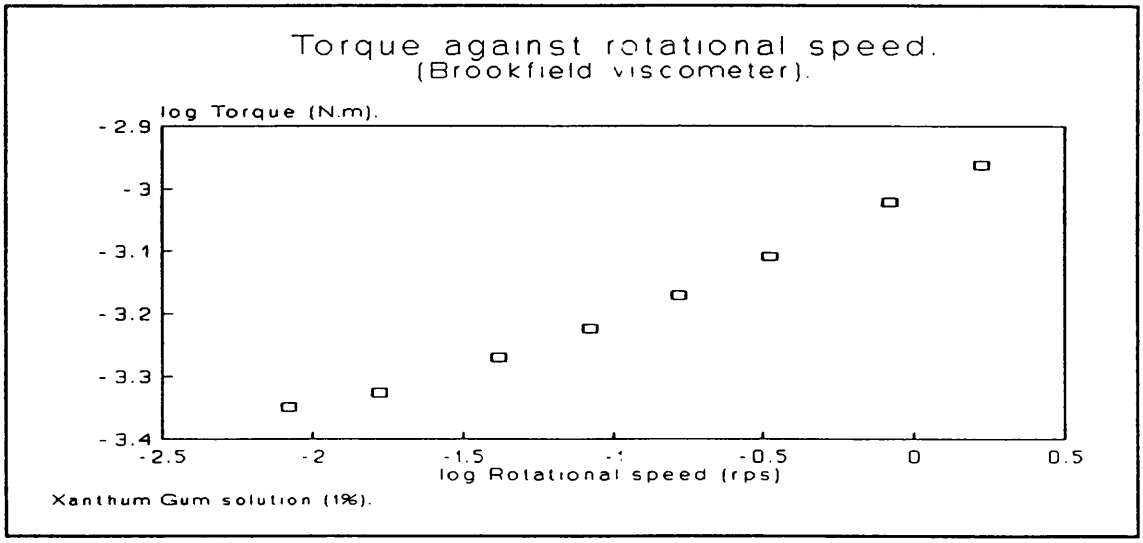

Figure 23

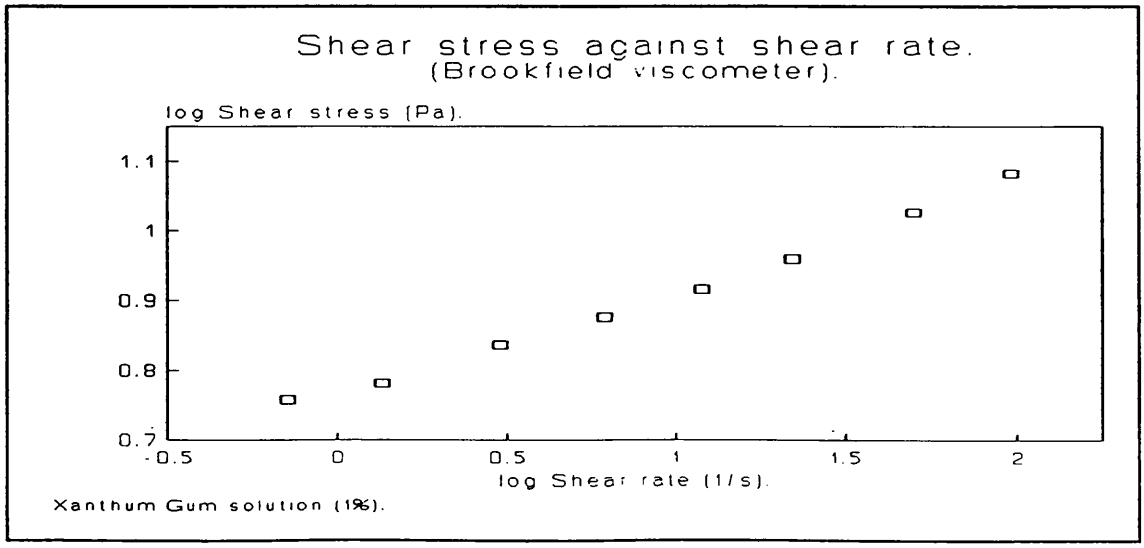

Figure 24

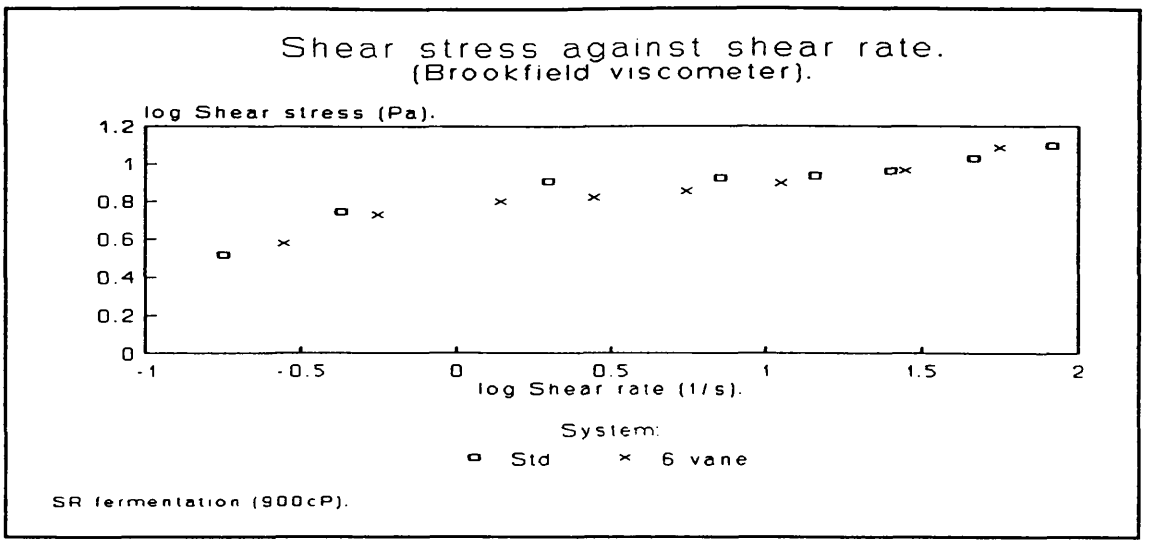

Figure 25

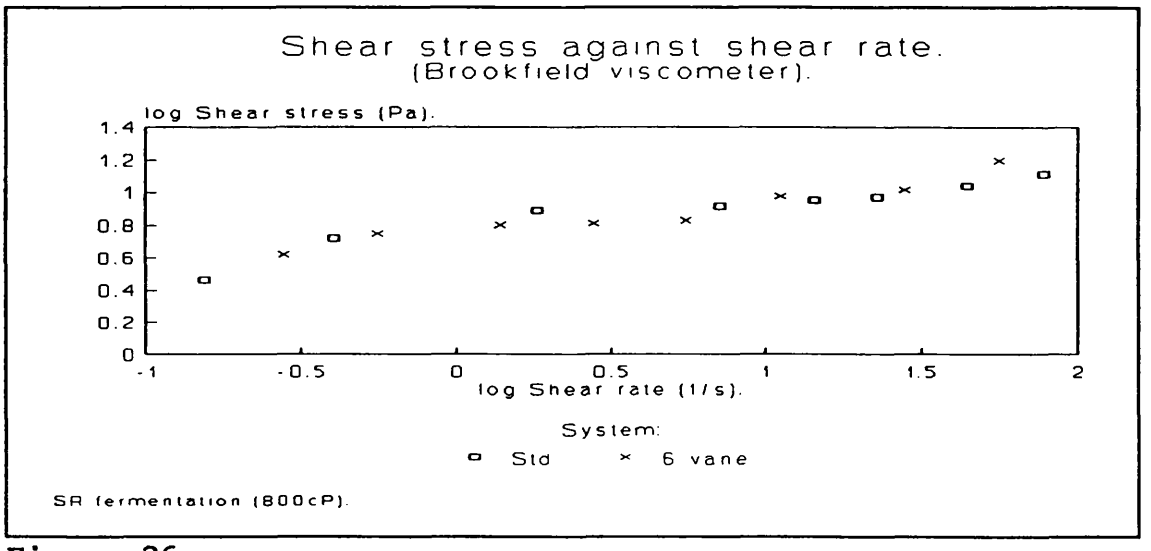

Figure 26

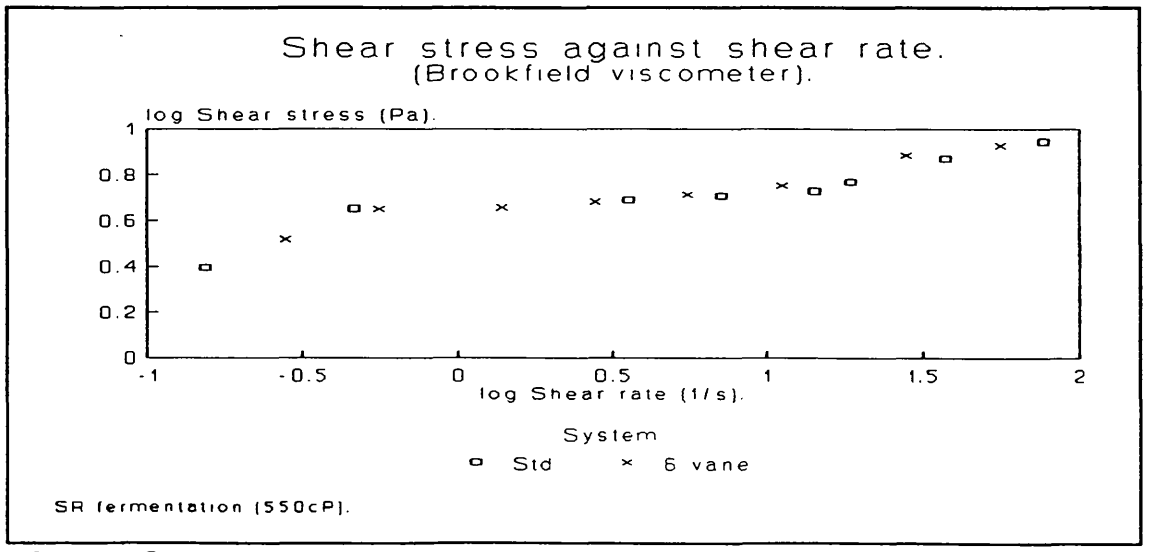

Figure 27

obtained for it. In contrast the standard data (std) was obtained using the theoretical equations for the co-axial cylinder viscometer.

The majority of the rheometry work in this project was to be undertaken using a Brookfield viscometer. Therefore, the use of a vane turbine measuring head on the Brookfield was the next logical step. Once again the Kemblowski and Kristiensen procedure was followed and figures 22, 23 and 24 show the calibration plots.

Figure 22 shows a plot of log Power number against log Reynolds number for the six vane turbine. Equation (13) gives the equation for the straightline plot. The value of the constants β and K_p which were calculated using linear regression analysis, are -0.95 and 1296.9, respectively.

Figure 23 shows a plot of log torque against log rotational speed for the six vane turbine. Linear regression analysis was used to evaluate the constants, n, and ,A for the straightline relationship; the values were 0.173 and 9.58×10^{-4}, respectively.

Figure 24 shows a plot of log shear stress against log shear rate for a 1% Xanthan Gum solution using the number two disc spindle. The straightline plot means that the Power law can be fitted. By using linear regression analysis the rheological characteristics of the Xanthum Gum solution can be determined. The values of the Power law index, n, and the consistency coefficient, K, are 0.153 and 5.805, respectively.

By using equation [ ] a value for K_s can be obtained for the Brookfield six vane turbine, it was calculated as 33.4.

Figures 25, 26 and 27 give a comparison of data from the standard Brookfield viscometer system and the six vane turbine. The figures display plots of log shear stress against log shear rate for three different *S. rimosus* production broths; the single point viscosities of the broths were 900 Cp, 800 Cp and 550 Cp. The plots show a good correlation between the two viscometer systems.

Table 5 displays the Power law index, n, and the consistency coefficient, K, determined using the standard and turbine systems for each *S. rimosus* fermentation broth.

Table 5. Standard and turbine rheological data.

	Standard Geometry		Turbine Geometry	
	n	log K	n	log K
900cP	0.178±0.025	0.751±0.076	0.184±0.021	**0.731±0.043**
800cP	0.200±0.026	0.732±0.078	0.214±0.030	0.747±0.061
550cP	0.165±0.026	0.593±0.073	0.158±0.021	0.629±0.042

The parameters are shown with 95% confidence limits. The standard geometry values are statistically equivalent to the turbine geometry values when the range of the confidence limits are considered.

Figures 28, 29, 30, and 31 also compare these two viscometer systems using a plot of log shear stress against log shear rate for different *A. roseorufa* fermentation broths. The plots show a reasonable similarity between the two measuring heads, however, the shear stress data for the six vane turbine seems to be consistently lower than the standard Brookfield geometry for a given shear rate. Table 6 presents the Power law index, n, and the consistency coefficient, K, that were determined using the standard and turbine geometries on the *A. roseorufa* fermentation broths. The values are shown with 99% confidence limits.

The standard geometry values are statistically equivalent to the turbine geometry values when the range of the confidence limits are considered, except for the consistency coefficients in broths 1 and 3. Therefore, it appears that the turbine head sometimes produces lower shear stresses than the standard system for the *A. roseorufa* system. The turbine system may have caused some rheodestruction in these *A. roseorufa* broths.

Kemblowski and Kristiansen [73] suggested that

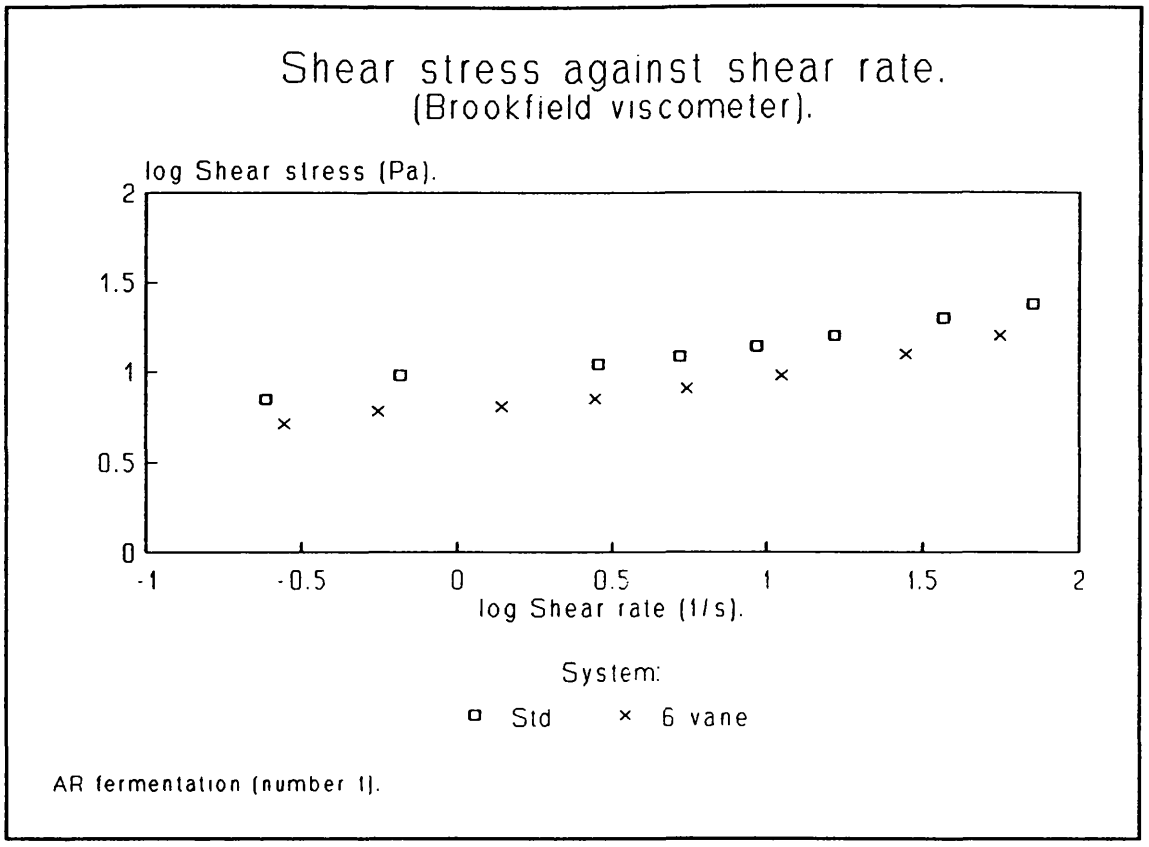

Figure 28

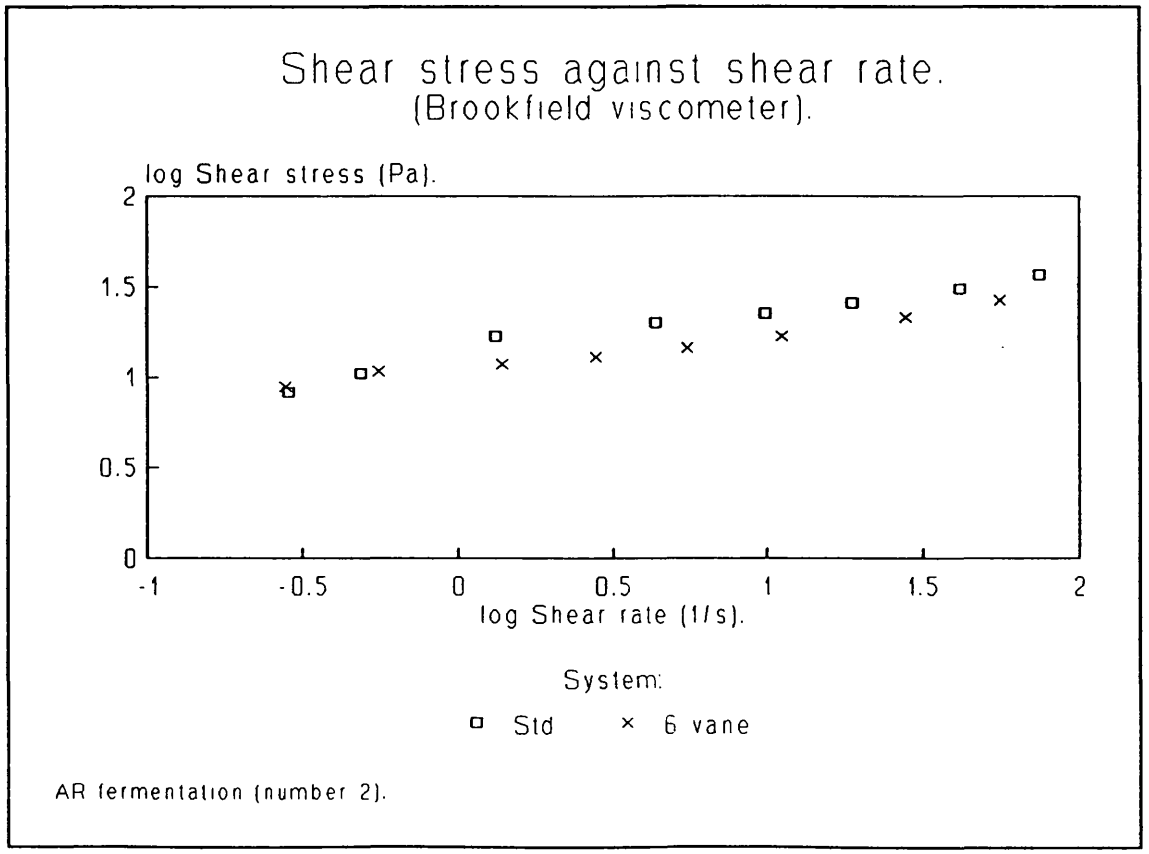

Figure 29

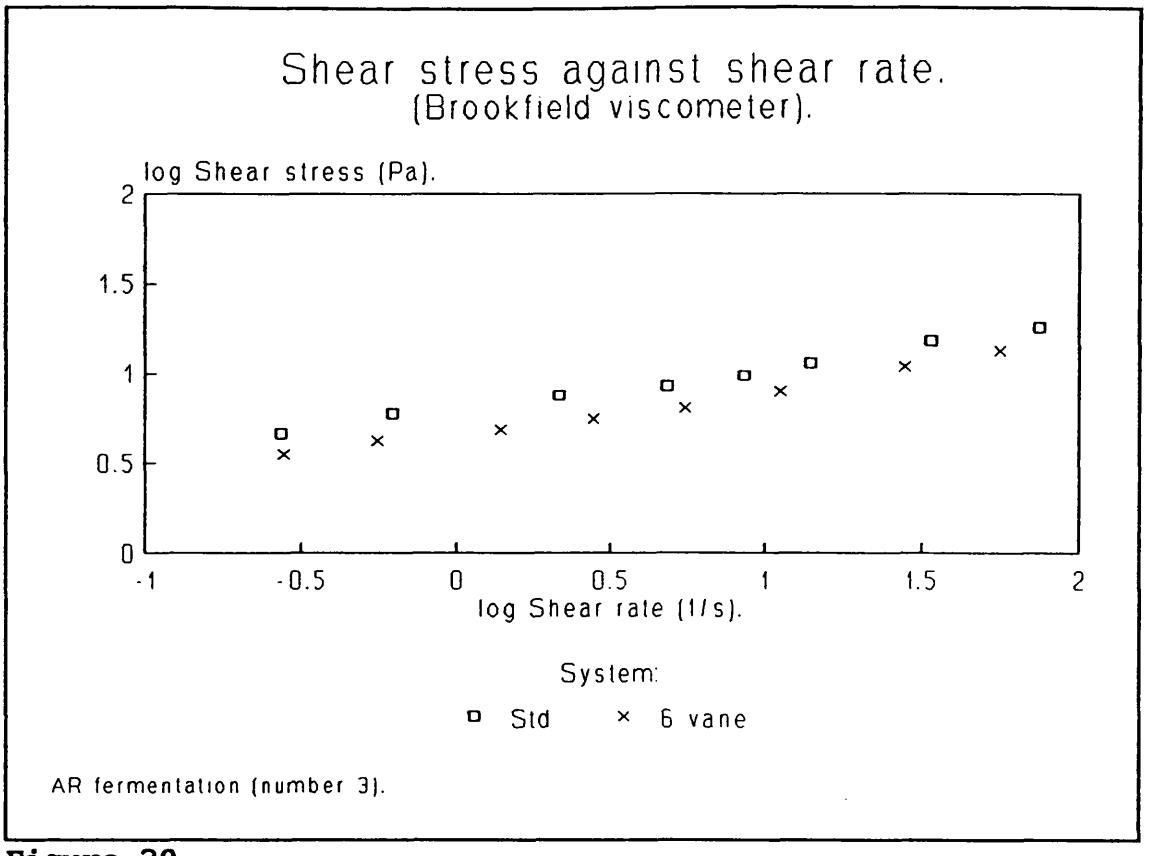

Figure 30

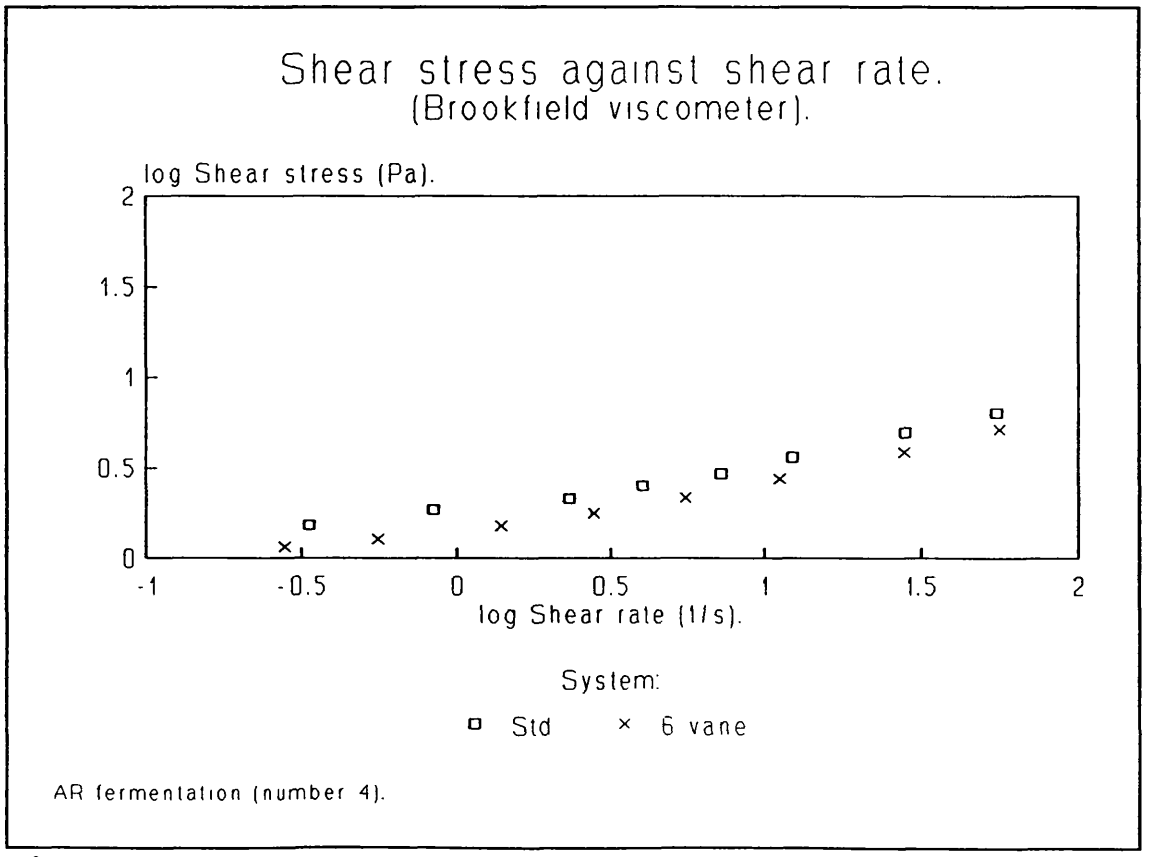

Figure 31

difficulties are encountered when measuring the rheological properties of a mycelial fermentation because of gravity settling and other forms of phase separation. The results in this section do not show any substantial differences between the traditional methods of rheological measurement and this turbine system proposed by Bongenaar [100] and Kemblowski [73]. Therefore, the advantages of turbine systems are only required in some mycelial fermentations.

Table 6. Standard and turbine rheological data.

	Standard Geometry		Turbine Geometry	
	n	log K	n	log K
1	0.201±0.024	0.970±0.058	0.203±0.032	0.796±0.067
2	0.246±0.032	1.110±0.080	0.194±0.023	1.048±0.045
3	0.238±0.018	0.796±0.044	0.248±0.024	0.662±0.050
4	0.280±0.039	0.270±0.076	0.283±0.035	0.166±0.070

9 Conclusions.

The advent of image analysis has provided an accurate and rapid technique for the examination and quantification of the morphology of filamentous microorganisms.

Many authors (see introduction) have suggested that as filamentous microorganisms grow longer and/or more branched they will become more entangled with each other and the resultant matting of the organisms causes a higher apparent viscosity of the fermentation broth. This hypothesis has been shown not to be the case for the three different Actinomycete fermentations investigated in this work; no correlation could be found between the rheology of the fermentation broth and the morphology of the filamentous microorganisms contained in the broth. Although the only morphological parameter discussed in the results is the mean main hyphal length, other morphology parameters were examined and also found to exhibit no correlation with the rheology of the fermentation. This image analysis technique has shown that the Actinomycetes used in this work were both shorter and less branched than the filamentous organisms morphologically examined in other literature [42, 123 and 124]. Figure 1 shows the change in mean main hyphal length (μm) with fermentation time for three different filamentous microorganisms; *S. clavuligerus* [123], *P. chrysogenum* [124] and *S. erythraeus*. The *S. erythraeus* represents the longest of the Actinomycetes analysed in this work but it is still much shorter than the *P. chrysogenum* and the *S. clavuligerus*. From observations using the image analysis system, the Actinomycetes investigated in this work appear to be too short to become entangled. Thus the entanglement hypotheses cannot apply to the Actinomycetes studied in this work and probably to many other filamentous organisms with similar physical features. The order of Actinomycetes contains filamentous microorganisms of widely differing morphologies. The three Actinomycetes all had short mycelia, probably because they were selected for use in an industrial process. The

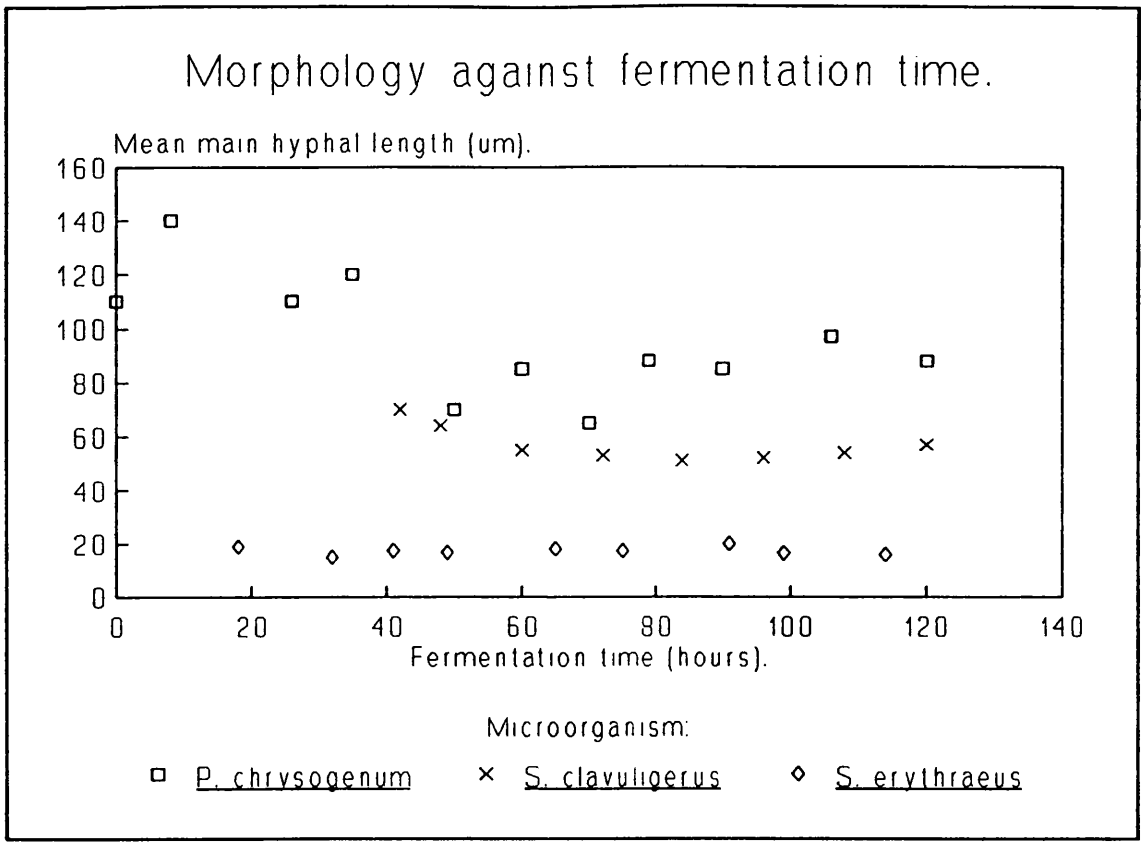

Figure 1

mutation work on the organisms to improve product yield has also selected the shorter filamentous microorganisms. The improved product yield of these nutrients may result in part from the enhanced mass and heat transfer in a less viscous fermentation broth.

In previous work Belmar et al [123] and Makagiansar [124] have successfully used a similar image analysis system to determine relationships between morphological parameters and other fermentation parameters for *S. clavuligerus* and *P. chrysogenum*. The *P. chrysogenum* and the *S. clavuligerus* are found to have a distinctive growth trend with time, see figure 1, whereas the Actinomycetes examined in this work exhibited no particular growth trend.

The application of the Power law provided rheological data which were independent of shear rate. The three Actinomycete fermentations produced similar profiles for the Power law parameters. In general the consistency coefficient was observed to increase to a peak and then

decrease as the fermentation proceeded. Therefore, over the duration of the fermentation, the apparent viscosity of the fermentation rose to a high point and then fell. The Power law index fell rapidly from a value near unity to somewhere in the range 0.2-0.4 and remained at this level for the remainder of the fermentation. Thus at the start of the process the fermentation broth quickly altered form a Newtonian fluid to a highly pseudoplastic fluid. Similar trends to those described above were seen by Tuffile and Pinho [55] while studying a highly viscous *S. aureofaciens* fermentation.

The rheology of the fermentation broth appears to be influenced by the concentration of cells and the ionic composition of the broth. As in the work by Gbewonyo et al [121], a relationship can be observed between the cell concentration for the Actinomycetes and the total oxygen consumption of the fermentation during the active growth phase. As a result of this discovery a further relationship was found between the cell concentration and the rheology of the fermentation during the active growth phase. An increase in the dry cell weight of the fermentation resulted in an increase in the apparent viscosity of the fermentation broth. Altering the pH or the salt concentration had a significant effect on the apparent viscosity of the fermentation broths. It is hypothesised that positive divalent ions form bridges between the filamentous microorganisms. These interparticular bonds cause the viscous nature of the fermentation broth by forming a matrix of bound organisms. More work needs to be done in this area.

Contrary to the views of Kemblowski and Kristiansen [73], the use of turbine impellers for the measurement of rheological characteristics on Actinomycete fermentations has shown no obvious benefits over more traditional procedures. The turbine systems were designed to overcome any form of phase separation, but the *S. rimosus* and *A. roseorufa* fermentations do not suffer from such problems. As was stated earlier, the organisms studied in this work

are by no means typical of all filamentous organisms and the ineffectiveness of the turbine system in this work should not preclude the use of this system for other filamentous microbial fermentations.

Recommendations for further work.

Several important issues were discovered during this study that deserve further investigation. These were as follows:

1) It was shown that biomass concentration had a strong influence on the apparent viscosity of the culture broth. The variation in culture rheology as a function of biomass concentration throughout the fermentation period could only be studied for one of the three microorganisms (*S. erythraeus*). Significant practical problems were encountered beyond the initial growth phase in the separation of the microorganisms from the fermentation liquor in the cases of *S. rimosus* and *A. roseorufa*. The use of defined nutrient media would eliminate the presence of insoluble particles normally associated with complex media and therefore ease the separation process. This will allow accurate measurements of the biomass concentration during the *S. rimosus* and *A. roseorufa* fermentations and the data should indicate whether or not the relationship between biomass concentration and apparent viscosity observed for *S. erythraeus* is dependent on the specific microorganisms.

2) As part of this investigation experiments were carried out to establish whether the presence of interparticle forces originating from charges around the microorganism influenced the rheology of the culture. This was achieved by manipulating the pH of the *S. rimosus* broth. The results indicated that rheology of the culture was sensitive to even minor changes in broth pH. It is recommended that these measurements be carried out with the other two microorganisms (*S. erythraeus* and *A. roseorufa*). Additionally, it is suggested that parallel with these measurements data be obtained on the zeta potential for these systems in order to establish the mechanisms by which pH influences rheology.

3) Experiments were done in which the biomass concentration of *S. rimosus* was reduced systematically by the addition of de-mineralised water and it was found that

while the magnitude of the flow behaviour index (n) was unaffected by the degree of dilution the value of the consistency coefficient (K) was strongly dependent on it. This further confirms that the rheology of the fermentation broth is affected by biomass concentration rather than by the morphology of the microorganism which clearly remains unaffected by the dilution process. However, it is important to study the effect of dilution on the rheology of the other two cultures (*S. erythraeus* and *S. rimosus*) in order to confirm these observations.

4) It is established that the morphology of the microorganisms does not correlate with the rheology of the fermentation for the specifically selected and industrial strains of Actinomycetes used in this work. It is suggested that similar experiments be carried out with other species both from the order of Actinomycetes and others to establish whether these observations apply to other fermentation broths.

Notation.

a - instrument constant (-).
A - area (m^2).
AR - *Actinomadura roseorufa*.
BL - branch length (µm).
C - the concentration of dissolved oxygen in the liquid ($mol.m^{-3}$).
C* - the concentration of dissolved oxygen in equilibrium with the partial pressure of oxygen in the gaseous phase ($mol.m^{-3}$).
CER - carbon dioxide evolution rate.
CL - confidence limit.
CMC - carboxy methyl cellulose.
d - impeller diameter (m).
D - sample holder diameter (m).
DCW - dry cell weight (g/l).
DOT - dissolved oxygen tension (%).
ET - equilibration time (s).
F - force (N).
G' - shear modulus (N/m^2).
HGU - hyphal growth unit (µm).
HL - total hyphal length (µm).
HRI - helical ribbon impeller.
K - consistency coefficient ($Pa.s^n$).
K_c - Casson viscosity ($Pa^{½}.s^{½}$).
K_La - the volumetric transfer coefficient (s^{-1}).
k_s - a constant (-).
l - length / impeller length (m).
L_0 - initial length (m).
L_h - total length of hyphae per unit of culture volume (µm).
L_i - length (m).
M - torque (N.m).
ML - main hyphal length (µm).
n - Power law index or flow behaviour index (no units).
N - impeller speed (1/s).

n_b - number of blades.

N_h - number of hyphae tips per unit of culture volume (no units).

NT - number of growth tips (-).

OSR - oxygen solution rate.

OUR - oxygen uptake rate (moles/l.hr).

p - pitch length (m).

P - power consumption (N.m/s).

P_0 - power number (-).

P_{ij} - the stress tensor.

P_{xy} - a stress component.

r - radius (m).

R - power index constant (-).

RQ - respiratory quotient (-).

S - instrument constant ($1/m^3$).

SE - *Streptomyces erythraeus*.

SR - *Streptomyces rimosus*.

t - time (hr).

TOC - total oxygen consumed (moles).

w - impeller blade width (m).

v - velocity (m/s).

V - the volume of the element (m^3).

x - a distance (m).

X - the mycelial concentration (g/L).

z - the manufactures constant for a viscometer (m^{-3}).

α - the mean apical growth rate (μm/s) and the viscometer reading (N.m).

β - the mean branching rate (1/μm.s).

$\dot{\gamma}$ - the shear rate (1/s).

γ - the average shear rate across a volume (1/s).

δ - morphology constant ($Pa.l^2/g^2$).

μ - the viscosity (Pa.s).

μ_a - the apparent viscosity (Pa.s).

α - blade inclination angle and a reduction ratio (-).

ν_1 - first normal stress difference.

ν_2 - second normal stress difference.

ρ - density of fluid (kg/m^3).

τ - the shear stress (Pa).

τ_0 - the yield stress (Pa).

γ - the angle of shear (radians).

Appendix.

Conversion of Brookfield readings into viscosity functions.

Mitschka [115] developed a procedure based on theoretical studies of the rotational flow of non newtonian fluids (obeying the Power law relationship) around bodies with simple geometry in well defined flow fields.

The procedure is specifically used for converting the primary (scale readings) readings from the Brookfield viscometer into corresponding values of shear stress and shear rate.

The procedure is described fully elsewhere [115] and only an outline of the technique with a worked out example using a fermentation broth is given below:

(1) As many pairs of values as possible of the scale deflection, α, on the torque dial (in scale units of the 0-100 scale) are taken with one, or preferably several, spindles for fixed values of rotational speed, N (rpm). In the present study only one spindle (number 2) was used.

(2) Values of α are converted to average shear stresses, τ (Pa), on the spindle used by equation (1).

$$\tau = S \cdot \alpha \qquad (1)$$

The value of S depends on both spindle geometry and the model of viscometer. For the spindle and model viscometer used in this study the value of S was 0.476 which is a value based on Mitschka's calculations but modified for the particular model of viscometer (2HA DVII) used in this work. The value of S was obtained from private communication with the Brookfield technical department.

(3) Pairs of τ - N valid for each particular spindle are plotted in the log-log form.

(4) When the dependence is sufficiently close to a linear one, the fluid under test is of the Power law type. The slope of the log τ - log N dependence in this case is simply equal to the flow index of the fluid, n.

The corresponding values of average shear rate, γ (1/s), are then calculated using equation (2).

$$\dot{\gamma} = R \cdot N \qquad (2)$$

Where R is a function of both the flow behaviour index and spindle geometry. Notice that the recommended value of R provides the shear rate values in 1/s whilst N is measured in rpm. Values of R are calculated and tabulated by Mitschka and table (1) gives these values of R for the particular spindle used in this work.

The above procedure is modified slightly for cases where log τ against log N is non-linear. For such plots point values of slope (and hence n) were obtained from the tangents drawn to each curve at different speed points. Again equation (2) was used to obtain values of average shear rate, γ (1/s).

Table one. Values for Mitchka's parameters.

n (-)	R (-)
0.1	1.431
0.2	0.875
0.3	0.656
0.4	0.535
0.5	0.458
0.6	0.404
0.7	0.365
0.8	0.334
0.9	0.310
1.0	0.291

A polynomial expression was fitted to the data in table one. This equation was used to calculate a value of R from the determined value of n, see equation (3).

$$R = 9.20.n^4-24.66.n^3+24.21.n^2-10.73.n+2.27 \qquad (3)$$

(5) The relevant pairs τ - γ are now assumed to be the points of the apparent viscosity function of the fluid sample tested.

Table (2) provides the raw data and shear stress/shear rate values calculated using the above procedure.

The torque readings were converted to shear stresses using equation (4).

$$\tau = 0.476.\alpha \qquad (4)$$

The values of log shear stress against log speed were plotted and a straightline was drawn through the points using linear regression analysis. After determining the flow behaviour index of the fluid, n, (the gradient of the line) R could then calculated using equation (3) and the shear rates could be determined using equation (5).

$$\dot{\gamma} = 0.76.N \qquad (5)$$

The plot of log Shear stress against log Shear rate is shown in figure (1).

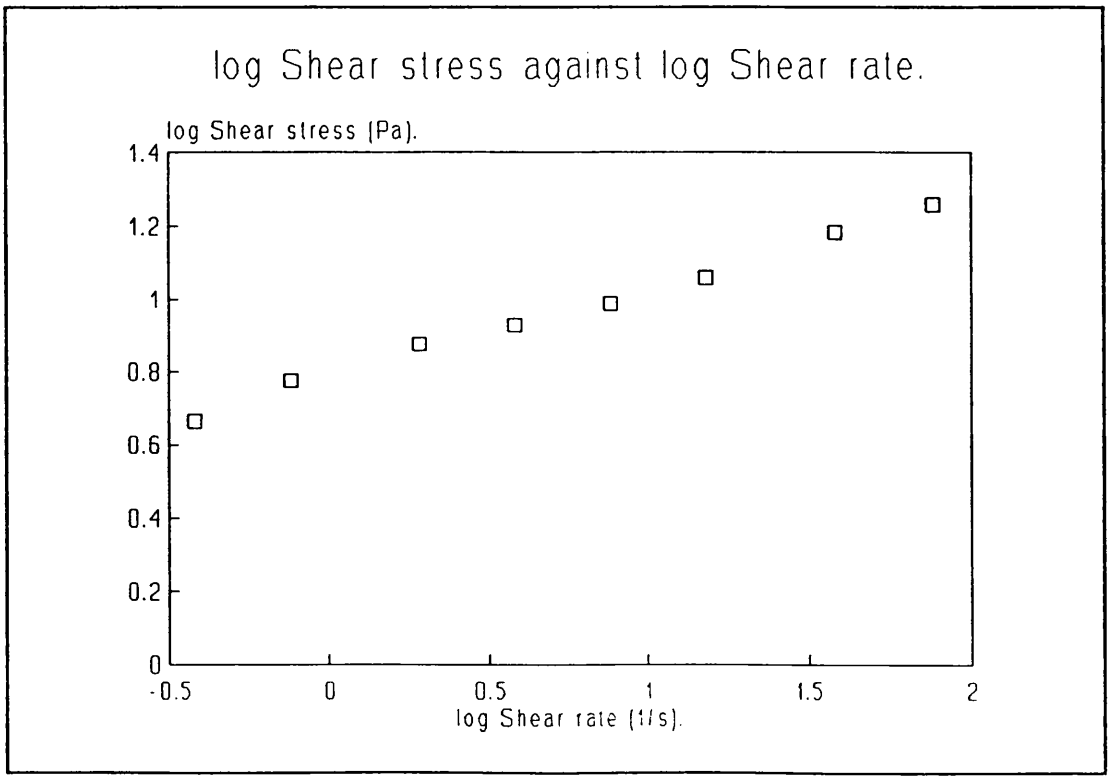

Figure 1

Table 2. Typical results of the Mitchka procedure.

Speed N (rpm)	Torque α (scale reading)	Shear stress τ (Pa)	log Shear stress	log Speed	Shear Rate γ (1/s)	log Shear rate
0.5	9.7	4.62	0.66	(0.30)	0.38	(0.42)
1.0	12.5	5.95	0.78	0.00	0.76	(0.12)
2.5	15.8	7.52	0.88	0.40	1.91	0.28
5.0	17.8	8.47	0.93	0.70	3.81	0.58
10.0	20.4	9.71	0.99	1.00	7.63	0.88
20.0	24.0	11.42	1.06	1.30	15.25	1.18
50.0	32.0	15.23	1.18	1.70	38.13	1.58
100.0	38.1	18.14	1.26	2.00	76.26	1.88

References.

1) J. A. Roels, J. Von Den Berg, and R. M. Voncken, The rheology of mycelial broths, Biotech. Bioeng.,16, 181-208 (1974).

2) M. Charles, Technical aspects of the rheological properties of microbial cultures, Adv. Biochem. Eng., 8, 1-62, (1978).

3) I. A. Fatile, Rheological characteristics of suspensions of *A. niger*, Appl. Microbiol. Biotechnol., 21, 60-64 (1985).

4) R. G. Buchanan, Studies on the nomenclature and classification of the bacteria II. The primary subdivisions of the Schizomycetes, J. Bacteriol., 2, 155-164 (1917).

5) S. A. Waksman, The Actinomyces of the soil, Soil Science, 1, 99-134 (1916).

6) Bacteriostatic and bactericidal substances produced by a soil actinomyces. Proceedings of the Society of Experimental Biology and Medicine, 45, 609-614.

7) A. Schalz, E. Bugie, and S. A. Waksman, Streptomycin, a substance exhibiting antibiotic activity against Gram-positive and Gram-negative bacteria, Proceedings of Soc. Exp. Biology Med., 55, 66-69 (1944).

8) C. Reeding, and M. Cole, Clavulanic acid: a beta-lactamase-inhibiting beta-lactam from *Streptomyces clavuligerous*, Antimicrobial agents and chromatography, 11, 852-857 (1977).

9) H. Prouser, Characters and genera arrangement in actinomycetales In: The actinomycetales, (Prouser ed.), pp407-418, Gustov Fischer, Jena (1970).

10) R. Locci, Developmental micromorphology of actinomycetes In: Actinomycetes the boundary organism, (Arai ed.), pp249-297, Toppen Company, Tokyo (1976).

11) S. A. Waksman, and A. T. Henrici, The nomenclature and classification of the actinomycetes, J. Bacteriol., 46, 337-341, (1943).

12) J. Lacy, and M. Goodfellow, A novel actinomycete from sugar cane bagasse: *Saccharopolyspora kirsula* gen. et sp. nov, . Gen. Microbiol., 88, 75-85 (1975).

13) S. T. Williams, G. P. Sharples, J. A. Serrano, A. A. Serrano, and J. Lacey, The micromorphology and fine structure of nocardioform organisms In: The biology of Nocardiae (Goodfellow, Brownell and Serrano eds.), pp120-140, Academic Press, London (1976).

14) Labeda D. P., Transfer of the type strain of *Streptomyces erythraeus* (Waksman and Henrici, 1948) to the genus Saccharopolyspora (Lacey and Goodfellow, 1975) as *Saccharopolyspora erythraea*, Int. J. of Systematic Bacteriology, 37, 19-22 (1987).

15) D. Da Riva Ricci, and R. Kendrick, Computer modelling of hyphal tip growth in fungi, Canadian J. Botany, 50, 2455-2462 (1972).

16) R. Locci, Micromorphology and development of actinomycetes. Zentralblatt für bakteriologie, mikrobiologie und hygiene 1 abteilung. Supplement II,119-130 (1979).

17) K. F. Chater, and M. J. Merrick, Streptomycetes in developmental biology of Prokaryotes, (Parish ed.), pp93-114, Blackwell Scientific Publications, Oxford (1979).

18) R. Locci, and K. P. Schaal, Apical growth in facultative aerobic actinomycetes as determined by immunofluorescent labelling. Zentralblatt für Bakterioloie, Parasitenkunde, Infektionskrunkheiten und Hygiene. Abteilung 1, Originale, 246, 112-118 (1980).

19) R. Locci, Developmental micromorphology of actinomycetes In: Actinomycetes the boundary microorganism, (Arai ed.), pp249-297, University Park Press, London (1976).

20) S. T. Williams, and E. M. H. Wellington, Micromorphology and fine structure of actinomycetes In: Microbiological classification and identification (Goodfellow and Board eds.), pp139-165, Academic Press, London (1980).

21) M. E. Bushell, Growth, product formation and fermentation technology In: Actinomycetes in biotechnology (Goodfellow, Williams, Nardarski eds.), Academic Press, London, pp185-217 (1988).

22) B. König, and K. Schügerl, Strategies for Penicillin fermentation in tower-loop reactors, Biotech. Bioeng., 24, 259-280 (1982).

23) S. Kretschmer, D. Riesenberg, and F. Bergler, Comparative analysis of mycelial growth in actinomycetes, Zentralblatt für bakteriologie, mikrobiologie und hygiene 1. Abteilung, supplement 11, 131-135 (1981).

24) D. Katz, D. Goldstein, and R. F. Rosenberger, Model for branch initiation in *Aspergillus nidulans* based on measurement of growth parameters, J. Bacteriol., 109, 1097-1102 (1972).

25) B. L. A. Carter, and A. T. Bull, The effect of oxygen tension in the medium on the morphology and growth kinetics of *Aspergillus nidulans*, J. Gen. Microbiol., 65, 255-273 (1971).

26) Y. Aharonowitz, and A. L. Demain, Thoughts on secondary metabolism, Biotech. Bioeng., 22, 5-9 (1980).

27) O. Hara, S. Huinouchi, T. Vozami, and T. Beppu, Genetic analysis of A-factor synthesis in *Streptomyces coelicolor* A3(2) and *Streptomyces griseus*, J. Gen. Microbiol., 129, 2939-2944 (1983).

28) G. T. Banks, Aeration of mould and streptomycete culture fluids In: Topics in enzyme and fermentation biotechnology 1 (Wiseman ed.), pp72-110, Ellis Horwood, Chichester (1977).

29) B. Metz, N. Kossen, and J. A. Van Suijdam, Rheology of mould suspensions, Adv. Biochem. Eng. 2, 103-156 (1979).

30) B. Atkinson, and F. Marituna, Biochemical engineering and biotechnology handbook, the Nature Press, London (1983).

31) F. H. Deindorfer, and J. M. West, Rheological examination of some fermentation broths, J. of Microbiol and Biochemical Technology and Engineering, 2, 165-175 (1983).

32) P. F. Stanbury, and A. Whitaker, Principles of fermentation technology, Pergamon Press, Oxford.

33) R. Bunch, and J. M. McGuire, US patent 2653899 (1953).

34) J. C. French, J. D. Howells, and L. E. Anderson, US patent 3551294 (1970).

35) Stark W. M., and Smith R. L., The Erythromycin fermentation, Progress in Ind. Microbiol., 3, 213-230 (1961).

36) R. L. Smith, H. R. Bungay, and R. C. Pittenger, Growth-biosynthesis relationships in Erythromycin fermentations, Appl. Microbiol.,10, 293-296 (1962).

37) H. G. Osman, A. A. Abou-Zeid, and A. A. El-Gamal, Factors influencing the biosynthesis of Erythromycin by *Streptomyces erythreus*, Zeitschrift f. Allg. Mikrobiologie, 8 (5), 421-428 (1968).

38) D. J. Wood, European patent 0314330A2 (1988).

39) A. C. Finlay, G. L. Hobby, S. Y. P'an ,et al, Terramycin, a new antibiotic, Science, 111, 85 (1950).

40) J. Doskoăl, B. Sikyta, J. Kaŝparová, et al, Development of the culture of *Streptomyces rimosus* in submerged fermentation, J. Gen. Microbiol., 18, 302-314 (1958).

41) H. L. Adams, and C. R. Thomas, The use of image analysis for morphological measurements on filamentous microorganisms, Biotech. Bioeng., 32, 707-712 (1988).

42) H. L. Packer, and C. R. Thomas, Morphological measurements on filamentous microorganisms by fully automated image analysis, Biotech. Bioeng., 35, 870-881 (1990).

43) B. Metz, E. W. de Bruijn, and J. C. van Suijdam, Method for quantitative representation of the morphology of molds, Biotech. Bioeng., 23, 149-162 (1981).

44) U. Björkman, Properties and principles of mycelial flow: experiments with a tube rheometer, Biotech. Bioeng., 29, 114-129 (1987).

45) N. Casson, Rheology of dispersed systems, Mill C C, Pergamon, London, 1959.

46) J. C. van Suijdam, and P. J. B. Dusseljee, Physical aspects of bioreactor performance. Chapter 6: concept of apparent morphology as a tool in fermentation technology (W. Crueger ed.), Dechema, 1987.

47) J. C. van Suijdam, and B. Metz, Influence of engineering variables upon morphology of filamentous molds, Biotech. Bioeng., 23, 111-148 (1981).

48) J. J. Smith, M. D. Lilly, and R. I. Fox, The effect of agitation on the morphology and Penicillin production of *Penicillium chrysogenum*, Biotech. Bioeng., 35, 1011, 1990.

49) Joyce Loebl, Image analysis, principles and practice, Joyce Loebl, Gateshead, England, 1985.

50) V. S. Mitev, and S. B. Popova, Computer morphological analysis in Baker's yeast production, Prog. Biotechnol., 6, 431-435 (1990).

51) British Standard Institution, British Standard glossary of rheological terms, BS5168 (1975).

52) K. Walters, Rheometry: industrial applications (Walters ed.), Research Studies Press, Chichester, 1980.

53) R. W Whorlow, Rheological techniques, Ellis Horwood Ltd., Chichester, 1980.

54) K. Walters, Rheometry, Chapman and Hall, London, 1975.

55) C. M. Tuffile, and F. Pinho, Determination of oxygen-transfer coefficients in viscous Streptomycete fermentations, Biotech. Bioeng., 12, 849-871 (1970).

56) H. Taguchi, The nature of fermentation fluids, Adv. Biochem. Eng., 1, 1-30 (1971).

57) K. Sato, Rheological studies on some fermentation broths (IV). Effect of dilution rate on rheological problems of fermentation broth, J. Ferment. Tech., 39, 517-520 (1961).

58) J. R. van Wazer, . W Lyons, and K. Y. Kim, Viscosity and flow measurement, Interscience, 1963.

59) H. Freundlich, Thixotropy, Hermann et Ae, Paris, 1935.

60) F. Moore, The rheology of ceramic slip bodies, Trans. Brit. Ceram. Soc., 58, 470-492 (1959).

61) D. C-H. Chang, A differential form of constitutive relation for thixotropy, Rheol. Acta., 12, 228-233 (1973).

62) D. C-H. Chang, and F. Evans, Phenomenological characterization of the rheological behaviour of inelastic reversible thixotropic and antithixotropic fluids, Brit. J. Appl. Phys., 16, 1599-1617 (1965).

63) J. M. Coulson, and J. F. Richardson, Chemical Engineering (Volume 3), Pergamon Press, Oxford, 1984.

64) A. G. Frederickson, Principles and applications of rheology, Prentice Hall, Englewood Cliffs N.J., 1964.

65) A. B. Metzner, and J. C. Reed, Flow of non-Newtonian fluids - correlation of the laminar, transition, and turbulent-flow regions, AIChE Journal, 1(4), 434 1955.

66) W. Ostwald, Kolloid-Z, 38, 261 (1926).

67) W. J. Frith, and J. Mewis, Rheology of concentrated suspensions: experimental investigations, 51, 27-34 (1987).

68) A. B. Metzner, and R. E. Otto, Agitation of non-Newtonian fluids, A. I. Ch. E. J., 3(1), 1-10 (1957).

69) N. Q. Dzuy, and D. V. Boger, Yield stress measurement for concentrated suspensions, J. Rheol., 27(4), 321-347 (1983).

70) W. H. Herschel, and R. Bulkley, Proc. Amer. Soc. Test Matls., 26, 621- (1926).

71) H. A. Barnes, and K. Walters, The yield stress myth, Rheol. Acta, 24, 323-326 (1985).

72) J. L. Sutterby, Laminar converging flow of dilute polymer solutions in conical sections: Part 1. Viscosity data, new viscosity model, tube flow solution, A. I. Ch. E. J., 12(1), 63-68 (1966).

73) Z. Kemblowski, and B. Kristiansen, Rheometry of fermentation liquids, Biotech. Bioeng., 28, 1474-1483 (1986).

74) F. H. Deindorfer, and J. M. West, Rheological properties of fermentation broths, Fermentation Symposium: broth rheology, 2, 265-273 (1960).

75) H. W. Blanch, and S. M. Bhavaraja, Non-Newtonian fermentation broths: rheology and mass transfer, Biotech. Bioeng., 18, 745-790 (1976).

76) G. W. Pace, and R. C. Righelato, Production of extracelluar microbial polysaccharides, Adv. Biochem. Eng., 15, 41-70 (1980).

77) N. Blakebrough, W. J. McManamey, and K. R. Tart, Rheological measurements on *Aspergillus niger* fermentation systems, J. Appl. Chem. Biotechnol., 28, 453-461 (1978).

78) Y. Cohen, and A. B. Metzner, An analysis of apparent slip flow of polymer solutions, Rheol. Acta, 25, 28-35 (1986).

79) D. G. Allen, and C. W. Robinson, Measurement of rheological properties of filamentous fermentation broths, Chem. Eng. Science, 45(1), 37-48 (1990).

80) U. Björkman, Properties and principles of mycelial flow: a tube rheometer system for fermentation fluids, Biotech. Bioeng., 29, 101-113 (1987).

81) C. R. Perley, J. R. Swartz, and C. L. Cooney, Measurement of cell mass concentration with a continuous flow viscometer, Biotech. Bioeng., 21, 519-523 (1979).

82) F. Moore, and L. J. Davies, The consistency of ceramic slips - a new rotational viscometer and some preliminary results, J. Trans. Brit. Ceram. Soc., 55, 313-338 (1956).

83) I. M. Kreiger, and S. M. Maron, Direct determination of the flow curves of non-Newtonian fluids III. Standardized treatment of viscometric data, J. Appl. Phys., 25, 72-75 (1954).

84) M. Mooney, Explicit formulas for slip and fluidity, J. Rheol., 2(2), 210-222 (1931).

85) W. L. Wilkinson, Non-Newtonian fluids, Pergamon Press, Oxford, 1960.

86) T. M. T. Yang, and I. M. Krieger, Comparison of methods for calculating shear ratesin coaxial viscometers, J. Rheol., 22(4), 413-421 (1978).

87) T. W. Barker, and J. T. Worgan, The application of air-lift fermenters to the cultivation of filamentous fungi, Eur. J. Appl. Microbiol. Biotechnol., 18, 17-23 (1983).

88) A. Leduy, A. A. Marsan, and B. Coupal, A study of the rheological properties of a non_newtonian fermentation broth, Biotech. Bioeng., 16, 61-76 (1974).

89) N. P. Ghildyal, M. S. Thakur, S. Stikanta, et al, Rheological studies on *Streptomyces fradiae* SeF-5 in submerged fermentation, J. Chem. Tech. Biotechnol., 38, 221-234 (1987).

90) R. Wittler, R Matthes, and K. Schügerl, Rheology of *Penicillium chrysogenum* pellet suspensions, Eur. J. Appl. Microbiol. Biotechnol., 18, 17-23 (1983).

91) G. I. Taylor, Phil. Trans. Roy. Soc. A., 233, 289-293 (1923).

92) H. Schlichting, Boundary layer theory (translated by Kestin), McGraw Hill, 1968.

93) R. N. Weltmann, and P. W. J. Kuhns, Effect of shear temperature on viscosity in a rotational viscometer measurement, J. Colloid Sci., 7, 218-226 (1952).

94) V. J. Vand, Viscosity of solutions and suspensions II - experiemntal determination of the viscosity-concentration function of spherical suspensions, Phys. Colloid. Chem., 52, 300-314 (1948).

95) K. H. Sweeny, and R. D. Geckler, The rheology of suspensions, J. Appl. Phys., 25(9), 1135-1144 (1954).

96) A. D. Maude, and R. C. Whitmore, The wall effect and the viscometry of suspensions, Brit. J. Appl. Phys., 7, 98-102 (1956).

97) C. Tangsathitkulchai, and L. G. Austin, Rheology of concentrated slurries of particles of natural size distribution produced by grinding, Powder Technol., 56, 293-299 (1988).

98) J. J. Vocadlo, and M. E. Charles, Measurement of yield stress of fluid-like viscoplastic substances, Can. J. Chem. Eng., 49, 576-583 (1971).

99) R. W. Higman, A new torque and normal thrust measuring system for the Weissenberg rheogoniometer, Rheol. Acta., 12, 533-539 (1973).

100) J. J. Bongenaar, N. W. F. Kossen, et al, A method for characterizing the rheological properties of viscous fermentation broths, Biotech. Bioeng., 15, 201-206 (1973).

101) M. Cooke, J. C. Middleton, and J. R. Bush, Mixing and mass transfer in filamentous fermentations, Biotech. Bioeng., 15, 37-64 (1973).

102) M. Reuss, D. Debus, and G. Zoll, Rheological properties of fermentation fluids, The Chemical Engineer, 233-236, June 1982.

103) D. G. Allen, and C. W. Robinson, The influence of `slip' on rheological measurements on a mycelial broth of *Aspergillus niger*, Annals N. Y. Acad. Sci., 506, 589-599 (1987).

104) P. Rapp, and F. Wagner, Cellulose degradation and monitoring of viscosity decrease in cultures of *Cellulomonus uda* grown on printed newspaper, Biotech. Bioeng., 26, 1167-1175 (1984).

105) Z. Kemblowski, and B. Kristiansen, and O. Ajayi, On-line rheometer for fermentation liquids, Biotech. Letters, 7(11), 803-808 (1985).

106) O. Ajayi, Z. Kemblowski, B. Kristiansen and V. F. Larsen, On-line rheometer for the monitoring of polymer fermentations: operating conditions, Biotechnol. Letts., 13(8), 583-588 (1991).

107) B. Metz, N. W. F. Kossen, and J. C. van Suijdam, The rheology of mold suspensions, Adv. Biochem. Eng., 11, 104-156 (1979).

108) J. H. Kim, J. M. Lebeault, and M. Reuss, Comparative study on rheological properties of mycelial broth in filamentous and pelleted forms, Eur. J. Microbiol. Biotechnol., 18, 11-16 (1983).

109) D. Picque, and G. Corrieu, New instrument for on-line viscosity measurement of fermentation media, Biotech. Bioeng., 31, 19-23 (1988).

110) G. Schramm, Introduction to practical viscometry, Gebrüder Haake GmbH, West Germany, 1981.

111) Brookfield, When viscosity is measured, Brookfield Engineering Laboratories, Massachusetts, USA.

112) Contraves, Rheomat 115 operating instructions, Contraves Industrial Products Ltd., Ruislip, England.

113) P. Mitschka, Simple conversion of Brookfield RVT readings into viscosity functions, Rheol. Acta, 21, 207-209 (1982).

114) R. W. Williams, Brookfield data analysis, Brookfield seminar, London, 1990.

115) Nikon, Optiphot biological microscope instructions, Nikon, Tokyo, Japan.

116) J. B. Kennedy, and A. M. Neville, Basic statistical methods for engineers and scientists, Harper and Row, New York, 1986.

117) J. H. Rushton, E. W. Costick, and H. J. Everett, Power characteristics of mixing impellers. II, Chem. Eng. Prog., 46, 467-476 (1950).

118) W. I. Patterson, P. J. Carreau, and C. Y. Yap, Mixing with helical ribbon agitators, A. I. Ch. E., 25(3), 508-521 (1979).

119) A. Mitard, and J. P. Riba, Rheological properties of *Aspergillus niger* pellet suspension, Appl. Microbiol. Biotechnol., 25, 245-249 (1986).

120) K. Takahashi, T. Yokota, and H. Konno, Power consumption of helical ribbon agitatorsin highly viscous pseudoplastic liquids, J. Chem. Eng. Japan, 17(6), 657-659 (1984).

121) K. Gbewonyo, D. Jain, S. W. Drew, and B. C. Buckland, On-line analysis of Avermectin fermentation cell growth kinetics in an industrial pilot plant, Biotech. Bioeng., 34, 234-241 (1989).

122) B. C. Buckland, K. Gbewonyo, D. DiMasi, G. Hunt, G, Westfield, and A. W. Nienow, Improved performance in viscous mycelial fermentations by agitator retrofitting, Biotech. Bioeng., 31, 737-742 (1988).

123) M. T. Belmar Campero and C. R. Thomas, The effect of stirrer speed on the morphology and clavulanic acid production of *S. clavuligerus*, paper E2, in the *2nd International Conference on Bioreactor Fluid Dynamics* (R. King ed.), London, 1988.

124) H. Y. Makagiansar, 1991, PhD thesis, University of London.

125) W. B. Russel, The dynamics of colloidal systems, University of Wisconsin Press, England, 1987.

126) G. D. Parfitt, In dispersion of powders in liquids (Parfitt G. D. ed.), Applied Science, London, 1973.

127) R. Hogg, I.Chem.E, 5th Int. Symp. on Agglomeration, UK, 483-495 (1989).

128) J. T. Davies and E. K. Rideal, Interfacial Phenomena, Academic Press, UK, 1961.

129) T. P. Elson, D. J. Cheesman and A. W. Nienow, X-ray studies of cavern sizes and mixing performance with fluids possessing a yield stress, Chemical Engineering Science, 41 (10), 2555-2562, 1986.